NANOPORE SENSING OF PEPTIDES AND PROTEINS

A Thesis Submitted to the College of Graduate Studies and Research
In Partial Fulfillment of the Requirements for the
Degree of Doctor of Philosophy
In the Department of Biochemistry
University of Saskatchewan
Saskatoon

By

Besnik Krasniqi

PERMISSION TO USE

In presenting this thesis in partial fulfillment of the requirements for a postgraduate degree from the University of Saskatchewan, I agree that the Libraries of this University may make it freely available for inspection. I further agree that permission for copying of this thesis in any manner, in whole or in part, for scholarly purposes may be granted by the professors who supervised my thesis work, or in their absence, by the Head of the Department or the Dean of the College in which my thesis work was done. It is understood that any copying or publication or use of this thesis or parts thereof for financial gain shall not be allowed without my written permission. It is also understood that due recognition shall be given to me and to the University of Saskatchewan in any scholarly use which may be made of any materials in my thesis.

Requests for permission to copy or make other use of material in this thesis in whole or in part should be addressed to:

Head of the Department of Biochemistry
University of Saskatchewan
Saskatoon, Saskatchewan S7N 0W0

ABSTRACT

In recent years the application of single-molecule techniques to probe biomolecules and intermolecular interactions at single-molecule resolution has expanded rapidly. Here, I investigate a series of peptides and proteins in an attempt to gain a better understanding of nanopore sensing as a single-molecule technique.

The analysis of retro, inversed, and retro-inversed isomers of glucagon and α-helical Fmoc-$D_2A_{10}K_2$ peptide showed that nanopore sensing utilizing a wild-type α-hemolysin pore can distinguish between all four isomers while circular dichroism can only distinguish between chiral isomers, but not between directional isomers.

The investigation of a series of proteins of different chemical and physical properties revealed important information about nanopore analysis of proteins. Contrary to some reports in the literature, all proteins analysed here induced large blockade events. The frequency of total events and the proportion of large blockade events were significantly reduced in tris(hydroxymethyl)aminomethane or 4-(2-hydroxyethyl)piperazine-1-ethanesulfonic acid buffers and were only restored by the addition of ethylenediaminetetraacetic acid or the use of phosphate buffer, both of which can sequester metal ions. Furthermore, the results obtained with the proteins in the presence of ligands demonstrated that transient or partial unfolding of proteins can be detected by nanopore analysis confirming the usefulness of this technique for conformational studies or for protein/ligand interactions. Interestingly, while the blockade current histograms were different for each protein there was no obvious correlation between the properties of the proteins and the blockade current histograms.

In an attempt to identify whether the large blockade events were translocation or intercalation, both an indirect and a direct approach were taken. The indirect approach which relies on the effect of voltage on the interaction of the molecule with the pore provided no conclusive answer to the question of protein translocation through the α-hemolysin pore. In contrast, the direct approach in which ribonuclease A is added to the *cis* side of the pore and then the *trans* side is tested for enzyme activity showed that ribonuclease A doesn't translocate through the α-hemolysin pore.

PUBLISHED WORKS

Krasniqi, B., and Lee, J.S. (2012). The importance of adding EDTA for the nanopore analysis of proteins. Metallomics *4*, 539-544.

Krasniqi, B., Scruten, E., Piller, J., Lee, J., and Napper, S. (2012). Stability, toxicity and biological activity of retro, inversed and retro-inversed glucagon isomers. J. Pept. Sci. *18*, 519-526.

Christensen, C., Baran, C., Krasniqi, B., Stefureac, R.I., Nokhrin, S., and Lee, J.S. (2011). Effect of charge, topology and orientation of the electric field on the interaction of peptides with the alpha-hemolysin pore. J. Pept. Sci. *17*, 726-734.

Meng, H., Detillieux, D., Baran, C., Krasniqi, B., Christensen, C., Madampage, C., Stefureac, R.I., and Lee, J.S. (2010). Nanopore analysis of tethered peptides. J. Pept. Sci. *16*, 701-708.

ACKNOWLEDGMENTS

There are a lot of people who have contributed in one way or another to this thesis. First and foremost I would like to thank Dr. Jeremy Lee. You have been an excellent advisor and mentor. Your constant support has been invaluable. I am grateful for the freedom you provided me with in exploring some of my own ideas. Thank you for not giving up on me even when at times it seemed like nothing was working and reminding me that "this is research". It has been my privilege to work with you.

I am thankful to my advisory committee (past and present members), Drs. Ramji Khandelwal, Rob Warrington, Stan Moore, Peter Howard, and Scott Napper for their advice throughout my program.

Special thanks to the staff of the Biochemistry student lab: Dr. Tricia Ulmer, Maureen Sinclair, James Talbot, and Cindy Farrar, for their support and for being such great friends. Thanks Tricia for trusting me as a teaching assistant for three years in a row. Thank you JT and Maureen for going out of your way in lending me equipment and showing me how to use it.

Enormous thanks go to my friends in Lee's lab: Dr. Radu Stefureac, Dr. Claudia Madampage, Meena Kumari, Omid Tavassoly, Christopher Christensen, and Elisabet Jakova, for keeping up with me and making my time here so much fun.

Last but not least, I thank my family for always believing in me and supporting me throughout my life.

DEDICATION

I dedicate this thesis to my parents, sister, and brother.

TABLE OF CONTENTS

LIST OF TABLES

LIST OF FIGURES

LIST OF ABBREVIATIONS

AC	alternating current
AFM	atomic force spectroscopy
ag	atto grams (10^{-18} g)
Al_2O_3	aluminium oxide
BPTI	basic pancreatic trypsin inhibitor
BSA	bovine serum albumin
CD	circular dichroism
cDNA	complementary DNA
ClyA	cytolysin A
DEPC	Diethylpyrocarbonate
dsDNA	double-stranded DNA
EDTA	ethylenediaminetetraacetic acid
fg	femto grams (10^{-15}g)
Fmoc	N-(9-fluorenyl)methoxycarbonyl
FRET	fluorescence resonance energy transfer
FuhA	ferric hydroxamate uptake component A
GdnHCl	guanidine hydrochloride
HEPES	4-(2-hydroxyethyl)piperazine-1-ethanesulfonic acid
HPr	histidine-containing phosphotransfer protein
MBP	maltose binding protein
mRNA	messenger RNA
MspA	*Mycobacterium smegmatis* porin A
NMR	nuclear magnetic resonance
nN	nano Newton
nS	nano Siemens
NTA	nitrilotriacetic acid
pA	pico ampere (10^{-12} A)
Pg	pico grams (10^{-12}g)
pM	pico molar (10^{-12} M)

RNase A	ribonuclease A
RT-PCR	reverse transcriptase-polymerase chain reaction
SiC	silicon carbide
SiN	silicon nitride
SiO_2	silicon dioxide
smFRET	single molecule fluorescence resonance energy transfer
SNP	single nucleotide polymorphism
SP1	stable protein 1
ssDNA	single-stranded DNA
TCEP	tris(2-carboxyethyl)phosphine
TEM	transmission electron microscope
TRIS	tris(hydroxymethyl)aminomethane

1.0 INTRODUCTION

Probing biomolecules and intermolecular interactions at single-molecule resolution plays a crucial role in understanding important biological processes that support the functioning of living cells. By studying biomolecules at single-molecule resolution it is possible to avoid averaging of ensembles (Cornish and Ha, 2007; Ritort, 2006; Selvin and Ha, 2008; Tinoco and Gonzalez, 2011). This, in turn, provides more specific data about the biomolecule being probed rather than an average of the total population. This is particularly valuable when studying molecular heterogeneity. For example, intrinsically disordered proteins may adopt multiple structural conformations and therefore it's extremely difficult or impossible to study conformational heterogeneity of these proteins with techniques such as circular dichroism (CD), X-Ray crystallography, and nuclear magnetic resonance (NMR) (Japrung *et al.*, 2013; Madampage *et al.*, 2012; Tavassoly and Lee, 2012). The level of sensitivity achieved by single-molecule techniques makes them particularly appealing. As a result, there has been a growing interdisciplinary effort in developing a low-cost, single-molecule technique with improved sensitivity and specificity. Over the past two decades several single-molecule techniques have been developed (Ritort, 2006; Selvin and Ha, 2008; Tinoco and Gonzalez, 2011). Until recently, most of the available single-molecule techniques, such as atomic force microscopy (AFM), single-molecule fluorescence resonance energy transfer (smFRET), and optical trapping, required substrate labelling and/or surface immobilization (see section 1.4 for more information on these techniques) (Ashkin, 2000; Binnig *et al.*, 1986; Cornish and Ha, 2007; Ha, 2001a; Selvin and Ha, 2008). With the emergence of the nanopore sensing technique, biomolecules can now be studied at the single-molecule level of sensitivity and at low-cost and label-free.

Nanopore sensing has recently emerged with the ultimate goal of sequencing the whole human genome for $1000 (Eisenstein, 2012; Kasianowicz *et al.*, 1996; Pennisi, 2012). While DNA sequencing continues to be one of the main driving forces of this technique, nanopore sensing has also been used for other single-molecule level applications such as studying protein folding, protein conformational heterogeneity, enzyme kinetics, intermolecular interactions, to name just a few (Baran *et al.*, 2010; Madampage *et al.*, 2010; Oukhaled *et al.*, 2007; Stefureac and Lee, 2008; Stefureac *et al.*, 2010a; Sutherland *et al.*, 2004; Zhao *et al.*, 2009a). However, until very recently most of the work was done on nucleic acids and peptides.

Therefore, the focus of this thesis will be on understanding nanopore sensing as applied to proteins. A series of proteins with different chemical and physical properties were studied to help understand what the limits of this technique are. In addition, the sensitivity of this technique was examined by studying isomers of peptides. Hence, the introduction will be mainly aimed towards the literature on the work done on peptides and proteins.

1.1 Nanopore detection as a single-molecule technique

The use of nanopore sensing as a single-molecule technique was first proposed in the mid-1990s (Kasianowicz *et al.*, 1996). Since then, nanopore sensing has been used to study a wide range of analytes at the single-molecule level. Nanopore sensing is achieved by monitoring ionic current changes as an analyte interacts with a nanometer-sized pore. The changes in current are characteristic of the molecule interacting with the pore. The concept of nanopore sensing is based on two earlier techniques: Coulter counting or resistive pulse sensing and single channel current recording (Bayley and Martin, 2000; Coulter, 1953; Graham, 2003; Hille, 2001; Neher and Sakmann, 1976; Wanunu, 2012).

1.1.1 A brief history: from Coulter counting to nanopore sensing

Prior to the mid-1950s, counting and sizing of blood cells was done manually. A highly skilled technician had to prepare stained microscope slides and then manually count and size the blood cells. This process was time consuming, had a very high error rate and had very little reproducibility (Coulter, 1953; Davis and Green, 1967; Graham, 2003; Hurley, 1970). To overcome some of these problems, in the mid-1950s, the Coulter counter was introduced as an apparatus for counting and sizing particles suspended in solution (Coulter, 1953). A typical Coulter counter consists of a pair of electrodes immersed in two chambers filled with electrolyte solution and connected through an orifice. The electrodes are used to drive an ionic current through the orifice. The ionic current is then measured as a function of time using an electrometer connected to the electrodes and a chart plotter (Bayley and Martin, 2000; Graham, 2003; Wanunu, 2012). A solution of the sample to be measured is added to one of the electrolyte filled chambers and caused to pass through the orifice and the presence of a particle such as a cell in the orifice, gives rise to a detectable change in the ionic current. These

changes in the ionic current are also known as resistive pulses. The frequency and magnitude of these pulses are related to the concentration of the sample and particle size, respectively (Mattern *et al.*, 1957). This became known as "Coulter Principle", named after its inventor, Wallace H. Coulter (Graham, 2003). The use of an orifice in the Coulter counter marked the first use of a pore as a sensor for detecting particles.

In 1970s, based on the Coulter Principle and the use of submicron-diameter pores, DeBlois and Bean developed a nanometer-particle analyzer that could detect nanometer analytes (DeBlois and Bean, 1970). They demonstrated that it was possible to detect and measure viruses (Henriquez *et al.*, 2004). The Coulter Principle played a crucial role in the development of the current nanopore sensing field. However, the current nanopore sensing field would not have thrived without the breakthroughs in ion-channel electrophysiology.

One of the most important innovations in electrophysiology was the discovery of the patch-clamp technique in 1976 (Neher and Sakmann, 1976). This technique gave electrophysiologists new prospects in ion-channel electrophysiology. The patch-clamp technique allowed high-resolution current recordings of single channels. In patch-clamp recording, a glass pipette filled with electrolyte solution forms a tight seal with the cell membrane and thus is able to isolate a single channel opening. An electrode immersed in the electrolyte solution and connected to an amplifier can then be used to record currents flowing through the channel (Hille, 2001; Molleman, 2003; Neher and Sakmann, 1976; Neher *et al.*, 1978; Penner, 1995). The ability to monitor single-channel current flow across a membrane together with the Coulter Principle led to the birth of the idea of using nanopores for sequencing DNA (Kasianowicz *et al.*, 1996).

In 1996, Deamer, Branton, and Kasianowicz demonstrated that by applying an electric field they could drive single-stranded DNA and RNA through a nanopore and detect their passage as a decrease in the ionic current flow (Kasianowicz *et al.*, 1996). Furthermore, they showed that the length of a polynucleotide could be determined by the amount of time the ionic current dropped. In addition, they suggested that this method could be used for sequencing DNA or RNA (Kasianowicz *et al.*, 1996).

Just last year in a conference in Florida, Oxford Nanopore Technologies (a commercial company) introduced a device smaller than the palm of the hand, which they claimed will decode a billion DNA bases in six hours (Eisenstein, 2012). However, to date the device is still not commercially available. While nanopore sensing started as a simple sensing tool, it has

been greatly refined to a general single-molecule technique that has been used to study a wide range of analytes and important biological processes at single-molecule resolution.

1.1.2 Principle of nanopore sensing

The principle behind nanopore sensing is simple: a voltage bias, V, is applied via two Ag/AgCl electrodes across a membrane separating two chambers filled with electrolyte solution (typically 0.1 to 1.0 M KCl or NaCl buffer) and then monitoring the ionic current flow through the nanopore embedded in the membrane using the patch-clamp technique (Figure 1.1) (Kasianowicz *et al.*, 1996; Ma and Cockroft, 2010). Under constant applied voltage, if there is no pore embedded in the membrane there will be no current flow between the two chambers (Figure 1.1a). In the presence of an open pore, there will be a steady flow of ionic current (Figure 1.1b). When a molecule is added to the electrolyte solution it interacts with the pore and reduces the ionic current relative to the open pore current as a result of partially blocking the flow of ions (Figure 1.1c). The magnitude (I) and duration (T) of the current block are characteristic of the molecule being analyzed. For example, a large molecule passing through the pore will cause a larger current block than a smaller molecule. Therefore, in theory (technology permitting) nanopore sensing can be used to distinguish differences between two molecules that differ in cross section by the size of an ion (i.e a few angstroms) (Wanunu, 2012).

Each interaction of the molecule with the pore is known as an event. The events can be of three general types: bumping, translocation, and intercalation (Figure 1.2) (Meng *et al.*, 2010). A bumping event will arise when a molecule bumps into the pore and will cause a small current blockade. In the case when a molecule goes through the pore, it is known as a translocation event and will result in greater reduction of the ionic current. The third type of event, intercalation, occurs when a molecule goes into the pore but diffuses away and does not translocate (Meng *et al.*, 2010).

Therefore, using the ratio of events produced together with their durations and blockade amplitudes as well as their frequencies, a molecule-specific profile can be constructed. The ability to do this makes nanopore sensing a very powerful single-molecule technique.

1.1.3 Types of pores

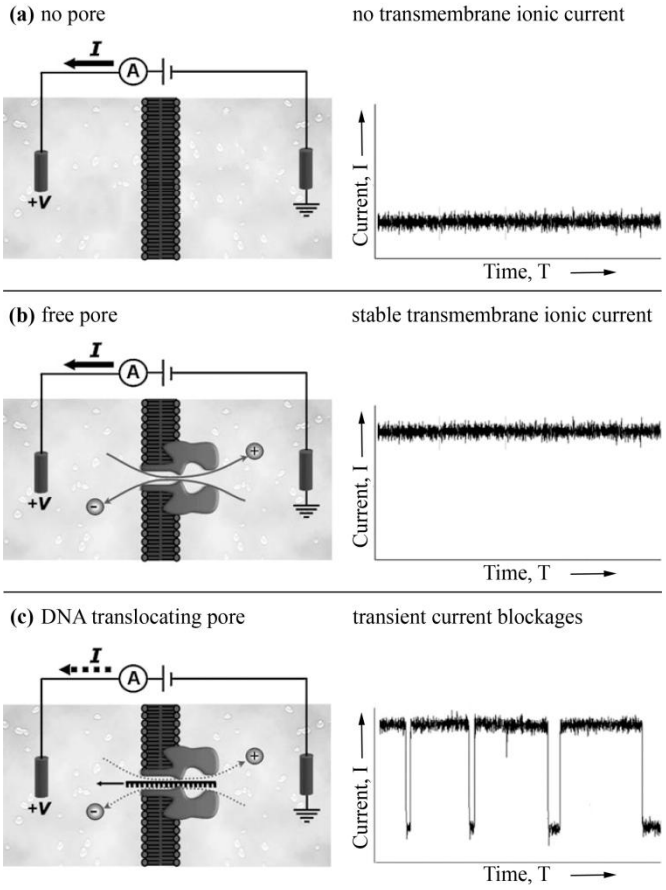

Figure 1.1. Schematic representation of the nanopore sensing principle. (a) An applied voltage (V) across a lipid bilayer will result in no ionic current (I) flow in the absence of a pore. (b) In the presence of a pore (eg. α-hemolysin) there will be an ionic current flow through the pore separating the two chambers. (c) If a molecule (eg. DNA) is added to one of the chambers it will interact with the pore (eg. translocate through the pore) and reduce the ionic current flow relative to the open pore current as a result of partially blocking the flow of ions. The magnitude (I) and duration (T) of the current block are characteristic of the molecule being analyzed. A large molecule passing through the pore will cause a larger current block than a smaller molecule. (Reprinted with permission from Ma and Cockroft, 2010. Copyright 2010 Wiley-VCH Verlag GmbH & Co. KGaA)

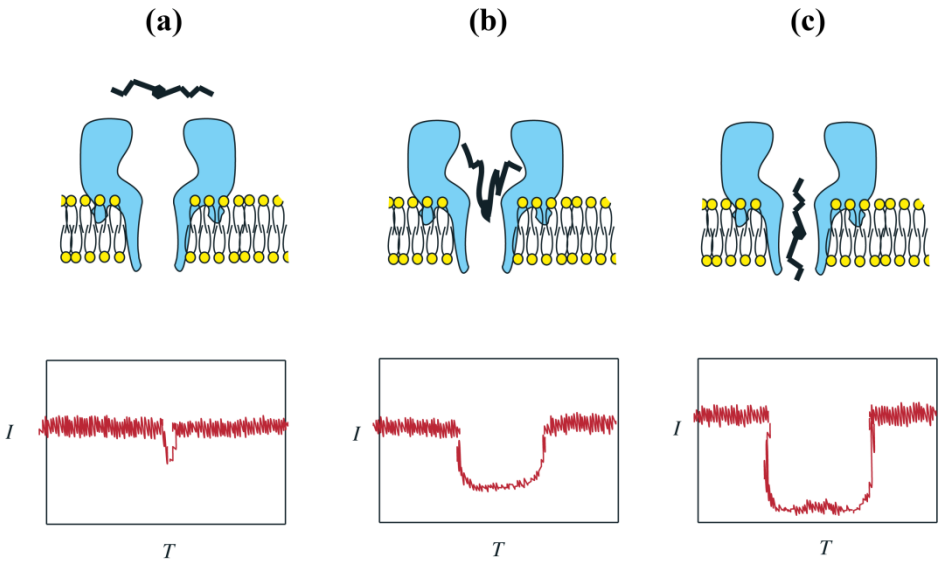

Figure 1.2. Schematic representation of the type of interactions/events between a molecule and the α-hemolysin pore. There are three general types of events observed: (a) bumping, (b) intercalation, and (c) translocation. A bumping event will arise when a molecule bumps into the pore and will cause a small current blockade. A translocation event will arise when a molecule goes through the pore. An intercalation event occurs when a molecule goes into the pore but diffuses away and does not translocate. The upper panel shows the interaction between a molecule and the pore while the bottom panel shows the corresponding event profiles where I is the current and T is the time. (Reprinted with permission from Meng *et al*, 2010. Copyright 2010 European Peptide Society and John Wiley & Sons, Ltd).

One of the main challenges of nanopore sensing is finding a suitable nanopore. Depending on the study, a pore that can withstand a range of experimental conditions and can remain stable for a long period of time is really desired. Currently there are two main sources of nanopores: biological pores (typically extracted from bacteria) and solid state-pores (typically fabricated from silicon material) (Bahrami *et al.*, 2012; Ma and Cockroft, 2010; Majd *et al.*, 2010; Miles *et al.*, 2013). Since the first nanopore sensing experiment in 1996, there have been numerous studies done with a variety of both solid-state pores and biological pores.

1.1.3.1 Biological Pores

In the cell, biological pores are responsible for controlling the flow of water, ions, and substrates (Majd *et al.*, 2010). This, in turn, maintains cell homeostasis or can lead to cell death. Biological pores can be simple short peptides (eg. gramicidin A) that self-assemble to form channels or can be large transmembrane proteins (eg. α-hemolysin) (Majd *et al.*, 2010). Their nanoscale dimensions and the ability to genetically engineer them make them particularly attractive for a range of applications. In 1996, Kasianowicz *et al*. demonstrated that the biological pore α-hemolysin can be used for single-molecule level studies (Kasianowicz *et al.*, 1996). Since then, other biological pores have been used, but α-hemolysin remains the most widely used (Butler *et al.*, 2008; Haque *et al.*, 2013b; Mohammad *et al.*, 2011; Soskine *et al.*, 2012; Stefureac *et al.*, 2006; Wang *et al.*, 2013; Wendell *et al.*, 2009).

α-Hemolysin is a toxin secreted by *Staphylococcus aureus* as monomer of 33.2 kDa which oligomerizes upon binding to a lipid bilayer to form a mushroom-shaped heptameric transmembrane pore (Song *et al.*, 1996). Its crystal structure was solved in 1996 and measures 100 Å in height and about 100 Å in diameter. The heptameric pore is solvent-filled with hydrophilic interior and hydrophobic exterior. It consists of a vestibule (i.e the cap and the rim domain) with an interior diameter of 36 Å which leads to the stem with a 14 Å constriction between the vestibule and the stem (Figure 1.3) (Song *et al.*, 1996). The stem domain makes up the transmembrane channel and is comprised of 14 antiparallel β-strands. Its robust structure makes it remarkably stable under a range of experimental conditions and can remain open for extended periods. For example, it remains functional up to 95 °C and can withstand concentrations of up to 2.0 M guanidine hydrochloride (GdnHCl) (Braha *et al.*, 1997; Oukhaled *et al.*, 2007). In 1 M KCl buffer, at room temperature, and under an applied voltage of 100 mV, the

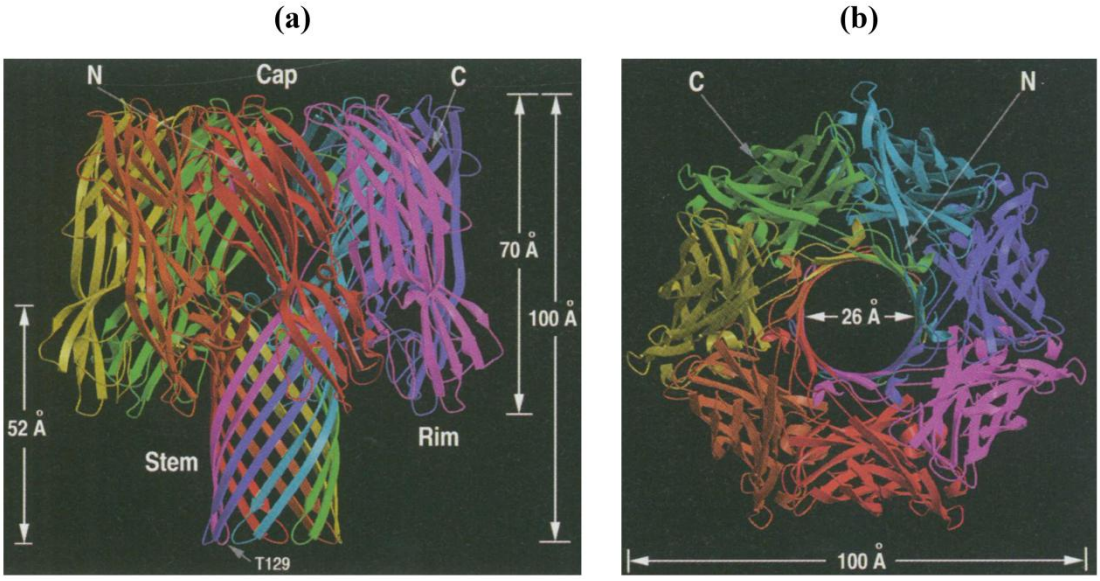

Figure 1.3. Ribbon representation of the α-hemolysin heptomeric structure (PDB ID: 7AHL). Part (a) shows the structure from a side view while part (b) show the structures from the top view of the structure. The monomers are presented in different colors. Each component of the pore and the respective dimension is marked. (Reprinted with permission from Song *et al*., 1996. Copyright 1996 American Association for the Advancement of Science)

open pore allows the flow of 100 pA ionic current, corresponding to a conductance of 1 nS (Akeson *et al.*, 1999; Bayley and Cremer, 2001; Menestrina, 1986). The conductance of the pore changes linearly with the conductivity of the solution (Menestrina, 1986). The α-hemolysin pore is slightly anion selective because of the charged residues found at the constriction between the vestibule and the stem, and this can be observed by simply reversing the potential (Aksimentiev and Schulten, 2005; Cozmuta *et al.*, 2005; Luo *et al.*, 2009; Menestrina, 1986). The ion selectivity of the pore is greater at lower pHs (Cozmuta *et al.*, 2005; Menestrina, 1986). While this is one of the most used biological pores for single-molecule studies, this hasn't stopped researchers from looking into alternatives. Figure 1.4 lists some of the other biological pores used so far in nanopore sensing.

The *Mycobacterium smegmatis* porin A (MspA) is another pore that has been gaining attention among researchers, especially those involved in DNA sequencing with nanopores (Figure 1.4a) (Bhattacharya *et al.*, 2012; Butler *et al.*, 2008; Faller *et al.*, 2004; Haque *et al.*, 2013b; Manrao *et al.*, 2012). For example, with the wild-type α-hemolysin pore it is not possible to distinguish between signals produced by each base because the pore's stem is too long to record the current of a single base (Manrao *et al.*, 2012; Pennisi, 2012; Schneider and Dekker, 2012; Wanunu, 2012). On the other hand, MspA is favoured because its smallest constriction is long enough to accommodate just four bases (Bhattacharya *et al.*, 2012; Butler *et al.*, 2008; Faller *et al.*, 2004; Haque *et al.*, 2013a; Manrao *et al.*, 2012; Schneider and Dekker, 2012).

Researchers involved in nanopore analysis of peptides and proteins have shown interest towards the aerolysin pore (Figure 1.4e) (Merstorf *et al.*, 2012; Pastoriza-Gallego *et al.*, 2011; Stefureac *et al.*, 2006; Tsitrin *et al.*, 2002). This pore has been shown to be more resistant to urea denaturation than α-hemolysin (Lesieur *et al.*, 1999; Pastoriza-Gallego *et al.*, 2011). This can be particularly attractive when studying the denaturation of proteins with urea (Pastoriza-Gallego *et al.*, 2009).

Just recently, three new biological pores have been introduced in nanopore sensing field. They are: cytolysin A (ClyA), stable protein 1 (SP1), and a mutated version of the monomeric ferric hydroxamate uptake component A (FuhA ΔC/Δ4L) (Mohammad *et al.*, 2011; Soskine *et al.*, 2012; Wang *et al.*, 2013). All three pores have larger dimensions than α-hemolysin, which makes them suitable for studying proteins. For example, it was shown that the lumen of ClyA

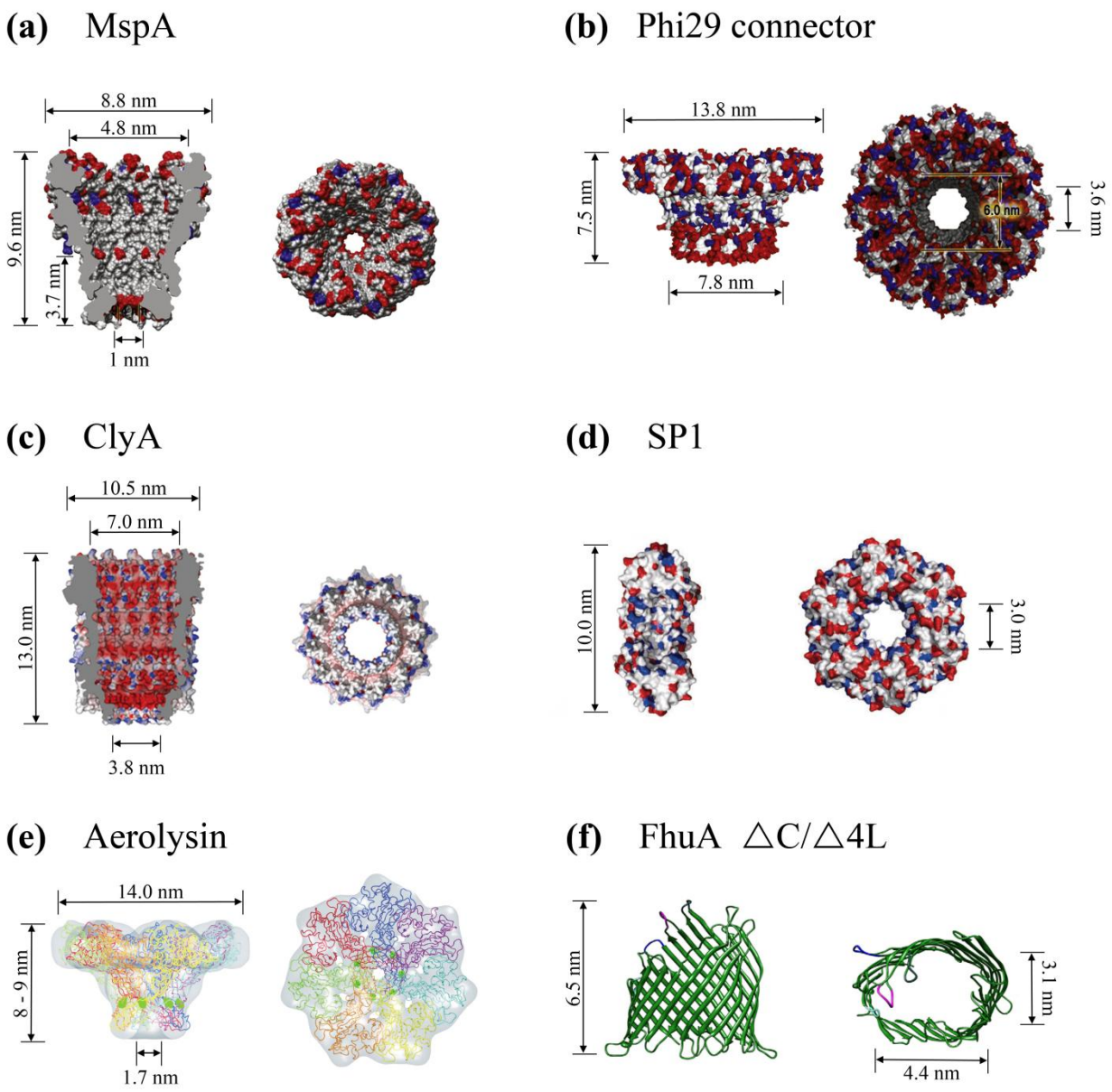

Figure 1.4. Structures of biological pores used in nanopore sensing. The side (left) and top (right) views of each pore are shown and the dimensions are marked. The pores shown are: (a) octomeric MspA (PDB ID: 1UUN), (b) dodecameric phi29 connector from the bacteriophae phi 29 DNA packing motor (PDB ID: 1FOU), (c) dodecameric ClyA (PDB ID: 2WCD), (d) dodecameric SP1 (PDB ID: 1TRO), (e) heptameric aerolysin, and (f) a mutated version of the FuhA (PDB ID of wild-type FuhA: 1BY3). (Reprinted with permission from: (a) and (b) Haque *et al*., 2013b. Copyright 2013 Elsevier Ltd, (c) Mueller *et al*., 2009. Copyright 2009 Macmillan Publishers Limited, (d) Wang *et al*., 2013. Copyright 2013 The Royal Society of Chemistry, (e) Tsitrin *et al*., 2002. Copyright 2002 Nature Publishing Group, and (f) Tomita *et al*., 2013. Copyright 2013 Elsevier B.V.)

could accommodate folded proteins of at least 40 kDa (Soskine *et al.*, 2012). Furthermore, these pores have other appealing features, such as protease resistance (eg. SP1) and great stability at low ionic concentration and low pHs (eg. FuhA ΔC/Δ4L) (Mohammad *et al.*, 2011; Wang *et al.*, 2013). The structures of these pores are shown in Figure 1.4.

Despite the usefulness and popularity of biological pores, there are limitations which prevent a single biological pore being used for studying a broad range of molecules. While one biological pore might be very suitable for studying one set of molecules, it may not be for another set of molecules. However, one of the main advantages of using biological pores for single-molecule level analysis is their ability to be genetically engineered (Miles *et al.*, 2013; Wanunu, 2012). Depending on the molecule being analyzed, biological pores can be engineered to interact with a specific molecule (Bayley and Cremer, 2001). The ability to modify biological pores enhances the potential of nanopore sensing with biological pores.

1.1.3.2 Engineered biological pores

To date there have been many studies performed at the single-molecule level with modified biological pores (Braha *et al.*, 2000; Braha *et al.*, 1997; Butler *et al.*, 2008; Gu *et al.*, 1999; Mohammad *et al.*, 2008; Mohammad *et al.*, 2011; Soskine *et al.*, 2012; Wolfe *et al.*, 2007; Zhao *et al.*, 2009b; Zhao *et al.*, 2008b). One of the most frequently modified biological pores is α-hemolysin. Hence, the focus of this section will be on the modified α-hemolysin pore. The knowledge of its three-dimensional structure at very high resolution has led to successful modifications of the pore by different approaches.

One such approach is mutations of amino acids within the β-barrel. In 1997, Bahra *et al*. introduced four histidine residues into the lumen of α-hemolysin by mutagenesis (Braha *et al.*, 1997). The resulting pore contained a divalent metal binding site. This turned the biological pore into a very sensitive and selective sensor for divalent metal ions (Braha *et al.*, 1997). It was shown that nanomolar concentrations of divalent metal ions could be detected and they could differentiate between different divalent metal ions. A decade later, Wolfe *et al*. designed three mutants of α-hemolysin by mutating a lysine residue to an aspartic acid at a specific site within the β-barrel domain (Wolfe *et al.*, 2007). This mutation near the constriction region of the pore caused the pore to become cation-selective. Furthermore, the replacement of positively-charged amino acids with negatively-charged amino acids enhanced the translocation

of cationic peptides. This allowed the authors to conclude that an electrostatic interaction between the peptide going through the pore and the pore lumen are an important factor in peptide translocation. Later in 2009, Zhao *et al*. examined the translocation of peptides containing mainly aromatic amino acids through mutants of α-hemolysin containing different number of aromatic residues (Zhao *et al.*, 2009b). By increasing the number of aromatic residues within the lumen of the pore they were essentially introducing more aromatic binding sides within the pore which, in turn, resulted in stronger binding affinities between the pore and the aromatic peptides. The stronger binding affinity resulted in enhanced resolution (i.e increased translocation times). With improved resolution they were able to quantify and differentiate between peptides differing by a single amino acid (Zhao *et al.*, 2009b). The authors suggest that with proper engineering of the biological pore it may be possible to sequence peptides and proteins (Zhao *et al.*, 2009b). Among other studies, designed biological pores have also been used for detection and characterization of single DNA molecules (Howorka *et al.*, 2001a).

Another common approach of biological pore modification is placement of a ring-shaped molecular adaptor, such as β-cyclodextrin, inside the lumen of the α-hemolysin pore (Gu *et al.*, 1999; Gu *et al.*, 2001; Kang *et al.*, 2006; Kang *et al.*, 2005). The adapter is lodged into the lumen of the pore either covalently or non-covalently (Wu *et al.*, 2007). By using a mutant $(M113F/K147N)_7$ pore with β-cylodextrin, a chiral molecule, lodged within the pore, Kang *et al*. showed that it was possible to discriminate between chiral drug molecules (Kang *et al.*, 2006). In the same study they were able to demonstrate that with this designed pore it was possible to study the kinetics of racemisation (i.e the conversion of (S)-thalidomide into (R)-thalidomide or vice versa in the presence and absence of human serum albumin). This approach could also be used to detect organic analytes, which bind within the hydrophobic interiors of cyclodextrins (Gu *et al.*, 1999). In 2009, Bayley and coworkers showed that, by using a mutant $(M113R)_7$ pore with covalently attached β-cyclodextrin, they were able to distinguish between all four nucleoside 5`-monophosphate molecules with an average accuracy of 99.8% (Clarke *et al.*, 2009). In addition, the modified pore was capable of distinguishing between normal cytosines and methylated cytosines. The β-cyclodextrin used here contained the primary amino groups required for base detection and a reactive linker enabling covalent attachment to a cytosine residue within the pore. The authors of this study proposed that this

approach in combination with an exonuclease can be developed as a method for DNA sequencing. In this proposed DNA sequencing method, an exonuclease covalently attached to the same mutant pore fitted with β-cyclodextrin would be used to degrade the strand one base at a time, while each base is fed into the pore where the residual ion current is measured and used to identify the base (more on this in section 1.2.1).

The third most common approach of biological pore modification has been covalent attachment of peptide, oligonucleotide, or a polymer group (eg. polyethylene glycol molecules) to a residue near the entrance of the pore (stem or vestibule side) or within the lumen of the pore through a disulfide bond (Howorka *et al.*, 2001a; Howorka *et al.*, 2001b; Movileanu *et al.*, 2000; Rotem *et al.*, 2012; Xie *et al.*, 2005). This approach enhances the sensitivity and selectivity of the pore. For instance, attachment of polymer group containing a biotinyl group at the untethered end to the lumen of the pore enabled Movileanu *et al*. to quantify and identify streptavidin mutants with different binding affinities for the biotin group (Movileanu *et al.*, 2000). In a separate study, Xie *et al*. constructed an α-hemolysin pore with covalently attached protein kinase inhibitor peptide which was linked though a linker to a cystine residue at the *trans* mouth of the pore (Xie *et al.*, 2005). The protein kinase inhibitor peptide has strong binding affinity for the C subunit of protein kinase A. In the presence of MgATP its affinity is further stimulated. Using nanopore sensing with the modified α-hemolysin pore, it was possible to measure the binding kinetics between the C subunit and the protein kinase inhibitor peptide at the single-molecule level. The results obtained were comparable to those done in bulk solution. These results indicate that the nanopore sensing technique equipped with a modified biological pore by this approach could essentially be developed into a method for screening kinase inhibitors (Xie *et al.*, 2005).

Recently, modified α-hemolysin pores with aptamers have been presented (Rotem *et al.*, 2012; Soskine *et al.*, 2012; Ying *et al.*, 2011). In this type of modification, an oligonucleotide is covalently attached to a cysteine residue near the mouth of the pore. This is followed by addition of an aptamer to the solution and subsequent hybridization to the oligonucleotide. This particular approach is very attractive because aptamers can adopt different three-dimensional structures allowing them to bind various analytes. Nanopore sensing equipped with aptamer-based biological pores can then be used to detect different analytes and study intermolecular interactions between two different molecules (eg. a molecule binding to an aptamer can also

bind to a different molecule through a different binding domain) (Rotem *et al.*, 2012).

Taken together, the above mentioned approaches show that by modifying biological pores, the sensitivity and selectivity of nanopore sensing at single-molecule level can be greatly improved. Furthermore, these modifications increase the diversity of nanopore sensing applications. Much of the growth in the nanopore sensing field can be attributed to the work done with biological pores. Biological pores have proven to be extremely reliable and have shown great promise. However, there are certain drawbacks in nanopore sensing with biological pores. One such drawback is the fixed diameter of the pores. In addition, as it will be shown later in the results section of this thesis, these pores are embedded in fragile lipid bilayers and their fragility limits the lifespan of an experiment and the conditions under which an experiment can be performed. To overcome these shortcomings, synthetic pores with various diameters have been successfully fabricated in solid-state materials.

1.1.3.3 Solid-state pores

The first successful fabrication of a solid-state pore was reported over a decade ago by Li *et al*. using a technique known as ion beam sculpting (Li *et al.*, 2001). With this technique they demonstrated that synthetic pores can be fabricated in solid-state membranes with diameters as small as 1.8 nm (i.e comparable to biological pores). Furthermore, it was shown that translocation of a 500 bp double-stranded DNA (dsDNA) through a 5 nm pore could be detected (Li *et al.*, 2001). Since then solid-state pores have gradually become popular due to the benefits they offer over biological pores.

The fabrication of synthetic or solid-state pores starts with the production of the membranes followed by drilling of the pores into the membranes. The solid-state membranes are produced from material such as silicon nitride (SiN), silicon dioxide (SiO_2), silicon carbide (SiC), aluminium oxide (Al_2O_3), and, recently, graphene (Garaj *et al.*, 2010; Li *et al.*, 2001; Merchant *et al.*, 2010; Schneider *et al.*, 2010; Storm *et al.*, 2003, 2005; Sugita *et al.*, 2013; Venkatesan *et al.*, 2009; Wu *et al.*, 2005). One of the most common types of material used for solid-state membrane fabrication is silicon nitride. This is because SiN is a good insulator, mechanically robust, and chemically stable over a wide range of conditions such as salt concentration, pH, and temperature (Dekker, 2007; Miles *et al.*, 2013). In addition, the material can be easily modified to incorporate the pores. Depending on the material used, the fabrication process of

membranes is a several step process. The fabrication of silicon nitride membranes can be described as a four-step process and the process flow for the fabrication of silicon nitride nanopores is outlined in Figure 1.5 (Miles *et al.*, 2013). First, a thin layer of silicon nitride is deposited on both sides of a silicon wafer using low-pressure chemical vapour deposition. The second step involves designating where the pore will go by using photolithographic techniques (eg. photoresist coating on the membrane). The third step is the removal of the earlier deposited SiN within the designated area using reactive ion etching. Finally, the silicon is removed as well within the designated area by anisotropic wet etching using potassium hydroxide aqueous solution. At the end of the fourth step there will be an etched well with an exposed free-standing SiN membrane. The freestanding membrane together with the support structure makes up a chip. The thickness of the membrane is generally between 10-40 nm (Miles *et al.*, 2013). Thinner membranes are preferred especially for DNA sequencing because the pore will be occupied by fewer DNA bases at the same time. A 10 nm thick membrane will make it impossible to obtain a signal at single base resolution. To overcome this challenge graphene, a single layer of carbon sheet, has recently been used as membrane material for fabrication of solid-state pores (Garaj *et al.*, 2010; Merchant and Drndic, 2012; Schneider *et al.*, 2010). This has generated excitement among the research groups in solid-state pore fabrication and DNA sequencing, because graphene is atomically thin. Single-layer graphene is 0.34 nm thick, which is smaller than the distance between DNA nucleotide bases (~0.3 nm) (Wells *et al.*, 2012). Therefore, nanopores made of a single layer of graphene will only have one base of DNA inside the pore at any time.

The production of solid-state pores continues with the drilling of pores into the solid-state membranes. The three most common techniques used for preparing synthetic pores are: ion-beam sculpting, electron-beam drilling, and ion track-etching (Figure 1.6) (Li *et al.*, 2001; Siwy *et al.*, 2002; Storm *et al.*, 2003). Ion-beam sculpting was the first technique to successfully fabricate nanometer solid-state pores for nanopore sensing. The technique has been successful in drilling pores as small as 1.8 nm. In this technique, after creating a large bowl-shaped cavity in a free-standing Si_3N_4 membrane as described in above paragraphs and Figure 1.5, a focused ion beam is then used to gradually break through the membrane and connect with the bowl-shaped cavity on the other side (Li *et al.*, 2001). The ion beam uses energies of several thousand electron volts (KeV) to remove layers of the silicon nitride membrane via sputtering

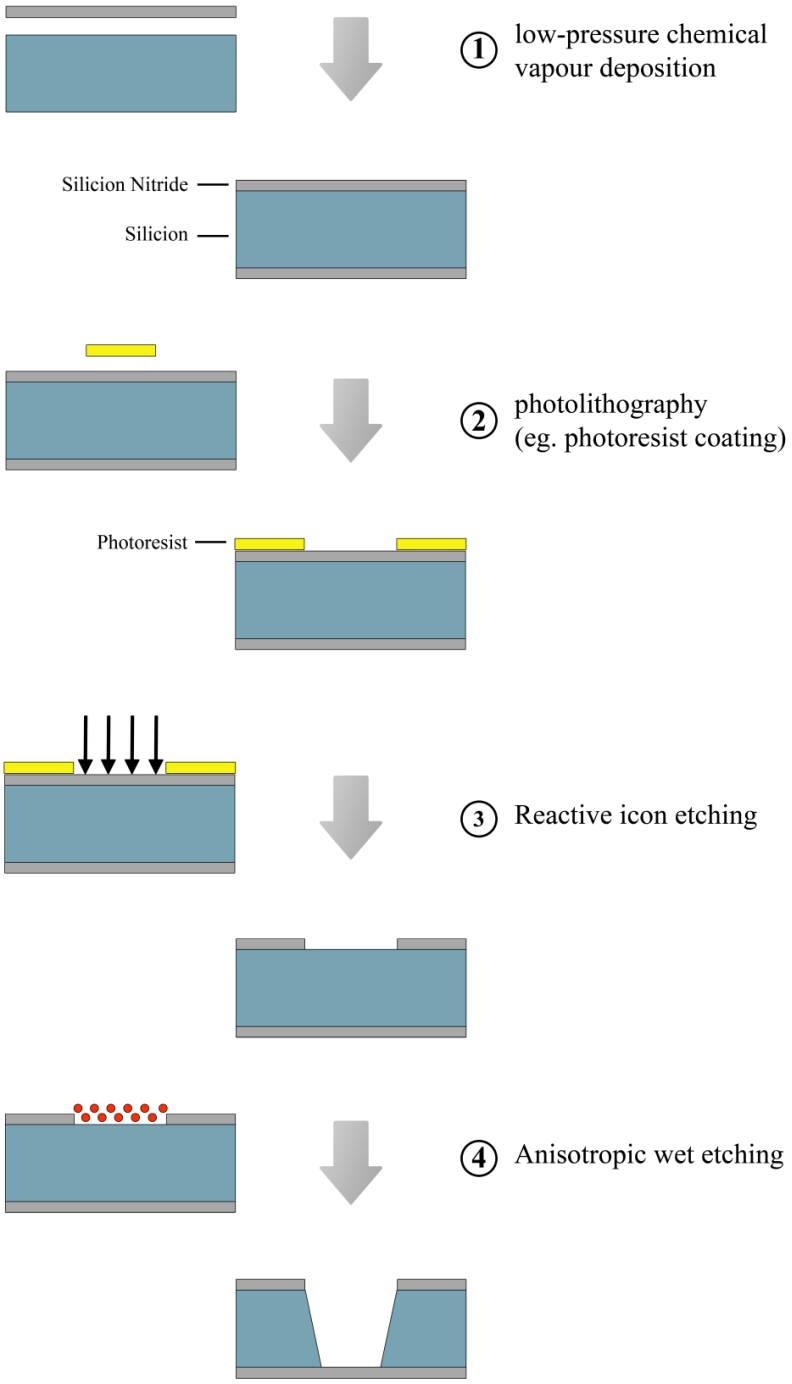

Figure 1.5. Workflow in the fabrication of silicon nitride membranes. First, a thin layer of silicon nitride is deposited on both sides of a silicon wafer using low-pressure chemical vapour deposition. Second, photolithographic techniques (eg. photoresist coating on the membrane) are used to designate where the pore will go. The third step is the removal of the earlier deposited silicon nitride within the designated area using reactive ion etching. Finally, in the fourth step the silicon is removed within the designated area by anisotropic wet etching using alkaline aqueous solution.

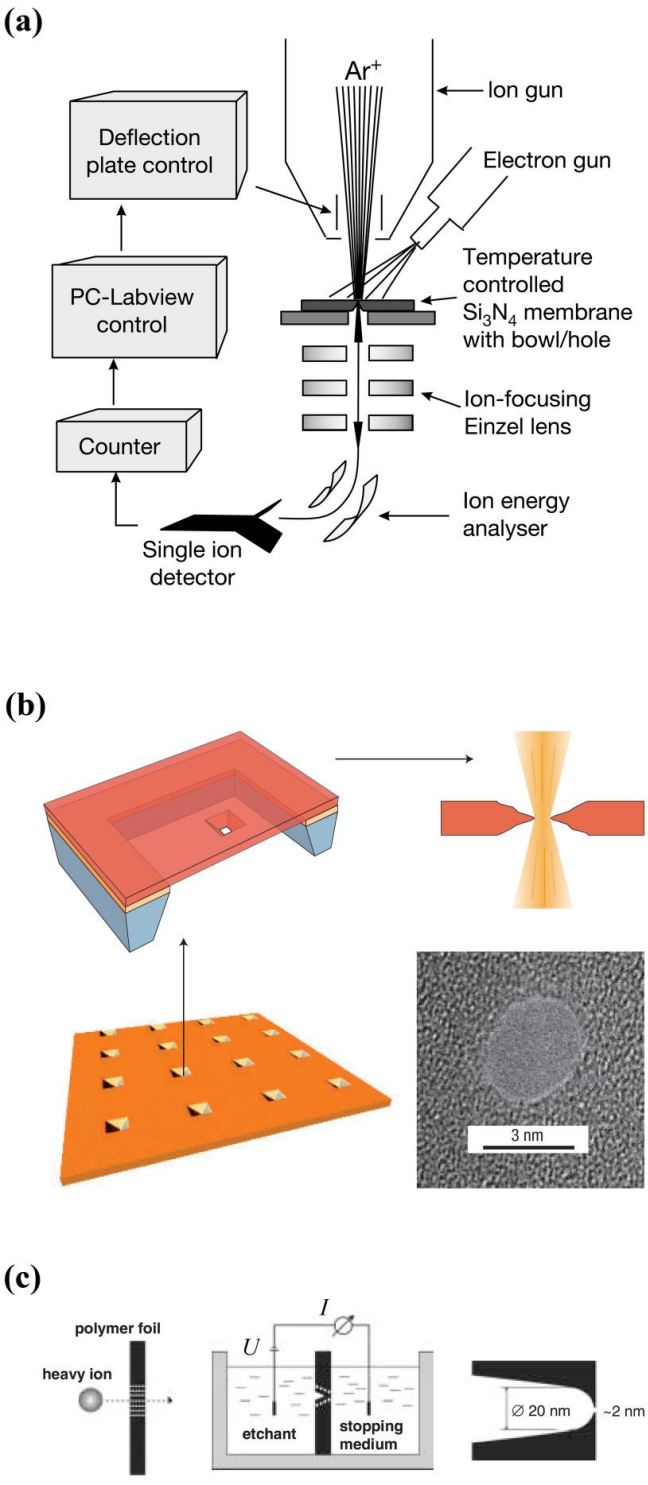

Figure 1.6. Solid-state nanopore drilling techniques. The three most common techniques used for drilling pores into solid state membranes are: (a) ion-beam sculpting, (b) electron-beam drilling, and (c) ion track-etching. (Reprinted with permission from Li *et al.*, 2011. Copyright 2001 Macmillan Magazines Ltd; Storm *et al.*, 2003. Copyright 2003 Nature Publishing Group; Siwy *et al.*, 2002. Copyright 2002 IOP Publishing)

erosion. The apparatus used in this technique (shown in Figure 1.6a) employs a feedback-control mechanism that counts the ions transmitted through the opening of the pore and stops the erosion process at the right time (Li *et al.*, 2001). In addition, the apparatus is responsible for controlling the sample temperature, the ion beam duty cycle, and the ion beam flux (in ions nm^{-2} s^{-1}). Depending on the ion rate and temperature, the pores can be opened or closed (Dekker, 2007). The sputter-erosion process is done at temperatures below 5 °C, whereas the closing is done at room temperature. Therefore, the opening of pores by this technique can be achieved by first opening larger pores and then with sufficient ion exposure at room temperature, the pore can be closed down to the desired diameter. While Ar^+ was used as a source of ions for the fabrication of the first pore, other ion sources such as He^+, Ne^+, Xe^+, Ga^+, and Kr^+ have also been employed (Cai *et al.*, 2006). In addition to the silicon nitride membranes, this technique has also been used to incorporate pores in SiO_2, Al, Cr, poly(methyl methacryate), and polyimide material. While ion beam sculpting continues to be popular among many researchers for solid-state pore fabrication, another technique termed electron beam drilling has become just as popular.

In 2003, Storm *et al*. reported successful fabrication of a pore at single nanometer precision in SiO_2 membranes using a transmission electron microscope (TEM) (Storm *et al.*, 2003). The procedure (as illustrated in Figure 1.6b) involved the use of electron-beam lithography and subsequent anisotropic potassium hydroxide wet etching to open pores of 20 nm diameter (Storm *et al.*, 2003). This was followed by thermal oxidation (i.e formation of a SiO_2 layer over silicon) by high-energy electron beam to reduce the pore diameter to a single nanometer. Depending on the initial diameter, the electron beam can have a different effect. For pores with initial diameter of 50 nm or lower, the electron beam will have a shrinking effect, but for those pores with diameters of 80 nm or higher the electron beam will produce an expansion effect. Simply controlling the beam intensity will control the shrinking process (Storm *et al.*, 2003). To date, electron beam drilling has been successfully employed to directly drill pores in membrane martial such as metal oxides, SiN, and graphene (Garaj *et al.*, 2010; Merchant *et al.*, 2010; Schneider *et al.*, 2010; Storm *et al.*, 2003; Venkatesan *et al.*, 2009). This technique has become quickly popular because of the availability of TEMs. In addition, this technique offers the advantage of monitoring the pore diameter in real-time using TEM.

The third technique used for fabricating nanopores is ion track-etching (Siwy *et al.*, 2002).

This method is based on blasting the membrane (eg. polycarbonate, polyethylene terephthalate, and polyimide material) with heavy ions (eg. Xe, Au) at high kinetic energies. Each ion will create a single track. The tracks are then chemically etched (Figure 1.6c). The number of pores produced is dependent on the number of ions that went through the sample (Siwy *et al.*, 2002). In 2002, Siwy *et al*. manufactured conical pores down to 2 nm diameter in polyethylene terephthalate material using this method. The conical shaped pores were generated by applying alkaline solution to only one of the sides of the blasted membrane while applying a neutralizing solution to the other side of the membrane. The etching process was done in a conductivity cell and controlled by monitoring the electric current through the pore. Once the current starts going through the membrane, the etching is stopped by simply flushing out the solution used as etchant. The size and shape of pores produced by this method can be controlled by controlling the type of etchant, temperature, and duration of etching (Cao and Wang, 2009; Siwy *et al.*, 2002).

As summarized above, reliable solid-state pores have been produced by all three drilling techniques. However, all solid-state pores produced to date exhibit noise levels larger than their biological counterpart (more on this issue in section 1.1.3.4) (Tabard-Cossa *et al.*, 2007). Furthermore, the selectivity of typical solid-state pores is not comparable to that of biological pores. To overcome some of these limitations, many research groups are working on different approaches of modifying the surface of these solid-state pores.

1.1.3.4 Surface modification of solid-state pores

Surface modification of solid-state pores has been explored by many research groups to compensate for deficiencies of the fabrication techniques. Furthermore, surface modification is performed to produce pores with desired chemical, physical, and even biochemical properties (Iqbal *et al.*, 2007; Mussi *et al.*, 2010a; Mussi *et al.*, 2010b; Mussi *et al.*, 2011; Venkatesan *et al.*, 2010; Wei *et al.*, 2012; Yusko *et al.*, 2011; Yusko *et al.*, 2012). Examples include controlling the surface charge, reducing the pore size, and attaching functional groups to make the pores more selective. One of the most common approaches of reducing the size of solid-state pores (excluding the direct fabrication techniques) is atomic layer deposition. Atomic layer deposition can be used to deposit layers of aluminium oxide with 0.1 nm precision (Venkatesan *et al.*, 2010). By using atomic layer deposition one can control the size of the pore

to sub-nanometer dimensions. Furthermore, depending on the material deposited the properties of the pore can also be controlled. For example, it's been shown that by depositing aluminium oxide layers, the pores show better signal-to-noise levels and no surface charge at near neutral pH values (Venkatesan *et al.*, 2010). Recently, Wei *et al*. used vapour deposition to coat the interior of the pores with layers of gold and titanium resulting in pore diameter reduction (Wei *et al.*, 2012).

Several studies have shown that surface modification of solid-state pores can be used to improve the sensitivity and selectivity of the pores. In this type of modification, functional groups are attached to the pore that can be used to interact and detect target molecules (Iqbal *et al.*, 2007; Mussi *et al.*, 2010a; Mussi *et al.*, 2010b; Mussi *et al.*, 2011; Siwy *et al.*, 2005; Wei *et al.*, 2012). The current block resulting from the interaction of the attached molecule with the target molecule can be detected and distinguished from that produced by molecules that do not bind to the functional group. This allows for very specific sensing and can be used to study the interaction of any two molecules. While the process of attaching a molecule to the pore varies from study to study, the principle remains the same. In 2005, Siwy *et al*. demonstrated that target proteins could be detected with extreme specificity (Siwy *et al.*, 2005). First, conically shaped nanopores were track-etched in poly(ethylene terephthalate) membrane. Then gold plating was used to deposit a conically shaped gold nanotube inside the pore. This was then followed by attachment of biotin, protein-G or an antibody specific for ricin to target and detect streptavidin, IgG, and ricin, respectively (Siwy *et al.*, 2005). The target analyte binding was detected as a permanent block. They could essentially detect two sets of target molecules. For example, the binding of streptavidin to biotin followed by subsequent binding of biotinyalated protein G to streptavidin already bound to biotin could also be detected.

In another interesting study, solid-state nanopores were designed to be selective towards a specific sequence of single-stranded DNA. This was accomplished by attachment of hairpin loop DNA to the surface of the pores with sequence complementary to the target DNA (Figure 1.7a) (Iqbal *et al.*, 2007). The hairpin loop DNA acted as a probe. By measuring the event duration, amplitude, and frequency, it was demonstrated that even a single base mismatch could be detected. Similar studies have been performed by Mussi *et al*. in 2010 and 2011 where DNA molecules have been attached to the pore and then used to selectively detect complementary target sequences (Mussi *et al.*, 2010a; Mussi *et al.*, 2010b; Mussi *et al.*, 2011).

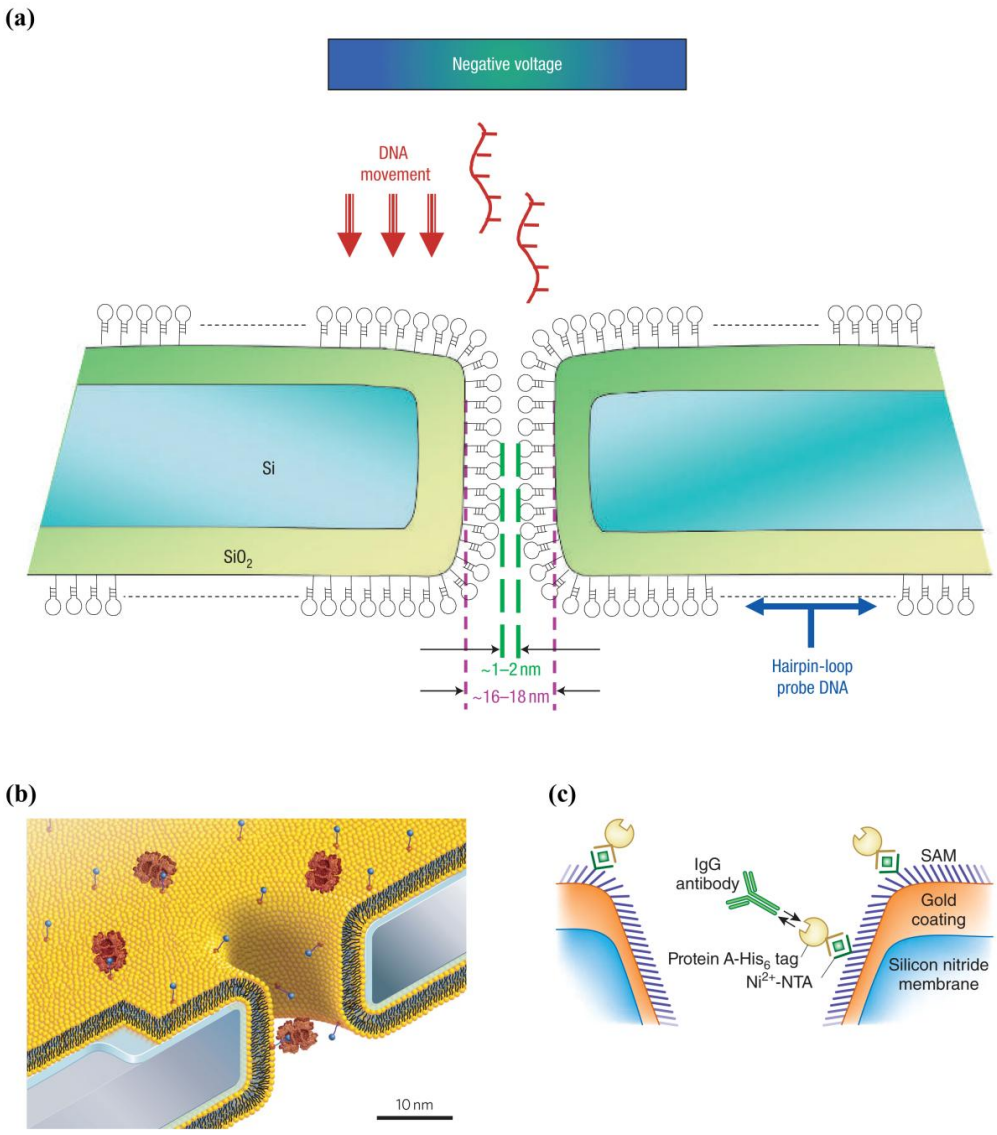

Figure 1.7. Examples of surface modifications of solid-state pores. (a) Schematic of hairpin loop DNA molecules attached to the surface of the pore with sequences complementary to the target DNA. The pores are designed to be selective towards target DNA of known sequence. (b) Schematic of nanopores coated with a lipid bilayers. By controlling the lipid bilayer composition it is possible to control the pore diameter, surface chemistry, and the selectivity of the pore. The selectivity is achieved by using ligand anchored lipids (eg. biotinylated lipids, blue circles). The target molecule (eg. streptavidin, brown structures) can then be detected by nanopore sensing. (c) Schematic of solid-state pores modified to contain specific receptors. First, a gold-coated nanopore is modified to contain a monolayer of ethylene glycol chains (blue lines) and nitrilotriacetic acid (NTA) receptors (green lines). The Ni^{2+} loaded NTA receptor specifically binds His-tagged proteins. The His-tagged protein can in turn be used to target secondary targets (eg. IgG). (Reprinted with permission from Iqbal *et al.*, 2007. Copyright 2007 Nature Publishing Group; Yusko *et al.*, 2007. Copyright 2011 Macmillan Publishers Limited; Howorka and Siwy, 2012. Copyright 2007 Nature Publishing Group)

Demonstrating the power of surface modification of solid-state pores, Mayer and coworkers designed nanopores coated with a fluid lipid bilayer that allowed control over the diameter, surface chemistry, and selectivity of the pores (Figure 1.7b) (Yusko *et al.*, 2011; Yusko *et al.*, 2012). The fluid lipid bilayer coating was done by simply dipping the pores in an aqueous suspension of liposomes. The control over the pore diameter and surface chemistry was achieved by controlling the lipid composition. The selectivity was achieved by preparing liposomes with a small fraction of biotinylated lipids (i.e ligand anchored lipids). The fluid lipid coating prevented pores from clogging, eliminated non-specific binding, and enabled the translocation of amyloid-beta oligomers and fibril which tend to bind to the pore surface and clog them (Yusko *et al.*, 2012). These pores also enabled them to capture proteins from very dilute solutions (picomolar concentrations) and slow their translocation, thus obtaining important information about the interaction between the target molecule and the ligands attached to the lipids (more on this study in section 1.2.2.2).

Recently, Rant and coworkers engineered receptor-modified solid-state nanopores (Figure1.7c) (Wei *et al.*, 2012). First, the interior of silicon nitride pores were covered with a layer of gold by means of evaporation. Then the gold surface was chemically modified to contain a molecular monolayer of alkane-thiols. The molecular monolayer mix contained a few nitrilotriacetic acid receptors (NTA). By controlling the mol% of NTA in the mixture it was possible to incorporate receptors to solid-state nanopores at a 1:1 stoichiometry. The NTA chelates Ni (II) ions and then the NTA-Ni^{2+} binds to His-tagged proteins. When adding his-tagged protein A to the solution it was possible to observe the binding between a single protein molecule and the receptor in real time. As a result of the high affinity between NTA_3-His_6 bond, the his-tagged protein A was immobilized very stably to the surface of the pore. This in turn, allowed to target and discriminate between secondary proteins (eg. subclasses of IgG) (Howorka and Siwy, 2012; Wei *et al.*, 2012). The ability to immobilize protein molecules as receptors on the surface of solid-state pores makes this approach extremely useful for examining protein-protein or protein-nucleic acid interactions. The details of this study are further discussed in section 1.2.2.2.

The fabrication and surface modification of solid-state pores has greatly advanced in recent years, as outlined here. Solid-state pores offer a "solid" alternative to biological pores. Each type of pore, solid-state or biological, exhibits advantages and disadvantages over the other

type. Their strengths and shortcomings are described in the next section.

1.1.3.5 Biological pores vs. solid-state pores

A decade after the first use of solid-state nanopores for biosensing, biological pores still remain the most popular type of pores. One of the main advantages of using biological pores is the ability to genetically engineer them. As outlined in section 1.1.3.2, genetic engineering broadens the range of experiments that can be performed with these pores. Furthermore, biological pores have an atomicically precise structure which means great pore-to-pore reproducibility. Both of these features are lacking in solid-state nanopores. While surface modification of solid-state pores has greatly advanced in recent years, it still does not offer the same level of precession as does genetic engineering. In addition, even with the state of the art fabrication techniques, solid-state pore reproducibility is still lacking (Beamish *et al.*, 2012; Wanunu, 2012). For example, it is possible to fabricate solid-state pores with similar diameters from the same material but they still exhibit different electrical properties (eg. different noise levels and conductance) (Smeets *et al.*, 2006). In addition, with biological pores there is no non-specific binding whereas with solid-state pores there is (Niedzwiecki *et al.*, 2010; Oukhaled *et al.*, 2011; Sexton *et al.*, 2007; Sexton *et al.*, 2010; Yang and Neimark, 2012). The binding of molecules to the interior walls of solid-state pores results in clogging (Yusko *et al.*, 2011). Finally, biological pores offer less current noise and therefore a better signal-to-noise level than their solid-state counterparts (Beamish *et al.*, 2012; Tabard-Cossa *et al.*, 2007). However, recently it's been reported that the electrical noise on solid-state pores can be reduced by application of high electric fields in an aqueous environment (Beamish *et al.*, 2012). Furthermore, the approach described by Beamish *et al.* can be used to rejuvenate pores that have been discarded due to high noise.

The main drawbacks of biological pores are their fixed diameters and limited stability. Unlike biological pores, solid-state pores allow control of diameter and channel length. This allows the study of analytes of various sizes. In addition, the stability of solid-state pores enables the use of nanopore sensing for diverse applications which would not be possible using biological pores (Beamish *et al.*, 2012). For example, solid-state pores can be used under a wide range of experimental conditions such as pH, salt concentration, temperature, applied potential, and so on (Cressiot *et al.*, 2012; Firnkes *et al.*, 2010; Freedman *et al.*, 2011; Oukhaled

et al., 2011; Plesa *et al.*, 2013). It should be noted that researchers are actively exploring different biological pores with the aim of finding a biological pore than can be used under a range of experimental conditions (Mohammad *et al.*, 2011; Pastoriza-Gallego *et al.*, 2011; Payet *et al.*, 2012; Wang *et al.*, 2013). While a biological pore may be stable in a fragile lipid bilayer only for hours, solid-state pores can remain functional for days (Fologea *et al.*, 2007). Another advantage of solid-state pores is the potential for integration into devices.

When comparing the quality and quantity of results published with both pores, that of the biological pores is superior. Solid-state pores emerged with promise of offering the same advantages as their biological counterparts and overcoming their limitations but this has yet to be shown. At the present, both pores have serious limitations. These limitations might be overcome by the use of a hybrid pore. A hybrid pore would combine the precise structure of a biological pore and the robustness of a solid-state pore.

In 2010 Dekker and coworkers constructed a hybrid pore by inserting a preassembled mutant α-hemolysin pore into a solid-state pore (Hall *et al.*, 2010). α-Hemolysin was mutated to include an additional 11-amino acid loop which contained a single cystine residue to which a DNA oligomer was attached though a disulphide bond. Then an additional 3 kbp dsDNA with a complementary end to the DNA oligomer was attached to the α-hemolysin. The DNA/α-hemolysin complex was then electrophoretically driven through a solid-state pore. The solid state pores were just large enough to allow the dsDNA and the stem of the pore enter, but not large enough to allow α-hemolysin to pass. This ensured that the vestibule of the biological pore would be facing the *cis*-side. In addition, it was demonstrated that this hybrid pore can be used for detection of single-stranded DNA (ssDNA) (Hall *et al.*, 2010). While this study showed the potential of a hybrid pore, there have been no more reports of hybrid pores for nanopore sensing since then.

1.2 Biochemical studies with nanopores

DNA sequencing continues to be one of the main driving forces of nanopore sensing technique. While this is true, nanopore sensing has been extensively used for other application such as detection of single nucleotide polymorphisms, detection of single amino acid mutations, study of protein folding, protein conformational heterogeneity, enzyme kinetics, intermolecular interactions, to name just a few (Kukwikila and Howorka, 2010; Madampage *et al.*, 2012;

Madampage *et al.*, 2010; Smeets *et al.*, 2009; Stefureac *et al.*, 2008; Stefureac *et al.*, 2010a; Stefureac *et al.*, 2010b; Talaga and Li, 2009; Tavassoly and Lee, 2012; Zhao *et al.*, 2009a). Last year alone, there were a few hundred papers published that had to do with the nanopore sensing technique. Therefore, in this section selected studies will be reviewed as it would be impossible to review the entire nanopore sensing literature in this limited space.

1.1.1 Nanopore sensing of polynucleotides

Nanopore sensing has been explored for analyzing the structure and composition of DNA and RNA molecules, for probing interactions between nucleic acids and protein molecules, and as a DNA sequencing platform. The idea of using nanopores for DNA sequencing was first proposed in 1996 (Kasianowicz *et al.*, 1996). Deamer and coworkers were first to demonstrate that single stranded DNA and RNA could be electrophoretically driven through the α-hemolysin pore. They observed that under an applied potential of 120 mV adding ssDNA or ssRNA resulted in numerous short lived current blockades with the frequency increasing with increasing concentration. The durations of the blockades were used to construct a histogram which revealed three different peaks. The blockade durations of two of the peaks were directly proportional to the polymer length, but indirectly proportional to the applied voltage. For this reason they attributed those as translocation events with one of the peaks belonging to molecules traversing the channel in a 5′ to 3′ direction and the other peak belonging to molecules going through the channel in a 3′ to 5′ direction. The blockade durations of the third peak were independent of the polymer length or applied potential and thus were attributed as bumping events. To prove that ssDNA did indeed translocate the α-hemolysin pore they PCR-amplified the *trans* chamber solution and as expected there was DNA present in the *trans* chamber. Furthermore, it was shown that upon addition of ribonuclease A (RNase A) to the *cis* chamber containing long polymers of polyuridylic acid, there was an initial increase in the event frequency because of the hydrolysis of the long polymers resulting in increased molar concentration of shorter polymers. With time the frequency would go down and with addition of fresh polyuridylic acid the rate would increase again. However, the same effect was not observed with RNase A and polyadenylic acid, which is not a substrate for RNase A. From these results they reasoned that, since only ssDNA or ssRNA would be able to translocate through the narrow channel and the channel can only accommodate one single strand, then the

single stranded polymers must translocate through the pore in a sequential, single-file order. From this they proposed that with further modification, this technique could be used to sequence DNA or RNA (Kasianowicz *et al.*, 1996).

To explore the idea that nanopore sensing can be used for sequencing DNA or RNA, Akeson and coworkers examined if different homopolymers (eg. polyadenylic acid, polycytidylic acid, polyuridylic acid, and polydeoxycytidylic acid) could be distinguished on the basis of blockade amplitude and time (Akeson *et al.*, 1999). Indeed, it was shown that each homepolymer produces a specific and distinguishable blockade signature. This was the first report of nanopore distinguishing between homopolymers of nucleic acids. The next step towards sequencing was to determine if the nanopore would distinguish between purines and pyrimidine bases when a single molecule of a nucleic acid passes through the pore. To do this, a single poly $A_{30}C_{70}$ molecule was synthesized and added to the *cis* compartment. As expected, it was possible to distinguish between the segment of purines and that of pyrimidines on the basis of blockade amplitude and duration (Akeson *et al.*, 1999).

In a similar study, Meller *et al*. demonstrated that different DNA polymers of similar length and composition that differ only in sequence could be differentiated (Meller *et al.*, 2000). Furthermore, it was shown that at lower temperatures the difference between polymers was more pronounced. In a different study, Meller *et al*. discovered that for DNA polymers of 12 nucleotides (length of β-barrel region of α-hemolysin pore) or more, the blockade amplitude was fairly constant and the velocity was independent of length (Meller *et al.*, 2001). From these studies it became apparent that the translocation of DNA molecules was occurring at a very fast rate, about 1-2 μs/base (similar velocities have also been observed for translocation of DNA molecules through solid-state pores). These translocation speeds are too fast to be detected by currently available sensors (Fologea *et al.*, 2005; Jetha *et al.*, 2011; Rosenstein *et al.*, 2012; Wanunu, 2012). For example, typically a 10 kHz low-pass Bessel filter is used with a rise time of the filter being $\approx 0.33 f_c^{-1}$ or 33 μs (f_c is the cut off frequency, i.e 10 kHz in this case). Any event with duration less than twice the filter rise time will be distorted (Pedone *et al.*, 2009; Plesa *et al.*, 2013). Furthermore, because the smallest constriction region of α-hemolysin pore is long enough to accommodate about 12 nucleotides, it is not possible to achieve single-nucleotide resolution without further improvements (Branton *et al.*, 2008). Therefore, time and geometry resolutions are the critical factors in achieving DNA sequencing

with nanopores. Geometric resolution can be described as the sharpness profile of the smallest constriction of the pore (Branton *et al.*, 2008; Maitra *et al.*, 2012; Wanunu, 2012).

Different research groups have reported different strategies to address the resolution factor. For example, changing the temperature and viscosity of the electrolyte solution (eg using organic salts or glycerol), using DNA hairpins, attachment of proteins to one end of DNA molecules, and mutating amino acids in the β-barrel region of α-hemolysin pore are some of the approaches taken to address the fast translocation velocities (Fologea *et al.*, 2005; Kowalczyk *et al.*, 2012; Luan *et al.*, 2012; Rincon-Restrepo *et al.*, 2011; Vercoutere *et al.*, 2001; Vercoutere *et al.*, 2003; Yeh *et al.*, 2012) . With the use if hairpin it was found that the hairpin molecules had to unzip in order to translocate, thereby improving the time resolution (Mathe *et al.*, 2004; Vercoutere *et al.*, 2001; Vercoutere *et al.*, 2003). Furthermore, to improve the geometric resolution researchers have used the MspA pore (shown in Figure 1.7a) with a constriction cross-section that can accommodate just four bases, the α-hemolysin pore fitted with an adaptor, solid-state pores drilled in very thin silicon nitride membranes, and the use of graphene solid-state pores with atomically thin membranes that can accommodate only one base of DNA inside the pore at any time (Butler *et al.*, 2008; Clarke *et al.*, 2009; Garaj *et al.*, 2010; Manrao *et al.*, 2012; Merchant *et al.*, 2010; Schneider *et al.*, 2010). Figure 1.8 highlights the most popular approaches being taken to achieve nanopore-based DNA sequencing. All these approaches try to address the resolution factor.

One method that has been gaining ground is the use of an adaptor-fitted α-hemolysin with a tethered exonuclease (Figure 1.8a) (Astier *et al.*, 2006; Clarke *et al.*, 2009). This method is also known as exonuclease sequencing. In 1999, Gu *et al*. first reported the use α-hemolysin pore equipped with an internal, non-covalently bound adapter. The adapter used was β-cyclodextrin, a 7 member sugar ring molecule. It was shown that β-cyclodextrin fits well inside the wild-type pore and only blocks 64 % of the open pore current. As a result, the α-hemolysin fitted with the adaptor proved to be suitable for detection of organic molecules (Gu *et al.*, 1999). Later, in 2001, Gu *et al*. showed that by using mutant α-hemolysin pores, the residence time of β-cyclodextrin inside the pore can be prolonged (Gu *et al.*, 2001). Eight years later, Clarke *et al*. reported successful differentiation of nucleoside monophosphates with the use of a mutant α-hemolysin pore $(M113R)_7$ fitted with a covalently-bound molecular adapter (a modified β-cyclodextrin), which interacts with nucleoside monophosphates and its cavity is similar in size

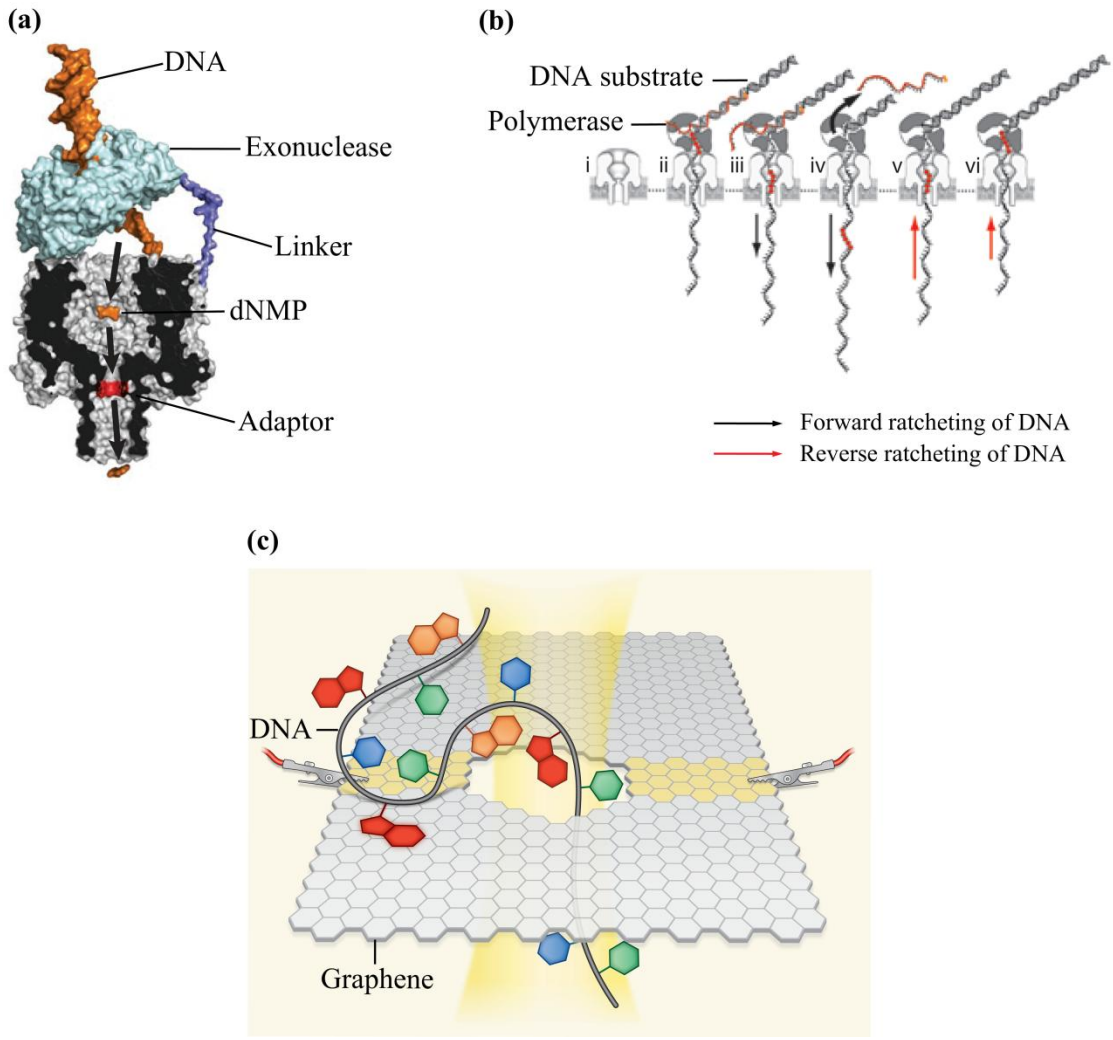

Figure 1.8. Popular approaches in nanopore-based DNA sequencing. (a) Schematic of the exonuclease sequencing approach. In this approach an exonuclease coupled to an adaptor-fitted α-hemolysin pore is used to degrade a DNA strand one base at a time and then each base translocates through the pore in the same sequential order as removed from the strand. Each base is identified based on blockade amplitude and time. (b) Schematic of a DNA polymerase based approach. In this approach a DNA substrate is bound by the DNA polymerase forming an inactive complex. The inactive complex is then drawn into the pore where the complex becomes active as a result of blocking oligomer (red ribbon) being removed from the DNA substrate by the applied force (i.e voltage). This in turn allows DNA polymerase to start synthesis of the new strand one nucleotide at a time. Addition of a nucleotide will induce a characteristic current block representative of the nucleotide being added. (c) Schematic of DNA sequencing with graphene nanopores. In this strategy a single-stranded DNA is passed through a solid-state pore made up of a graphene monolayer with thickness comparable to the dimensions of a single base. As each base passes through the pore, the current is recorded and the base is identified. (Reprinted with permission from Branton *et al*., 2008. Copyright 2008 Nature Publishing Group; Cherf *et al*., 2012. Copyright 2012 Nature Publishing Group; Bayley, 2010. Copyright 2010 Nature Publishing Group)

to a nucleotide (Clarke *et al.*, 2009). Using the mutant α-hemolysin pore with the covalently-bound β-cyclodextrin, the deoxynucleoside monophosphates were identified with 99.8% accuracy. In addition, it was possible to distinguishing between normal cytosines and methylated cytosines with the same accuracy level. The deoxynucleoside monophosphates detected and identified were either added directly to the solution (*cis* side) or produced in solution from ssDNA and Exonuclease I from *E. coli*. The next step in this DNA sequencing approach, yet to be achieved, is to tether the exonuclease onto the modified α-hemolysin pore which would cleave single bases from DNA and feed them to the pore in a sequential order as they appear in the DNA molecule, enabling identification of bases. Coupling the exonuclease to the pore would slow the translocation of the DNA through the pore and thereby increasing the identification accuracy (Deamer, 2010). This exonuclease sequencing strategy is being applied in the development of commercial, nanopore-based DNA sequencing product by Oxford Nanopore Technologies (Eisenstein, 2012; Pennisi, 2012).

Another popular nanopore-based DNA sequencing strategy takes advantage of a DNA polymerase and a biological pore (Figure 1.8b) (Benner *et al.*, 2007; Cherf *et al.*, 2012; Lieberman *et al.*, 2010; Manrao *et al.*, 2012). Again, the reason why a DNA polymerase is being explored is because this approach will control the speed of DNA through the pore. For example, a typical polymerase adds free nucleotides to the newly forming strand at a rate of about few milliseconds per nucleotide (Deamer, 2010). Therefore, this would overcome the time resolution issue. Moreover, by using DNA polymerase a ratcheting effect will be produced in which each nucleotide pauses in the pore as the enzyme adds a new nucleotide to the strand (Cherf *et al.*, 2012). The idea of using a DNA polymerase for controlling the translocation speed of DNA through the pore has been investigated by Akeson and coworkers since 2007 (Benner *et al.*, 2007). In 2007 it was shown that a nanopore can be used to distinguish between the signal produced by unbound DNA, DNA/Klenow fragment (a fragment of DNA polymerase I from *E. coli* without the exonuclease activity) complex, and DNA/Klenow fragment/dNTPs complex. This was a critical discovery towards the use of a DNA polymerase in a nanopore-based sequencing method because it shows that each component involved in the polymerase reaction can be identified. Then in 2010, Akeson and coworkers discovered that the bacteriophage phi29 DNA polymerase was a suitable candidate for this approach because it remained bound to the DNA substrate while held atop the α-

hemolysin pore even under an applied voltage potential of 180 mV (Lieberman *et al.*, 2010). Furthermore, it was demonstrated that the phi29 DNA polymerase controls the movement of the DNA strand through the pore at a rate that is suitable for base detection and identification. In 2012 the DNA polymerase approach received even more attention when two different groups reported that a DNA polymerase-coupled biological pore (MspA and α-hemolysin) could be used to obtain sequence information from a DNA translating the pore (Cherf *et al.*, 2012; Manrao *et al.*, 2012; Schneider and Dekker, 2012).

In the study by Cherf *et al*., a DNA substrate made up of a primer, a template, a blocking oligomer, and a single-stranded end was designed (Figure 1.9a). The primer was annealed to the template's 3′ end. The blocking oligomer was annealed adjacent to the primer-template junction and its function was to prevent extension and excision of the primer in bulk phase by the phi29 DNA polymerase. On the other hand the 3′ end of the template was protected by a protecting group. Addition of the phi29 DNA polymerase to the *cis* chamber in the presence of protected DNA substrate resulted in formation of a stable but enzymatically inactive complex. Upon an applied voltage, the single-stranded end of the substrate DNA is drawn into the pore and hence pulls the complex to the entrance of the pore (Figure 1.9b). The complex becomes active only when the blocking oligomer is unzipped (3′ to 5′) as a result of the applied force (i.e applied voltage). With the removal of the blocking oligomer, the 3′ end of the primer is exposed, allowing synthesis to start. As the polymerase synthesizes the new strand, it acts as a motor that pulls the DNA through the pore in single-nucleotide steps (these steps are illustrated in Figure 1.9b) (Cherf *et al.*, 2012). This strategy was successful in slowing the DNA translocation speed to approximately 25 ms/nt during synthesis and 400 ms/nt during unzipping (Maitra *et al.*, 2012). However, they were unable to directly match the current blocks with individual nucleotides due to the lack of sensitivity of α-hemolysin. By analyzing a number of different DNA substrates with known sequences they managed to construct an ionic current map. Using the map, as well as performing four additional experiments for each template, where the concentration of one of the four dNTPs was lowered, it was demonstrated that the sequences of DNA templates could be determined. This has yet to be demonstrated with DNA templates of unknown sequences. The same phi29 DNA polymerase and blocking oligomer strategy was pursued by Manrao *et al*. with a mutated MspA pore (Manrao *et al.*, 2012). It should be noted that the current blocks observed with MspA as a DNA molecule translocates

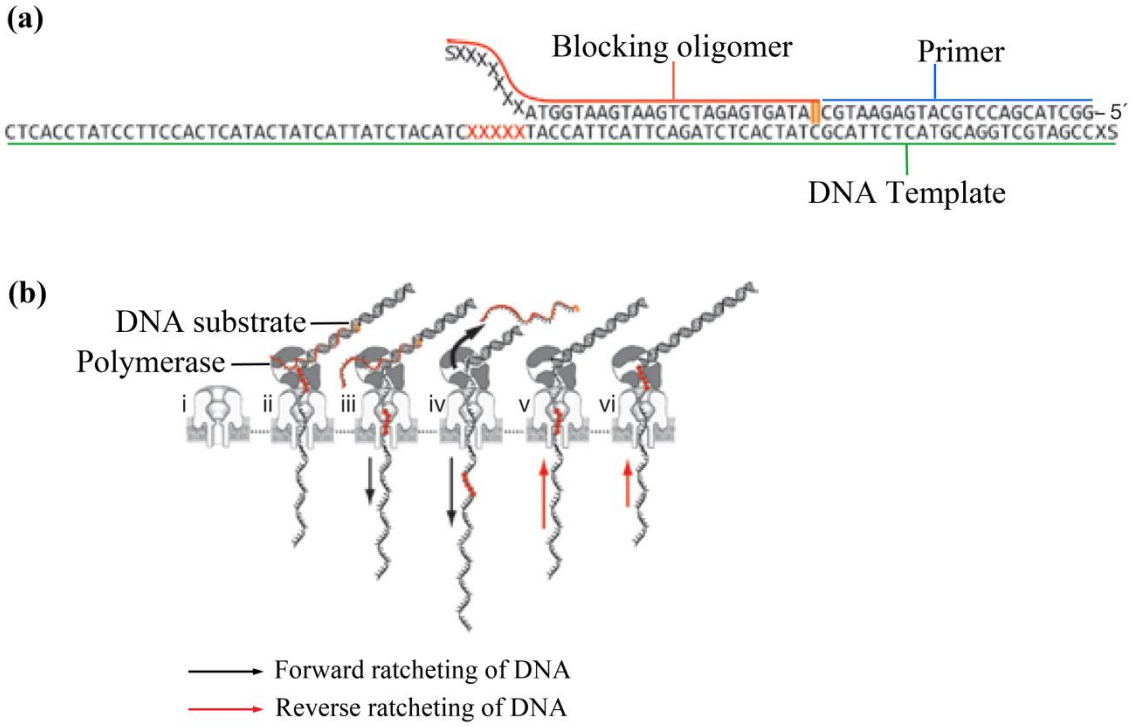

Figure 1.9. DNA polymerase based sequencing approach. (a) DNA substrate. The DNA substrate is made up of a DNA template, a primer, and a blocking oligomer. The blocking oligomer prevents extension of the primer by the DNA polymerase in solution before being drawn into the pore. The blocking oligomer is removed by the applied voltage once pulled into the pore. (b) An illustration of the steps involved in a DNA polymerase based sequencing approach. (Reprinted with permission from Cherf *et al.*, 2012. Copyright 2012 Nature Publishing Group)

through the pore are as a result of about 4 nucleotides occupying the pore compared to about 10 nucleotides for the α-hemolysin pore. Manrao *et al*. showed that the current levels could be related to a known DNA sequence but further work was required to be able to sequence unknown DNA. The important conclusion reached from both of these studies is that the polymerase can be used to control the DNA translocation through the nanopore in single-nucleotide steps. Furthermore, because DNA molecules are forced to pass through the pore twice - once during unzipping and once during synthesis - this provides double reading of the same sequence. While this approach might provide the most compelling results to date in DNA sequencing with nanopores, there is still further work required to achieve direct strand sequencing.

Recently a third DNA sequencing approach by nanopores is being explored where the pores are solid-state pores made of graphene (Figure 1.8c) (Garaj *et al.*, 2010; Merchant and Drndic, 2012; Merchant *et al.*, 2010; Postma, 2010; Schneider *et al.*, 2010; Wells *et al.*, 2012). DNA sequencing with graphene nanopores provides an attractive strategy because of the thickness of graphene. As stated earlier, graphene is an atomically thin layer of carbon atoms arranged in a honeycomb lattice. The thickness of graphene pores is comparable to the dimensions of a base and therefore graphene nanopores present an intriguing alternative for DNA sequencing. Translocations of DNA through solid-state pores made of graphene were first reported in 2010 by three different groups, all within a month. While graphene is atomically thin, it is still very robust. In addition, unlike other solid-state pore material, graphene is a good electrical conductor. However, translocation of dsDNA through graphene nanopores occurs at very fast rate (about 10 ns/base). These translocation velocities are two fast to allow the resolution of current blockades arising from individual bases for the reasons mentioned in the beginning of this section. Since graphene is electrically conductive, it might be possible to identify each base as they pass through the pore by running a tunneling current through the DNA molecule with the graphene acting as an electrode. In 2010, Postma *et al*. proposed a technique for identifying individual bases by using graphene nanogaps to read DNA's conductance as it passes through (Figure 1.8c). Electrodes on each side of the gap are used to measure the conductance of each base as it passes through. While DNA sequencing with graphene nanopores presents an alternative approach to DNA sequencing with biological pores, there are a number of obstacles that must be overcome before this approach is established as a serious

competitor to the approaches using biological pores. For example, graphene nanopores exhibit very high levels of current noise due to their atomically thin structures. Additionally, DNA is known to adhere to graphene.

The above outlined approaches for DNA sequencing might be the most popular approaches but are not the only ones being pursued (Maitra *et al.*, 2012; Wanunu, 2012). Due to limited space, it's impossible to list all the approaches. For example, in 2012 Kasianowicz and coworkers proposed another method for nanopore-based DNA sequencing which they termed as "nanopore-based sequencing by synthesis" (Kumar *et al.*, 2012). The principle behind this approach involves the use of DNA polymerase, DNA substrate (primer and template), and four poly(ethylene glycol) molecules of different length and chemical structure as tags to modify nucleotides, with each nucleotide having a different tag. During a polymerase reaction, as each nucleotide is incorporated into the growing DNA strand, its tag is released and enters a nanopore in release order. In order for the tags to enter the nanopore in the same order as they were released, the polymerase would have to be coupled to the pore. Kasianowicz and coworkers demonstrated that large poly(ethylene glycol) molecules could be used as tags without effecting polymerase recognition. Furthermore, because of the large size of the tags and their distinct chemical structures, discrimination between the tags was achieved very easily as they produced distinct blockade currents (Kumar *et al.*, 2012). This nanopore-based sequencing by synthesis strategy is a promising method because there is already a great amount of work with polymerase coupled pores.

While DNA sequencing continues to be the main focus of nanopore sensing technique, various groups have extended this technique to other applications such as probing nucleic acid structures. Ang *et al*. showed that nanopore sensing could be successfully applied to detection of single-nucleotide polymorphisms (SNPs), which are important biomarkers for many diseases (Ang and Yung, 2012). In this study they designed two sets of non-complementary probes made up of a gold nanoparticle and ssDNA. One set contained a longer sequence of ssDNA and the other contained a shorter sequence of ssDNA. These two probes are linked together via hybridization to the target DNA to form an assembly structure. The assembly structure is formed only in the presence of perfect complementary sequence. In the presence of a single-mismatch the assembly structure is not formed because the intermediate duplex structure is energetically unstable. Using solid-state pores they were able to detect the assembly structures

which corresponded to a "yes" signal, indicating perfect complementarity. In the presence of a single-mismatch, there were no events observed, thus indicating the presence of SNPs. The reason why there were no events observed was because the pore size was designed such that probes or target DNA alone would be much smaller compared to the pore size and thus produce negligible current block as they pass through. It was also shown that the detection limit of this technique is down to 5.0 pM of target sample and only 30 min analysis is required to confirm the presence of SNPs with no false positives.

An interesting study conducted by Wanunu *et al*. demonstrated the ability of nanopore sensing to detect and quantify microRNAs down to picogram levels (Wanunu *et al.*, 2010). It was shown that microRNAs can be detect from total RNA using a solid-state pore with a 3 nm diameter fabricated in a 7 nm thick membrane. Before the nanopore detection step could be performed, it was necessary to perform an enrichment step of the target microRNA. The microRNA enrichment began with the isolation of the total RNA from tissue and subsequent hybridization to an RNA probe complementary to the target microRNA. This was followed by incubation of the viral p19 protein, specific for 21–23 bp dsRNA, with the probe-hybridized total RNA. Any RNA which did not bind the probe was washed away followed by elution of the probe/microRNA complex from the p19 protein. The probe/microRNA complex was then finally detected using nanopore sensing. In order to quantify the microRNA, a standard curve of the event frequency vs. a known concentration of a synthetic probe/microRNA was constructed. Then, using the standard curve they demonstrated the ability to determine the concentration of the microRNA in the solution and in turn the amount of target microRNA per 1 μg of rat liver of total RNA. Just 4 minutes of nanopore sensing was sufficient to determine the microRNA concentration with 93% certainty. This study shows the capability of nanopore sensing as a suitable microRNA detection and quantification technique.

In a similar study, Wang *et al*. showed that nanopore sensing with α-hemolysin can be used to detect specific microRNAs in plasma samples in lung cancer patients without amplification or labelling of the microRNA (Wang *et al.*, 2011b). Total plasma RNAs was extracted from blood samples of lung cancer patients and healthy volunteers and then added to the *cis* chamber with a designed probe targeting a specific microRNA. The probe was designed such that the sequence complementary to the target microRNA would be in the middle, thus leaving single stranded ends. Upon applying a voltage, the probe/microRNA complex would be drawn into

the pore and forced to unzip, thus producing a distinct current block. The authors of the study went on to quantify the levels of a specific microRNA in lung cancer patients using nanopore sensing and real-time reverse transcription polymerase chain reaction and found that the nanopore sensing method demonstrated a higher accuracy level while requiring no labelling or amplification.

In conclusion, nanopore sensing has emerged as a powerful tool for studying nucleic acids at single-molecule resolution. Moreover, the development of nanopore-based DNA sequencing platforms in the near future seems promising.

1.2.2 Nanopore sensing of peptide and proteins

The nanopore sensing field has grown rapidly over the last two decades. It emerged as a potential high speed, low-cost DNA sequencing platform. Today, it is used as a general platform for a wide range of peptide and protein studies. The quality of research conducted on nucleic acids inspired many groups to start employing the same techniques to peptides and proteins. However, as can be seen from selected studies presented in this section as well as much of the results and discussion section of this thesis, applying nanopore sensing as a single-molecule technique to peptides and proteins is much more difficult than applying it to nucleic acids. For example, unlike nucleic acids, peptides and proteins are not uniformly charged. Furthermore, as reported recently, translocation of proteins through nanopores exhibit anomalous behaviour (Plesa *et al.*, 2013). In order to have a better understanding of the technique, many groups started with simple sensing of peptides and gradually moved to more complex protein folding and conformational studies and just recently nanopore sensing is being explored as a protein sequencing platform.

1.2.2.1 Nanopore sensing of peptides

Almost a decade after the first report of nanopore sensing of nucleic acids came the first report of nanopore sensing of peptides (Sutherland *et al.*, 2004). In 2004, Lee and coworkers were the first to report the study of peptides with nanopores. In their study they examined peptides of sequence $(Gly\text{-}Pro\text{-}Pro)_n$, where n was either one, two, or three, using the α-hemolysin pore. The triple repeat peptides form single, double, or triple collagen-like helices

and exist as a heterogeneous mixture. Each species in the mixture was successfully identified for all three peptides using nanopore sensing. This was possible because all species produced distinct current blocks. In addition to the triple repeat peptides, they also examined a heptapeptide of unknown structure and using nanopore analysis they were able to show that it folds as it translocates through the α-hemolysin pore. This was a very important study because it truly showed the potential of nanopore sensing as a single-molecule technique. For example, CD spectra of the triple repeat peptides only provided an average of all the species present for each peptide, whereas nanopore analysis clearly showed the presence of multiple species (Sutherland *et al.*, 2004).

In 2005, Movileanu *et al*. examined the effect of peptide length and charge on free energy barrier as the peptides translocate the α-hemolysin pore (Movileanu *et al.*, 2005). The peptides they examined were cationic α-helical peptides of 11 to 36 residues and with a net charge ranging between +2 to +7. They discovered that with an increase in peptide length there was a decrease in the frequency of events because of the entropic penalty experienced as a result of translocating across a nanometer-sized pore. On the other hand, an increase in the applied voltage potential resulted in an increase in the frequency of events because the applied voltage reduces the effective barrier. In addition, it was shown that with an increase in peptide length there was an increase in the event duration which was expected. In a follow-up study, Wolfe *et al*. wanted to further examine what drives peptide transport through biological pores and whether the binding sites within the pore lumen effect the translocation of peptides across the pore (Wolfe *et al.*, 2007). The authors hypothesized that the positively charged amino acid residues found at the constriction site and also at the *trans* exit site of the wild-type α-hemolysin pore, contribute to the energy barrier experienced by translocating cationic peptides. To test this hypothesis they examined the interaction of three cationic peptides of similar length and charge, but of different hydrophobicity with wild-type α-hemolysin and with three different α-hemolysin mutants. The mutants had a lysine residue mutated to an aspartic acid either at the constriction site, *trans* exit site, or both. The results obtained showed that the negatively charged binding sites facilitated the translocation of the peptides across the pores through attractive electrostatic interactions between the translocating peptide and the pore lumen (Wolfe *et al.*, 2007). Basically, the attractive electrostatic forces provided a substantial reduction of the free energy barrier. In addition, the strong interactions between the translocating peptide and

the pore lumen resulted in longer residence times inside the pore. However, the concentration of the peptide had no effect on the residence times but did have a linear effect on event frequency. It was also demonstrated that the interaction between the peptides and the pore was dependent on the nature of the peptides. For example, the frequency of events was greater for hydrophilic peptides than for hydrophobic ones. This is because the energy barrier is greater for hydrophobic peptides due to the hydrophilic nature of the interior of the pore (Wolfe *et al.*, 2007).

In a similar study, Zhao *et al*. used a series of peptides containing mainly aromatic amino acids with various lengths to investigate the effect of length and structure of peptides on their interaction with wild-type and engineered α-hemolysin pores (Zhao *et al.*, 2009b). The engineered α-hemolysin pores contained either one or two aromatic binding sites obtained through introduction of aromatic residues by mutagenesis. It was apparent that with an increase in the peptide length there was an increase in blockade duration and amplitude. In addition to the peptide length, it was also demonstrated that peptide composition affected the blockade amplitude and duration. Peptides containing aromatic amino acids had higher binding affinities to the engineered pores with aromatic binding sites, thus producing blockades with longer duration and amplitudes. Again, with higher affinity there was an enhancement in time resolution (i.e longer durations) and signal-to-noise ratio which in turn allowed differentiation of peptides of different lengths, including those differing by one amino acid. In a separate study, Zhao *et al*. have also shown that the ionic strength of the electrolyte solution can be used to improve the resolution and sensitivity of nanopore sensing (Zhao *et al.*, 2008a). It was shown that the ionic strength of the electrolyte solution affects non-covalent interactions (electrostatic, aromatic, and hydrophobic) between peptides and the pores. For peptides interacting with the pore through hydrophobic or aromatic interactions, the event frequency was decreased with an increase in the salt concentration whereas for those peptides interacting through electrostatic interactions, the opposite was observed. However, an increase in the blockade duration was observed for all peptides (independent of the non-covalent interaction) at higher ionic strength, thus providing improved resolutions. Taken together, the ionic strength of the electrolyte solution and a properly engineered pore can be used to improve the sensitivity of nanopore sensing. The authors of these studies also suggested that with a properly engineered pore it might be possible to develop a nanopore-based protein sequencing platform

(Zhao *et al.*, 2009b).

In an attempt to better understand nanopore sensing, Lee and coworkers examined the translocation of a series of negatively charged α-helical peptides of different length through α-hemolysin and aerolysin pores (Stefureac *et al.*, 2006). Unlike α-hemolysin, aerolysin has no vestibule but has a larger stem and similar diameter. This was the first report of the aerolysin pore being utilized in nanopore sensing. In the analysis of these peptides the authors observed two types of events: bumping and translocation. For the α-hemolysin pore, the peptides produced mainly translocation events whereas for aerolysin the events were a mixture of bumping and translocation events. The authors reasoned that the vestibule of the α-hemolysin pore facilitates the translocation of peptides because of the larger capture radius compared to aerolysin. Furthermore, it was found that larger dipoles facilitate the alignment of the peptide with the pore channel and hence aid the translocation of the peptides across the pores. Peptides with smaller dipoles produced a larger proportion of bumping events compared to those with higher dipoles. Thus it's important not to discard bumping events in nanopore analysis as they can provide critical information. In addition to dipole moment, the net charge density was found to have an effect on the translocation of the peptide. For the translocation events, the duration increased with peptide length and decreased with net charge density. For neutral peptides, the frequency of events was greatly reduced and the proportion of bumping events was increased, suggesting a diffusion-controlled interaction with the pore rather than voltage-driven. Together, these results showed that nanopore sensing can provide important structural information about the molecule interacting with the pore.

To further understand peptide translocation through nanopores and also gain insight into protein translocation, Lee and coworkers conducted a two part study where they analyzed a series of peptides with increasing structural complexity (Christensen *et al.*, 2011; Meng *et al.*, 2010). The peptides were of linear, circular, and branched (x- and y-shaped). In the first part of the study, the interaction of the peptides with the α-hemolysin pore as a function of voltage was investigated, with the peptides being added to *cis* side of the pore and the *trans* electrode being grounded (Meng *et al.*, 2010). Two of the peptides studied had similar composition and sequence of amino acids with exception of a single amino acid residue being positioned at either the N- or C-terminus. The position of this single amino acid on the peptide had a significant effect on the interaction of the peptide with the pore, resulting in different blockade

current signatures. This analysis allowed the authors to conclude that the interaction between the peptide and the pore is sequence-dependent. Furthermore, addition of a single benzyl group to a peptide facilitated its translocation through the pore because of the increase in hydrophobicity, which agrees with results previous results obtained by Stefureac *et al*. with the Fmoc-protected alpha-helical peptides (Stefureac *et al.*, 2006). The third observation made from the analysis of some of these peptides was the presence of a third type of event, which the authors termed as "intercalation events" (Figure 1.2b). An intercalation event was described as an event resulting from a molecule that enters the pore and diffuses to the same side without translocating and their residence time within the pore increases with increasing voltage. In the second part of the study, Lee and coworkers studied the effect of charge, topology, and orientation of the electric filed on the interaction of peptides with the α-hemolysin pore (Christensen *et al.*, 2011). The peptides analyzed were of 12 amino acid residues and of opposite charge. The peptides were added to either vestibule or stem side of the pore and the grounded electrode was either in the *cis* or *trans* side, thus for a single peptide there were four experiments conducted. In two of the experiments a peptide would have to go against the electric field in order to translocate through the pore. Together, these experiments allowed them to conclude that beside electrophoresis, other factors such as electroosmotic flow and current rectification due to the pore play an important role on the interaction of peptides with the pore. Furthermore, it was stated that the only way of determining whether an event was a translocation or intercalation event was to study the effect of voltage on the duration times. Intercalation events were also observed by Asandei *et al*. on the analysis of antimicrobial peptides (Asandei *et al.*, 2011). Asandei *et al*. showed that placing aromatic amino acids at the ends of an antimicrobial peptide results in stabilization of the peptide within the lumen of the pore through reversible aryl-Met interactions between aromatic residues placed at a peptide's ends and the methionines present at the constriction region of the α-hemolysin pore. Upon increasing of the applied voltage, the duration and frequency of the events increased, thus indicating intercalation events.

In their quest towards understanding peptide translocation through biological pores, Movileanu and coworkers also studied β-hairpin peptides (Goodrich *et al.*, 2007). The peptides investigated varied in their folding properties, with the folded fraction ranging between 5-50%. The β-hairpin peptides with the lowest degree of folding translocated the pore in an extended

conformation and their translocation times were very fast. On the other hand, the translocation of the β-hairpin peptides with the highest fraction of folding translocated the pore in a misfolded or fully folded confirmation and at a much slower rate. In general, the translocation times of all the β-hairpin peptides were strongly dependent on the electrophoretic force and related to the folding degree of the peptides. Therefore, this study showed that translocation of the peptides through α-hemolysin pore is also dependent on the folding features of the translocating peptide.

In a different approach, Lee and Stefureac studied the effect of alternating current (AC) field, superimposed on the direct current field, on the translocation of peptides through the α-hemolysin pore (Stefureac *et al.*, 2012). The AC frequencies chosen were in the MHz range to prevent the headstage or amplifier used from detecting and filtering those frequencies. Increasing the AC frequency resulted in higher proportion of bumping events for the peptides with large dipole moment due to an increase in peptide rotation and therefore a decrease in probability of the peptide entering the narrow constriction of the pore. This study has important implications because it shows that nanopore analysis can be performed under an applied AC field and translocation of peptide can be controlled by controlling the AC frequency. Furthermore, this could be developed into a biosensor that can discriminate peptides or other molecules based on dipole moment differences.

Following these preliminary studies with peptides, more complex studies were conducted such as detection and differentiation of multiple confirmations of the same molecules in a single sample. For example, nanopore sensing has been used to examine folding in Zif168, a 28 amino acid Zn-finger peptide (Stefureac and Lee, 2008). In the folded state, Zif168 is bound by Zn (II) and contains β-sheet, α-helix, and turn motifs. In contrast, in the absence of the Zn (II) the peptide is unfolded. The dimensions of the folded peptide are larger than the diameter of the α-hemolysin pore, and thus cannot translocate through the pore. Using nanopore analysis, Stefureac and Lee examined the peptide in the presence and absence of the Zn (II) and demonstrated that it was possible to differentiate between the folded and unfolded state. The folded peptide (i.e Zif268 in the presence of Zn (II)) was unable to translocate and therefore produced mainly bumping events. The proportion of bumping events was shown to be directly proportional to the molar concentration of Zn (II). However, in the presence of other divalent metal ions which bind Zif268 with much lower affinities, the peptide still translocated the pore,

suggesting weaker free energy of folding. In a similar study, conducted by the same research group, conformational changes in prion peptides caused by metal ion binding were detected (Stefureac *et al.*, 2010a). Three prion peptides isolated from the octarepeat region of the cellular prion protein were examined in the presence and absence of divalent metal ions. The octarepeat region located within the N-terminal region of the normal cellular prion protein is responsible for binding to metal ions. Some metal ions bind the peptides with higher affinities than others. Depending on the binding affinity between the peptide and the divalent metal ion, different degrees of conformational changes were observed. For example, higher binding affinity resulted in tighter complexes which in turn resulted in a higher proportion of bumping events. Together, these studies illustrate the capability of nanopore sensing for detecting conformational changes in a molecule upon binding to a ligand and studying protein or peptide folding. Furthermore, they show that the technique can be used to determine the degree of binding affinity between a molecule and its ligand.

Finally, nanopore analysis has also been used to study β-Amyloid (Aβ) peptides which are implicated in Alzheimer's disease (Madampage *et al.*, 2012; Wang *et al.*, 2011a; Yusko *et al.*, 2011; Yusko *et al.*, 2012). These peptides are derived from amyloid precursor protein and are known to readily aggregate into fibrils and plaques. The Aβ peptides are the main component of amyloid plaques in the brains of people suffering from Alzheimer's disease (Wang *et al.*, 2011a). Three different research groups have subjected Aβ peptides to nanopore analysis. One group studied the aggregation states of Aβ42 by analyzing Aβ42 in the presence and absence of a promoter (eg. β-cyclodextrin) or inhibitor (eg. Congo red) of Aβ42 aggregation (Wang *et al.*, 2011a). By using α-hemolysin pore and analyzing the blockade durations and times it was possible to detect and differentiate between conformational changes caused by β-cyclodextrin and Congo red. The second research group demonstrated that it is possible to differentiate between Aβ42, Aβ40, and a Aβ40 mutant using nanopore analysis (Madampage *et al.*, 2012). Finally, the third research group has shown that Aβ40 oligomers can be characterized using lipid-coated, solid-state pores (Yusko *et al.*, 2011; Yusko *et al.*, 2012). The aggregation of Aβ40 was successfully followed as a function of time by monitoring the size distribution of Aβ40 aggregates in solution. Furthermore, using the blockade durations and amplitudes it was possible to characterize the size and shape of the aggregates from a heterogeneous mixture. This highlights the ability of nanopore sensing technique to study molecules in solution without

labelling or immobilization.

1.2.2.2 Nanopore sensing of proteins and intermolecular interactions

In this section different reports of nanopore analysis of proteins are presented. In contrast to the study of nucleic acids using nanopores, the study of proteins has been more challenging due to variable charge distribution and structure and this will be highlighted as selected studies are reviewed. However, these challenges have not prevented nanopores from becoming a valuable tool for studying proteins and their interactions with different molecules at the single-molecule level. A good indication of this is the quantity and diversity of studies on proteins employing nanopores. These studies can be grouped into three very general categories: protein sensing and differentiation, protein conformation studies, and most recently, protein sequencing. Some of the earliest studies on proteins with nanopores were simple detection and differentiation between different proteins or its mutants.

Over the years different approaches have been pursued for protein detection by nanopores. One of the most common approaches of detecting proteins with nanopores is to use unmodified nanopores (eg. biological or solid-state pores). Such approach has been employed for detection of numerous proteins by different research groups. For example, in 2006 Staufer and coworkers reported the first protein detection using solid-state pores (Han *et al.*, 2006). By monitoring the ionic current through the pore it was possible to detect bovine serum albumin (BSA) protein. In the presence of the protein there were current blockades observed, but in the absence or after washing the protein from the chamber there were no blockades observed. Furthermore, an interesting observation was made that events were observed only when the protein translocation was in the same direction as the electrophoretic force. Using the amplitudes of the blockade current it was possible to estimate the diameter of the protein. These results were also confirmed by Fologea *et al*. (Fologea *et al.*, 2007). In addition, Fologea *et al*. demonstrated that BSA could be differentiated from a larger protein, fibrinogen, on the basis of blockade amplitudes. Direct proof linking the blockade events with translocation of the protein across a solid-state pore was also provided. The direct proof of BSA translocation through a solid-state pore was obtained by conducting a nanopore experiment for a period of about 50 hrs to allow enough molecules to translocate through the pore followed by detection of BSA in the opposite chamber using a chemiluminescent BSA enzyme linked immunosorbent

assay. This marked the first direct proof of protein translocation through a solid-state pore. Direct proof of protein translocation through biological pores has yet to be achieved (more on this in the results and discussion section of this thesis).

In 2008, Stefureac *et al*. utilized two different biological pores, α-hemolysin and aerolysin, to detect histidine-containing phosphotransfer protein (HPr) and two of its mutants, T34N and S46D (Stefureac *et al.*, 2008). This was the first report of employing nanopores for distinguishing different mutants. The mutants detected were single amino acid mutants yet the blockade events produced by all three proteins were dramatically different, thus demonstrating the power of the nanopore sensing method. In comparison to wild-type protein and the T34N which are uncharged at neutral pH, the negatively charged S46D mutant gave rise only to translocation events as a results of the electrophoretic force acting on it being greater than on the other proteins and thus facilitating translocation. The authors also noted that the proteins were translocating the pore by unfolding because the dimensions of the folded confirmation were too big to allow passage through the pore. Similarly, nanopore analysis has been used to detect and distinguish between mutants of α-synuclein, mutants of bovine prion protein, and prion proteins from different species (eg. human and bovine) (Jetha *et al.*, 2013; Madampage *et al.*, 2012; Merstorf *et al.*, 2012).

In a very recent study, Soskine *et al*. exploited the large size of the ClyA pore to detect and differentiate between several different proteins, including human and bovine thrombins which have 86% sequence identity (Soskine *et al.*, 2012). With a *cis* entrance of 7.0 nm, ClyA pore could accommodate proteins as large as 40 kDa into its lumen (Soskine *et al.*, 2012). The interactions of the proteins with the pore were detected as distinct blockade events. Human and bovine thrombins could also be readily differentiated even when in solution as a mixture. To improve distinction between several proteins in a solution and identify them with higher precision, ligands specific for the proteins were used. For example, addition of ligands specific for human thrombin into the mixture almost completely suppressed the events induced by the thrombin protein because of the complex (ligand-protein) was too big to induce events. Using this approach and the frequency of events, one can determine the concentration of an analyte in a mixture where several analytes are present. In spite of the ability of using unmodified nanopores to detect and distinguish different proteins on the basis of the current blockades, it is very challenging to distinguish between binding of a protein to a pore and translocation through

the pore. Therefore, the specificity is low when sensing with unmodified nanopores. To further improve selectivity and force specific targeting, many research groups have reported various sophisticated strategies.

One such strategy was employed by Bayley and coworkers in 2000 for detection of streptavidin (Movileanu *et al.*, 2000). A polyethylene glycol chain was tethered to the lumen of the pore at one end and covalently-attached to a biotin molecule at the other end. Addition of streptavidin to the solution resulted in biotin binding which was detected as changes in ionic current. Similar results were obtained with an antibody specific for biotin. Using the linear relationship between frequency of events and the concentration it was possible to quantify proteins at very low concentrations. The use of biotin as a ligand was just proof of principle but other immobilized ligands can be used to detect other proteins and in turn study the protein-ligand interactions. Indeed, a similar approach was reported for the detection and study of the interaction between the catalytic subunit of cyclic adenosine monophosphate-dependent protein kinase and a protein kinase inhibitor peptide (Xie *et al.*, 2005). The inhibitor peptide was covalently attached to the *trans* entrance of the pore and its interaction with the catalytic subunit was monitored as current blockade events. The effect of MgATP on the interaction of the peptide with the catalytic subunit was also assayed by examining the frequency of events and the duration of the events. At higher concentrations of MgATP, the binding is stimulated and this is evidenced with an increase in the frequency of events. Furthermore, at higher concentrations of MgATP, the duration of events is longer. The authors proposed that nanopore sensing could be used as a sensor for screening protein kinases for interaction with peptides.

In a recent study by Rotem *et al*., protein detection was performed using the α-hemolysin pore equipped with aptamers (Rotem *et al.*, 2012). Aptamers are DNA or RNA oligonucleotides that can adopt three-dimensional structures that can recognize and bind a broad range of analytes, including proteins, with very high affinity (Ying *et al.*, 2011). Aptamers are sometimes referred to as "synthesized antibodies" because they are generated *in vitro* by scanning a large library of random oligonucleotides and then repeating a cycle of selection and amplification until oligonucleotides with high affinity for the target is obtained (Rotem *et al.*, 2012). In this report, Rotem *et al*. used an aptamer (15-mer DNA) specific for the thrombin protein. The α-hemolysin pore was genetically engineered to introduce a single

cysteine residue to the *cis* entrance of the pore to which a DNA oligonucleotide (DNA adapter) was attached through a disulfide bond. The aptamer used was made up of a thrombin-binding domain and a hybridization domain with a sequence complementary to the DNA oligonucleotide. The two domains were linked together through a thymine linker. For the thrombin to be detected, first the aptamer had to be added to the *cis* chamber to ensure binding between the aptamer hybridization domain and the α-hemolysin coupled DNA oligonucleotide, followed by addition of thrombin to the same chamber. Upon addition of thrombin a new class of events were detected with increased current amplitude. However, this class of events was not detected in the presence of other proteins or denatured thrombin, suggesting that the events were indeed caused by binding of the native thrombin to the attached aptamer. Furthermore, addition of excess aptamer into the solution reduced the frequency of this class of events, indicating a reduction in the number of unbound thrombin. Based on the rate constants for the aptamer, it was possible to calculate the equilibrium dissociation constant for the thrombin-aptamer interaction, which was similar to what has been determined before by other methods. Detection of thrombin and investigation of aptamer-thrombin interactions was impeded at high voltages due to unzipping of the aptamer hybridization domain from the DNA adapter. The α-hemolysin pore used here can be rapidly configured simply by changing the protein-binding domain of the aptamer to detect any target protein at very high specificity. An aptamer based approach was also used by Maglia and colleagues to detect lysozyme and thrombin (Soskine *et al.*, 2012). Twelve thrombin or lysozyme aptamers were conjugated to the ClyA pore (one per pore monomer), and used for detecting thrombin or lysozyme proteins. By attaching 12 aptamers to the entrance of the pore, this essentially created a very selective filter that allowed capture of only proteins specific for the aptamer and excluded non-specific capturing. This approach can be very useful if the aim is to introduce selectivity towards a specific analyte in solution. Immobilized aptamers on glass solid-state pores have also been used to detect both IgE and ricin (Ding *et al.*, 2009).

In nanopore sensing of proteins, protein specificity has also been obtained by incorporating biological receptors into solid-state nanopores (Wei *et al.*, 2012). In a recent report, Wei *et al*. demonstrated for the first time a method for attaching biological receptors to solid-state nanopores at a 1:1 stoichiometry. In their method, first, a solid-state pore covered with a layer of gold was generated and then the gold surface was covered with a monolayer of ethylene

glycol to prevent nonspecific binding of proteins to gold. The ethylene glycol layer contained NTA receptors, whose mol% fraction was controlled to ensure the incorporation of a single receptor per pore. Using this method the authors reported successful detection of a single molecule of His-tagged protein A in real time (this is illustrated in Figure 1.7c). To confirm that the events observed were a result of the interaction between the His-tagged protein and NTA receptor, a high concentration of a competitive binder of NTA (i.e imidazole) was added to the solution and a decrease in the blockade duration times was observed (Wei *et al.*, 2012). When adding only proteins without His-tags, faster events were observed, thus indicating no binding to the NTA receptor. It was also observed that the duration times for the events induced by the interaction of the protein with the receptor molecules decreased with increasing voltage. Based on this method, they were able to detect and discriminate between secondary target proteins (i.e proteins that bind to His-tagged protein A, Figure 1.7c). First a solid state-state pore was prepared with one or few His-tagged primary proteins (i.e receptors) immobilized inside the pore through high affinity binding to the NTA molecules. Then, secondary proteins (eg. IgG subclasses) with differing affinities for the His-tagged protein were added to the solution and detected. Based on the duration times it was possible to discriminate between different antibodies. Antibodies with lower affinity for His-tagged protein A showed shorter duration times, whereas antibodies with higher affinities induced blockades with longer durations. Voltage-dependent measurements can also be used for this purpose. It should be noted that this type of sensitivity and specificity is not possible with non-modified solid-state pores. This approach can be extremely useful as it can be directly applied for examining a wide range of interactions between proteins and other analytes.

Finally, embedding of ligands into bilayer surface of lipid-coated solid-state pores has also been successful in detection of specific proteins (Yusko *et al.*, 2011; Yusko *et al.*, 2012). Mayer and colleagues reported that coating solid-state pores with a fluid lipid bilayer allows control over nanopore diameters and surface chemistry and also prevents non-specific binding of proteins to the pore walls (Figure 1.7b). The lipid bilayer coating of solid-state pores was achieved by exposing the nanopore chips to an aqueous solution of small unilamellar vesicles and allowing the liposomes to spread on the pores (the inside and outside walls of the pore). By choosing the lipids it was possible to control the bilayer thickness and in turn the diameter and surface chemistry of the pores. For example, the lipid length and number of double bonds

control the bilayer thickness, while the nature of the polar head groups are responsible for the surface chemistry of the pores. In addition to fine-tuning of the diameter of the pores, the authors showed that bilayer coating provides a strategy for rendering the pore specific for any analyte by simply introducing desired functional groups (eg. ligands or receptors) to the bilayer surface. These functional groups can be introduced during liposome preparation. In one of their experiments they used mole fractions of biotinylated lipids to prepare liposomes which were then used for coating of pores. As a result of the fluid nature of the lipid bilayer, the lipid-anchored ligands are mobile within the bilayer and can be used to concentrate very dilute analytes from the bulk solution and deliver these analytes to the pore. Lipid coated pores with bilayers containing biotinylated lipids were used to detect streptavidin, polyclonal anti-biotin Fab fragments, and monoclonal anti-biotin IgG antibodies (Figure 1.7b). The use of pores coated with bilayers containing biotinylated lipids showed reduced translocation speed of streptavidin and improved frequency of events compared to the lipid coated pores without biotinylated lipids (Yusko *et al.*, 2011; Yusko *et al.*, 2012). For example, it was possible to detect streptavidin from a bulk solution containing 6 pM streptavidin. The resolution of translocation times was also improved as a function of acyl chain length and degree of saturation due to the effect on viscosity of the bilayer. Using the frequency of translocation events and the blockade amplitudes it was possible to compare the affinity of proteins for the ligand and determine their molecular volume, respectively. This lipid coating strategy shows, yet another method of rendering nanopore sensing of proteins highly sensitive and selective.

While nanopore sensing has become a powerful tool for detecting and distinguishing proteins, it has also proved to be a valuable tool for studying protein folding. As a single-molecule technique, nanopore sensing offers the opportunity to study unfolded, partially folded, and fully folded confirmations in the same sample which is not possible with bulk measurements. In the analysis of the HPr proteins, both wild-type and mutants, folded and partially folded states could be observed (Stefureac *et al.*, 2008). The folded state was marked by bumping events whereas the partially unfolded state was marked by translocation events. This is because in its folded state, HPr is too big to translocate through α-hemolysin or aerolysin pore and thus it must unfold to go through the pores. The unfolding of the protein was facilitated by the protein's low activation energy of unfolding and the electrophoretic force acting on it.

The protein folding pathway of maltose binding protein (MBP) has been extensively studied by Juan Pelta's group (Cressiot *et al.*, 2012; Merstorf *et al.*, 2012; Oukhaled *et al.*, 2012; Oukhaled *et al.*, 2011; Oukhaled *et al.*, 2007; Pastoriza-Gallego *et al.*, 2007; Pastoriza-Gallego *et al.*, 2011; Payet *et al.*, 2012). The protein is 370 amino acid residues and has dimensions of 3 x 4 x 6.5 nm^3, thus cannot translocate the α-hemolysin pore folded. In 2007, MBP was studied as a function of the concentration of a denaturing agent, GdnHCl (Oukhaled *et al.*, 2007). In the absence of denaturing agent, there were no events observed. However, in the presence of 0.8 M GdnHCl long and short duration events were observed and the event frequency increased with increasing concentration of GdnHCl, with the frequency rate eventually reaching a plateau. The frequency rate vs. the concentration of the denaturant followed a typical sigmoid denaturation curve. As the concentration of the denaturant increased, the long duration events disappeared. Furthermore, with increased protein concentration and applied voltage, the frequency of the short duration events increased. These observations allowed the authors to conclude that the long duration events are induced by the partially folded protein, while the short duration events are induced by unfolded protein. They reasoned that at higher denaturant concentrations the partially folded species convert to unfolded species and hence the disappearing of the long duration events. In an attempt to repeat the results obtained by Juan Pelta's group, discrepancies were noted between the results obtained in our lab and those obtained by their group. These discrepancies have been addressed in detail as part of the research in this thesis, which have lead to the discovery of the importance of EDTA in nanopore analysis of proteins (more details will be provided in the results and discussion sections).

To confirm their initial results with MBP, Pelta and coworkers have also analyzed the unfolding of a less stable mutant of MBP (Merstorf *et al.*, 2012). As expected, the frequency of events as a function of the denaturant followed an identical sigmoid curve with the curve shifting more towards lower concentration of denaturant. This makes sense since the less stable protein will require lower concentration of denaturant to unfold. The unfolding of wild-type and mutant MBP has also been investigated with the aerolysin pore (Merstorf *et al.*, 2012; Oukhaled *et al.*, 2012). The unfolding curves obtained with both pores are similar. In order to provide indirect proof that the events observed with the denatured proteins are translocation events and not only interaction between the pores and the proteins, the authors generated a

double MBP (i.e two proteins linked together) and used the aerolysin pore to analyze it under the same conditions (Pastoriza-Gallego *et al.*, 2011). The duration times for the double-sized unfolded protein was twice that obtained for the single protein at the same concentration and applied voltage, suggesting that the events observed are indeed due to translocations of the unfolded proteins. In a separate study, Payet *et al*. investigated thermal unfolding of the MBP destabilized mutant using the α-hemolysin and aerolysin pores (Payet *et al.*, 2012). They observed very few events at room temperature but as they increased the temperature from 20 to 70 °C the event frequency increased. A similar sigmoid curve fit was used to fit the frequency of events vs. temperature. Again, for both pores, two types of events were observed: short and long events corresponding to bumping and translocation events, respectively. The frequency of translocation events increased with temperature as a result of thermal unfolding of the protein and as expected the translocation of the protein through the pores happens at a higher rate for higher temperatures. Similar data were obtained with both pores, thus indicating that the unfolding curve does not depend on the structure or the net charge of the nanopore. The thermal unfolding curved obtained with both nanopores show the same melting temperature as that obtained by CD (Payet *et al.*, 2012). This shows nanopore sensing as a reliable single-molecule technique for studying thermal unfolding of proteins.

In addition to the biological pores, Pelta and colleagues have also studied protein folding using solid-state pores (Cressiot *et al.*, 2012; Oukhaled *et al.*, 2011). MBP has been investigated in the presence and absence of GdnHCl as a function of voltage through a 3 nm and 20 nm solid-state pores (Oukhaled *et al.*, 2011). For the large pore, they reported an exponential increase in the event frequency of current blockades and an exponential decrease in translocation times as a function of applied voltage for folded and unfolded protein. The duration times obtained for the natively folded protein were larger than those obtained for the unfolded proteins. This was explained by fact that the folded and unfolded proteins differ in shape and surface charge distribution and therefore the interaction of proteins with the pore will be different. The percent current block remained constant for the folded protein but decreased for the unfolded protein as a function of voltage. This suggests that the volume occupied by the unfolded protein in the pore is smaller than that of folded protein. The authors reasoned that this is a result of the unfolded protein being stretched by increased voltage and therefore occupies smaller volume of the pore. The data obtained with the large pore contained a few

anomalies. For example, the translocation times for the proteins were much larger (millisecond range), than what they were expected to be (microsecond range). This has also been reported in other studies (Niedzwiecki *et al.*, 2010; Sexton *et al.*, 2007; Sexton *et al.*, 2010). The reason for this phenomenon is not yet fully understood. Generally, there are two explanations proposed for this anomaly. First, interaction of the protein with the pore walls leads to longer durations (Niedzwiecki *et al.*, 2010; Sexton *et al.*, 2010). Second, due to the charged walls of the pore there is an electroosmotic effect (Firnkes *et al.*, 2010). Electroosmosis is movement of the solvent across a charged channel as a result of an applied electric and is directly proportional to the applied electric field (Firnkes *et al.*, 2010; Oukhaled *et al.*, 2012). The Si_3N_4 membranes used and the MBP protein are negatively charged, thus the electroosmosis and electrophoresis will be in opposite directions. Therefore, the electroosmosis could slow or even prevent the translocation of the protein. However, the electroosmotic effect under their experimental conditions is not dominant. To gain a better understating of these results, the same experiments were repeated with a smaller 3 nm pore, comparable diameter to the biological pores. With the smaller pore, the protein adsorption and the electroosmotic effect are minimized. Furthermore, the energy barrier was reported to be two times smaller for the smaller pore than for the larger pore.

Other groups have also reported the use of solid-state pores for studying protein folding and unfolding. In 2009, Talaga and Li investigated translocation of β-lactoglbulin and HPr proteins in the presence and absence of urea, a chemical denaturant (Talaga and Li, 2009). Under different concentrations of urea, different folded states of proteins were observed. For example, in the presence of 5 M urea the proteins were mostly in a partially folded state whereas in the presence of 8 M urea the proteins were in an unfolded state. Based on the blockade current amplitudes and durations it was possible to differentiate between different folding states of proteins. Furthermore, based on the amplitude of the blockades it was possible to calculate the excluded volume. However, the calculated excluded volume, as obtained from the blockade amplitudes in the absence and presence of urea, was much smaller in most cases than that of a folded protein. Thus, they reasoned that if the proteins were to translocate through the pore in a linear unfolded confirmation then the excluded volume would be a result of a linear segment of a polypeptide chain within the pore. Taking into account the pore length, the number of the amino acids that can fit within that pore length, and the average volume of a single amino acid,

they were able to calculate the excluded volume for a linear segment of amino acids. This calculated linear segment volume was similar to the calculated excluded volume as obtained from the blockade current amplitudes. Therefore, the authors concluded that the proteins were translocating mostly in the linear unfolded confirmation with only a small portion of proteins translocating in a folded confirmation. However, the authors failed to address how the β-lactoglobulin protein, which contains disulfide bonds, can translocate in linear unfolded confirmation in the absence of a denaturing agent or reducing agent. These results were later contradicted by Strefureac *et al*. (Stefureac *et al.*, 2010b). In the latter study, translocation of HPr, MBP, and calmodulin through 7 nm and 5 nm pores were examined as a function of increased applied voltage. They reasoned that for a molecule translocating through a pore, the resulting excluded volume is expected to remain constant independent of the applied voltage. Since the current block is directly related to the excluded volume, then the current block as a percentage of the open pore current will remain constant as a function of voltage. Furthermore, for molecules being driven across the pore by electrophoresis, the event duration times will decrease with increasing voltage. For HPr and calmodulin the percent current block remained constant independent of the applied voltage while the duration times decreased with increasing voltages, thus suggesting translocations. As for MBP, the percent current block decreased with increasing voltage and the duration times remained roughly constant with change in applied voltage, allowing the authors to conclude that MBP did not translocate the pores. To determine if the translocating proteins translocate unfolded or folded, Stefureac *et al*. calculated the volumes for the folded confirmations and the expected percent block if proteins were to translocate in a folded confirmation and then compared the two. Interestingly, the percent block for translocating calmodulin was twice that of HPr as was the case with their folded state volumes. The possibility that the proteins translocate in linear unfolded confirmation was further rejected because if the proteins were to translocate in linear unfolded confirmation, the excluded volume of the electrolyte inside the pore will be equal to that of a linear segment within the pore as shown by the illustration in Figure 1.10. This is because a pore of 15 nm in length can only fit about 39 amino acids (0.38 nm/amino acid) and this is independent of the protein being investigated and therefore the percent block for HPr and calmodulin would have been the same if that was the case. Therefore the authors concluded that proteins with dimension smaller than the pore translocate in folded confirmation whereas those proteins with

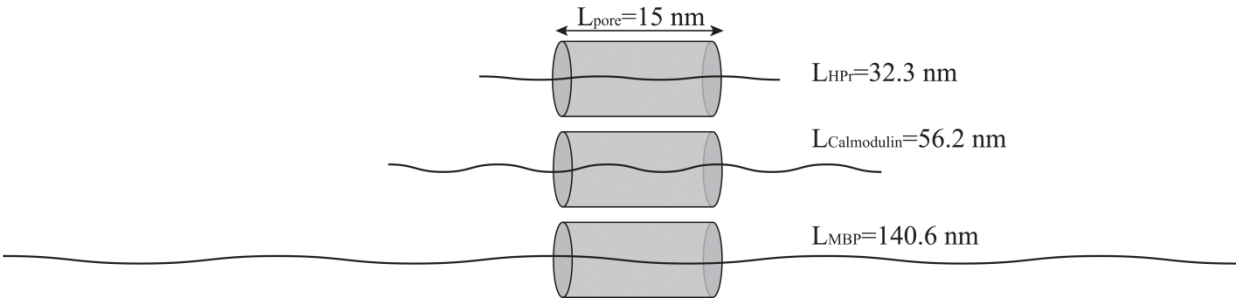

Figure 1.10. A diagram showing the translocation of completely unfolded proteins (histidine-containing phosphotransfer protein, calmodulin, and maltose binding protein) through a solid-state pore. The approximate lengths of the proteins are marked. (Reprinted with permission from Stefureac *et al*., 2010. Copyright 2012 IOP Publishing.)

similar or larger dimensions than the pore will not translocate.

In a recent study by Bayley and coworkers, a new approach is proposed for studying protein unfolding using α-hemolysin pore (Figure 1.11) (Rodriguez-Larrea and Bayley, 2013). In this approach an oligonucleotide is attached to a protein substrate through a linker to facilitate co-translocational unfolding of a protein through the pore. In earlier sections of this thesis it was shown that single-stranded nucleic acids translocate through α-hemolysin pore by electrophoresis at a very fast rate. Thus, by attaching a negatively charged oligonucleotide to an end of a protein, it will provide a driving force for protein translocation as well as protein unfolding. In their study a mutant of the thioredoxin protein was used which mimics the reduced form of the protein and includes additional stabilizing mutations. The wild-type thioredoxin has been studied in a different approach as part of the research performed in this thesis (see results and discussion) (Krasniqi and Lee, 2012). To observe the co-translocational unfolding of the protein, the ionic current passing through the α-hemolysin pore was monitored (Rodriguez-Larrea and Bayley, 2013). The translocation of the protein through the pore appeared as a four-step translocation (i.e a four-step blockade event). It starts with the oligonucleotide entering the pore and pulling on the protein, followed by partial unfolding of the protein as a result of the pulling forces. The rest of the protein is then fully unfolded in the third step and subsequently translocated across the pore in the final step (Figure 1.11). The rate constant for the first and second step increases with increasing voltage while the rate constant for the last two steps is independent of voltage. This could be because during the last two steps the oligo is no longer in the α-hemolysin pore. Furthermore, the charge density on the protein is very low compared to the charge density on the oligo. Therefore, the electrophoretic force acting on the oligo is more pronounced than on the polypeptide. The rate constant of the first step is also dependent on the concentration of the protein-oligonucleotide analyte. To ensure that the first step is related to threading of the oligonucleotide through the pore the authors attached different oligonucleotides to the protein and observed changes in the first step of the event while the other steps were not affected, thus confirming entrance of the oligonucleotide into the pore and subsequent threading. Furthermore, this shows that the oligonucleotide enters the pore first and not the protein. The oligo enters first because it has much higher net charge density than the protein thus the electrophoretic force acting on it is greater. To confirm that steps two and three represent unfolding, the translocation of the oligonucleotide-protein was

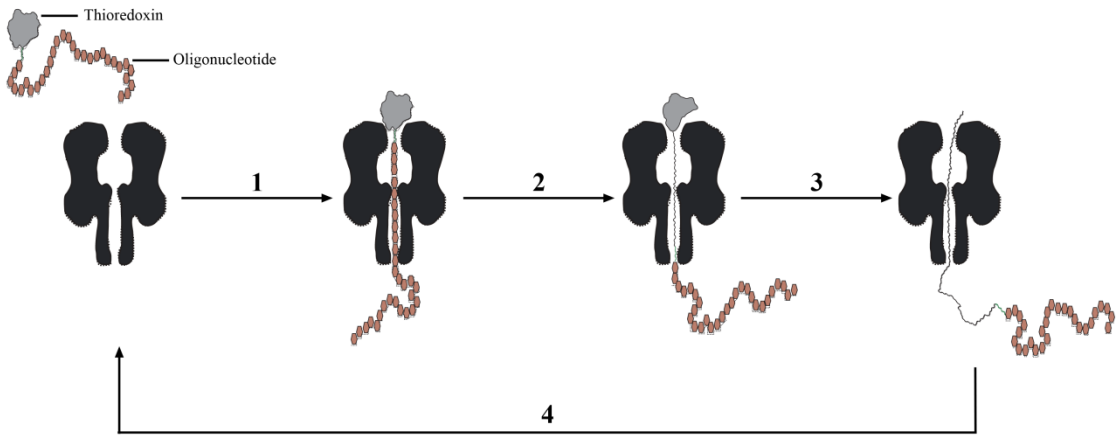

Figure 1.11. A diagram illustrating co-translocational unfolding of a protein molecule through the α-hemolysin pore. A folded protein molecule attached to an oligonucleotide is drawn into the pore due to an applied potential with the oligonucleotide entering the pore first (step 1). Due to the applied potential, the oligonucleotide pulls on the protein causing partial unfolding of the protein (step 2). This continues with the remainder of the protein unfolding and translocating the α-hemolysin pore (step 3). The whole process starts again with another folded protein molecule. (Reprinted with permission from Rodriguez-Larrea and Bayley, 2013. Copyright 2013 Macmillan Publishers Limited.)

examined in the presence of urea. If steps two and three are indeed a result of protein unfolding then their rate constants will increase with increasing urea concentrations. This is because of urea lowering the free energy of unfolding and in turn unfolding proceeding at a faster rate (Rodriguez-Larrea and Bayley, 2013). As expected, the rate constants for steps two and three did increase with increasing concentration of urea, suggesting that these two steps are produced by the unfolding of the protein. The rate constant for the first step decreased at high urea concentration because of the change in viscosity of the electrolyte solution. However, the rate constant for step four was not affected by urea concentration because at that point the protein is fully unfolded and just exiting the pore. Furthermore, at high urea concentrations two types of events were observed: four-step events and single blocked level events (i.e lacking steps 2 and 3). The proportion of the single blockade level events increased as the concentration of urea increased, suggesting that the protein is fully unfolded before entering the pore. Further experiments were conducted to confirm that steps two and three are related to the protein unfolding. Therefore, the results suggest that the unfolding of the thioredoxin protein is a two step process and there is an intermediate species. These findings show that nanopore sensing can be used for studying protein unfolding and can reveal important information, such as existence of intermediates in an unfolding pathway whether or not they are rate limiting.

Lee's group has performed comprehensive studies on protein conformational changes using the α-hemolysin pore (Baran *et al.*, 2010; Madampage *et al.*, 2012; Madampage *et al.*, 2010; Stefureac and Lee, 2008; Stefureac *et al.*, 2010a; Tavassoly and Lee, 2012). The group has studied conformational changes of many proteins induced by metal binding, drug binding, and interaction with other molecules. One such an example is the analysis of myelin basic protein, an intrinsically disordered protein (Baran *et al.*, 2010). Baran *et al*. showed that this highly basic protein translocates through the α-hemolysin pore freely (no bumping events). The translocation of the protein was confirmed indirectly by examining the protein at different voltages. However, upon addition of divalent metal ions (eg. Cu^{2+} and Zn^{2+}), the protein forms a folded conformation and is unable to translocate through the pore. This is evidenced by an increase in proportion of bumping events. The process is readily reversible with the addition of ethylenediaminetetraacetic acid (EDTA). The effect of EDTA on nanopore analysis of proteins has been examined in great detail as part of this thesis and will be discussed in sections 3 and 4 (Krasniqi and Lee, 2012). In a different study, Lee and colleagues investigated the interaction

of divalent metal ions with the full-length bovine recombinant prion protein (Stefureac *et al.*, 2010a). Depending on the metal ion, translocation of the protein molecule was either facilitated or hindered. For example, in the presence of copper, zinc, and nickel metal ions, the proportion of bumping events was increased whereas in the presence of manganese, the opposite was observed. The authors reason that the translocation of this large protein is possible because the proportion of translocation events decreases with voltage. Thus, the applied voltage (100 mV) must be sufficient in facilitating the translocation of the protein. The authors proposed a model for the translocation of the prion protein in which a loop of the protein enters the vestibule and then the rest of the protein is pulled in. A similar model has been previously supported by theoretical studies (Makarov, 2009). The changes in blockade current profiles observed in these studies are clearly an indication of changes in protein confirmation since metal ions alone do not induce any blockade events (Braha *et al.*, 1997). While the authors' explanations for the large blockade events are reasonable, it is difficult to conclude if those events are translocations since the effect of voltage on the blockade times was not examined. As discovered by Meng *et al*. these large blockade events could be intercalation or translocation (Meng *et al.*, 2010). Furthermore, as stated earlier, as of yet there is no direct evidence of protein translocation through the α-hemolysin pore and as it will be shown in the results section, the effect of voltage on blockade times does not always identify whether the large blockade events are translocations or intercalations. A large part of the work done on this thesis addresses this issue.

Conformational changes as a result of ligand binding have also been reported for α-synuclein, another intrinsically disordered protein (Tavassoly and Lee, 2012). The misfolding of this 140 amino acids protein plays a crucial role in Parkinson's disease. It's been reported that people with methamphetamine addiction (a recreational drug) are more prone to development of Parkinson's disease (Tavassoly and Lee, 2012). For this reason, Tavassoly *et al*. investigate the effect of methamphetamine binding to α-synuclein and subsequent conformational changes using α-hemolysin pore. By monitoring the ionic current passing through the α-hemolysin pore it was possible to observe conformational changes to α -synuclein protein in the presence of methamphetamine. In the absence of drug binding, the protein translocates through the pore freely, with 80% of the events being translocation events. Upon drug binding, the proportion of translocation events decreases and that of bumping events increases, indicating a conformational change. The methamphetamine binding to α-synuclein

was also investigated using CD, but CD failed to detect any conformational changes. This implies that the conformational change caused by the binding of the methamphetamine to the protein does not induce an α-helical or β-sheet conformation. This shows that nanopore sensing is a good technique for detecting very subtle conformational changes. Furthermore, by investigating the interaction of the drug with different regions of the protein, the authors were able to demonstrate that methamphetamine binds to the N-terminal region of the protein.

Similarly, Madampage *et al*. have shown that antibody-protein and antibody-peptide interactions can be detected using nanopore sensing (Madampage *et al.*, 2010). It was shown that the prion protein alone induces certain types of events while the prion-antibody complex induces other types of events. The authors were able to subtract those events produced by antibody alone as background and demonstrate prion-antibody binding. The authors went to suggest that by employing the sensitivity of nanopore sensing and the specificity of the antibody, it would be possible to develop a prion detector device.

Lastly, just this year, Mark Akeson's group has proposed a nanopore-based method, analogous to DNA sequencing with polymerase, for sequencing proteins (Nivala *et al.*, 2013). In this method, an enzyme is used to facilitated unfolding and translocation of native proteins through α-hemolysin pore. The enzyme exploited for this purpose was ClpX from the ClpXP proteasome-like complex which is responsible for drawing proteins through pores into a proteolytic chamber for degradation. More specifically, they chose *E. coli* ClpX because it provides sufficient force (~20 pN) for denaturing stable protein folds at a rate suitable for sensing changes in primary sequence using nanopores (~ 80 amino acids per second) (Nivala *et al.*, 2013). The protein substrates were modified to contain an anionic peptide tail which facilitates entry into the pore (see Figure 1.12). In addition, the peptide tail was capped with an 11 amino acid tag for targeting ClpX. In order for ClpX protein to function it requires ATP. Therefore, ClpX together with ATP were added to the *trans* side of the pore and the protein substrate was added to the *cis* side of the pore (see Figure 1.12). Once the peptide tag was translocated to the *trans* side, it was bound by the ClpX enzyme and then the enzyme moved along the chain, thereby pulling the chain towards the *trans* side. The applied pulling force was sufficient to unfold the protein and cause it to translocate through α-hemolysin pore. By monitoring the ionic current flow it was possible to identify different segments of protein as it passed through the pore, based on sequence-dependent features. While this study is just a

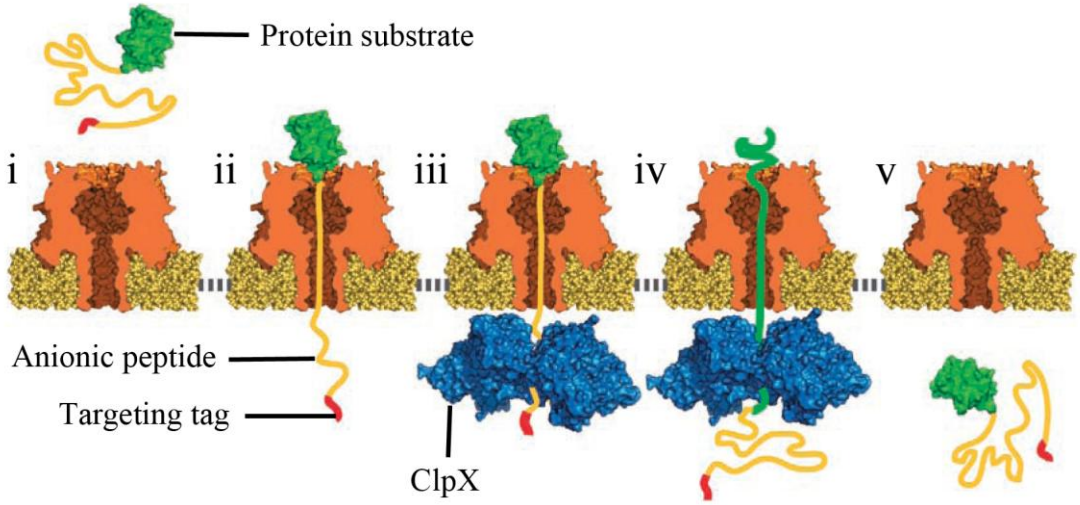

Figure 1.12. A diagram illustrating controlled unfolding and translocation of native proteins through the α-hemolysin using ClpX enzyme. A native protein substrate added to the *cis* chamber is attached to an anionic peptide which is pulled into the pore as a result of applied potential (steps i and ii). The anionic peptide contains targeting tag specific for ClpX enzyme. Once the peptide tag is translocated to the *trans* side, it is bound by the ClpX enzyme and then the enzyme moves along the chain, thereby pulling the chain towards the *trans* side (steps iii and iv). The applied pulling force is sufficient to unfold the protein and cause it to translocate through α-hemolysin pore in unfolded confirmation (step v). (Reprinted with permission from Nivala *et al*., 2013. Copyright 2013 Nature Publishing Group.)

proof-of concept, it shows the potential for a nanopore-based protein sequencing platform.

In summary, the selected studies presented in this section demonstrate the ability of nanopore sensing to provide detailed information about structure and function of a protein and the potential of using this technique for sequencing proteins.

1.2.3 Nanopore sensing of enzyme kinetics

In 1996, the first nanopore sensing publication, reported the hydrolysis of long polymers of polyuridylic acid by RNase A (Kasianowicz *et al.*, 1996). With the addition of RNase A to the *cis* chamber containing polyuridylic acid the frequency of events increased dramatically, suggesting increased molar concentration of short polymers as a result of hydrolysis of the long polymers by RNase A. While the purpose of this study was to show that nanopore sensing can be used for sequencing DNA, it also showed the potential of this technique as a tool for monitoring enzyme activity. Over a decade later, Zhao *et al*. successfully demonstrated the possibility of probing enzyme kinetics with nanopores (Zhao *et al.*, 2009a). In their study, they are able to monitor peptide cleavage by trypsin in real-time. Trypsin is a serine protease enzyme that cleaves peptide bonds after arginine or lysine amino acid residues. Upon nanopore analysis of a peptide substrate alone, a single type of blockade events with large duration times and small blockade amplitudes were observed. However, after addition of trypsin to the chamber containing the peptide substrate, two new types of events with short duration times and large blockade amplitudes were observed. These two types of events were confirmed to be induced by the breakdown products from the enzymatic reaction. After an hour the events corresponding to the full peptide substrate disappeared, indicating that all of the substrate had been cleaved. Therefore, the concentration of the products after 1 hr would be equal to the initial concentration of the peptide substrate. Since the frequency of the events is directly related to the concentration of substrate, one can calculate the concentration of the substrate at any time using the frequency of events. Furthermore, the rate of the reaction at any time is proportional to the change in frequency of the breakdown products. Therefore, plotting the reciprocals of the substrate concentrations vs. the reciprocals of the change in frequency of the breakdown products will yield a Lineweaver-Burk curve. Of course, the Michaelis constant, K_m, and maximum reaction rate, V_{max}, can be obtained from the inverse of x- and y-intercepts of the Lineweaver-Burk curve, respectively.

In a different report, Fennouri *et al*. utilized the aerolysin pore to monitor the hydrolysis of hyaluronic acid, an anionic carbohydrate, by the hyaluronidase enzyme (Fennouri *et al.*, 2012). Hyaluronic acid is a polymer of disaccharides, D-glucuronic acid and D-N-acetylglucosamine, which can reach in size up to couple million Da. The enzyme, hyaluronidase is responsible for hydrolyzing the glycosidic bonds between D-glucuronic and D-N-acetylglucosamine residues. The authors chose a hyaluronic acid with very high degree of polymerization (i.e high molecular weight) and added it to the *cis* side of the aerolysin pore. However, due to its large size there were no events observed. Shortly after adding the enzyme to the same chamber, events with very long duration started appearing, suggesting translocation of long hyaluronic acid fragments. With time, the frequency of events increased and the duration of the events observed decreased, indicating higher molar concentration of fragments and higher number of smaller fragments. Using high-resolution mass spectrometry the authors provided direct evidence of carbohydrate translocation through a nanopore.

Together these studies show that nanopore sensing can be used to monitor enzyme reactions and explore enzyme kinetics without immobilization or labelling of the substrate.

1.3 Applications of nanopore sensing

Two decades ago, the number of research groups and publications in the nanopore field were just a few and DNA sequencing was the focus of this technique. Today, the ease, cost, speed, and quality has made nanopore sensing an attractive single-molecule technique to over a hundred research groups around the world for a wide range of applications (Albrecht *et al.*, 2010; Majd *et al.*, 2010; Mulero *et al.*, 2010; Oukhaled *et al.*, 2012; Rhee and Burns, 2006; Stoloff and Wanunu, 2012). Various technical improvements and discoveries have been made which allow nanopore sensing to achieve high efficiency, sensitivity, and selectivity. The ability to detect and differentiate single nucleoside 5'-monophosphate molecules with 99.8% accuracy, as well as the ability to control translocation of DNA across a pore shows great potential for development of nanopore-based DNA sequencing platform (Cherf *et al.*, 2012; Clarke *et al.*, 2009; Manrao *et al.*, 2012). Successful detection and differentiation between methylated cytosines and normal cytosines by nanopores can be useful in investigation of epigenetic modifications (Clarke *et al.*, 2009; Jetha *et al.*, 2011). Furthermore, as Ang *et al*. showed, nanopores are capable of detecting SNPs (Ang and Yung, 2012). SNPs are the most

common genetic variations between two individuals. In addition, some SNPs predispose individual to have a certain disease or drug reaction. Therefore, they are important biomarkers for many diseases and play a critical role in the development of personalized medicine. This in turn indicates that nanopores could be applied in early detection of diseases and drug discovery and development. As detailed in section 1.1.1, nanopores can also be successfully applied to detection and quantification of specific microRNAs (Wang *et al.*, 2011b; Wanunu *et al.*, 2010). Wang *et al*. reported that nanopore sensing can be used to quantify specific microRNAs in lung cancer patients with very high accuracy and speed while requiring no labelling or amplification. Hence this study could inspire the use of nanopores for early detection of cancer or for other applications, as microRNAs are implicated in many biological processes.

New reports in protein studies with nanopores show that nanopore sensing technique is already being applied for the study of neurodegenerative diseases such as Alzheimer disease, Parkinson's disease, and prion related diseases (Jetha *et al.*, 2013; Madampage *et al.*, 2012; Tavassoly and Lee, 2012; Wang *et al.*, 2011a). All of these diseases are associated with protein misfolding and aggregation. The proteins involved are prone to aggregation at high concentrations. Therefore, the employment of nanopores for these studies is particularly intriguing, because very low concentrations of these proteins are required for their analysis. Furthermore, these proteins can adopt multiple conformations and therefore nanopore sensing is an ideal technique since it can detect multiple species in the same sample (Sutherland *et al.*, 2004; Tavassoly and Lee, 2012). Lee's group has proposed that by using the sensitivity of the pore and the specificity of a prion antibody, a prion detector may be potentially developed (Madampage *et al.*, 2010). In addition, the findings by Fennouri *et al*. indicate that nanopore sensing is a valuable tool for detecting and probing glycosaminoglycans (Fennouri *et al.*, 2012). Glycosaminoglycans have been recently considered as important biomarkers for metabolic disorders, cancer, and immune diseases (Fennouri *et al.*, 2012). Therefore, the study of these diseases is another potential utilization of nanopores.

As it's been shown by several groups by modifying the biological pores or solid-state pores, the sensitivity and selectivity of the technique is greatly improved and can be used to detect target analytes in very dilute solutions (Rotem *et al.*, 2012; Soskine *et al.*, 2012; Wei *et al.*, 2012; Yusko *et al.*, 2011; Yusko *et al.*, 2012). The detection and differentiation capability of this technique continues to be the most common use. This feature of the technique has been

explored in detection and/or differentiation of wide range of analytes, including bioterrorist agent ricin (Ding *et al.*, 2009). Therefore, the application of this specific feature of the technique can be left to the researcher's imagination.

1.4 Other single-molecule techniques

Over the past two and a half decades, the popularity of single-molecule techniques has grown tremendously as evidenced by a constant increase in the number of publications utilizing these techniques. This is because of their power in providing the ability to study biological processes at the single-molecule level. Unlike nanopore sensing, other single-molecule techniques require substrate immobilization and/or labelling. Here I will outline the principles behind some of these techniques. The most common techniques used for probing biomolecules at the single-molecule level are: AFM, optical tweezers, and smFRET. AFM and optical tweezers are force manipulation based techniques (Cornish and Ha, 2007).

AFM was developed in 1986 as an instrument which can be used for producing an image of the sample being probed, measure forces, and manipulating matter at the nanometer scale (Binnig *et al.*, 1986). The apparatus consists of a flexible cantilever with an attached sharp tip, a laser beam, a photo-diode, and a piezoelectric tube (Binnig *et al.*, 1986; Kasas *et al.*, 1997). To produce an image, a sample is fixed on the piezo tube and then the sharp tip of the cantilever is used to scan the surface of the sample with the laser beam shining onto the cantilever. As the tip interacts with the surface of the sample, forces between the tip and the sample lead to cantilever displacement, resulting in deflections of the laser beam and these deflections are detected by the photodiode. The deflections are then recorded and used to construct a topography image of the sample. The applied force by the cantilever is kept well below the force which would disturb the sample and thus the sample is imaged non-destructively. The resolution of the image is depended on the size of the cantilever and on the shape of the tip. For example, sharper the tip and small cantilever indicate better resolution (Kasas *et al.*, 1997; Santos and Castanho, 2004). The AFM technique can achieve a resolution of 1 nm (Santos and Castanho, 2004). In terms of imaging applications, AFM has been used to study the structure of different biomolecules, viruses, bacteria, cells, and morphology of organs (Billingsley *et al.*, 2012; Bockelmann, 2004; Bornschlogl and Rief, 2011; Casuso *et al.*, 2011; Kasas *et al.*, 1997; Samorì *et al.*, 2005; Santos and Castanho, 2004). Besides imaging, AFM can also be used for

measuring forces and manipulating matter at the nanometer scale. For example, AFM can be used to mechanically unfold a protein and measure unfolding and refolding forces (Bornschlogl and Rief, 2011; Casuso *et al.*, 2011; Samorì *et al.*, 2005). To do this, one end of the protein molecule is bound to the cantilever tip and the other end to a surface. The surface and the tip are moved relative to each other and the forced applied to the protein molecule is measured by deflections of the cantilever. After unfolding the protein, the applied force is released by changing the direction of the movement and then the refolding forces are measured. A similar approach is used to measure interactions between two molecules (Bockelmann, 2004). For example, one molecule is attached to the tip and the other to the surface. Molecules are brought in close proximity to interact and then the tip is pulled back. The binding strength between the two molecules is measured by the cantilever deflections. To date the technique has been successfully applied in measuring forces in protein unfolding and refolding and intermolecular interactions. It can be used to measure interactions as weak as 1 pN (eg. single hydrogen bond) (Kasas *et al.*, 1997). While the AFM technique is capable of high forces (up to 10 000 pN) and therefore can be used to study large molecules, the force noise is high as well. On the other hand, optical tweezers provide lower applied forces and the force noise is lower than that of AFM technique (Samorì *et al.*, 2005).

Optical tweezers (or optical traps) is another single-molecule technique which relies on force manipulation of the substrate (Cornish and Ha, 2007). This technique was developed in the early 1970s. It relies on the use of a highly focused laser beam with an objective lens of high numerical aperture to trap and manipulate objects as small as atoms (Neuman and Block, 2004). The objective lens is the most important part of optical tweezers apparatus. It is the objective lens that is responsible for focusing the laser beam to a spot which is known as an optical trap. Any small particle (eg a bead) near the optical trap will be trapped by the force of the laser beam. The force acting on the particle is generated as a result of the change in momentum of the incoming light from the laser as the light hits the object. In the case of biomolecule studies, the molecule is attached to the trapped bead and then manipulated so that physical properties can be studied. For example, optical tweezers have been used to induce mechanical unfolding and refolding of protein molecules (Ashkin, 2000; Bockelmann, 2004; Cecconi *et al.*, 2005). Optical tweezers can measure forces with sensitivity of down to 100 aN (Zhang and Liu, 2008). Furthermore, optical tweezers have become an essential tool for

manipulating single cells (eg. cell sorting, transporting foreign materials into single cells, and delivering cells to specific locations) (Zhang and Liu, 2008).

SmFRET is another powerful single-molecule technique which is commonly used for probing conformational changes of biomolecules and intermolecular interactions (Cornish and Ha, 2007). SmFRET is an application of FRET. In FRET, energy is transferred from a donor molecule, which is excited by a light source, to an acceptor molecule, which is within a distance of 2-8 nm, via an induced-dipole, induced-dipole interactions (Ha, 2001a, b; Ha *et al.*, 1996). As the donor and acceptor come closer together the donor emission decreases in intensity while the acceptor emission increases. If the two are far apart then there is no interaction between the two and therefore no energy transfer. The use of FRET was first demonstrated by Streyer and Haugland in 1967 for ensemble measurements and since then it has been extensively used for probing intermolecular interactions and conformational changes (Michalet *et al.*, 2006). In 1996, Ha *et al*. extended FRET to single-molecule level by demonstrating the measuring of energy transfer between a single donor fluorophore and a single acceptor fluorophore with the aid of near-field scanning optical microscopy (Ha *et al.*, 1996). Near-field scanning optical microscopy allows optical measurements with sub-wavelength resolution. Therefore, in smFRET the energy transfer can be measured on a single donor-acceptor pair allowing monitoring conformational changes down to 0.5 nm (Cornish and Ha, 2007; Ha *et al.*, 1996). SmFRET has been successfully utilized to study replication, transcription, translation, RNA folding, RNA catalysis, signal transduction, protein folding, and protein conformational changes (Roy *et al.*, 2008). For example, when studying protein folding, the donor and acceptor dyes are attached to the protein such that the folded state has high FRET whereas the unfolded state has very low FRET.

As detailed here, all three single-molecule techniques (AFM, optical tweezers, and smFRET) are used extensively for a wide range of studies and they are highly sensitive. However, unlike nanopore sensing, all three techniques require substrate immobilization and/or labeling.

1.5 Thesis objectives

Nanopore sensing has proved to be a valuable single-molecule technique for characterizing peptides and proteins. More specifically, it has been demonstrated that nanopore-sensing

utilizing wild-type α-hemolysin pore can distinguish between different peptides and proteins, including single-amino acid mutants. However, there are a number of anomalies and disagreements in the literature. So the overall objective is to address some of these issues.

The first set of experiments were designed to investigate what structural features do nanopores interrogate. This aim is to be achieved by analyzing retro, inversed, and retro-inversed isomers of glucagon and α-helical Fmoc-$D_2A_{10}K_2$ peptide. It has been shown that the engineered α-hemolysin pore can differentiate between chiral drug molecules and chiral amino acid isomers (Boersma and Bayley, 2012; Kang *et al.*, 2006). However, there have been no reports on detection and differentiation of chiral and/or directional peptide isomers using the wild-type α-hemolysin pore. By subjecting both chiral and directional peptide isomers to nanopore analysis it will allow examination of the sensitivity of the technique and determine if the pore is recognizing structure, sequence, or both.

The next objective of the project was to gain a better understanding of nanopore analysis of proteins by examining a series of native proteins with different physical and chemical properties. Until recently most of the work with this technique has been focused on peptides and nucleic acids. In addition, as stated earlier, there have been reports of anomalies in protein analysis (Oukhaled *et al.*, 2012; Plesa *et al.*, 2013). Therefore, it's important to understand what the limits of the technique might be in regards to proteins. Further analysis of these proteins under different experimental condition (eg. different applied voltages, different buffers, different ligands, in the presence of denaturing agents and/or reducing agents, etc.) will provide a better understanding of the interaction of proteins with the α-hemolysin pore.

While there have been reports of protein translocation through α-hemolysin pore, there is no direct evidence, as yet, that proteins can translocate the α-hemolysin pore. The evidence provided in these reports is indirect at best because it’s based on the interaction of the proteins with the pore as a function of voltage. Most proteins analyzed with nanopore sensing are larger than the smallest constriction of the α-hemolysin pore. Therefore, in order for proteins to translocate through the pore, they must unfold. If proteins are unfolding to translocate, then nanopore sensing would be a powerful single-molecule technique for studying protein folding and unfolding. Hence, the final set of experiments was designed to determine if proteins translocate the α-hemolysin pore. For this purpose, an enzyme was chosen where direct evidence would be possible by demonstrating activity on the *trans* side of the pore, thus

providing an amplification of the signal. More specifically, RNase A was chosen because even if it unfolds to translocate through the pore, it would readily refold to an active conformation once in the *trans* chamber (Cao *et al.*, 2001; Neira and Rico, 1997; Reinstadler *et al.*, 1996; Wedemeyer *et al.*, 2000). However, the α-hemolysin pore on average remains viable for only few hours, thus few putative translocations can be achieved. Therefore, as part of this objective, an RNase A detection assay needed to be designed.

Lastly, the final experiments were set up to use solid-state pores as positive controls for protein translocation through the α-hemolysin pore. This objective can be achieved through the use of solid-state pores with dimensions larger than RNase A, where translocation would not be prohibited by the size of the pores (Fologea *et al.*, 2007; Stefureac *et al.*, 2010b). Together, these experiments will provide a basis for the future nanopore analysis of proteins.

2.0 MATERIALS AND METHODS

2.1 Reagents, supplies, and equipment

The list of reagents, supplies, and equipment used in conducting this research are presented in Table 2.1. Table 2.2 lists the names and addresses of companies where the reagents, supplies, and equipment were purchased.

2.2 Nanopore sensing and patch-clamp experimental setup

The nanopore sensing apparatus consist of the patch-clamp hardware, solid-state pores or the lipid bilayer and biological pores, and the patch-clamp data recording and processing software. Each component of the apparatus is described below.

2.2.1 The patch-clamp hardware

The patch-clamp apparatus/hardware is shown in Figure 2.1 and consists of six main components: the perfusion unit, the electrodes, the Faraday Cage, the headstage, the amplifier, and the digitizer. All components are connected together and the information is relayed from one component to the next. The whole patch-clamp apparatus is connected to a computer which is used for data recording and processing. Each component of the hardware is described below.

The perfusion unit varies between experiments conducted with biological pores and those conducted with solid-state pores. In the experiments with biological pores (i.e α-hemolysin), the perfusion unit (Warner Instruments) consist of a holder (black) and cup (white) (shown in Figure 2.1a) which are made up of black and white Derlin, respectively. The cup is mounted into the holder with a screw holding the cup in place. Both the holder and cup contain wells of 1 mL volumes which are filled with the same electrolyte solution, unless stated otherwise. A 150 μm aperture is incorporated into the cup wall which separates the two electrolyte-filled wells/chambers. In most of the experiments in this thesis (unless stated otherwise), the cup well will be referred to as the *cis* chamber whereas the holder well will be referred to as the *trans* chamber. The perfusion unit is placed in a copper block which is set on top of an air floating table (Kinnetic Systems) to shield it from electrical and vibrational interference (Figure 2.1c).

Table 2.1. Chemical and biological reagents, equipment, and supplies.

Item	Supplier
Chemical and biological reagents	
1,2-diphytanoyl-*sn*-glycero-3-phosphocholine in chloroform	Avanti Polar Lipids
4-(2-Hydroxyethyl)piperazine-1-ethanesulfonic acid (HEPES)	BDH
Acetic acid, glacial ($C_2H_4O_2$)	BDH
Agarose	EMD
Alpha-globin primers	Sigma-Genosys
Alpha-hemolysin	Sigma-Aldrich
Avidin , hen's egg white	ProSpec
Beta-globin primers	Sigma-Genosys
Basic pancreatic trypsin inhibitor (BPTI), bovine lung	ProSpec
Citric Acid	BDH
Copper sulfate ($Cu_2SO_4 \cdot 5H_2O$)	Sigma-Aldrich
Decane (anhydrous)	Sigma-Aldrich
Diethyl pyrocarbonate (DEPC)	Sigma-Aldrich
Disodium ethylenediaminetetraacetate dehydrate (EDTA-Na_2)	Sigma-Aldrich
D-Lactose monohydrate	Sigma-Aldrich
D-Maltose monohydrate	Sigma-Aldrich
DNA Ladder	New England Biolabs
E. coli thioredoxin, recombinant	Sigma-Aldrich
Ethanol	EMD
Ethidium Bromide	Sigma-Aldrich
Fmoc-$D_2A_{10}K_2$ peptide	Sigma-Genosys
Fmoc-$D_2A_{10}K_2$ peptide, all D amino acids	CHI Scientific
Fmoc-$K_2A_{10}D_2$ peptide	CHI Scientific
Fmoc-$K_2A_{10}D_2$ peptide, all D amino acids	CHI Scientific
Gel loading dye	New England Biolabs

Guanidine hydrochloride (GdnHCl)	Sigma-Aldrich
Human thioredoxin, recombinant	Sigma-Aldrich
Hydrochloric acid (HCl)	BDH
Hydrogen peroxide (H_2O_2)	EMD
Lysozyme, hen's egg white	Sigma-Aldrich
Magnesium chloride ($MgCl_2$)	BDH
Maltose binding protein, recombinant (MBP)	VLI Research
Nitric acid (HNO_3)	EMD
Nitrogen (gaseous)	Praxair
Nuclease-free Water	Life Technologies
Potassium chloride (KCl)	EMD
Potassium phosphate dibasic (K_2HPO_4)	Thermo Fisher Scientific
Potassium phosphate monobasic (KH_2PO_4)	Thermo Fisher Scientific
Rabbit Globin mRNA	Sigma-Aldrich
Ribonuclease A, bovine pancrease (RNase A)	MP Biomedicals
RNaseZap	Life Technologies
RT-PCR Kit (One Step RT-PCR kit)	Qiagen
Sephadex G-50	GE Healthcare Life Sciences
Sodium Acetate (CH_3COONa)	Sigma-Aldrich
Sodium bicarbonate ($NaHCO_3$)	Sigma-Aldrich
Sodium carbonate, Na_2CO_3	Sigma-Aldrich
Sodium hydroxide (NaOH), pellets	EMD
SP Sepharose Fast Flow	GE Healthcare Life Sciences
Sulfuric acid (H_2SO_4)	EMD
Tris(2-carboxyethyl)phosphine hydrochloride (TCEP)	Sigma-Aldrich
Tris-[hydroxymethyl] aminomethane (Tris)	Thermo Fisher Scientific
Trisodium citrate dehydrate	Sigma-Aldrich
Ubiquitin, Bovine red blood cells	Sigma-Aldrich
Zinc chloride ($ZnCl_2$)	EMD

Equipment and supplies

Active-air floating table	Kinetic Systems
Aerosol-barrier filter tips with low binding properties	Ultident Scientific
Amplifier, Axopatch 200B	Axon Instruments
Digitzer, DigiData 1440A	Axon Instruments
Faraday cage	Warner Instruments
Folded capillary cells	Malvern Instruments
Gel imaging platform, AlphaDigiDoc	Alpha Innotech
Gel loading pipette tips	Ultident Scientific
Glass capillary tubes	World Precision Instruments
Glass vials with caps	Kimble Chase & VWR
Headstage, CV203BU	Axon Instruments
Microcentrifuge, Hettich Mikro 20	Hettich Zentrifugen
Microcentrifuge tubes, non-stick	Life Technologies
Origin 7 graphing software	OriginLab
Paintbrushes, size 000	Island Blue
Parafilm	VWR
Pasteur pipettes	VWR
pClamp 9.0 and 10.1 software suite	Axon Instruments
PCR microcetrifuge tubes	VWR
PCR thermocycler	MJ Research
Perfusion bilayer chamber and cup	Warner Instruments
pH meter	Thermo Fisher Scientific
Pipettes	Eppendorf
Power supply, ONEAC PC750A	Oneac
Silicone elastomer sheet	McMaster-Carr
Silver wire	Alfa Aesar
Solid-state pores	NanoPore Solutions
Syringe filters, 0.2 μm	Thermo Fisher Scientific
Syringe needles	Becton Dickinson

Syringes, microliter	Hamilton
Syringes, milliliter	Becton Dickinson
Ultrasonic cleaner, Branson 1510	Branson Ultrasonics
Vacuum desiccators	Bel-Art Products
Zetasizer Nano ZS	Malvern Instruments
Other laboratory consumables (eg. PCR microcentrifuge tubes, gloves, conical tubes, etc)	VWR

Table 2.2. Companies and Addresses

Company	Address
Alfa Aesar	Alfa Aesar, Ward Hill, MA, USA
Alpha Innotech	Protein Simple, Toronto, ON, Canada
Avanti Polar Lipids	Avanti Polar Lipids, Alabaster, AL, USA
Axon Instruments	Molecular Devices,Sunnyvale, CA, USA
BDH	VWR International, Edmonton, AB, Canada
Becton Dickinson	Becton Dickinson Canada, Mississauga, ON, Canada
Bel-Art Products	Bel-Art Products, Wayne, NJ, USA
CHI Scientific	CHI Scientific, Maynard, MA, USA
EMD	EMD Millipore, Gibbstown, NJ, USA
Branson Ultrasonics	Branson Ultrasonics, Danbury, CT, USA
Eppendorf	Eppendorf Canada, Mississauga, Ontario, Canada
GE Healthcare Life Sciences	GE Healthcare Life Sciences, Baie d'Urfe, Quebec, Canada
Hamilton	Hamilton Company, Reno, NV, USA
Hettich Zentrifugen	Hettich Lab Technology, Beverly, MA, USA
Island Blue	Island Blue Print, Victoria, BC, Canada
Kinetic Systems	Kinetic Systems, Boston, MA, USA
Life Technologies	Life Technologies, Burlington, ON, Canada
Malvern Instruments	Malvern Instruments, Malvern, Worcestershire, UK
McMaster-Carr	McMaster-Carr, Santa Fe Springs, CA, USA
MJ Research	Bio-Rad Laboratories Canada, Mississauga, Ontario, Canada
MP Biomedicals	MP Biomedicals Solon, OH, United States
NanoPore Solutions	NanoPore Solutions, Cascais, Portugal
New England Biolabs	New England Biolabs Canada, Whitby, ON, Canada
Oneac	Powervar Canada, Ajax, ON, Canada
OriginLab	OriginLab, Northampton, MA, USA
Praxair	Praxair, Saskatoon, SK, Canada
ProSpec	ProSpec-Tany TechnoGene, Rehovot, Israel
Qiagen	Qiagen Canada, Mississauga, ON, Canada

Sigma-Aldrich	Sigma-Aldrich Canada, Oakville, ON, Canada
Sigma-Genosys	Sigma-Aldrich Canada, Oakville, ON, Canada
Thermo Fisher Scientific	Fisher Scientific Company, Ottawa, ON, Canada
Ultident Scientific	Ultident Scientific, St. Laurent, QC, Canada
VLI Research	VLI Research, Malvern, PA, USA
VWR	VWR International, Edmonton, AB, Canada
Warner Instruments	Warner Instruments, Hamden, CT, USA
World Precision Instruments	World Precision Instruments, Sarasota, FL, USA

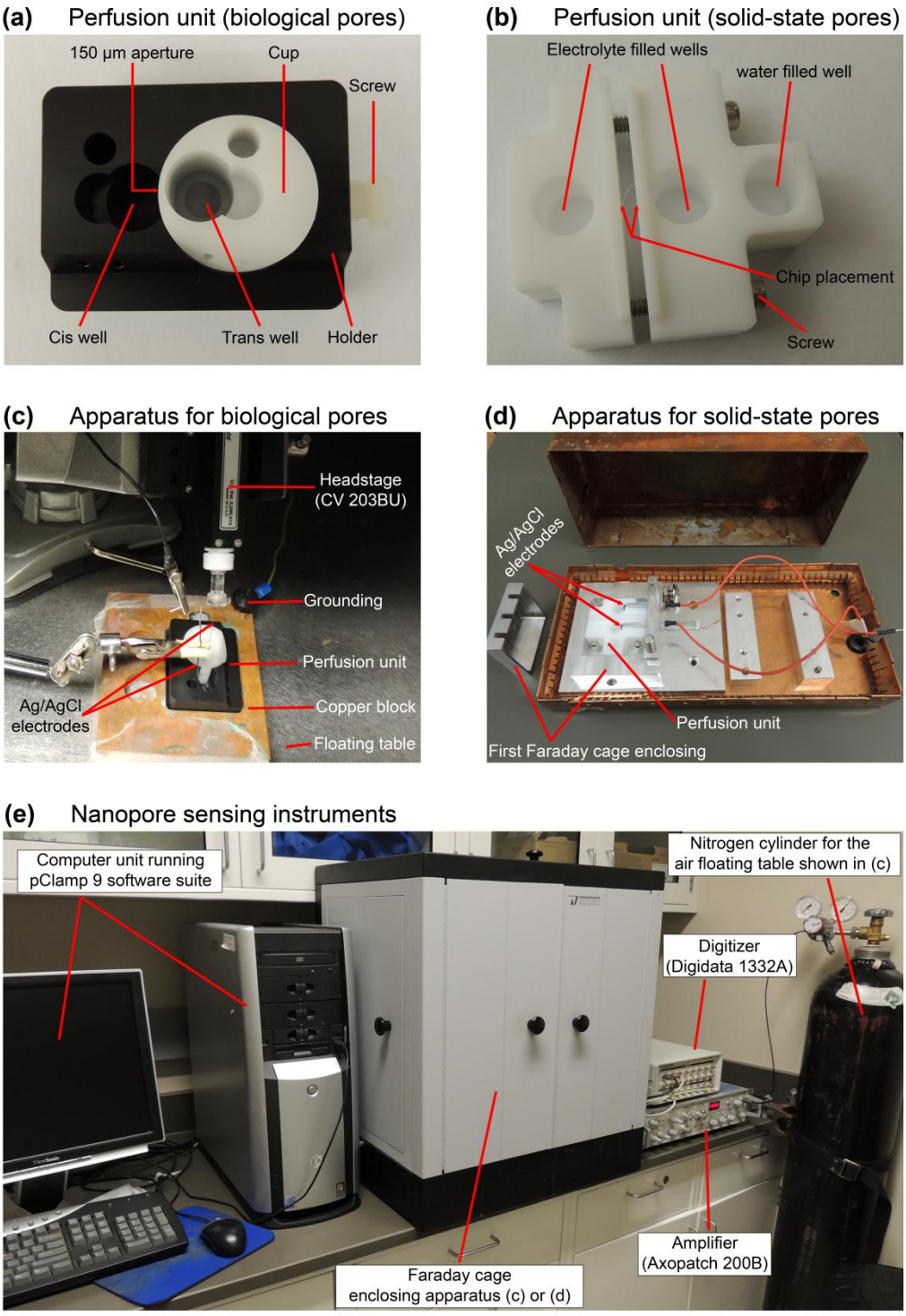

Figure 2.1. Nanopore sensing experimental setup. (a) Perfusion unit used in experiments with biological pore. (b) Perfusion unit used in experiments with solid-state pores. (c) Typical set up of a nanopore sensing experiment utilizing biological pores. (d) The apparatus used in nanopore sensing experiments utilizing solid-state pores. The whole unit sits on top of the air floating table enclosed in the Faraday cage. (e) The patch-clamp instruments and other equipment used in nanopore sensing experiments.

In contrast, for nanopore sensing experiments with solid-state pores, the perfusion unit consists of a two piece polytetrafluoroethylene cell which contains 3 wells with volumes of 0.5 mL (Figure 2.1b). Two of the wells (one from each piece) are filled with electrolyte solution whereas the extra well is filled with water to help minimize the evaporation of the electrolyte during an experiment. The silicon support chip which incorporates the solid-state pore is sandwiched between two silicone elastomer gaskets which are used to ensure a gigaohm seal between the two wells of the cell. The sandwiched silicon chip is placed between the two electrolyte-filled wells and the two pieces of the cell are then held together by screws. The whole cell assembly is placed into an aluminum housing unit which is used to reduce electromagnetic noise. This aluminum housing unit containing the electrodes and the perfusion unit is placed into a small Faraday cage (Figure 2.1d). This is followed by placing the small Faraday cage on top of an air floating table (Kinnetic Systems) to shield it from electrical and vibrational interference. The floating table is housed in a larger Faraday cage (Warner Instruments) shown in Figure 2.1e. Everything inside the cage is grounded to a copper rod found on the metal cover of the cage and then connected to the amplifier's signal ground. The solid-state apparatus shown in Figure 2.1d was provided by Dr. Andre Marziali from the University of British Columbia (Tabard-Cossa *et al.*, 2007).

The Ag/AgCl electrodes were prepared by soaking silver wire (Alfa Aesar) into a bleach solution for at least 2 hours to allow coating with AgCl (i.e anodizing). After an experiment the electrodes were revived by sanding them with sand paper and re-soaking them in bleach solution. The electrodes were replaced frequently with new silver wire. For those experiments performed without the use of salt bridges, one end of the electrode was immersed directly into one of the wells of the perfusion unit and the other end was connected to the headstage unit (model CV203BU, Axon Instruments). In contrast, when using salt bridges, the electrodes were immersed into microcentrifuge tubes to avoid direct contact with the wells of the perfusion unit. The solution used in the microcentrifuge tubes is the same as the electrolyte solution in the perfusion unit wells. The salt bridges (U-shaped) are used to make a connection between the microcentrifuge solution and the well solution. The salt bridges were prepared by filling U-shaped glass tubing with 1.5% nuclease free and PCR pure agarose (EMD Chemicals) in 3 M KCl (w/v). Upon preparation, the U-shaped agarose bridges were placed in fresh 3 M KCl solution and stored for up to a week. For most experiments the measuring electrode is

connected to the *trans* chamber while the reference electrode was connected to the *cis* chamber. It's important to note that the term "salt bridges" used in this thesis does not refer to salt bridges occurring in proteins between amino acid side-chains.

The voltage bias, controlled through the patch-clamp amplifier (Axopatch 200B, Axon Instruments) using the voltage clamp recording mode, is applied via the two Ag/AgCl electrodes. The signal is then transmitted from the electrodes through the headstage back to the patch-clamp amplifier which converts the voltage to current. The analog signal from the amplifier is then further filtered and converted to a digital signal by the digitizer (DigiData 1322A, Axon Instruments).

2.2.2 Lipid bilayer formation and pore insertion

The lipid bilayer formation process can be divided into three steps. First, the lipid solution is prepared before performing a nanopore experiment. In this step, 75 µL aliquots of 10 mg/mL 1,2-diphytanoyl-*sn*-glycero-3-phosphocholine in chloroform (Avanti Lipids) are prepared and stored at -20 °C until needed for an experiment. When needed an aliquot is taken and dried under vacuum and then re-dissolved in decane solution at a final concentration of 30 mg/mL. In the second step of the process, the 150 µm aperture found on the wall of the cup is prepared to accept lipids prior to cup/holder assembly and membrane formation. The preparation is done by pre-coating the aperture (on both sides of the wall) twice with a lipid solution using a paintbrush of size 000. The excess lipid solution on the wall of the cup is dried with nitrogen gas. The perfusion unit is then assembled and the wells in the cup and holder are filled with 1.0 mL of electrolyte solution. The electrolyte solution varies with experiments. Finally, the membrane is formed over the 150 µm aperture by applying the lipid solution with the paintbrush.

The membrane formation is confirmed by monitoring the electrical current flow through the 150 µM aperture under an applied transmembrane potential of 100 mV. In the presence of membrane there is no current flow between the *cis* and *trans* chambers. Initial coating of the aperture with the lipid solution results in formation of a multilayer membrane. To facilitate the insertion of the α-hemolysin pore, the multilayer is thinned to a bilayer through repeated brush strokes. The bilayer formation is confirmed through capacitance readings performed by the pClamp 9.0 software.

Upon obtaining a stable bilayer a solution of monomeric α-hemolysin (Sigma Aldrich), typically 5 µL of 2 µg/mL solution, is added to the *cis* compartment in proximity to the aperture/lipid bilayer. If the first addition of α-hemolysin solution results in no pore insertions, more α-hemolysin solution is added until achieving a stable pore insertion. α-Hemolysin pore insertions are characterized by current jumps of 100 pA at an applied potential of 100 mV with the electrolyte being 1 M KCl buffer and the experiment conducted at a temperature of 22 ± 1 °C. Following successful pore insertions (eg. 1 to 3 pores), the solution of the molecule to be analyzed is added to the *cis* compartment (unless stated otherwise) in proximity to the pore (more details on this in later sections). This results in spontaneous appearance of blockade events which are then recorded using the pClamp 9.0 software.

2.2.3 The solid-state pore setup

Prior to assembling the solid-state pore perfusion units, the solid-state pore chips and the two piece polytetrafluoroethylene cell are cleaned in different solutions. Solid-state pore chips (NanoPore Solutions) are cleaned in a piranha solution (a mixture of H_2SO_4 and H_2O_2, 1:3) for 30 minutes at 95 °C. The piranha solution is used to remove organic contaminants and improve nanopore wettability (i.e render the surface of the pore hydrophilic) (Miles *et al.*, 2013). The chip is then rinsed twice with distilled water. In contrast, the two piece polytetrafluoroethylene cell are first boiled in 20% HNO_3 for 10 minutes followed by boiling in distilled water for another 10 minutes. The boiling in distilled water is done twice to ensure the removal of the HNO_3 solution. Following boiling, the cell is dried under a jet of nitrogen air and the whole perfusion unit is assembled as described earlier and shown in Figure 2.1b.

The two wells of the cell connected through the nanopore are filled with degassed ethanol and the whole cell is placed in a plastic vacuum desiccator under vacuum to get rid of any bubbles inside the channels. Once a few bubbles have escaped through the pore the vacuum line is broken gently to ensure no re-entering of bubbles. The ethanol solution is then exchanged with degassed electrolyte solution by perfusion. The perfusion is done gently to ensure no bubble formation in the process. As stated earlier, the third well in the cell is filled with water. The whole perfusion unit is then placed in the aluminum housing and the electrodes are immersed into the electrolyte filled wells followed by placement in the first Faraday Cage (Figure 2.1d).

2.2.4 Data recording and processing

Once the molecule to be analyzed is added to the *cis* chamber, the interactions of the molecule with the pore are observed as blockade events or current traces (i.e drops in the current flow through the pore). As stated in section 2.2.1 the signal is transmitted from the electrodes through the headstage to the patch-clamp amplifier which converts the voltage to current. The analog signal from the amplifier is then further filtered and converted to a digital signal by the digitizer. For all experiments conducted in this thesis, the signals are low-pass filtered at a cut-off frequency of 10 kHz (100 µs) using the Axopatch 200B amplifier (Axon Instruments) and acquired (i.e digitized) at 100 kHz (10 µs) frequency using the DigiData 1322A digitizer (Axon Instruments). The acquisition frequency is set at 100 kHz because based on the Nyquist-Shannon sampling theorem the acquisition frequency has to be at least twice the filter cut-off frequency (Oukhaled *et al.*, 2012).

All events are recorded using Clampex 9 software which is part of the pClamp 9 suite (Axon instruments). The acquisition mode of the Clampex 9 software is set to "Fixed-length events" mode. In this mode the digitized data is displayed in real time during data acquisition but only saved onto hard disk whenever a signal passes the set threshold level. This acquisition mode works well for molecules inducing low frequency of events (e.g. proteins) because it uses less space on the computer's hard drive since typically there are thousands of events recorded. For all experiments performed with the α-hemolysin pore at 100 mV the threshold level was set about 20 pA from baseline. This ensures that any events smaller than 20 pA are ignored and the events recorded are well above the noise level. For those experiments performed at different voltages, the threshold level was adjusted accordingly. For each experiment there were at least five thousand raw (unprocessed) events recorded. The data recorded is stored in Axon Binary Format file.

The data acquired with Clampex is then analyzed with the Clampfit software, which is also part of the pClamp software suite. The data is opened in the analysis window of the Clampfit software and the events are displayed as concatenated traces. Using the event detection mode of the software, a single-channel search is carried out to detect and characterize each event (i.e obtain the amplitude and duration of each event). Two out of the 4 cursors available on the analysis window are used to specify the region where the single-channel search is performed. In addition, for all the data presented here two threshold levels were configured for the single-

channel search. One threshold level was used for the small blockade events and the other was used for large blockade events, thus providing a better separation between the two populations of events. The selected region as defined by the cursors and levels is then scanned by the software and each detected event is displayed on the event viewer window. The events on the event viewer window are examined and any event which is not recognized/detected properly by the program is rejected. In addition to the event viewer, the properties of each detected event are added to the event sheet of the results window of the software. Among the properties measured are the event amplitude and duration. The data in the event sheet is then transferred to a different sheet of the results window and the whole cycle with event detection for another region of traces is repeated till all files recorded are processed.

Once the data is processed, only events with duration times of 50 μs or higher are kept while those with lower duration times are deleted. The reason for deleting events of 50 μs or faster is because the low-pass filter cut-off frequency (f_c) used is 10 kHz (100 μs) and the finite rise time of the filter employed in our experiments is about $0.33 f_c$ or 33 μs. The rise time of the filter is defined as the time it takes for the instrument to respond to a signal (Pedone *et al.*, 2009). Furthermore, in order for the events to be measured accurately the event duration has to be twice the rise time (Pedone *et al.*, 2009). Therefore events faster than about 66 μs are too fast to be measured accurately. For this reason we only kept events with durations of 50 μs or higher for analysis.

The blockade amplitudes and duration times obtained with Clampfit are transferred to Origin 7 graphing software (OriginLab Corporation). Origin software is used to construct blockade current and time histograms. First, the blockade amplitudes are plotted as statistical histograms. This is followed by setting the bin size of the histogram to 1 (corresponding to 1 pA) and then re-plotting the number of events within each bin vs. the blockade current as a column graph. Each event population (eg. translocation and bumping) is fitted with the Gaussian function to obtain the peak/population blockade current value. On the other hand the duration time data for each population is plotted separately and the data is fitted with a single exponential decay function.

2.3 Analysis of glucagon and α-helical Fmoc-$D_2A_{10}K_2$ peptide isomers

2.3.1 Nanopore discrimination of retro, inversed, and retro-inversed isomers of glucagon and α-helical Fmoc-$D_2A_{10}K_2$ peptide

Retro (R), inversed (D), and retro-inversed (RI) isomers of glucagon and α-helical Fmoc-$D_2A_{10}K_2$ peptide were subjected to nanopore analysis. The glucagon peptide family were generous gifts from Dr. Scott Napper from Vaccine and Infectious Disease Organization (Saskatoon, Canada) and were over 95% pure. The respective sequences of the glucagon isomers analyzed are presented in Table 2.3. The L-Fmoc-$D_2A_{10}K_2$ peptide was synthesized as described previously (Stefureac *et al.*, 2006). The D-, R-, and RI-Fmoc-$D_2A_{10}K_2$ were purchased from CHI Scientific Inc (Maynard, MA) with over 95% purity. The Fmoc-D2A10K2 and glucagon peptides were prepared at 2.0 and 2.1 mg/mL, respectively, in 1.0 M KCl in 10 mM potassium phosphate buffer, pH 7.8. Aliquots were prepared and stored at -20 °C. An aliquot per nanopore experiment was used to avoid freeze and thaw cycles.

The α-hemolysin and lipid solutions were prepared and used as outlined in section 2.2.2. The same electrolyte solution, 1 mL of 1.0 M KCl in 10 mM potassium phosphate buffer, pH 7.8, was used in both chambers (*cis* and *trans*) for all experiments expect for the analysis of L-glucagon in the presence of GdnHCl (Sigma Aldrich). In the latter experiment the electrolyte used was 1 mL of 1.0 M GdnHCl and 1.0 M KCl in 10 mM potassium phosphate buffer, pH 7.8. After successful stable pore insertions (maximum of three), 10-20 µL of the peptide solutions were added to the *cis* chamber. The experiments were carried out at 22 ± 1 °C. A transmembrane potential of 100 mV was applied through the Ag/AgCl electrodes with the *cis* chamber being negatively biased. The blockade current and time histograms were obtained as described in section 2.2.4.

2.3.2 Circular dichroism discrimination of retro, inversed, and retro-inversed isomers of glucagon and α-helical Fmoc-$D_2A_{10}K_2$ peptide

Glucagon and α-helical Fmoc-$D_2A_{10}K_2$ peptide isomers were also subjected to circular dichroism (CD). The CD spectra for both peptide families were obtained with the PiStar-180 spectrometer (Applied Photophysics) which was connected to an Acorn PC. The experiments were conducted at 22 ± 1 °C using 1 mm path length quarts glass cuvettes. All peptide solutions were prepared in 1 M KCl in 10 mM phosphate buffer, pH 7.8 in an attempt to mimic

Table 2.3. Amino acid sequences of glucagon isomers.

Isomer	Sequence
Glucagon (all L-configuration)	His-Ser-Gln-Gly-Thr-Phe-Thr-Ser-Asp-Tyr-Ser-Lys-Tyr-Leu-Asp- Ser-Arg-Arg-Ala-Gln-Asp-Phe-Val-Gln-Trp-Leu-Met-Asn-Thr
D-Glucagon (all D-configuration)	His-Ser-Gln-Gly-Thr-Phe-Thr-Ser-Asp-Tyr-Ser-Lys-Tyr-Leu-Asp- Ser-Arg-Arg-Ala-Gln-Asp-Phe-Val-Gln-Trp-Leu-Met-Asn-Thr
R-Glucagon (all L-configuration)	Thr-Asn-Met-Leu-Trp-Gln-Val-Phe-Asp-Gln-Ala-Arg-Arg-Ser- Asp-Leu-Tyr-Lys-Ser-Tyr-Asp-Ser-Thr-Phe-Thr-Gly-Gln-Ser-His
RI-Glucagon (all D-configuration)	Thr-Asn-Met-Leu-Trp-Gln-Val-Phe-Asp-Gln-Ala-Arg-Arg-Ser- Asp-Leu-Tyr-Lys-Ser-Tyr-Asp-Ser-Thr-Phe-Thr-Gly-Gln-Ser-His

the nanopore experimental conditions. Glucagon peptides were prepared at concentrations ranging between 2 - 8 µM, while the Fmoc-$D_2A_{10}K_2$ peptides were prepared at concentrations between 100 - 200 µM. The raw ellipticity (θ) in mdeg units was determined for each peptide by scanning from 190 to 260 nm. This ellipticity was then converted to mean residue ellipticity (θ_{res}) and plotted against the wavelengths scanned to allow comparison between isomers. The mean residual ellipticity was calculated using the following equation (Kelly *et al.*, 2005; Kelly and Price, 2000):

$$\theta_{res} = \frac{\theta M}{10lcN} \qquad \text{Equation 2.1}$$

where θ is the ellipticity in mdeg, M is the molar mass of the peptide in g/mol, l is the path length of the cuvette in cm, c is the peptide mass concentration in mg/mL, and N is the number of amino acids in the peptide. The mean residue ellipticity is reported in deg·cm^2·dmol^{-1}.

2.4 Nanopore analysis of proteins

Eight different proteins (RNase A, lysozyme, bovine pancreatic trypsin inhibitor, ubiquitin, human thioredoxin, calmodulin, *E. coli* thioredoxin, and MBP) were subjected to nanopore analysis. The analysis of all proteins was carried out at 22 ± 1 °C. In all experiments, α-hemolysin and lipid solutions were prepared and used as outlined in section 2.2.2. Furthermore, a transmembrane potential of 100 mV, except for the voltage studies (section 2.4.5), was applied through Ag/AgCl electrodes with the *cis* chamber being negatively biased. In addition, all proteins were added to the *cis* chamber. The blockade current and time histograms were obtained as described in section 2.2.4. For protein and experiment specific details please see sections 2.4.1 - 2.4.5.

2.4.1 Nanopore analysis of ribonuclease A

RNase A protein purchased from MP Biomedical with purity of greater than 70% and activity of greater than 70 Kunitz units/mg was subjected to nanopore analysis under different experimental conditions. The natively folded and reduced RNase A were examined in the presence and absence of GdnHCl. The protein was prepared fresh at 5 mg/mL in 1 M KCl in

10 mM KPi, pH 7.0 before each experiment. Nanopore experiments were carried out using 30-60 µL of the 5 mg/mL solution. In the absence of GdnHCl, the electrolyte used was 1 M KCl in 10 mM KPi, pH 7.0, while in the presence of GdnHCl the electrolyte (for *cis* and *trans* chamber) was 1 M GdnHCl, 1 M KCl in 10 mM KPi, pH 7.0. For the analysis of the reduced RNase A, the protein was preincubated with a 10 fold excess (per disulphide bond) of tris-2-carboxyethyl-phosphine hydrochloride (TCEP) for 15 minutes before adding to the cup. TCEP (Sigma Aldrich) was also prepared fresh before each experiment to avoid oxidation.

For the analysis of completely unfolded RNase A, the protein was prepared in 4 M GdnHCl and 100 mM TCEP at a concentration of 1 mg/mL. The protein was prepared fresh before each experiment and left for incubation overnight at 22 ± 1 °C prior to adding it to the cup. The electrolyte used for these experiments was 1 M KCl in 10 mM KPi, pH 7.0.

In the analysis of purified RNase A, the protein purchased from MP Biomedical was subjected to purification by ion-exchange and size-exclusion chromatography prior to adding it to the *cis* chamber. Gel exclusion chromatography was performed on a 40 cm (32 mL) G-50 Sephadex (GE Healthcare Life Sciences) column in a buffer of 100 mM KPi, pH 7.0. The column was loaded with 2 mL of 10 mg/mL RNase and 35 fractions of 1 mL were collected. The fractions with the highest absorbance at 280 nm were pooled. The pooled fractions were then dialyzed into 10 mM Sodium Acetate buffer, pH 5.5. The dialyzed RNase A was further purified by ion exchange chromatography on SP Sepharose Fast Flow (GE Healthcare Life Sciences), a strong cation exchanger, as per manufacturer's instructions. The salt gradient used was 0 - 0.4 M KCl. There were 60 fractions of 1 mL collected and the fractions with the highest absorbance at 280 nm were pooled again and used for nanopore experiments. The protein concentration of the pooled fractions was determined by measuring the absorbance at 280 nm and using the molar absorption coefficient (ε) of 9800 M-1·cm-1 for RNase A (Sela and Anfinsen, 1957). The calculated concentration was 101.5 µM or 1.39 mg/mL. 30-60 uL of this solution was used for nanopore analysis.

2.4.2 Nanopore analysis of lysozyme, basic pancreatic trypsin inhibitor, ubiquitin, human thioredoxin, and calmodulin

Lysozyme (hen egg white), ubiquitin (bovine red blood cells), and recombinant human thioredoxin were purchased from Sigma-Aldrich, while basic pancreatic trypsin inhibitor

(BPTI) was purchased from ProSpec. Calmodulin was a generous gift of Dr. Louis Delbaere from the Department of Biochemistry at the University of Saskatchewan (Saskatoon, Canada). All proteins were high purity (greater than 90%). Stock solutions of 1 mg/mL were prepared in 1 M KCl in 10 mM KPi, pH 7.8. The analysis of the proteins was conducted with 30-60 µL of the stock solution added to the *cis* chamber. The electrolyte solution (1 M KCl in 10 mM KPi, pH 7.8) was the same for all experiments except for examination of lysozyme in the presence of GdnHCl. In the case of natively folded and reduced lysozyme in the presence of GdnHCl, the electrolyte solution was 1 M GdnHC and 1 M KCl in 10 mM KPi, pH 7.8. The reduction of disulfide bonds in lysozyme was carried out similar to RNase A reduction described in section 2.4.1

2.4.3 Nanopore analysis of *E. coli* thioredoxin and maltose binding protein in different buffers with and without EDTA

E. coli thioredoxin was purchased from Sigma Aldrich and MBP was from VLI Research Inc. Both proteins were high purity. *E. coli* thioredoxin was prepared at 1 mg/mL in 1 M KCl with 10 mM Tris-HCl buffer (pH 7.8) and a fresh aliquot was used for each experiment. MBP was prepared at 1 mg/mL in 1 M KCl with either 10 mM KPi buffer (pH 7.8) or 5 mM HEPES-NaOH buffer with or without 1 mM EDTA (pH 7.5). The analyses of the proteins were conducted with 30-60 µL of the stock solution added to the *cis* chamber. The electrolyte solution used varied with proteins and whether there was EDTA used or not. For *E. coli* thioredoxin the electrolyte solution was 1 M KCl with either 10 mM KPi (pH 7.8) or 10 mM Tris-HCl with or without 1 mM EDTA (pH 7.8). For MBP experiments the electrolyte solution was 1 M KCl with either 10 mM KPi (pH 7.8) or 5 mM HEPES-NaOH with or without 1 mM EDTA (pH 7.5). When the buffer with EDTA was used it was only added to the *cis* chamber because addition to both chambers chamber interferes with the Ag/AgCl electrode. Furthermore, for the experiments conducted in the presence of EDTA the α-hemolysin and protein solution added to the *cis* chamber also contained 1 mM EDTA to avoid introduction of metal ions.

For the analysis of MBP in the presence of GdnHCl, the 1 mg/mL stock solution prepared in 1 M KCl with 10 mM KPi (pH 7.8) was used and the electrolyte (in both chambers) was 1 M GdnHCl and 1 M KCl with 10 mM KPi (pH 7.8).

2.4.4 Nanopore analysis of maltose binding protein in the presence of metal ions, maltose, and lactose

The interaction of MBP with divalent metal ions (i.e Cu^{2+}, Zn^{2+}, and Mg^{2+}), maltose, and lactose was studied with nanopore analysis. The protein was made at 1 mg/mL in 1 M KCl in 5 mM HEPES-NaOH (pH 7.5) with or without EDTA. For sugar studies the protein solutions contained 1 mM EDTA, whereas for the metal studies the protein solution contained no EDTA. $CuSO_4$, $ZnCl_2$, and $MgCl_2$ (Sigma) were prepared in Millipore water (18 MΩ·cm) and used as a source of Cu^{2+}, Zn^{2+}, and Mg^{2+} divalent metal ions, respectively. The maltose and lactose sugars were purchased from Sigma and prepared fresh daily in 1 mM EDTA at 0.5 mg/mL. The electrolyte used in all experiments was 1 M KCl in 5 mM HEPES-NaOH, pH 7.5. However, for the study of interactions between the sugars and MBP, the *cis* chamber electrolyte contained 1 mM EDTA.

Upon successful pore insertions 30-60 µL of the stock protein solution was added to the *cis* chamber. This was followed by adding the ligand solution (eg. metal ions or sugars) to the *cis* chamber and gently mixing the *cis* chamber solution with a pipette. The protein was incubated with the respective ligand for 30 min before proceeding with recording of the data. Metal ions were added to the *cis* chamber at a final concentration of 10 µM. Lactose and maltose were added to the *cis* chamber at a final concentration of 3 moles sugar per mole of protein.

2.4.5 Nanopore analysis of ribonuclease A, calmodulin, *E. coli* thioredoxin, and maltose binding protein at different voltages

The interactions of RNase A, calmodulin, *E. coli* thioredoxin, and MBP with the α-hemolysin pore were investigated at 50, 100, and 150 mV. RNase A was prepared at 5 mg/mL in 1 M KCl, 10 mM KPi, pH 7.0. Calmodulin and *E. coli* thioredoxin were prepared at 1 mg/mL in 1 M KCl, 10 mM KPi, pH 7.8. MBP, on the other hand, was prepared at 1 mg/mL in 1 mM EDTA and 1 M KCl in 5 mM HEPES-NaOH, pH 7.5. The 1 M KCl buffers which were used to prepare the stocks solutions of the proteins were also used as electrolyte for the respective protein. For the analysis of MBP at different voltages, the *cis* chamber electrolyte also contained 1 mM EDTA.

For all proteins, 30-60 µL of the stock solution was added to the *cis* chamber and blockade

events were recorded at all three different voltages (i.e 50, 100, and 150 mV). When recording at different voltages, the threshold level (see section 2.2.4) was adjusted accordingly for each applied voltage. For example, at 100 mV the threshold recoding level was kept at about 20 pA from baseline, at 50 mV the threshold level was kept at about 12 pA from baseline, and at 150 pA the threshold level was kept at about 25 pA.

Additionally, MBP was also studied at 75 mV and 100 mV in the presence of 1.5 M GdnHCl. At this GdmHCl concentration, MBP is completely unfolded and should translocate the α-hemolysin pore (Betton and Hofnung, 1996; Oukhaled *et al.*, 2007). The electrolyte solution used in these experiments was 1.5 M GdnHCl and 1 M KCl in 5 mM HEPES-NaOH (pH 7.5) with the *cis* chamber electrolyte containing 1 mM EDTA. The protein solution was added to the *cis* chamber (30-60 µL). At 150 mV the membrane and pore were highly unstable and thus the nanopore experiment could not be carried out long enough to record sufficient data. Similarly, sufficient data could not be recorded at 50 mV because of the extremely low frequency of events. Therefore, data was recorded only at 75 and 100 mV.

2.5 Zeta potential measurements of proteins

Zeta Potential measurements were carried out for RNase A, Calmodulin, MBP, and Avidin. Avidin was purchased from ProSpec Bio with greater than 97% purity. The zeta potential of proteins were determined in different buffers and pHs with or without KCl. All proteins were prepared fresh at 1.25 mg/mL and the solutions were filtered by 200 nm pore size filters (Thermo Fisher Scientific) prior to measuring the zeta potentials. RNase A was prepared in the following solutions: (a) 10 mM KPi (pH 7), (b) 0.1 M KCl in 10 mM KPi (pH 7), (c) 0.1 M KCl in 10 mM KPi, (d) 10 mM TRIS-HCl (pH 8.0), (e) 50 mM KCl in 10 mM TRIS-HCl (pH 8.0), (f) 50 mM KCl in 10 mM Sodium Citrate (pH 4.0), and (g) 50 mM KCl in 10 mM Sodium Carbonate/Biocarbonate (pH 10.0). Calmodulin and MBP were prepared in 0.1 M KCl in 10 mM KPi (pH 7.8) and 0.1 M KCl in 5 mM HEPES (pH 7.5), respectively. Avidin was prepared in the following solutions: (a) 10 mM TRIS-HCl (pH 8.0), (b) 50 mM KCl in 10 mM TRIS-HCl (pH 8.0), (c) 50 mM KCl in 10 mM Sodium Citrate (pH 4.0), and (d) 50 mM KCl in 10 mM Sodium Carbonate/Biocarbonate (pH 10.0).

The zeta potential of each protein was measured with a Zetasizer Nano ZS instrument (Malvern Instruments) belonging to Dr. Ildiko Badea from the College of Pharmacy and

Nutrition at the University of Saskatchewan (Saskatoon, Canada). The Zetasizer Nano ZS instrument first determines the electrophoretic mobility and then applies the Henry equation to calculate the zeta potential. The electrophoretic mobility of the particle (i.e the velocity of that particle in an electric field) is measured by employing laser Doppler velocimetry. The Henry equation is:

$$\cup_E = \frac{2\varepsilon z f(Ka)}{3\eta} \qquad \text{Equation 2.2}$$

where *z* is the zeta potential, U_E is the electrophoretic mobility, ε is the dielectric constant, η is viscosity, and f(Ka) is Henrys function (Delgado *et al.*, 2005; Hunter, 1988). For all our measurements the Huckel approximation (f(Ka) = 1.0) was used. The protein samples were loaded slowly with a syringe into folded capillary cells (Malvern Instruments) to avoid formation of air bubbles. The samples were equilibrated for 15 minutes at 25 °C before starting the measurements. All measurements were done using the mono-modal measurement mode with a maximum of 100 runs. The voltage was set 50 V for those solutions containing KCl and 150 V for those containing no KCl. This was done to ensure no heating of the sample. The measurement cells were replaced frequently due to the corrosion of the electrodes. Specifically, for those solutions containing KCl a measurement cell was used only for a single measurement.

2.6 Reverse transcription polymerase chain reaction detection of ribonuclease A

Reverse transcription polymerase chain reaction (RT-PCR) is used here as a method for detecting RNase A. In RT-PCR, the RNA template is first reversed transcribed by reverse trasncriptase into a complementary DNA (cDNA) (Haddad and Baldwin, 2010). The cDNA is then used as template for amplification by PCR. However, in the presence of RNase A the RNA template will be degraded and thus the reverse transcription step will be interrupted. Therefore, RNase A detection will be confirmed by absence of amplified end-product. The end-product can be visualized on an agarose gel.

For all our experiments, the RNA template was rabbit globin messenger RNA (mRNA) purchased from Sigma (Flashner and Vournakis, 1977). Globin mRNA was prepared at 20 µg/mL in RNase-free water (Ambion), not DEPC-treated, and stored at -20 °C. Several aliquots of different concentrations were prepared.

Initially two primers sets were designed: one for the alpha-globin and another for beta-globin cDNA. However, for all our experiments only beta-globin primers were used because the alpha-globin primers didn't amplify well under our experimental conditions. There was an additional product visible on the agarose gel beside the target product. The primers were designed using the Primer-BLAST tool from NCBI. The primers with the desired properties were purchased from Sigma-Genosys. The properties of the primers selected are listed in Table 2.4. Stock solutions of 100 µM were prepared in RNase-free water (not DEPC-treated) and stored at -20 °C. Additionally, small aliquots of working solutions (10 µM) were prepared to avoid repeated thawing and freezing.

The RT-PCR was performed using a one-step RT-PCR kit from Qiagen. The RT-PCR was set up as per manufacturer's instructions unless otherwise stated. The PCR product was visualized on a 2.5% agarose gel. The agarose used was PCR quality (EMD Chemicals). The DNA ladder used was purchased from New England Biolabs and was a low molecular weight DNA ladder which included fragments ranging from 25-766 base pairs. For all experiments there was 1.15 µg of the DNA ladder used.

2.6.1 The detection assay

A detection assay utilizing RT-PCR was designed to detect RNAase A activity. A stock solution of RNase A (5 mg/mL) was prepared fresh daily in 1 M KCl with 10 mM KPi (pH 7.4). This stock solution was then used to prepare serial dilutions of RNase A in 0.5 M KCl in 10 mM KPi (pH 7.4), ranging from 100 µg/mL to 0.01 ag/mL in 500 µL final volume. The 0.01 ag/mL dilution should contain no molecules of RNase A. All RNase A solutions were set up in non-sticky RNase-free microcentrifuge tubes (Applied Biosystems) to avoid sticking of RNase A to the walls of the tubes. In addition, the dilutions were prepared using RNase free barrier tips with low-binding surface (Sorenson BioScience) to avoid loss of RNase A molecules in the process of dilution. Without the use of the non-sticky tubes and pipette tips with low-binding surface, the detection assay was not reproducible.

Following the set up the dilutions, globin mRNA was added to the 100 pg/mL, 1 pg/mL, 10 fg/mL, 100 ag/mL, 10 ag/mL, 1 ag/mL, 0.1 ag/mL, and 0.01 ag/mL RNase A dilutions at final concentration of 100 pg/mL. Additionally, there are two more solutions set up containing

Table 2.4. DNA Primer Properties.

Name	Sequence (5` - 3`)	Length	Tm (°C)	% GC	Product Length
alpha-globin forward	CCACGGTGGCGAGTATGGCG	20	74.9	70.00	320
alpha-globin reverse	CCAGGGAGGCATGCACCGCA	20	77.9	70.00	
beta-globin forward	TGCCCTGTGGGGCAAGGTGAA	21	75.9	61.90	354
beta-globin reverse	TAGGCAGCCTGCACCTGAGGA	21	71.4	61.90	

no RNase A: one of these solutions (i.e positive control for RT-PCR) was 100 pg/mL globin mRNA in 0.5 M KCl , 10 mM KPi (pH 7.4) and the other was the 0.5 M KCl buffer only (i.e negative control for RT-PCR reaction). These 10 reactions were then incubated at 37 °C for 24 hrs.

Following incubation, all ten solutions were used as a source of template RNA for setting up ten RT-PCR reactions of 50 µL final volume. The RT-PCR reactions were set up based on the OneStep RT-PCR kit handbook (Qiagen). Each RT-PCR reaction, except the negative control, contained 300 fg of globin mRNA. The thermal cycler conditions were set up as outlined in the RT-PCR kit handbook. Based on the Tm of the primers the annealing temperature was set at 65 °C. The number of cycles used for PCR amplification was 34. Finally, the end products were run on an agarose gel stained with ethidium bromide and visualized using the gel imaging platform, AlphaDigiDoc (Alpha Innotech).

The RNase A dilutions and RT-PCR reactions were performed on a RNase A free working area. All the consumables were RNase A free. The pipettes and laboratory benches were decontaminated with RNase Zap solution (Applied Biosystems) as per manufacturer's instructions.

2.6.2 Testing for ribonuclease A activity in the *trans* chamber

In this thesis, experiments were run to determine if folded or unfolded RNase A translocates through the α-hemolysin pore. The detection assay developed in section 2.6.1 was used to determine if RNase A translocates thorugh the α-hemolysin pore. In the first part of the process, a typical nanopore experiment utilizing agarose salt bridges was carried out.

The salt bridges used in nanopore experiments were prepared as outlined in section 2.2.1. The 3 M KCl solution, the agarose, and the glass tubing used for salt bridge preparation were all RNase free. The glass tubing was first soaked in RNase Zap solution followed by thoroughly rinsing with RNase free water. The perfusion unit was also soaked in RNase Zap solution followed by thoroughly rinsing with RNase free water and then boiling for couple of hours with RNase free water.

For those experiments with the folded protein, RNase A was prepared fresh daily in 1 M KCl in 10 mM KPi (pH 7.4) at 5 mg/mL. The electrolyte used was 1 M KCl in 10 mM KPi (pH 7.4). The electrolyte solution (1 M KCl buffer) was prepared fresh weekly with RNase

free chemicals in RNase-free water (not DEPC-treated). For the experiments with the unfolded protein, RNase A was prepared fresh daily in 4 M GdnHCl and 100 mM TCEP at 1 mg/mL. The electrolyte used in these experiments was 1 M KCl in 10 mM KPi (pH 7.4) with or without 1 M RNase free GdnHCl. In all of the nanopore experiments for this section, α-hemolysin was prepared in RNase free buffer (1 M KCl in 10 mM KPi, pH 7.4) at 2 µg/mL. Furthermore, as with any RNA experiment, extreme caution was taken to ensure an RNase free work area, apparatus, and lab consumables.

The protein (30-60 µL of the stock solution) was added to the *cis* chamber only after stable pore insertions. If the membrane was broken after adding the protein, the experiment was abandoned and a new experiment (with clean apparatus) was started. Upon successful completion of the nanopore experiment, 245 µL from *cis* and *trans* chambers was collected. These solutions were collected while ensuring the membrane and α-hemolysin pores remain intact (i.e no RNase a contamination). The solutions collected from each chamber were transferred to non-sticky RNase-free microcentrifuge tubes. Additionally 245 µL of RNase free water and 10 µL of 5 ng/mL globin mRNA was added to each tube to a final volume of 500 µL.

In the second part of the process, the RT-PCR detection assay outlined in section 2.6.1 was used to test for RNase A activity in solutions collected from the nanopore experiments. The whole process described in this section is illustrated in Figure 2.2.

2.7 The solid-state pore experiments

Si_3N_4 solid-state nanopores were purchased from Nanopore Solutions with diameters of 10 and 20 nm (10 of each). The pores were fabricated in silicon nitride membranes with 20 nm thickness. The perfusion units and the solid-state apparatus shown in Figure 2.1c were provided by Dr. Andre Marziali from the University of British Columbia. The pores were mounted as described in section 2.2.1.

The electrolyte used for solid-state pore experiments was 1 M KCl, 10 mM Tris-HCl (pH 7.4) and the proteins studied were MBP and RNase A. MBP and RNase A were prepared in 1 M KCl, 10 mM Tris-HCl (pH 7.4) at 1 and 5 mg/mL, respectively. The proteins were added to the *cis* chamber and the grounded electrode was either in the *cis* or *trans* chamber.

Prior to adding the proteins to the *cis* chamber open pore currents were recorded at different voltages in order to construct an open pore current versus applied voltage curve (I/V curve).

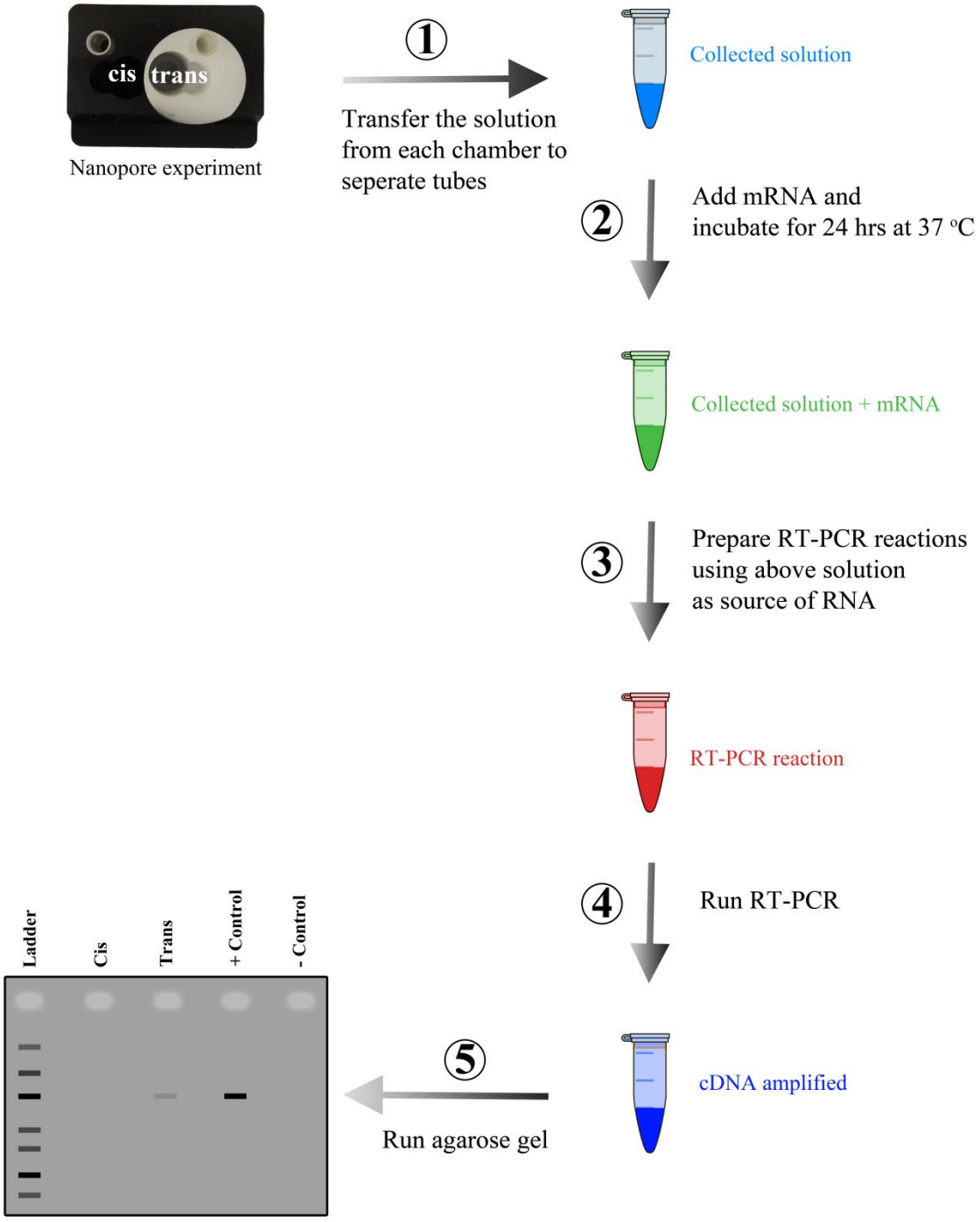

Figure 2.2. RNase A detection workflow. First, a nanopore experiment is conducted and at the end the solution from each chamber is collected and transferred to a microcentrifuge tube. Second, mRNA is added to the solution collected in step 1 and incubated for 24 hrs at 37 °C. Third, after incubation the solution from step 2 is used as source of template RNA for RT-PCR reaction. Fourth, RT-PCR is performed. In the fifth step, the end product from RT-PCR is run on an agarose gel. If there is RNase A present in solutions collected in step 1 then there will be a faint band or no band (depending on RNase A quantity) on the agarose gel.

The applied voltage ranged between -100 mV to +100 mV. The I/V curve was used to calculate the experimental pore conductance (i.e the slope of the I/V curve). The theoretical pore conductance for pores with diameters of comparable size to their lengths can be calculated using the following equation:

$$G = \frac{k\pi d_p^2}{4(\mathrm{h_p} + 0.8\mathrm{d_p})} \qquad \text{Equation 2.3}$$

where G is the pore conductance, k is the buffer conductivity, h_p is the thickness of the pore, and d_p is the diameter of the pore (DeBlois and Bean, 1970; Stefureac *et al.*, 2010b). The experimental pore conductance can be used in equation 2.3 to approximate the pore diameter. The volumes of the pores were calculated by assuming a cylindrical geometry and using a calculated effective length of 15 nm. The volumes of the proteins without the water shell were calculated using their dimensions and assuming an ellipsoidal shape. In contrast, the volumes of the proteins with the water shell were calculated based on a sphere shape (Stefureac *et al.*, 2010b). The expected blockade amplitude as a result of a protein passing through the pore was calculated by multiplying the percent excluded volume with the open pore current of the pore.

3.0 RESULTS

3.1 Nanopore and circular dichroism discrimination of glucagon and α-helical peptide isomers

3.1.1 Introduction

Lee and Stefureac have reported that nanopore sensing utilizing wild-type α-hemolysin pore can distinguish between different peptides and proteins, including single-amino acid mutants (Madampage *et al.*, 2012; Stefureac *et al.*, 2006; Stefureac *et al.*, 2008). Furthermore, other groups have shown that the engineered α-hemolysin pore can differentiate between chiral drug molecules and chiral amino acid isomers (Boersma and Bayley, 2012; Kang *et al.*, 2006). However, it's not yet understood what structural features the pores are interrogating. Is it structure, sequence, or both? Therefore, it was reasoned that by subjecting chiral and directional peptide isomers to nanopore analysis it would be possible to determine what the pore is interrogating and test the sensitivity of the technique. For this purpose the retro (R), inversed (D), and retro-inversed (RI) isomers of glucagon and Fmoc-$D_2A_{10}K_2$ peptide were considered. In D peptides the chirality of each amino acid residue is inverted, while in RI peptides the direction of the sequence is reversed and the chirality of each amino acid residue is inverted. In contrast, R peptides have reversed sequences, but the chirality of amino acids is unchanged (Fischer, 2003). The sequences of the glucagon peptides analyzed are presented in Table 2.3. For example, an antibody can distinguish between L and D peptides, but some cannot distinguish between L and RI peptides (Benkirane *et al.*, 1995; Briand *et al.*, 1995; Muller *et al.*, 1995). RI peptides are known to elicit a good immune response and they can be used to raise antibodies against the L peptide (Benkirane *et al.*, 1995; Briand *et al.*, 1995; Muller *et al.*, 1995). This is because; an antibody has to make contact with the peptide in at least three positions. These positions are different on L and D peptides but they remain the same between L and RI peptides (Figure 3.1a). Therefore, this study will be an important sensitivity test for nanopore sensing.

Glucagon and Fmoc-$D_2A_{10}K_2$ were selected as model peptides based on their physical and chemical properties. Glucagon is a small (29 amino acids), largely unstructured, and neutral peptide at physiological pH (Sasaki *et al.*, 1975; Unger and Orci, 1976). On the other hand,

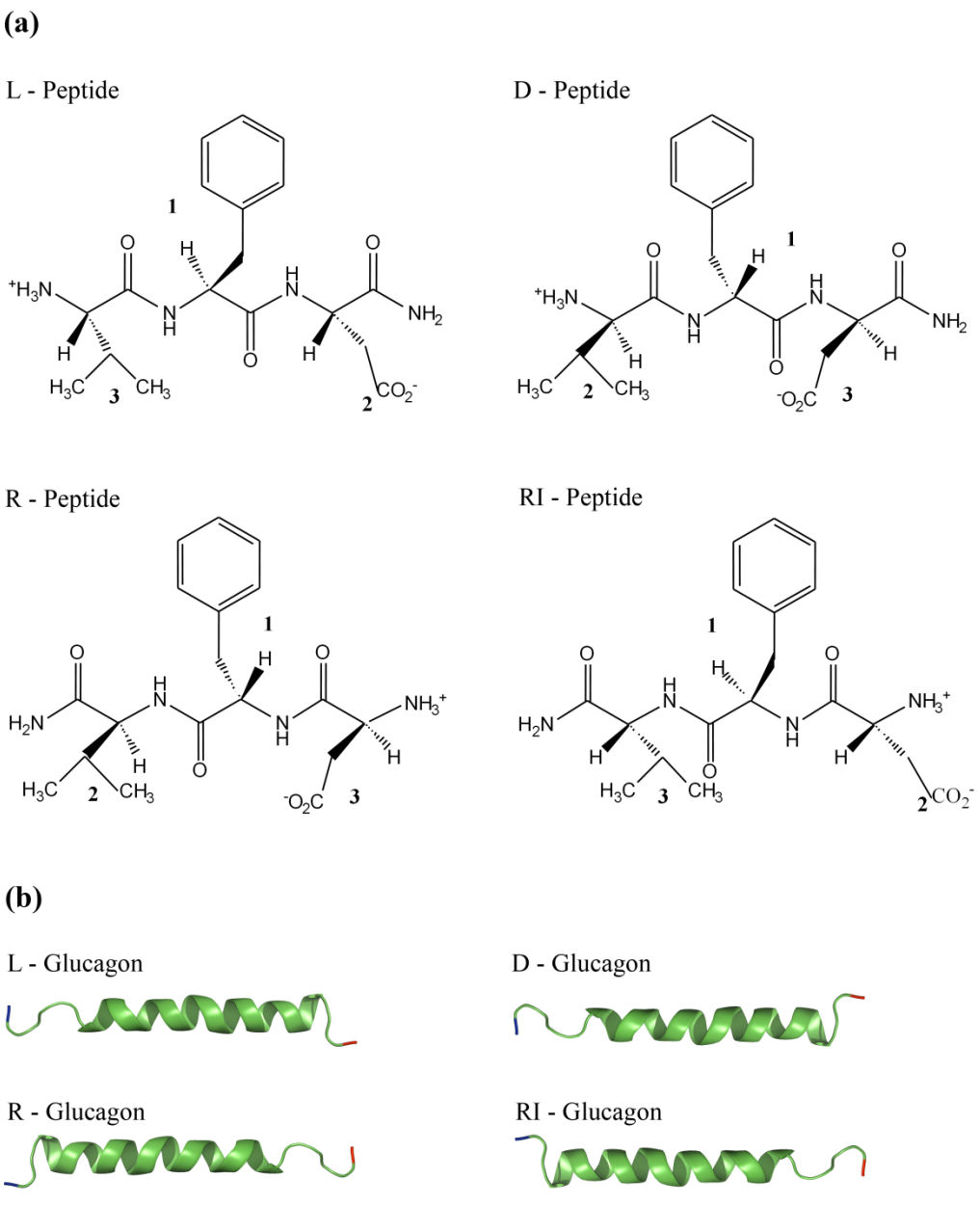

Figure 3.1. Schematic representations of the L, D, R, and RI isomers. Part (a) illustrates the change in position of different groups, marked as 1, 2 or 3 in the four isomers. These positions are different on L and D peptides but they remain the same between L and RI peptides. Part (a) was prepared with ChemDraw software. Part (b) shows the glucagon isomers. The D-glucagon is a mirror image of the L-glucagon where the sequence is the same but the chirality of each amino acid is inverted. In R-glucagon the direction of the sequence is changed but the chirality remains the same. In RI-glucagon the direction of the sequence is reversed and the chirality of each amino acid residue is inverted. Part (b) was prepared with PyMOL software using PDB ID 1GCN for the glucagon.

Fmoc-$D_2A_{10}K_2$ is negatively charged at pH 7, forms a stable α-helix, and the L-Fmoc-$D_2A_{10}K_2$ peptide has been previously studied by our laboratory and found to readily translocate the α-hemolysin pore (Stefureac *et al.*, 2006).

3.1.2 Nanopore discrimination of retro, inversed, and retro-inversed isomers of glucagon and α-helical Fmoc-$D_2A_{10}K_2$ peptide

Directional and chiral isomers of Fmoc-$D_2A_{10}K_2$ were subjected to nanopore analysis and the data obtained is presented in Figure 3.2 and Table 3.1 (see section 2.2.3 on how the data is obtained). The L and D peptides induced single types of events (i.e translocation events) with blockade currents of about -63 pA (Figure 3.2a, c). In contrast, both R and RI peptides gave rise to two types of events (Figure 3.2e, h). Less than 10% of the events belonged to the bumping population with blockade currents of about -25 pA, while more than 90% belonged to translocation population with large blockade currents of about -57 pA. The translocation times for the reversed peptides are about half that of the L and D peptides (Figure 3.2b, d, f, i and Table 3.1). Furthermore, the distribution of events for the translocation population of the reversed-sequenced peptides is sharper in comparison to the normal-sequenced peptides. From this data, it's clear that the chirality of the amino acids does not have a big effect on the blockade current amplitudes and duration times. However, the direction of the sequence affects the interaction of the pore with the peptide. Therefore, for the Fmoc-$D_2A_{10}K_2$ family the pore can differentiate between the directional isomers but not between chiral isomers. To confirm these results, retro, inversed, and retro-inversed isomers of glucagon were subjected to nanopore analysis.

Nanopore analysis of the four glucagon isomers is shown in Figure 3.3 and the event parameters are summarized in Table 3.2. It is clear that the blockade histograms are more complex than for the Fmoc-$D_2A_{10}K_2$ family and there are three distinct peaks in each case. For L-glucagon and D-glucagon, these occur at -26, -41, and -65 pA with event times of about 0.07, 0.27 and 0.30 ms, respectively. By comparison with other α-helical peptides (and with Fmoc-$D_2A_{10}K_2$), the peak at -41 pA is unlikely to represent translocation events because the current blockade is too small for a peptide of this size (Christensen *et al.*, 2011; Meng *et al.*, 2010; Movileanu *et al.*, 2005; Stefureac *et al.*, 2006). Initially it was thought that this might be due to

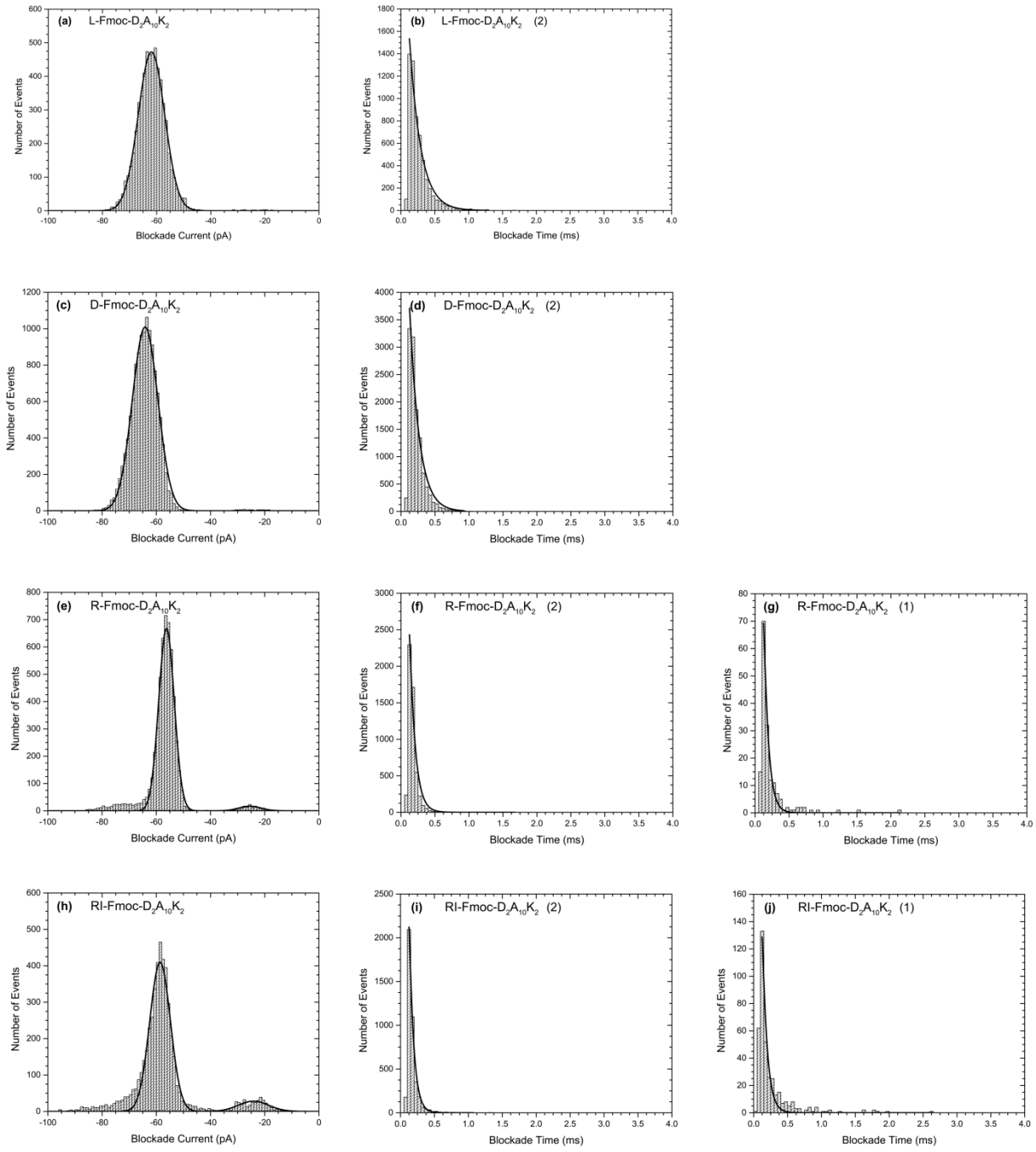

Figure 3.2. Nanopore discrimination of D, R, and RI isomers of α-helical Fmoc-$D_2A_{10}K_2$ peptide. Blockade current histograms obtained for (a) L-Fmoc-$D_2A_{10}K_2$, (c) D-Fmoc-$D_2A_{10}K_2$, (e) R-Fmoc-$D_2A_{10}K_2$, and (h) RI-Fmoc-$D_2A_{10}K_2$ peptides. Each event population is fitted with the Gaussian function to obtain the peak/population blockade current value. The corresponding blockade time histograms for L-Fmoc-$D_2A_{10}K_2$, D-Fmoc-$D_2A_{10}K_2$, R-Fmoc-$D_2A_{10}K_2$, and RI-Fmoc-$D_2A_{10}K_2$ are shown in (b), (d), (f,g), and (i, j), respectively. The duration time data is fitted with a single exponential decay function. The peak blockade current values and the duration times for each population are presented in Table 3.1.

Table 3.1. Interaction parameters of Fmoc-$D_2A_{10}K_2$ isomers with the α-hemolysin pore.

Parameter[a]	Peptide Isomer			
	L-Fmoc-$D_2A_{10}K_2$	**D-Fmoc-$D_2A_{10}K_2$**	**R-Fmoc-$D_2A_{10}K_2$**	**RI-Fmoc-$D_2A_{10}K_2$**
I_1 (pA)[b]	-	-	-25.4	-24.2
I_2 (pA)	-61.9	-64.1	-56.2	-58.6
T_1 (ms)[c]	-	-	0.07	0.07
T_2 (ms)	0.16	0.14	0.08	0.06
W_1 (pA)[d]	-	-	7.8	11.0
W_2 (pA)	9.6	9.2	5.4	7.4
A_1 (%)[e]	-	-	3.4	9.1
A_2 (%)	100	100	96.6	90.9

[a] I_1, I_2, T_1, and T_2 represent the amplitudes and the durations of the current blockades of the respective event populations presented in Figure 3.2. A_1 and A_2 are percent of total events forming each respective population and W_1 and W_2 represent width at half the maximum height. The peaks are numbered from right to left. A dash indicates the absence of the respective event population.
[b] The error is estimated to be ±1 pA.
[c] The error is estimated to be ± 10%.
[d] The error is estimated to be ± 1%.
[e] The error is estimated to be ± 1%.

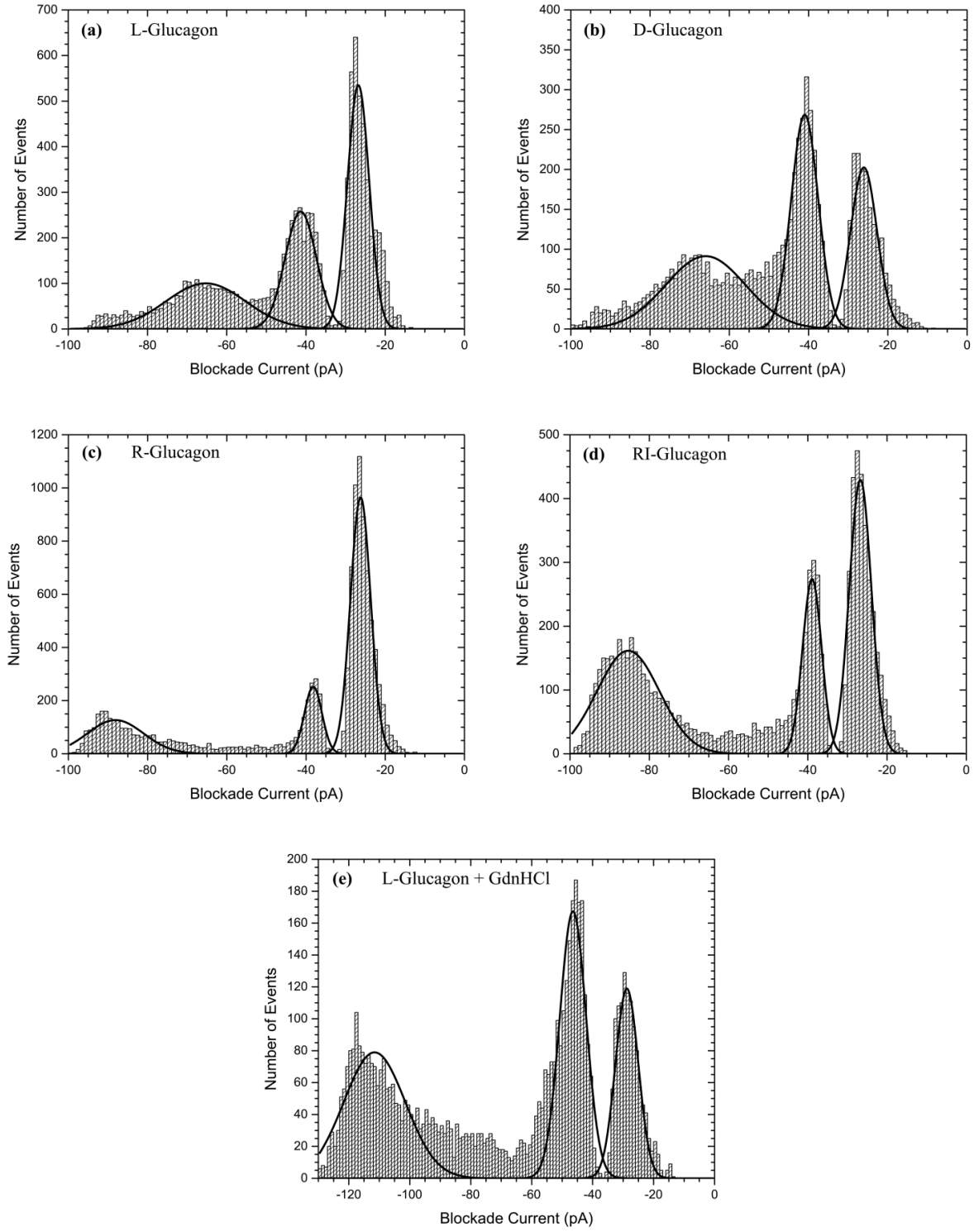

Figure 3.3. Nanopore discrimination of D, R, and RI isomers of glucagon. Blockade current histograms obtained for (a) L-glucagon, (b) D-glucagon, (c) R-glucagon, (d) RI-glucagon, and (e) L-Glucagon in the presence of 1 M GdnHCl. Each event population (three populations per isomer) is fitted with the Gaussian function to obtain the peak/population blockade current value. The peak blockade current values are presented in Table 3.2.

Table 3.2. Interaction parameters of glucagon isomers with the α-hemolysin pore.

Parameter[a]	Peptide Isomer				
	L-Glucagon	**D-Glucagon**	**R-Glucagon**	**RI-glucagon**	**L-Glucagon + GdnHCl**
I_1 (pA)[b]	-26.8	-26.1	-26.2	-26.7	-28.8
I_2 (pA)	-41.3	-41.0	-38.2	-38.9	-46.5
I_3 (pA)	-65.3	-66.0	-88.1	-85.3	-111.6
T_1 (ms)[c]	0.08	0.06	0.19	0.07	0.12
T_2 (ms)	0.27	0.27	0.22	0.19	0.31
T_3 (ms)	0.28	0.33	1.63	0.91	1.16
W_1 (pA)[d]	5.1	6.4	4.7	5.2	7.0
W_2 (pA)	7.6	6.5	4.0	4.4	8.2
W_3 (pA)	20.0	20.0	14.0	15.7	20
A_1 (%)[e]	28.9	27.0	62.9	38.1	40.6
A_2 (%)	29.1	36.4	14.2	21.0	36.7
A_3 (%)	42.0	36.6	22.9	22.9	22.7

[a] I_1, I_2, I_3, T_1, T_2, and T_3 represent the amplitudes and the durations of the current blockades of the respective event populations presented in Figure 3.3. A_1, A_2, and A_3 of total events forming each respective population and W_1, W_2, and W_3 represent their width at half the maximum height. The peaks are numbered from right to left.

[b] The error is estimated to be ±1 pA.

[c] The error is estimated to be ± 10%.

[d] The error is estimated to be ± 1%.

[e] The error is estimated to be ± 1%.

dimer formation. To test this theory L-glucagon was analyzed in the presence of 1 M GdnHCl (Figure 3.3e). Since the middle peak doesn't disappear in the presence of GdnHCl, dimer formation was ruled out. Thus, the peaks at -26 and -41 pA might represent bumping of the glucagon into the pore in two different orientations. Although the three peaks have similar current blockades and event times, the ratio of the peak heights are different between L-glucagon and D-glucagon, and thus, the pore is showing some discrimination. The reversed-sequence peptides also give three peaks (at -26, -39, and -86 pA), but the translocation peak at -86 pA has a significantly larger current blockade and longer blockade times than that of the L-glucagon and D-glucagon. Again, the direction of the sequence is being detected better than the chirality. That is, the difference in the interaction parameters (Table 3.2) between the peptides and the pore is greater for directional isomers than for chiral isomers. However, taking all parameters into consideration, the pore is able to distinguish between all four glucagon isomers.

These sets of experiments show that nanopore sensing coupled with the wild-type α-hemolysin pore can be used to differentiate between chiral and directional isomers of complex peptides. Hence, nanopore sensing is a very sensitive technique and is interrogating both structure and sequence of the peptide.

3.1.3 Circular dichroism discrimination of retro, inversed, and retro-inversed isomers of glucagon and α-helical Fmoc-$D_2A_{10}K_2$ peptide

Circular dichrosim (CD) was also employed in evaluating secondary structures of glucagon and Fmoc-$D_2A_{10}K_2$ isomers under similar experimental conditions as those used for nanopore analysis (i.e 1 M KCl 10 mM KPi, pH 7.8 buffer as solvent). The purpose of these experiments is to confirm that the chiral isomers (L vs D and R vs RI) exhibit CD spectra that are mirror images of each other and directional isomers (L vs R and D vs RI) have similar CD spectra when using the same solvent as that used in nanopore analysis (Kindrachuk *et al.*, 2011). Indeed, the CD spectra obtained for the chiral isomers (i.e enantiomers) in the KPi buffer are consistent with formation of symmetry-related structures (Figure 3.4).

Together, nanopore analysis and CD results indicate that nanopore sensing is able to discriminate all four isomers, while CD can only discriminate between chiral isomers. Thus, nanopore sensing offers greater sensitivity than CD in discrimination of isomers.

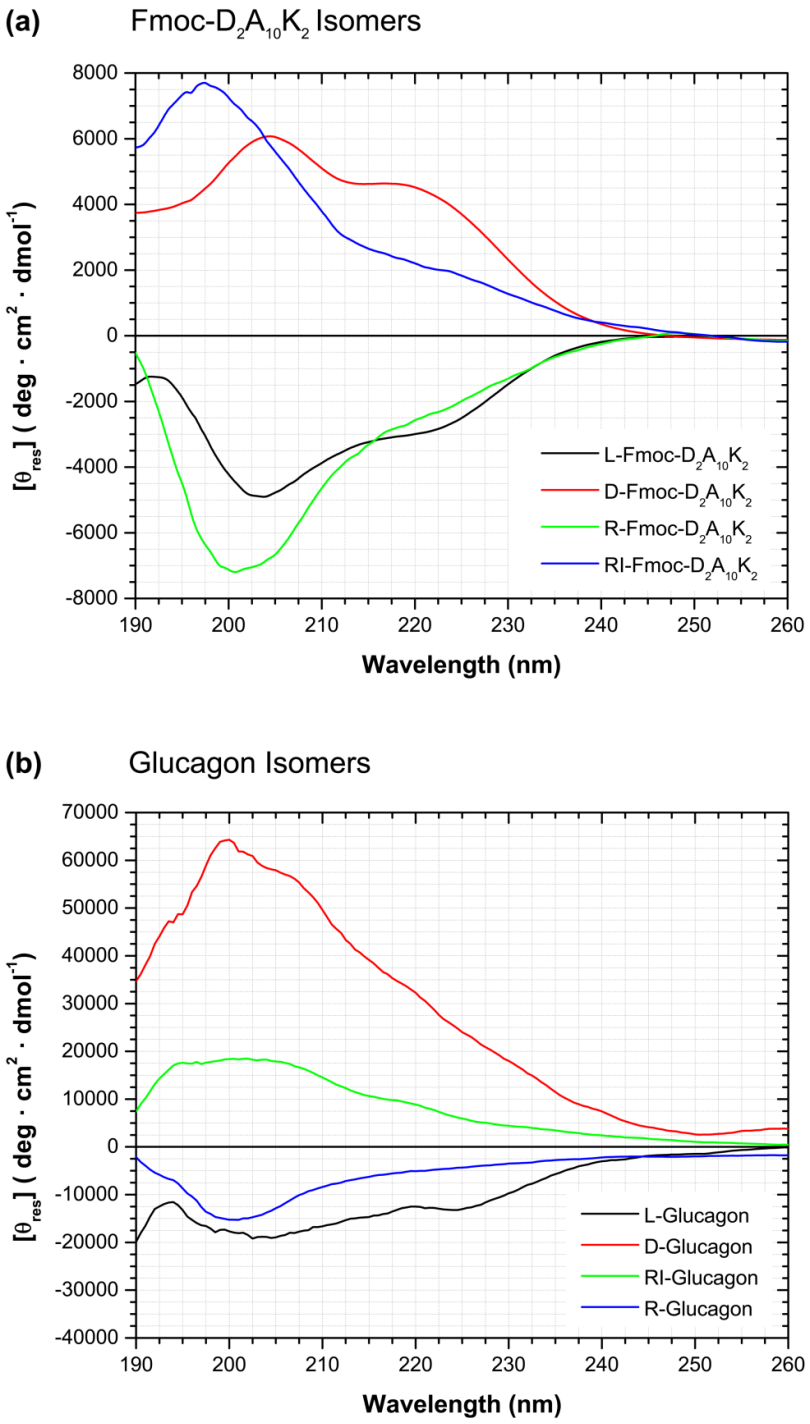

Figure 3.4. Circular dichroism of glucagon and Fmoc-$D_2A_{10}K_2$ isomers. The ellipticity in mdeg unit was determined for (a) Fmoc-$D_2A_{10}K_2$ and (b) glucagon isomers, prepared in 1M KCl 10 mM KPi, pH 7.8, by scanning from 190 to 260 nm at 22 ± 1 °C using 1 mm path length quarts glass cuvettes and a PiStar-180 spectrometer (Applied Photophysics, Leatherhead, Surrey, UK). This ellipticity was then converted to mean residue ellipticity and plotted against the wavelengths scanned to allow comparison between isomers.

3.2 Nanopore analysis of proteins

3.2.1 Nanopore analysis of ribonuclease A

3.2.1.1 Introduction

Nanopore analysis employing the α-hemolysin pore has been applied to both peptides and proteins. With peptides it is clear that size, overall charge, hydrophobicity, degree of folding, and dipole moment, all affect the interaction with the pore (Christensen *et al.*, 2011; Meng *et al.*, 2010; Stefureac *et al.*, 2006; Sutherland *et al.*, 2004; Zhao *et al.*, 2009b). However, as detailed in the introduction of this thesis, with proteins there are number of anomalies and disagreements in the literature. Furthermore, while there have been reports of protein translocation through α-hemolysin, there is no direct evidence (Oukhaled *et al.*, 2007; Stefureac *et al.*, 2008). Thus, it was reasoned that one method to provide direct evidence would be to translocate an enzyme and then demonstrate activity on the *trans* side of the pore thus providing an amplification of the signal. RNase A was chosen as a model enzyme for this analysis because it is very robust and after unfolding with denaturants and/or disulphide reducing agents, it readily refolds to an active conformation (Cao *et al.*, 2001; Miyamoto *et al.*, 2009; Neira and Rico, 1997; Reinstadler *et al.*, 1996; Wedemeyer *et al.*, 2000). RNase A is 124 amino acid protein with a molecular weight of 13.7 kDa and contains four disulfide bonds (Raines, 1998). It is positively charged (+4) at physiological pH with a pI of 9.3 (Raines, 1998). Its dimensions are 3.8 x 2.8 x 2.8 nm^3 (Joseph-McCarthy *et al.*, 1996). Therefore based on its dimensions it would have to unfold to translocate. Considering the presence of four disulfide bonds, the electrophoretic force might not be sufficient in facilitating unfolding and subsequent translocation of the protein. For this reason, the protein was examined under different conditions, including in the presence and absence of denaturing and/or reducing agents.

3.2.1.2 Nanopore analysis of native and reduced ribonuclease A in the presence and absence of a denaturing agent

RNase A was subjected to nanopore analysis under different experimental conditions.

Initially, native RNase A was analyzed in the absence of reducing agents and/or denaturing agents. Upon addition of RNase A to the *cis* side (grounded), a significant, but unexpected, number of events were recorded (Figure 3.5a). The number of events was unexpected because the protein is positively charged, thus the protein would be driven against the electric field. A histogram of blockade currents (Figure 3.6a) revealed two populations of events, one with large blockade currents (-70 pA) and the other with small blockade currents (-26 pA). Over 60% of the events were large blockade events with blockade times of 0.07 ms (Table 3.3). At the point when these experiments were conducted there were no reports of intercalation events.

Based on today's literature, the large blockade events could be either translocation or intercalation events. However, translocations might be unlikely because RNase A contains four disulfide bonds. To ensure that these events are not a result of impurities, RNase A was first purified by size exclusion chromatography to remove any small contaminants followed by ion exchange chromatography to remove any contaminants of similar size to RNase A, but of different charge. The purified RNase A was then re-examined under the same experimental conditions (Figure 3.6b). It is clear that the blockade histogram profile still remains the same with 60% of the events being large blockade events (i.e translocation or intercalation events, Table 3.3). Therefore, the blockades observed for RNase A are not as a result of impurities.

Next, the effect of reducing the disulfide bonds of RNase A with TCEP (a reducing agent) was examined (Figure 3.6c). As shown in Figure 3.6c there are still two populations of events observed for the reduced protein. Furthermore, both populations have similar blockade amplitudes and proportions as those observed for the native protein (Table 3.3). In contrast, when examining native RNase A in the presence of 1 M GdnHCl, the frequency of events is dramatically increased as seen in Figure 3.5b and the proportion of the large blockade events is also increased from 62% to 87% (Figure 3.6d and Table 3.3). Similar results were obtained with reduced RNase A in the presence of GdnHCl (Figure 3.6e). It should be noted that in the presence of GdnHCl the open pore current changes as a result of higher conductivity of the GdnHCl. Therefore, the large blockade peaks are shifted more to the left in the blockade current histograms. However, when comparing the blockade current peaks as a percentage of the open pore current they all remain the same. Furthermore, the times for the large blockade events are similar for purified native RNase A and reduced RNase A in the presence and absence of GdnHCl. Based on these results it can be concluded that TCEP has little or no effect

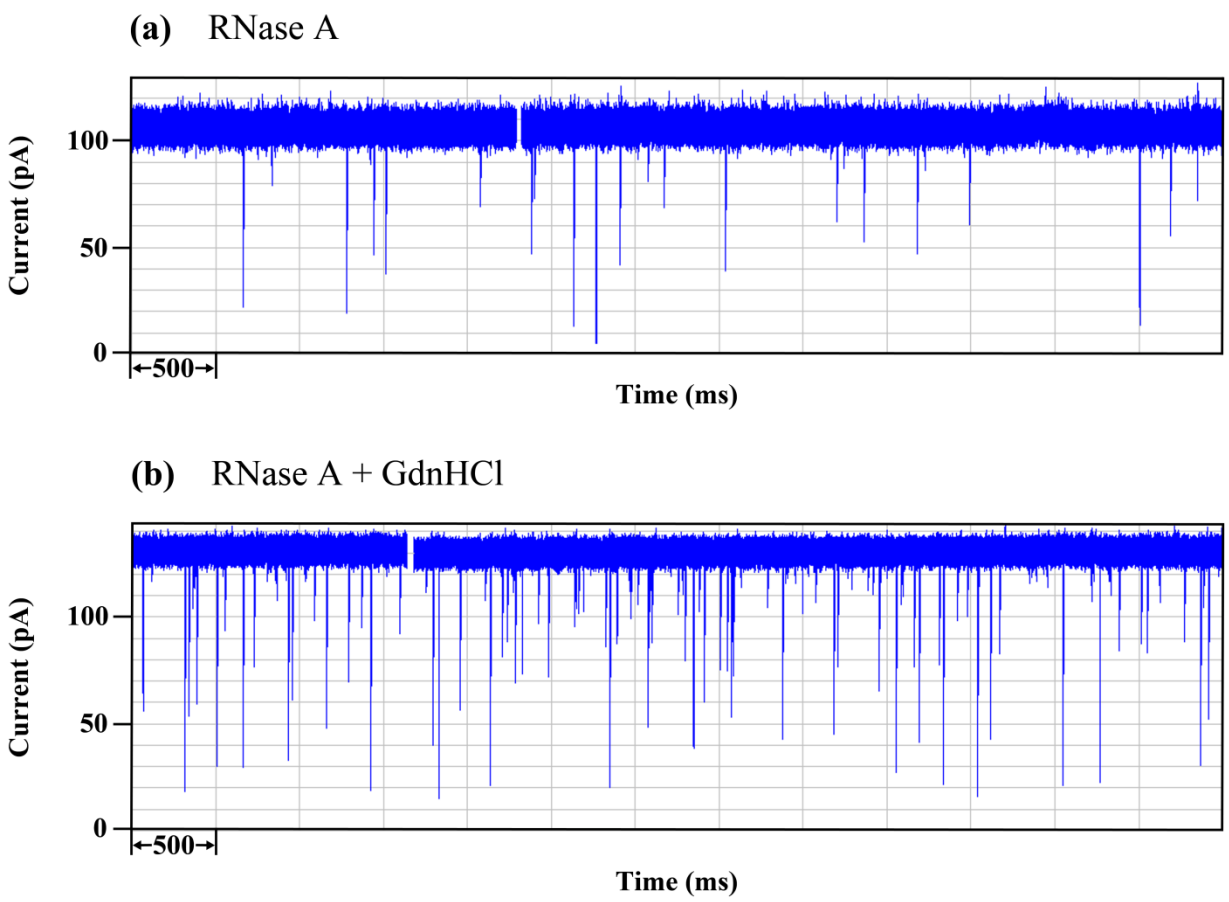

Figure 3.5. Segments of current traces for the interaction of RNase A with the α-hemolysin pore in (a) the absence and (b) the presence of 1 M GdnHCl. The open pore current is higher in the presence of GdnHCl as a result of higher conductivity of GdnHCl. Note the increase in frequency of the events and the change in proportion of large blockade events in the presence of GdnHCl.

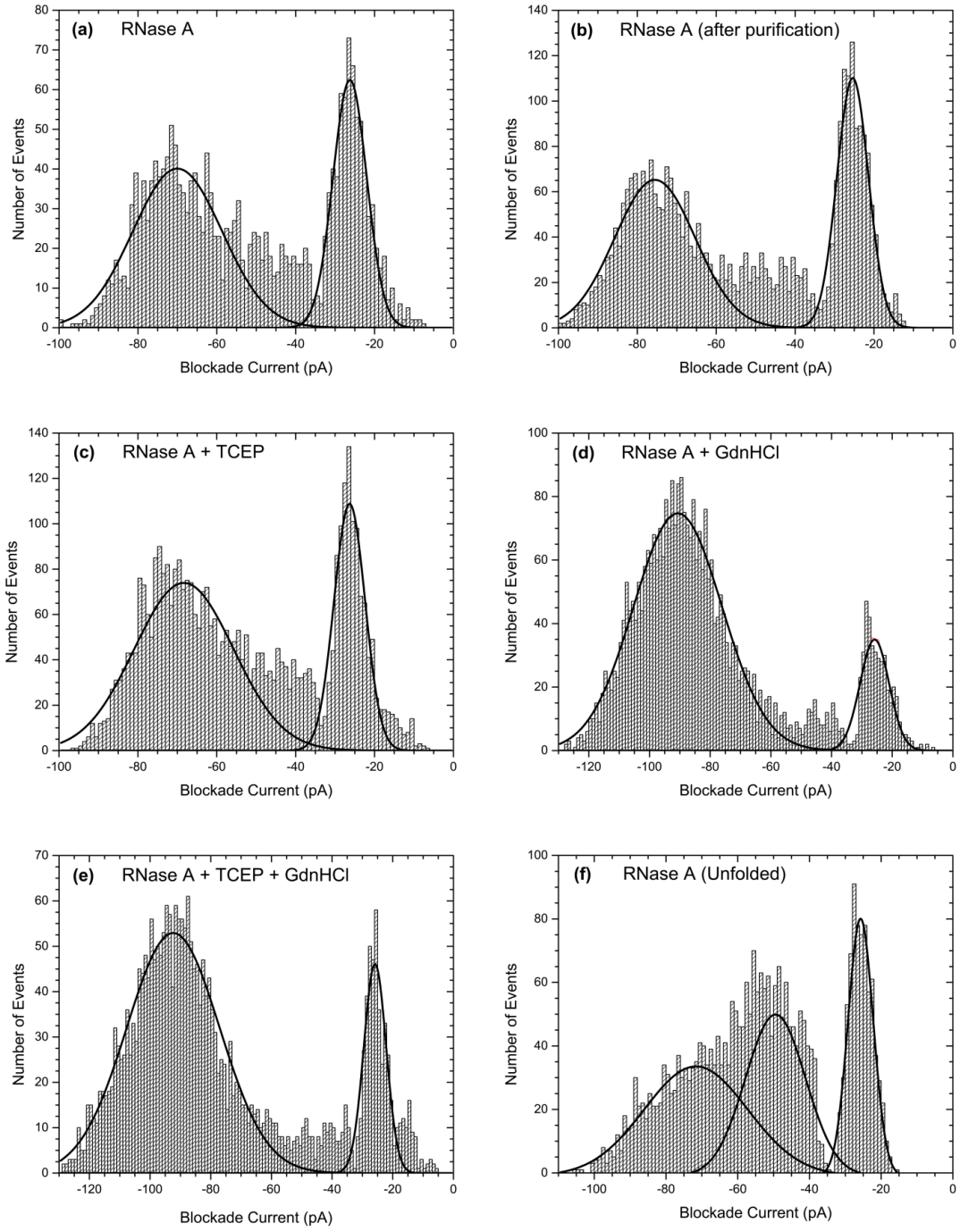

Figure 3.6. Nanopore analysis of RNase A. Blockade current histograms obtained for (a) natively folded RNase A, (b) natively folded RNase A after being subjected to size exclusion and ion exchange chromatography, (c) reduced RNase A, (d) RNase A in the presence of 1 M GdnHCl, (e) reduced RNase A in the presence of 1 M GdnHCl, and (f) completely unfolded RNase A. For the analysis of completely unfolded RNase A, the protein was pre-incubated in 4 M GdnHCl and 100 mM TCEP prior to adding it to the *cis* chamber. Each event population is fitted with the Gaussian function to obtain the peak/population blockade current value. The peak blockade current values are presented in Table 3.3.

Table 3.3. Interaction parameters of RNase A with the α-hemolysin pore under various experimental conditions.

Parameter[a]	RNase A	RNase A (after purification)	RNase A + TCEP	RNase A + GdnHCl	RNase A + TCEP + GdnHCl	Unfolded RNase A
I_1 (pA)[b]	-26.3	-25.4	-26.3	-25.8	-25.9	-25.7
I_2 (pA)	-70.0	-75.5	-68.3	-90.7	-92.4	-49.5
I_3 (pA)	-	-	-	-	-	-71.6
T_1 (ms)[c]	0.02	0.05	0.03	0.08	0.04	0.16
T_2 (ms)	0.07	0.11	0.11	0.14	0.10	0.21
T_3 (ms)	-	-	-	-	-	0.19
A_1 (%)[d]	37.2	39.7	31.5	13.28	17.3	23.5
A_2 (%)	62.8	60.3	68.5	86.72	82.7	35.2
A_3 (%)	-	-	-	-	-	41.3

[a] I_1, I_2, I_3, T_1, T_2, and T_3 represent the amplitudes and the durations of the current blockades of the respective event populations presented in Figure 3.6. A_1, A_2, and A_3 of total events forming each respective population. The peaks are numbered from right to left. A dash indicates the absence of third event population.

[b] The error is estimated to be ±1 pA.

[c] The error is estimated to be ± 10%.

[d] The error is estimated to be ± 1%.

on the interaction of the protein with the pore. On the other hand GdnHCl has a large effect on the frequency of the events and on the proportion of the translocation/intercalation events. Overall the results obtained were unexpected since the protein is much larger than the pore, contains disulfide bonds, and has a positive net charge.

3.2.1.3 Nanopore analysis of unfolded ribonuclease A

RNase A examined in the presence of 1 M GdnHCl induced a large number of events with large blockade amplitudes. Since the protein could only be partially unfolded at this denaturant concentration and partially folded protein might or might not translocate through the pore, it is not clear whether the events observed are intercalation or translocation. Therefore, it's important to examine the interaction of completely unfolded RNase A with the α-hemolysin pore and compare the results. RNase A is completely unfolded and reduced in 4 M GdnHCl and 100 mM TCEP (Bastings *et al.*, 2008). Since α-hemolysin pore cannot withstand these denaturant concentrations, the protein was denatured and reduced outside the cup and then added to the *cis* chamber (Oukhaled *et al.*, 2007).

Interaction of unfolded RNase A with α-hemolysin induced three event populations (Figure 3.6f). There is a clear bumping peak at around -26 pA (far right peak). The other two populations are partially merged together which made it extremely difficult to obtain good Gaussian fits. The middle peak at around -50 pA must be bumping events as well because their current blockade is too small to be an intercalation or translocation event for a protein of this size. On the other hand, the far left peak (around -72 pA) could be translocation events since the protein is fully unfolded. Interestingly, both folded and unfolded RNase A molecules give events with blockade currents of about -70 pA. In contrast, the blockade times for unfolded RNase A are almost twice as large as those observed for reduced, native, and partially folded RNase A (Table 3.3). Considering that the protein is fully unfolded one would expect it to freely translocate through the pore. However, the proportion of the large blockade events is only a fraction of the total events. One explanation for this might be that the protein refolds over time after being added to the *cis* chamber (Bastings *et al.*, 2008; Miyamoto *et al.*, 2009; Reinstadler *et al.*, 1996). From these results, it's difficult to conclude with confidence whether the large blockade events are translocation or intercalation events. This is why direct evidence is required to confirm protein translocation. Due to the unexpected results obtained for

nanopore analysis of RNase A, the enzyme detection experiments were temporarily abandoned and other proteins with variable chemical and physical properties were investigated.

3.2.2 Nanopore analysis of lysozyme

3.2.2.1 Introduction

The results described in section 3.2.1 are clearly different from those reported earlier for MBP where no bumping or translocation events were observed in the absence of denaturant even after 1 hour (Oukhaled *et al.*, 2007). Therefore, a protein with similar properties to RNase A was needed so as to confirm the results obtained with RNase A. Thus, lysozyme was selected for this analysis. Lysozyme is a 129 amino acid protein with a molecular weight of 14.7 kDa and contains four disulfide bonds (Merlini and Bellotti, 2005). It has a +8 net charge at physiological pH and a pI of 11 (Petkova *et al.*, 2002). Its dimensions are 4.5 X 3.0 X 3.0 nm^3 (Sethuraman and Belfort, 2005). Again, based on these properties the protein is not expected to translocate through the pore.

3.2.2.2 Nanopore analysis of native and reduced lysozyme in the presence and absence of a denaturing agent

Similar to RNase A, lysozyme was subjected to nanopore analysis under different experimental conditions to determine what conditions promote its translocation. Initially native lysozyme was analyzed in the absence of reducing agents and/or denaturing agents. Upon addition of natively folded lysozyme to the *cis* side (grounded), events with variable blockade amplitudes were recorded (Figure 3.7a). Again, this was unexpected because the protein is positively charged, thus the protein would be driven against the electric field. The blockade current histogram (Figure 3.7a) shows a clear bumping peak at around -23 pA and no clear peak for the events with blockades of -40 pA or higher. Therefore, it's impossible to fit those events with a Gaussian function. Interestingly, after reducing the disulfide bonds of the protein there are no changes in the blockade current histogram (Figure 3.7b and Table 3.4). In addition, analyzing the reduced or native protein in the presence of 1 M GdnHCl has no effect on the interaction of the protein with the pore. In contrast to RNase A, lysozyme induces a smaller

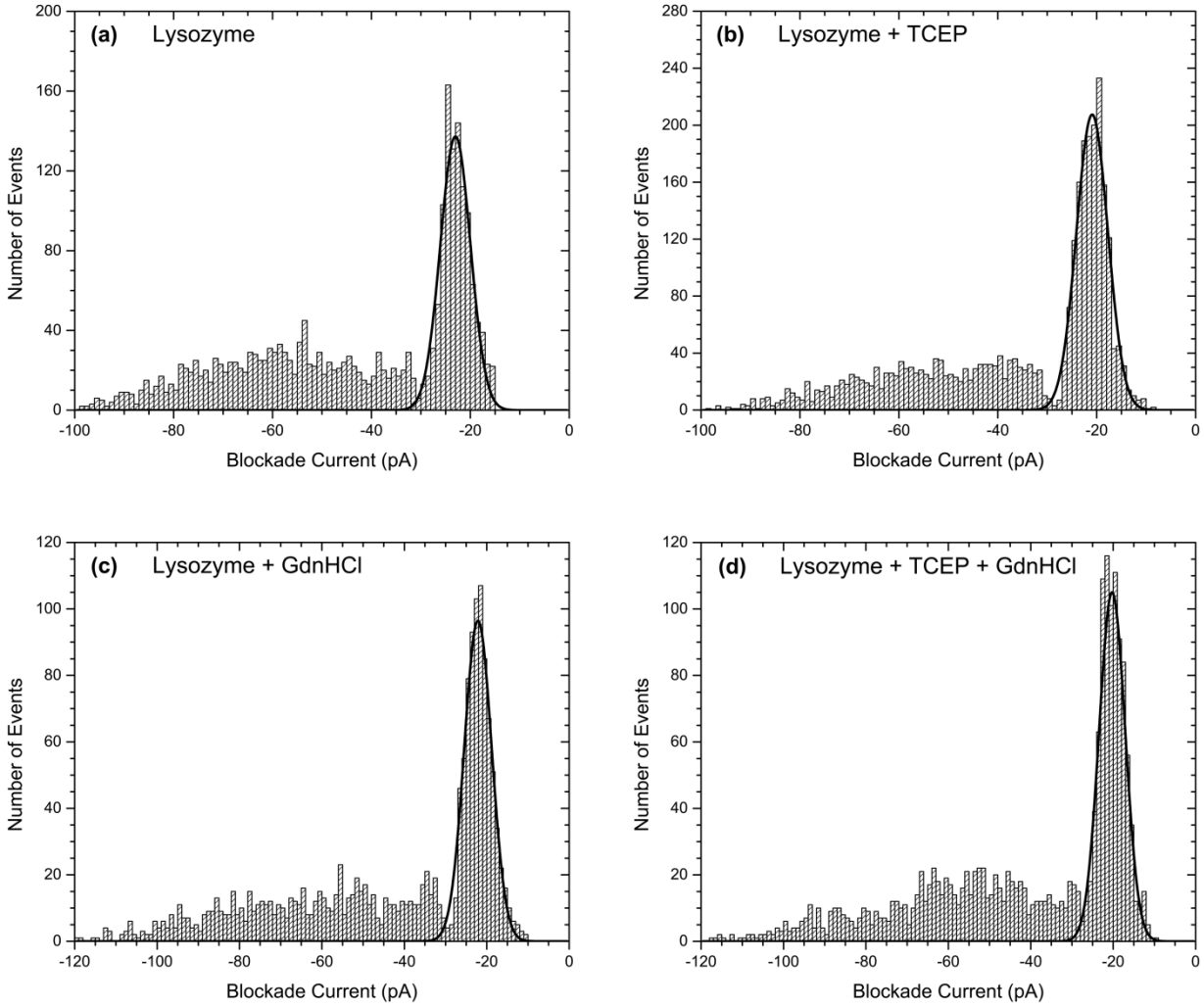

Figure 3.7. Nanopore analysis of lysozyme. Blockade current histograms obtained for (a) natively folded lysozyme, (b) reduced lysozyme, (c) lysozyme in the presence of 1 M GdnHCl, and (d) reduced lysozyme in the presence of 1 M GdnHCl. The large blockade event population (left) was too broad to be fitted with the Gaussian function. The small blockade event population (bumping peak) was fit with the Gaussian function and the peak blockade current values are presented in Table 3.4.

Table 3.4. Interaction parameters of lysozyme with the α-hemolysin pore under various experimental conditions.

Parameter[a]	Lysozyme	Lysozyme + TCEP	Lysozyme + GdnHCl	Lysozyme + TCEP + GdnHCl
I_1 (pA)[b]	-23.0	-20.9	-22.1	-20.3
I_2 (pA)	BR	BR	BR	BR
T_1 (ms)[c]	0.02	0.03	0.05	0.03
T_2 (ms)	0.13	0.13	0.17	0.13
A_1 (%)[d]	49.2	50.1	50.8	50.0
A_2 (%)	50.8	49.9	49.2	50.0

[a] I_1, I_2, T_1, and T_2 represent the amplitudes and the durations of the current blockades of the respective event populations presented in Figure 3.7. The peaks are numbered from right to left. BR indicates that the population was too broad to be fit with the Gaussian function.
[b] The error is estimated to be ±1 pA.
[c] The error is estimated to be ± 10%.
[d] The error is estimated to be ± 1%.

fraction of large blockade events which could be explained by the larger positive net charge. Overall these results do confirm that events are observed even with positively charged proteins containing disulfide bonds.

3.2.3 Nanopore analysis of proteins with different physical and chemical properties

3.2.3.1 Introduction

The results obtained with RNase A and lysozyme were not consistent with the literature at the time when these studies were conducted. One report showed that there were no events observed for natively folded MBP when analyzed with the α-hemolysin pore (Oukhaled *et al.*, 2007). Another study showed that even for a protein smaller than a pore (i.e a solid-state pore), there were no events observed when the electric field was against the translocation direction (Talaga and Li, 2009). However, the results obtained with RNase A and lysozyme clearly showed a large number of events even though the proteins were going against the electrophoretic field. Therefore these results were very intriguing. For this reason it was decided to study additional proteins with variable chemical and physical properties; namely, calmodulin, human thioredoxin, ubiquitin and bovine pancreatic trypsin inhibitor (refer to Table 3.5 for their properties). The study of these model proteins will provide more insight into protein interaction with the α-hemolysin pore.

3.2.3.2 Nanopore analysis of native basic pancreatic trypsin inhibitor, ubiquitin, human thioredoxin, and calmodulin

First, the interaction of calmodulin with the α-hemolysin pore was analyzed. Calmodulin is slightly larger than lysozyme and RNase A and is highly acidic (-25). Therefore, under the experimental set up used, its translocation would be facilitated by the electrophoretic field. However, the protein would have to unfold in order to translocate. The blockade current histogram profile (Figure 3.8a) shows a very broad translocation/intercalation peak centered around -76 pA and a typical bumping peak centered at -24 pA. The proportion of the large blockade events (i.e translocation/intercalation events) is over 70% of the total events recorded (Table 3.6). This is reasonable since the electrophoretic force acting on it is greater than for the

Table 3.5. Physical and chemical properties of the proteins analyzed in this thesis.

Protein	Property					
	Net charge	**Net charge density[i]**	**MW (kDa)**	**No. of amino acids**	**pI**	**No of S-S bonds**
Lysozyme[a]	+ 8	+ 0.062	14.3	129	11.0	4
BPTI[b]	+ 6	+ 0.103	6.5	58	10.5	3
RNase A[c]	+ 4	+ 0.032	13.7	124	9.5	4
Ubiquitin[d]	0	0	8.6	76	6.8	0
E. coli thioredoxin[e]	- 5	- 0.046	12.1	108	4.5	1
Human thioredoxin[f]	- 5	-0.048	11.1	105	4.8	1
MBP[g]	- 8	- 0.021	40.8	370	5.2	0
Calmodulin[h]	- 25	- 0.169	16.9	148	3.9	0

[a] References (Merlini and Bellotti, 2005; Petkova *et al.*, 2002; Sethuraman and Belfort, 2005).
[b] References (Ascenzi *et al.*, 2003; Braz and Howard, 2009; Gottschalk *et al.*, 2003)
[c] References (Raines, 1998)
[d] References (Kerscher *et al.*, 2006; Pickart, 2001; Vijay-Kumar *et al.*, 1987)
[e, f] References (Eun, 1996; Holmgren, 1985; Katti *et al.*, 1990; Stefankova *et al.*, 2005; Weichsel *et al.*, 1996)
[g] References (Betton and Hofnung, 1996; Doring *et al.*, 1999; Spurlino *et al.*, 1991; Telmer and Shilton, 2003)
[h] References (Barford *et al.*, 1986; Chin and Means, 2000; Kurokawa and Nonomura, 1988; Walsh, 1983)
[i] Calculated from the net charge divided by the number of amino acids

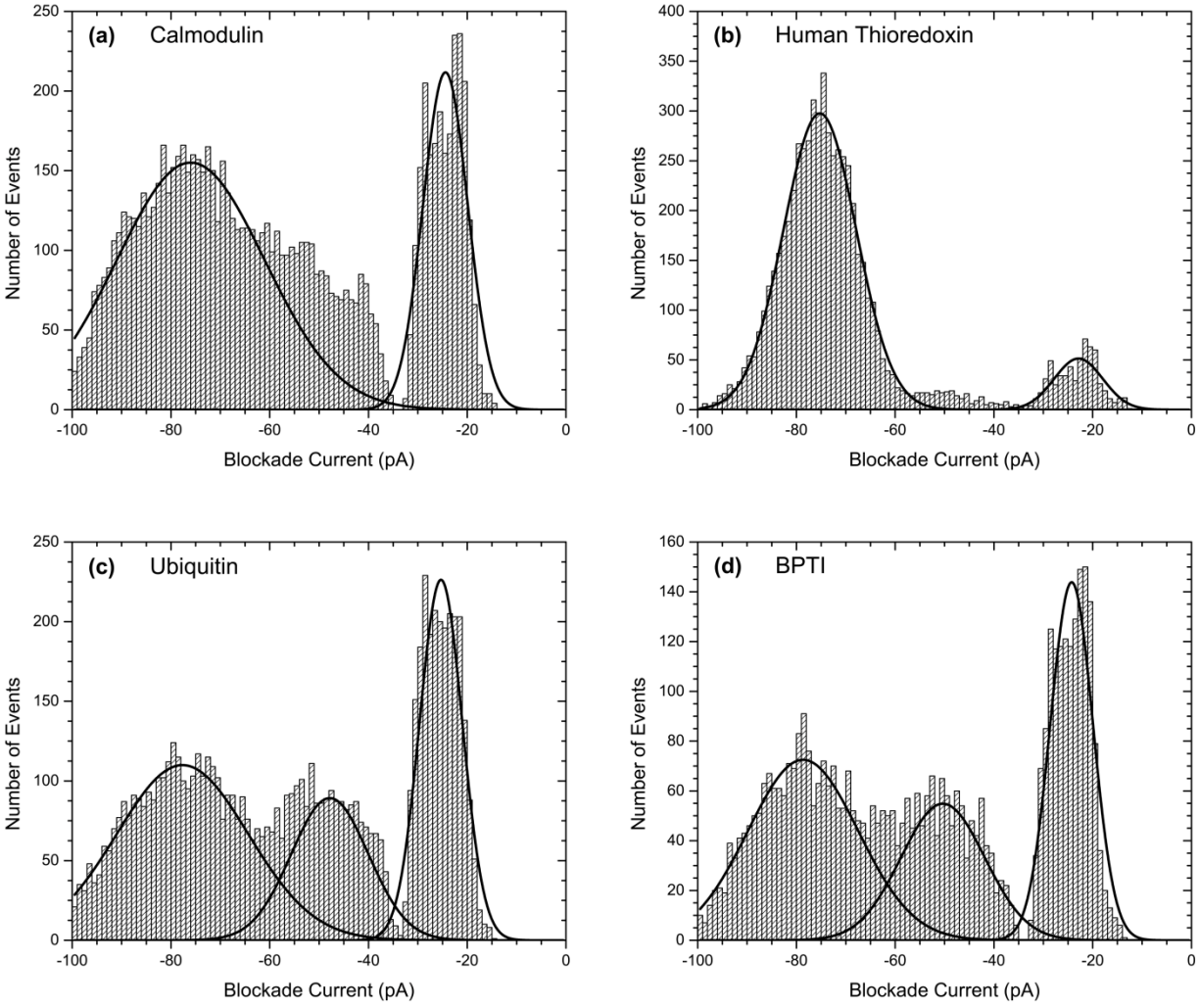

Figure 3.8. Blockade current histograms obtained for the interaction of (a) calmodulin, (b) human thioredoxin, (c) ubiquitin, and (d) basic pancreatic trypsin inhibitor with the α-hemolysin pore. Each event population is fitted with the Gaussian function to obtain the peak/population blockade current value. The peak blockade current values are presented in Table 3.6.

Table 3.6. Interaction parameters of calmodulin, human thioredoxin, ubiquitin, and BPTI with the α-hemolysin pore.

Parameter[a]	Calmodulin	Human Thioredoxin	Ubiquitin	BPTI
I_1 (pA)[b]	-24.4	-22.9	-25.3	-24.3
I_2 (pA)	-76.0	-75.2	-47.8	-50.3
I_3 (pA)	-	-	-77.7	-78.7
T_1 (ms)[c]	0.13	0.11	0.10	0.10
T_2 (ms)	0.17	0.10	0.19	0.14
T_3 (ms)	-	-	0.23	0.21
A_1 (%)[d]	29.3	10.3	31.2	32.7
A_2 (%)	70.7	89.7	22.1	24.5
A_3 (%)	-	-	46.7	42.8

[a] I_1, I_2, I_3, T_1, T_2, and T_3 represent the amplitudes and the durations of the current blockades of the respective event populations presented in Figure 3.8. A_1, A_2, and A_3 of total events forming each respective population. The peaks are numbered from right to left. A dash indicates absence of a third population of events.
[b] The error is estimated to be ±1 pA.
[c] The error is estimated to be ± 10%.
[d] The error is estimated to be ± 1%.

previously analyzed proteins because the protein has a higher net charge density (Table 3.5). Analysis of human thioredoxin, another negatively charged protein, yielded about 90% large blockade events (Figure 3.8b and Table 3.6). This protein is smaller than the other three proteins and has one disulfide bond. However, from the examination of the crystal structure, it appears that the disulfide bond position might not hinder the entrance of the protein into the pore, independent of whether the protein intercalates or translocates. On the other hand the current blockade histograms for ubiquitin and BPTI, which are very small proteins but with different properties showed three very similar peaks (Figure 3.8c, d). The far left peak (i.e the translocation/intercalation peak) for both proteins is centered around -78 pA, which is very similar to calmodulin and human thioredoxin. However, the duration times for the events within that peak are larger than for calmodulin or human thioredoxin (Table 3.6). Overall there seems to be little correlation between the event parameters summarized in Table 3.6 and the protein properties summarized in Table 3.5.

3.2.4 Nanopore analysis of maltose binding protein and *E. coli* thioredoxin

3.2.4.1 Introduction

A puzzling but consistent observation from the above results is that all proteins analyzed give rise to a significant number of events with both large and small % current blockades even in the absence of denaturants. It should be noted that these results are unlikely to be due to low molecular weight impurities in the proteins. First, they are highly purified recombinant proteins. Second, as shown in Figure 3.6b, RNase A was subjected to a second purification by gel exclusion and ion exchange chromatography and there was no significant change in the event frequency and profile. For this reason, it was decided to study MBP which had been previously studied by another research group where there were no events observed in the absence of denaturant (Oukhaled *et al.*, 2007). Furthermore, this protein is stably folded and does not contain a metal binding site, its crystallographic structures are available with and without maltose (a MBP ligand), and it's commercially available in a highly purified form for use as an NMR standard (Duan and Quiocho, 2001; Spurlino *et al.*, 1991; Telmer and Shilton, 2003). MBP is a 370 amino acid protein with a molecular weight of 40.8 kDa and contains no

disulfide bonds (Telmer and Shilton, 2003). It has -8 net charge at physiological pH and a pI of 5.2. Its dimensions are 3.0 x 4.0 x 6.5 nm^3, which make it larger than the previously analyzed proteins (Oukhaled *et al.*, 2007). Together, these properties make this protein ideal model protein for studying protein-α-hemolysin interactions and protein-ligand interactions.

3.4.2 Nanopore analysis of maltose binding protein in different buffers, with and without EDTA

The analysis of proteins and peptides reported in sections 3.1, 3.2, and 3.4 of this thesis were all done in phosphate buffer. However, the analysis of MBP reported by Oukhaled *et al*. was done in HEPES buffer (Oukhaled *et al.*, 2007). Previous work has shown that metal ions have an effect on the interaction of proteins and peptides with the α-hemolysin pore (Baran *et al.*, 2010; Stefureac and Lee, 2008; Stefureac *et al.*, 2010a). In addition, it has been shown that plastic, glass, and other materials are a potential source of metal ions and by necessity proteins are in constant contact with these materials (Huang *et al.*, 2004). While phosphate buffer chelates divalent metal ions, HEPES buffer does not (Sambrook and Russell, 2001). For this reason we examined MBP in both KPi and HEPES buffers. As shown in Figure 3.9a, b the frequency of events is much greater when analyzed in KPi buffer than in HEPES buffer. Furthermore, in KPi buffer the majority of the events are large blockade events with blockade currents of about -76 pA and duration times of 0.2 ms (Figure 3.10a and Table 3.7). The duration times are similar to those reported earlier for MBP in the presence of 1 M GdnHCl (Oukhaled *et al.*, 2007). Surprisingly, there are fewer large blockades and the peak for these events becomes larger and less prominent when the experiment is repeated in a HEPES buffer (Figure 3.10b and Table 3.9). However, in a buffer of HEPES with 1 mM EDTA (Fig. 3.9c) the event frequency reverts back to the same levels as those observed in KPi buffer. In addition, the proportion of the large blockade events is much greater in the presence than in the absence of EDTA, 80% versus 53% (Figure 3.10c). Furthermore, the duration time for the large blockade events in the HEPES buffer with 1 mM EDTA are the same as those obtained in KPi buffer. MBP was also examined in KPi buffer in the presence of 1 M GdnHCl (Figure 3.9d) and the frequency of events was much lower than what was reported by Oukhaled *et al*. (Oukhaled *et al.*, 2007). In addition, the proportion of large blockade events was dramatically lower than what was reported. As will be shown in later sections, even in the presence of

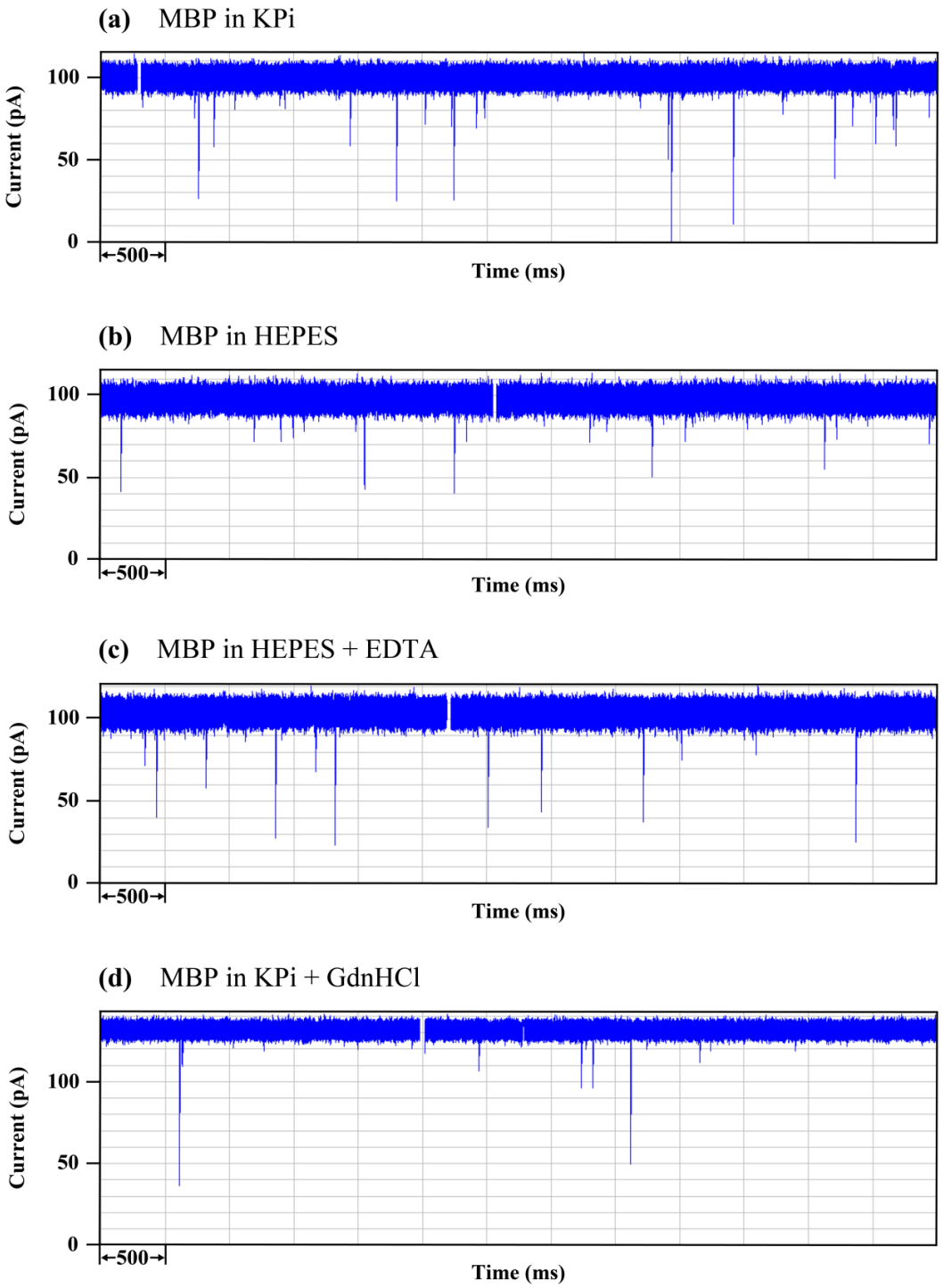

Figure 3.9. Segments of current traces for the interaction of MBP with the α-hemolysin pore in (a) KPi buffer, (b) HEPES buffer, (c) HEPES buffer with 1 mM EDTA, and (d) KPi buffer with 1 M GdnHCl. The open pore current is higher in the presence of GdnHCl as a result of higher conductivity of GdnHCl. Note the change in frequency and type of events observed with the change in the electrolyte solution.

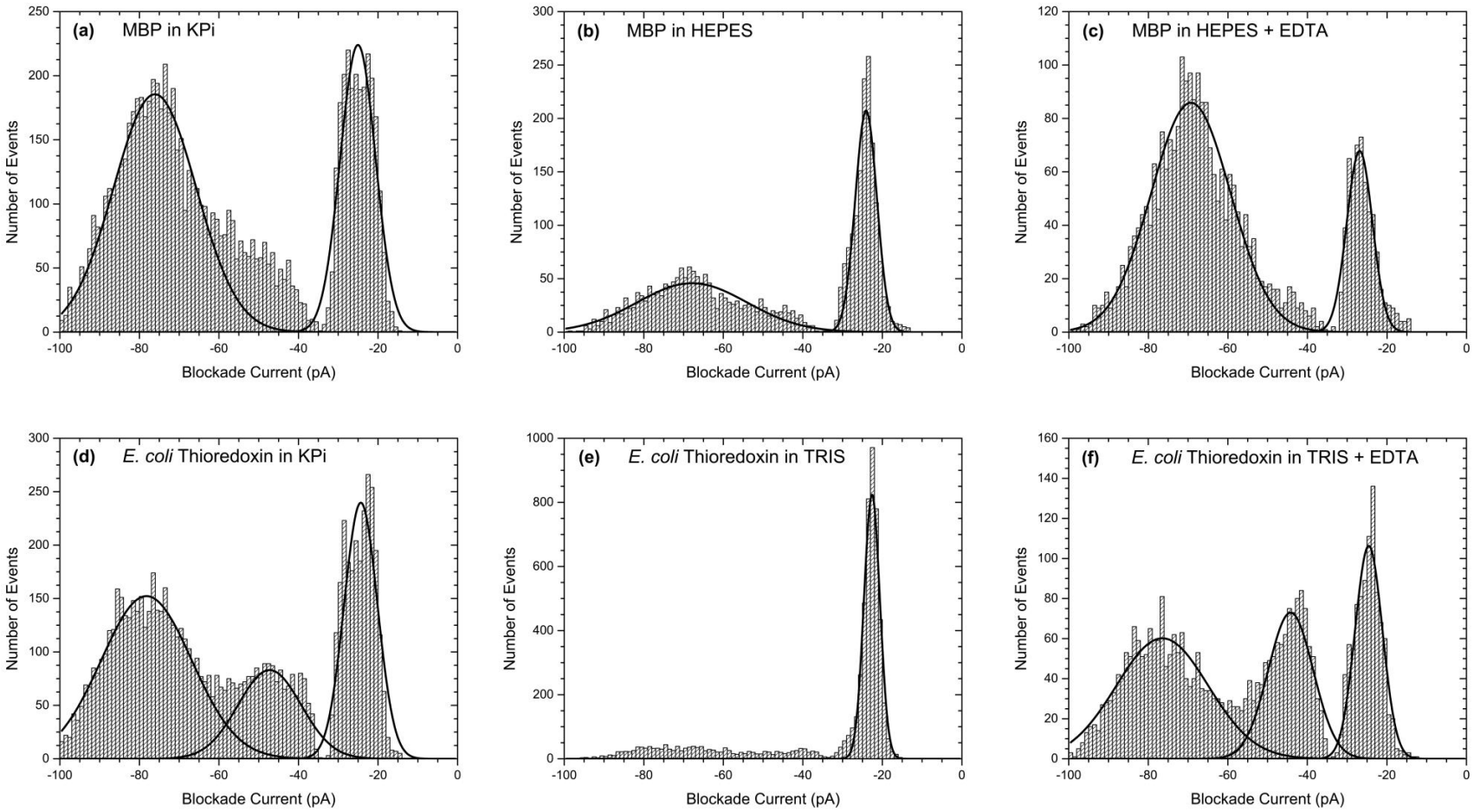

Figure 3.10. Effect of EDTA and buffer on the interaction of MBP and *E. coli* thioredoxin with the α-hemolysin pore. Current blockade histograms were constructed for the analysis of MBP in (a) KPi buffer, (b) HEPES buffer, and (c) HEPES buffer with 1 mM EDTA present in the *cis* chamber. Similarly, current blockade histograms were constructed for the analysis of *E. coli* thioredoxin in (d) KPi buffer, (e) TRIS buffer, and (f) TRIS buffer with 1 mM EDTA present in the *cis* chamber. Each event population present in the current blockade histograms was fitted with the Gaussian function to obtain the peak/population blockade current value. The peak blockade current values are presented in Table 3.7.

Table 3.7. Effect of EDTA and buffer on the interaction of MBP and *E. coli* Thioredoxin with the α-hemolysin pore.

Parameter[a]	MBP			*E. coli* Thioredoxin		
	KPi	HEPES	HEPES + EDTA	KPi	TRIS	TRIS + EDTA
I_1 (pA)[b]	-25.1	-24.1	-26.9	-24.3	-22.6	-24.6
I_2 (pA)	-76.1	-67.9	-69.3	-47.3	BR	-44.2
I_3 (pA)	-	-	-	-78.2	-	-76.5
T_1 (ms)[c]	0.11	0.20	0.14	0.11	0.16	0.10
T_2 (ms)	0.19	0.14	0.17	0.14	BR	0.16
T_3 (ms)	-	-	-	0.19	-	0.21
A_1 (%)[d]	34.0	47.1	20.3	29.5	76.0	24.8
A_2 (%)	66.0	52.9	79.7	19.4	24.0	28.0
A_3 (%)	-	-	-	51.1	-	47.2

[a] I_1, I_2, I_3, T_1, T_2, and T_3 represent the amplitudes and the durations of the current blockades of the respective event populations presented in Figure 3.10. A_1, A_2, and A_3 of total events forming each respective population. The peaks are numbered from right to left. A dash indicates absence of a third population of events. BR indicates that the population was too broad to be fit with the Gaussian function.

[b] The error is estimated to be ±1 pA.

[c] The error is estimated to be ± 10%.

[d] The error is estimated to be ± 1%.

higher concentrations of denaturant, the frequency of events remains unchanged. Thus, these results are in contradiction with the results obtained by Oukhaled *et al*. (Oukhaled *et al.*, 2007).

In order to confirm the importance of the buffer and EDTA, *E. coli* thioredoxin was examined in KPi, TRIS buffer, and TRIS with 1 mM EDTA (Fig. 3.10d, e, f and Table 3.7). In KPi there are two populations with large current blockades greater than -40 pA as are shown on the current blockade histogram in Fig. 3.10d. However, in TRIS buffer both of these peaks are suppressed (almost non-existent) and the peak belonging to bumping events, at about -25 pA, is significantly narrower (Fig. 3.10e). Upon addition of 1 mM EDTA to the *cis* side, the original profile is restored with a decrease in the proportion of bumping events compared to KPi (Fig. 3.10f). Again, duration times for the large blockade events at -77 pA are similar in the KPi buffer and the TRIS buffer with 1 mM EDTA (Table 3.7). It should be noted that the structures of *E. coli* thioredoxin and human thioredoxin are very similar (Katti *et al.*, 1990; Weichsel *et al.*, 1996). In addition, they have the same overall net charge (Table 3.5), dimensions, and number of disulfide bonds. However, the results obtained from the analysis of these two proteins are very different (Figure 3.8b and Table 3.6 versus Figure 3.10d and Table 3.7). The histogram of the blockade current values for the *E. coli* protein shows three peaks present in comparison to the human protein which yields only two peaks. It's very puzzling how two different proteins such as ubiquitin and BPTI give very similar results, but two similar proteins such as the human and *E. coli* thioredoxin give totally different results.

Overall, these results suggest that EDTA plays a critical role in nanopore analysis of proteins. In the absence of EDTA, different results might be obtained for the same protein. Another conclusion reached from these results is that events are observed with all proteins, independent of the buffer used.

3.2.4.3 Nanopore analysis of maltose binding protein in the presence of metal ions

The dramatic effect of EDTA and phosphate buffer, both of which can sequester metal ions, suggested that metal ion contamination might be involved. To test this hypothesis, MBP was examined in HEPES buffer in the presence of metal ions. Upon addition of 10 µM Cu^{2+}, Zn^{2+} or Mg^{2+} to the *cis* chamber, the large blockade events almost disappear (Figure 3.11 and Table 3.8). This concentration of metal ions is well below the concentrations reported to alter the

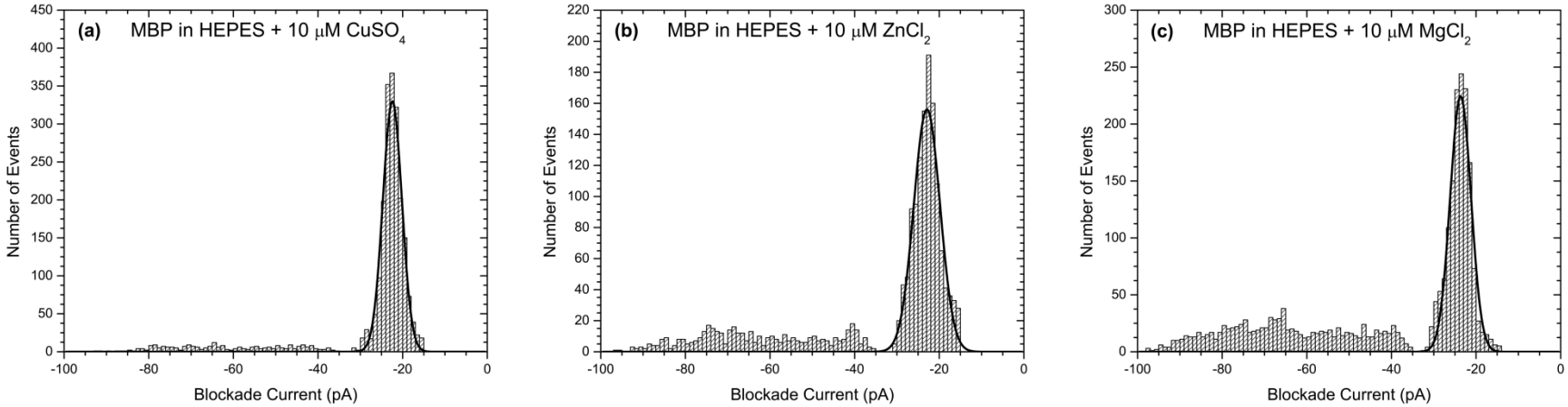

Figure 3.11. Effect of metal ions on the interaction of MBP with the α-hemolysin pore. The effect of (a) 10 μM $CuSO_4$, (b) 10 μM $ZnCl_2$, and (c) 10 μM $MgCl_2$ on the interaction of MBP with the α-hemolysin pore was investigated in HEPES buffer and the corresponding current blockade histograms were constructed for each experiment. The peak blockade current values are presented in Table 3.8.

Table 3.8. Effect of metal ions on the interaction of MBP with the α-hemolysin pore in HEPES buffer.

Parameter[a]	**$CuSO_4$**	**$ZnCl_2$**	**$MgCl_2$**
I_1 (pA)[b]	-22.4	-22.9	-23.7
I_2 (pA)	BR	BR	BR
T_1 (ms)[c]	0.43	0.17	0.22
T_2 (ms)	BR	BR	BR
A_1 (%)[d]	87.9	72.5	59.2
A_2 (%)	12.1	27.5	40.8

[a] I_1, I_2, T_1, and T_2 represent the amplitudes and the durations of the current blockades of the respective event populations presented in Figure 3.11. A_1 and A_2 are percent of total events forming each respective population. The peaks are numbered from right to left. BR indicates that the population was too broad to be fit with the Gaussian function.
[b] The error is estimated to be ±1 pA.
[c] The error is estimated to be ± 10%.
[d] The error is estimated to be ± 1%.

conductivity of the pore. While all three metal ions reduce the proportions of large blockade events, Cu^{2+} is the most effective. This effect is readily reversible with the addition of EDTA to the *cis* chamber. Therefore, the difference in results between different buffers (section 3.2.4.2) is as a result of metal ion contamination.

3.2.4.4 Nanopore analysis of maltose binding protein in the presence of maltose or lactose

The binding of metal ions by MBP is likely to be non-specific since there is no evidence that MBP has a metal binding site. MBP does however have a specific ligand, maltose, with a Kd of 1200 nM (Telmer and Shilton, 2003). The effect of maltose was examined in HEPES buffer with 1 mM EDTA at a ratio of three molecules of sugar for every molecule of protein (Figure 3.12a and Figure 3.13a). MBP binds only one molecule of maltose but an excess of maltose was added to ensure that most of MBP present in the *cis* chamber is bound by the ligand. Addition of maltose to the *cis* chamber decreased the proportion of the translocation/intercalation events, from 80% to 37% (Table 3.9). Furthermore, the duration times for both populations increased in the presence of maltose. Under the same conditions, there were no events observed for maltose alone (Figure 3.12b). Thus the reduction in translocation/intercalation events is in fact because of the binding of maltose to MBP. As a control, the effect of lactose which does not bind MBP was also investigated in HEPES buffer with 1 mM EDTA (Figure 3.12c and Figure 3.13b) (Doring *et al.*, 1999; Telmer and Shilton, 2003). Curiously, this resulted in the appearance of an additional peak at around -40 pA. Upon examination of the lactose alone a significant number of events were recorded including a peak at -40 pA (Figure 3.12d and Figure 3.13c). Lactose is too small to be detected by nanopore analysis under the current experimental set up so these events must be due to a higher molecular weight impurity (Rosenstein *et al.*, 2012). Therefore, the effect of maltose strongly supports the view that the observed large blockade events are indeed due to MBP and not peptide impurities since there is no evidence that maltose binds to peptides. However, it's not clear if these events are translocation or intercalation events. It has been shown that with peptides the best method to differentiate between translocation and intercalation events it to study the effect of voltage on duration times. Thus, the proteins must be examined at different voltages.

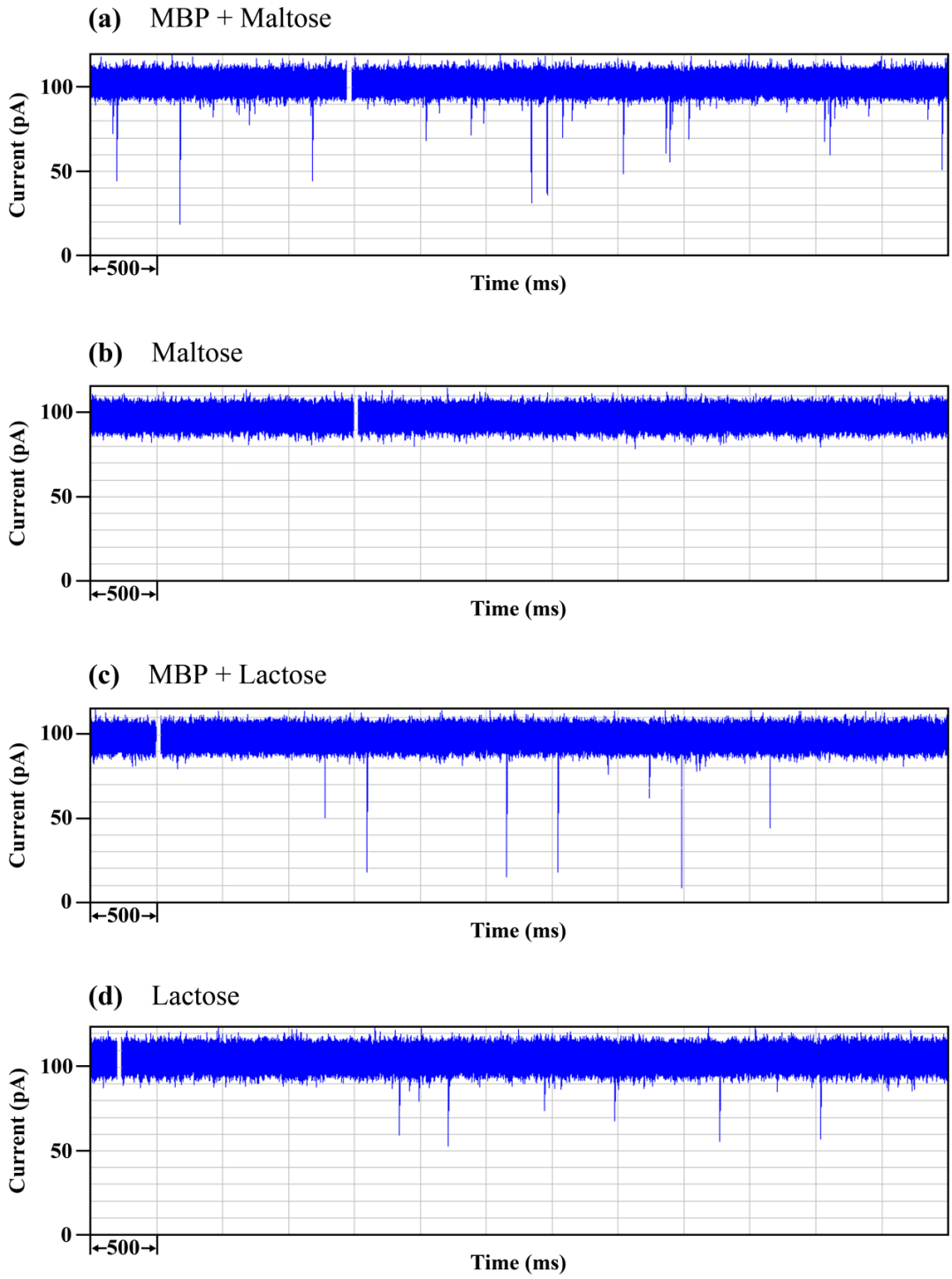

Figure 3.12. Segments of current traces for the interaction of MBP with the α-hemolysin pore in the presence of 3 moles of (a) maltose or (c) lactose per mole of MBP with the *cis* electrolyte being 1 M KCl in 5 mM HEPES buffer (pH 7.5) with 1 mM EDTA. The interaction of (b) maltose alone with the α-hemolysin pore induces no events. The interaction of (c) lactose alone with the α-hemolysin pore induces short blockade events.

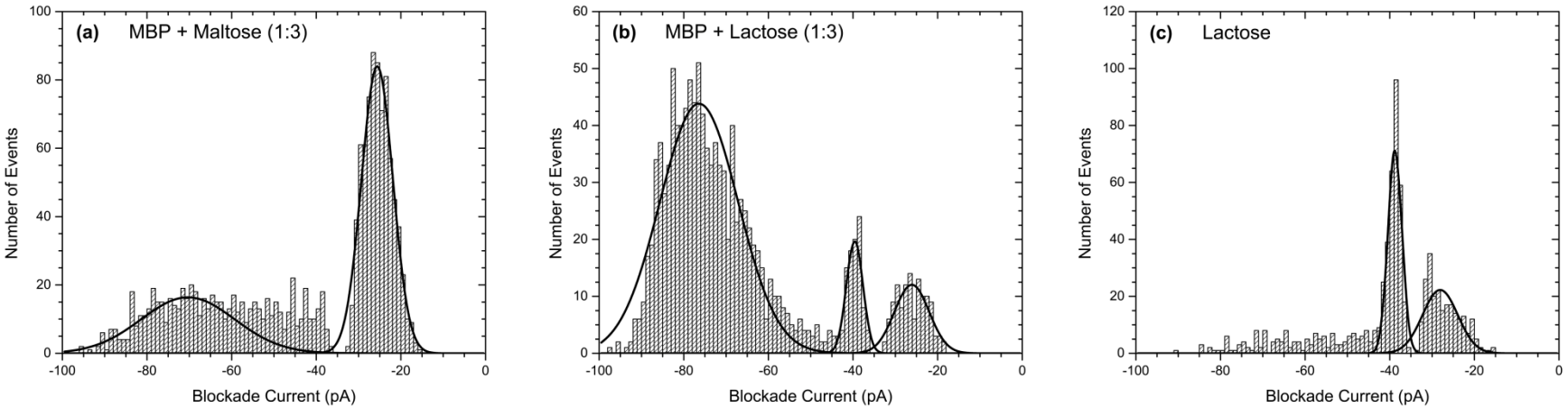

Figure 3.13. Effect of (a) maltose and (b) lactose on the interaction of MBP with α-hemolysin pore in HEPES buffer with 1 mM EDTA. The analysis was performed in the presence of three moles of sugar per mole of protein. Part (c) shows the current blockade histogram obtained for lactose alone as a control. The peak blockade current values are presented in Table 3.9.

Table 3.9. Effect of maltose and lactose on the interaction of MBP with α-hemolysin pore in HEPES buffer with EDTA.

Parameter[a]	MBP + Maltose (1:3)	MBP + Lactose (1:3)	Lactose only
I_1 (pA)[b]	-25.6	-26.1	-28.1
I_2 (pA)	-70.3	-39.6	-38.8
I_3 (pA)	-	-76.6	-
T_1 (ms)[c]	0.18	0.08	0.13
T_2 (ms)	0.22	0.39	0.31
T_3 (ms)	-	0.13	-
A_1 (%)[d]	63.2	10.1	43.8
A_2 (%)	36.8	7.8	56.2
A_3 (%)	-	82.1	-

[a] I_1, I_2, I_3, T_1, T_2, and T_3 represent the amplitudes and the durations of the current blockades of the respective event populations presented in Figure 3.13. A_1, A_2, and A_3 of total events forming each respective population. The peaks are numbered from right to left. A dash indicates absence of a third population of events. The results are the averages of at least three independent measurements.

[b] The error is estimated to be ±1 pA.

[c] The error is estimated to be ± 10%.

[d] The error is estimated to be ± 1%.

3.2.5 Effect of voltage on interaction of proteins with the α-hemolysin pore

3.2.5.1 Introduction

The effect of voltage on the translocation parameters of peptides and proteins has been studied previously by our group and others (Christensen *et al.*, 2011; Movileanu *et al.*, 2005; Oukhaled *et al.*, 2007; Pastoriza-Gallego *et al.*, 2011; Stefureac *et al.*, 2010b). It has been suggested that the voltage effect on the interaction of a molecule with the pore can be used to provide indirect evidence of protein or peptide translocation through the pore. For example, for an electrophoretically driven translocation, the duration times are expected to be inversely proportional to the applied voltage. On the other hand, the frequency of events is expected to be linearly proportional to the applied voltage (Baran *et al.*, 2010; Christensen *et al.*, 2011; Movileanu *et al.*, 2005). Furthermore, a molecule translocating the pore should induce the same percent current blockade independent of the voltage (Oukhaled *et al.*, 2012; Stefureac *et al.*, 2010b). This is because the volume occupied by the pore is not dependent on the voltage. If these three conditions are met then one can assume that the molecule has translocated the pore. In the case of an intercalation event, the duration times are expected to increase with the applied voltage (Meng *et al.*, 2010). Thus, in an effort to determine if the large blockade events observed with the proteins are translocations or intercalations we examined RNase A, Calmodulin, MBP, and *E. coli* thioredoxin at different voltages.

3.2.5.2 Nanopore analysis of proteins at different voltages

RNase A was subjected to nanopore analysis at different voltages (50 mV, 100 mV, and 150 mV) and the blockade current histograms obtained for each voltage are shown in Figure 3.14a. As stated in section 3.2.1, RNase A is positively charged protein (+4) and therefore under the experimental set up used here, the protein would have to go against the electric field to translocate through the pore. Hence, if the protein is indeed translocating the pore, an increase in the applied voltage should result in an increase in the blockade duration times. If the protein is intercalating then the duration times would increase with increased applied voltage. Figure 3.14a shows the same percent current block (about 71% block) for the translocation/intercalation events independent of the applied voltage. In addition, the frequency

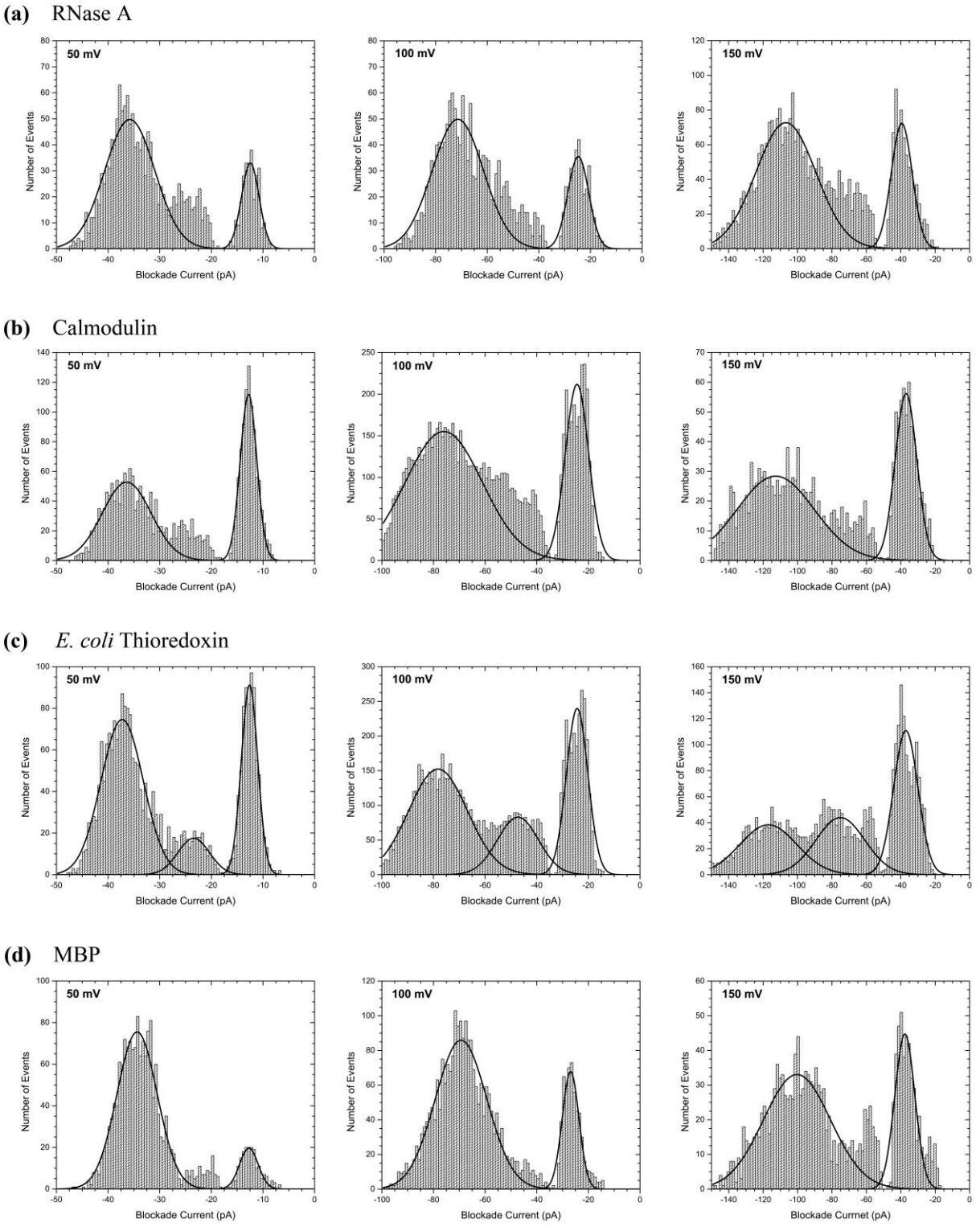

Figure 3.14. Current blockade histograms for (a) RNase A, (b) calmodulin, (c) *E. coli* thioredoxin, and (d) MBP with the α-hemolysin pore under applied potentials of 50 mV, 100 mV, and 150 mV. The peak blockade current values and the duration times are presented in Table 3.10.

of the events increased with voltage. These are two indications of a molecule translocating through the pore. However, the duration times for the large blockade events remained unchanged at all three voltages (Table 3.10). Therefore, the indirect approach does not provide an answer on whether the protein is translocating or intercalating. The lack of change in duration times as a function of voltage might be as a result of low net charge density on RNase A (+0.032). For this reason, Calmodulin, MBP, and *E. coli* thioredoxin with different net charge densities (Table 3.5) were examined at three different voltages.

Similar to RNase A, the blockade current histograms for all three proteins (Figure 3.14) showed that their respective percent current block for the large blockade events remained the same independent of the voltage. In contrast, the duration times for Calmodulin and *E. coli* thioredoxin increased with increasing voltage while remaining the same for MBP (Table 3.10). This indicates that Calmodulin and *E. coli* thioredoxin do not translocate the α-hemolysin pore. As for MBP, it cannot be concluded if the protein is translocating or intercalating since there is no change in times as a function of voltage. It should be noted that Calmodulin which has the largest net charge density showed the largest change in duration times with change in voltage. The effect of voltage on duration times observed for MBP and RNase A were surprising since there have been no such reports in literature.

To better understand these results we investigated the effect of voltage on blockade current and time for MBP in the presence of a denaturant, GdnHCl. MBP was studied at 75 mV and 100 mV in the presence of 1.5 M GdnHCl (Figure 3.15). At this GdmHCl concentration, MBP is completely unfolded and should translocate the α-hemolysin pore (Betton and Hofnung, 1996; Oukhaled *et al.*, 2007). As shown in Figure 3.15, the open pore currents for 100 mV and 75 mV were 200 pA and 150 pA, respectively. This is as a result of a conductance increase in the presence of 1.5 M GdnHCl. The blockade current as a percent of open pore current remained roughly the same for both applied voltages (Table 3.11). This fits one of the criteria for the indirect evidence of protein translocation. In addition, the times for the high blockade current events increased as the voltage decreased (Table 3.11). This further provides indirect evidence that those events are translocation. As a result of the high concentration of denaturant it was impossible to conduct this experiment at higher voltages because the pore was becoming frequently blocked. Furthermore, the event frequency was extremely low at voltages lower than 75 mV. However, based on the data obtained it is reasonable to conclude that the protein

Table 3.10. Effect of voltage on the interaction of RNase A, calmodulin, MBP, and *E. coli* thioredoxin with the α-hemolysin pore.

	RNase A			**Calmodulin**			**MBP**			***E. coli* Thioredoxin**		
Parameter[a]	50 (mV)	100 (mV)	150 (mV)	50 (mV)	100 (mV)	150 (mV)	50 (mV)	100 (mV)	150 (mV)	50 (mV)	100 (mV)	150 (mV)
I_1 (pA)[b]	-12.5	-24.7	-39.4	-12.8	-24.4	-37.0	-12.7	-26.9	-37.6	-12.6	-24.3	-37.0
I_2 (pA)	-35.8	-71.4	-106.7	-36.4	-76.0	-112.7	-34.4	-69.3	-100.3	-23.4	-47.3	-75.1
I_3 (pA)	-	-	-	-	-	-	-	-	-	-37.3	-78.2	-116.9
T_1 (ms)[c]	0.09	0.15	0.12	0.05	0.13	0.14	0.06	0.14	0.12	0.04	0.11	0.09
T_2 (ms)	0.17	0.18	0.18	.12	0.17	0.25	0.16	0.17	0.18	0.13	0.14	0.23
T_3 (ms)	-	-	-	-	-	-	-	-	-	0.13	0.19	0.23
A_1 (%)[d]	18.9	22.6	25.6	41.9	29.3	35.7	10.7	20.3	28.8	28.7	29.5	38.3
A_2 (%)	81.1	77.4	74.4	58.1	70.7	64.3	89.3	79.7	71.2	10.7	19.5	30.6
A_3 (%)	-	-	-	-	-	-	-	-	-	60.6	51.0	31.1

[a] I_1, I_2, I_3, T_1, T_2, and T_3 represent the amplitudes and the durations of the current blockades of the respective event populations presented in Figure 3.14. A_1, A_2, and A_3 of total events forming each respective population. The peaks are numbered from right to left. A dash indicates absence of a third population of events.

[b] The error is estimated to be ±1 pA.

[c] The error is estimated to be ± 10%.

[d] The error is estimated to be ± 1%.

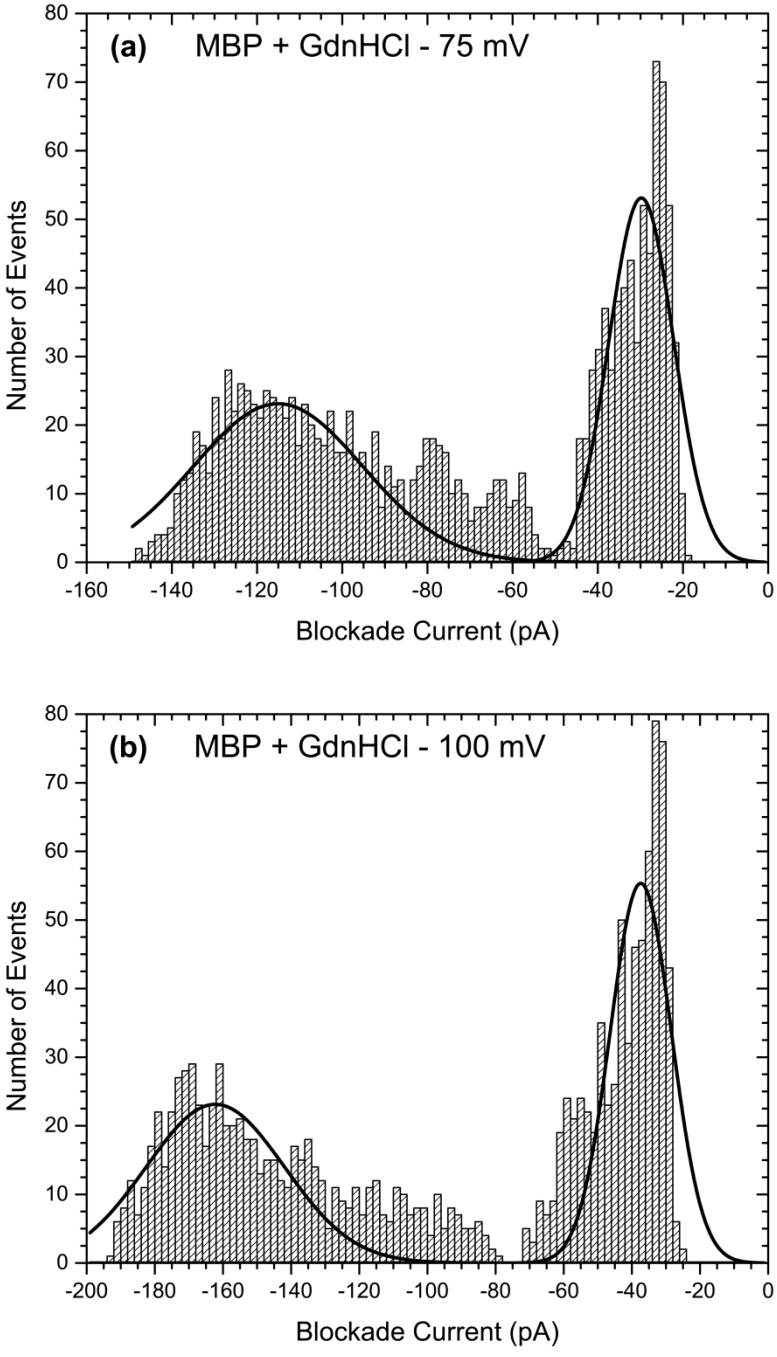

Figure 3.15. Current blockade histograms for MBP in HEPES buffer with 1 mM EDTA and 1.5 M GdnHCl under applied potentials of (a) 75 mV and (b) 100 mV. The peak blockade current values and the duration times are presented in Table 3.11.

Table 3.11. Effect of voltage on interaction of MBP with the α-hemolysin pore in HEPES buffer with 1 mM EDTA and 1.5 M GdnHCl.

Parameter[a]	Applied Voltage	
	75 mV	**100 mV**
I_1 (pA)[b]	-29.8	-37.4
I_2 (pA)	-115.1	-162.2
T_1 (ms)[c]	0.16	0.13
T_2 (ms)	0.20	0.14
A_1 (%)[d]	46.9	51.6
A_2 (%)	53.1	48.4

a I_1, I_2, T_1, and T_2represent the amplitudes and the durations of the current blockades of the respective event populations presented in Figure 3.15. A_1 and A_2 are percent of total events forming each respective population. The peaks are numbered from right to left.

[b] The error is estimated to be ±1 pA.

[c] The error is estimated to be ± 10%.

[d] The error is estimated to be ± 1%.

does translocate when unfolded by a denaturing agent. While, Oukhaled *et al*. reported very high frequency of events for MBP in the presence of 1.5 M GdnHCl, this was not the case here (Oukhaled *et al.*, 2007). This is yet another disagreement between their results and ours.

3.2.5.3 Zeta potentials of proteins

The high event rate observed with RNase A cannot be explained by electrophoresis because of the positive net charge on the protein. This is because under the experimental conditions used, RNase A would move away from the pore rather than towards the pore. To investigate this anomalous behaviour, zeta potential measurements were conducted under similar conditions to the ones used for nanopore analysis in order to determine the charged state of the protein in solution. Zeta potential is the potential generated as a result of a charged particle (eg. a protein) attracting ions of opposite charge in solution as illustrated in Figure 3.16 (Arjmandi *et al.*, 2012; Firnkes *et al.*, 2010; Hunter, 1988; Schuhmann and Muller, 1998). The ions which are close to the surface of the particle, will be strongly bound to the particle while those which are further away will not bind as strongly. This will result in the formation of a diffuse layer and any ions which are within that layer will move together with the particle whereas those ions which are outside this boundary will stay where they are (see Figure 3.16). This build up of counter ions can result in charge reversal of the protein. Such a case has been reported by Japrung *et al*. for the positively charged nuclear coactivator binding domain of CREB-binding protein (Japrung *et al.*, 2013). Therefore, the zeta potential of RNase A, calmodulin, MBP, and avidin were measured in different buffers and pHs, including similar buffers to the ones used for nanopore analysis. Avidin was chosen because its zeta potential has been reported before and thus can be used to compare our values with those in the literature (Firnkes *et al.*, 2010). While the nanopore experiments were performed in 1 M KCl buffers, the zeta potential measurements were conducted at lower salt concentrations. This is because the determination of zeta potentials at high salt concentration was impeded by high voltages and currents. Firnkes *et al*. showed that the zeta potential of avidin and streptavidin decreases with increasing salt concentration and eventually reaches a plateau at a concentration above 0.1 mM KCl (Firnkes *et al.*, 2010). On the other hand, Japrung *et al*. noted that at salt concentrations above 0.25 M KCl the nuclear coactivator binding domain of CREB-binding protein was becoming more negative (i.e charge reversal) (Japrung *et al.*, 2013). Typically, a positive zeta potential is

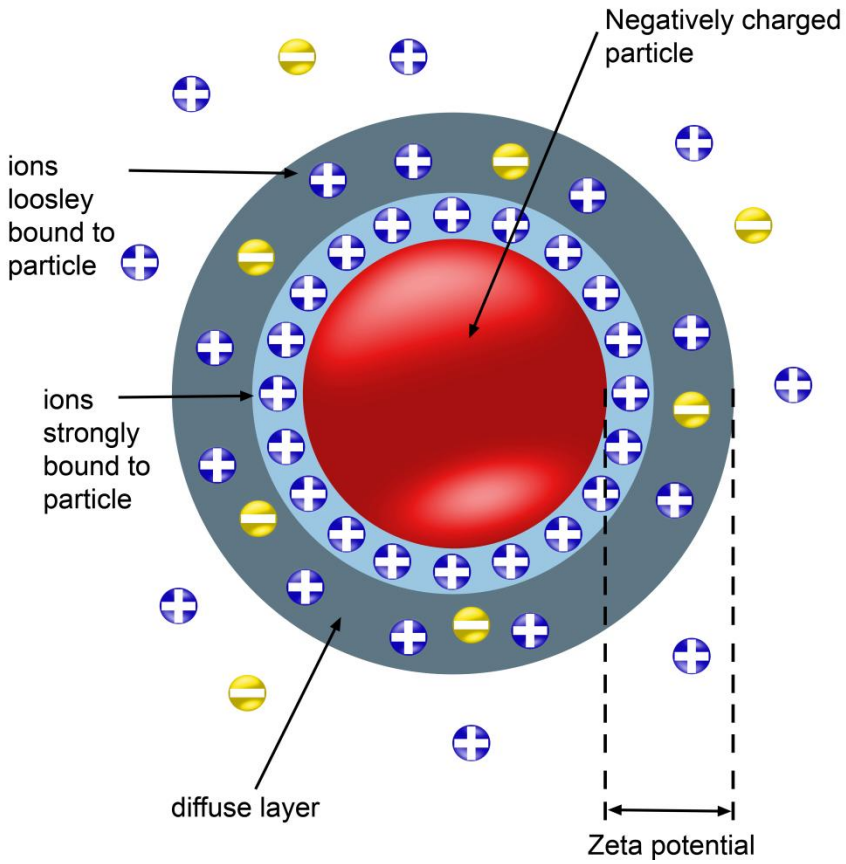

Figure 3.16. Schematic representation of zeta potential. The negatively charged particle (red) is bound by ions of opposite charge (positive) resulting in formation of a zeta potential.

expected at a pH below the pI (Firnkes *et al.*, 2010). However, the zeta potential obtained for RNase A (pI 9.5) in 0.1 M KCl, 10 mM KPi pH 7.0 was -1.62 mV (Table 3.12). This indicates charge reversal similar to that observed for the nuclear coactivator binding domain of CREB-binding protein. Based on the protein's pI, the protein would be expected to be positively charged in a buffer of pH 7.0 (calculated net charge at pH 7.0 = +4.6). However, based on the zeta potential the protein is negatively charged. While this is an unexpected result, the small and negative zeta potential explains the very small voltage effect on duration times and the large blockade events observed with RNase A even though it has a positive net charge. The zeta potentials obtained for MBP and Calmodulin were as expected (i.e negative at pH above their pI). In addition, the measurements obtained for avidin are in agreement with the literature (Firnkes *et al.*, 2010).

3.3 Reverse transcription polymerase chain reaction detection of ribonuclease A

3.3.1 Introduction

As indicated in earlier sections of this thesis, there have been reports of protein translocation through α-hemolysin pores (Baran *et al.*, 2010; Nivala *et al.*, 2013; Oukhaled *et al.*, 2012; Oukhaled *et al.*, 2007; Pastoriza-Gallego *et al.*, 2011; Rodriguez-Larrea and Bayley, 2013; Stefureac *et al.*, 2008). However, as of yet, there is no direct evidence that proteins, folded or unfolded, translocate the α-hemolysin pore. While the indirect approach does provide an answer for some proteins, it doesn't provide an answer for all proteins. For example, the indirect approach applied to MBP and RNase A did not provide an answer as to what type of events are the large blockade events: translocation or intercalation. In other words, applied voltage had no effect on duration times for the large blockade events. Therefore, the experiments in this section are designed to provide a direct approach in determining if proteins translocate the α-hemolysin pore. For these experiments, an enzyme was chosen where direct evidence would be possible by demonstrating activity on the *trans* side of the pore (opposite from the side where the enzyme is initially added), thus providing an amplification of signal. More specifically, RNase A was chosen because even if it unfolds to translocate through the pore, it would readily refold to an active conformation once in the *trans* chamber (Bastings *et al.*, 2008; Miyamoto *et al.*, 2009; Neira and Rico, 1997; Wedemeyer *et al.*, 2000). Hence, the

Table 3.12. Protein zeta potentials at various buffers and pHs.

Buffer (pH)	Zeta Potential (mV)			
	RNase A[a]	**Calmodulin**[b]	**MBP**[c]	**Avidin**
10 mM KPi (pH 7.0)	-0.9 ± 0.1	-	-	-
100 mM KCl, 10 mM KPi (pH 7.0)	-1.6 ± 0.9	-	-	-
500 mM KCl, 10 mM KPi (pH 7.0)	-8.0 ± 1.4	-	-	-
10 mM TRIS-HCl (pH 8.0)	-0.7 ± 0.1	-	-	22.5 ± 4.2
50 mM KCl, 10 mM TRIS-HCl (pH 8.0)	-1.8 ± 0.3	-	-	11.3 ± 1.8
50 mM KCl, 10 mM Sodium Citrate (pH 4)	13.2 ± 0.9	-	-	4.6± 1.0
50 mM KCl, 10 mM Sodium Carbonate / Bicarbonate (pH 10.0)	-13.3 ± 2.5	-	-	-18.4± 2.2
100 mM KCl, 10 mM KPi (pH 7.8)		-15.7 ± 0.9	-	-
100 mM KCl, 5 mM HEPES-NaOH (pH 7.5)		-	-20.2 ± 1.8	-

[a] Calculated charge at pH 7.0 (buffer pH used for nanopore sensing) = + 4.6
[b] Calculated charge at pH 7.8 (buffer pH used for nanopore sensing) = - 24.4
[c] Calculated charge at pH 7.5 (buffer pH used for nanopore sensing) = - 8.1

presence of RNase A can be detected using an activity based assay. However, the α-hemolysin pore on average remains viable for only 2-3 hours, thus if a protein does indeed translocate only a few thousand molecules will go through the pore within that time frame. For this reason, reverse transcription polymerase chain reaction (RT-PCR) was chosen as the technique of choice because of its high sensitivity. Basically, as detailed in the Materials and Methods section (see Figure 2.2), RNase A will be introduced into the *cis* chamber and if translocation of the enzyme through α-hemolysin is successful then some enzyme molecules will be present in the *trans* chamber. The solution of the *trans* chamber will be collected and mRNA will be added to it. Incubating RNase A with the mRNA will result in degradation of the mRNA which in turn will result in inhibition of the reverse transcription step of RT-PCR (Safarian and Moosavi-Movahedi, 2000; Takahashi *et al.*, 1969). While this approach should successfully detect RNase A, the detection limit must be determined before conducting an experiment. It's important to determine the detection limit of mRNA and RNase A. Lower detection limit for RNA means lower detection limit for the protein.

3.3.2 Determining the reverse transcription polymerase chain reaction detection assay limits

Initial experiments were carried out to determine the minimum amount of mRNA that can be successfully amplified. These experiments were conducted under conditions which would mimic RNase A detection experiments. As described in detail in the Materials and Methods section, this in turn meant incubation of the mRNA prior to being used as template for RT-PCR reaction. Therefore, it was important to examine the experimental conditions required to achieve the lowest level of detection (eg incubation period and temperature, number of cycles, buffer, etc.). After numerous experiments under different experimental conditions it was found that the lowest amount of mRNA that could be reproducibly amplified was 300 fg per RT-PCR reaction or 6.0 pg/mL. In order to be able to amplify amounts as small as these, the incubation period and temperature had to be 24 hrs and 37 °C, respectively. Furthermore, the number of cycles for amplification was kept at 34 and the salt concentration in the incubation buffer was 0.5 M rather than 1.0 M which is used in typical nanopore experiments. While it was possible to amplify even lower amounts of mRNA by changing the experimental conditions, this was at

the expense of the RNase A detection level. For example, increasing slightly the number of cycles increased the detection level of mRNA but that in turn reduced the detection limit for RNase A.

Next, experiments were performed to obtain an estimate of the amount/number of molecules of RNase A that can be detected with RT-PCR. To do this, a number of serial dilutions of RNase A were prepared to which the mRNA was added and then incubated for 24 hrs at 37 °C. The amount of mRNA added here was such that when using 3 µL of this solution as a source of RNA template for RT-PCR reactions it would result in 300 fg per RT-PCR reaction (i.e the detection limit for mRNA). It should be noted that different incubation periods and temperatures were examined but the values reported here were optimal. For example, while the optimal temperature for RNase A activity is about 60 °C this could not be used because incubating the mRNA alone at this temperature resulted in some degradation (Takahashi *et al.*, 1969). Furthermore, to prevent RNase A or RNA from binding to the tubes and/or pipette tips, non-sticky microcentrifuge tubes (polished with a diamond mold) and pipette tips with low binding properties were used. RNase A is known to stick to glass and plastic. Without the use of these special pipette tips and microcentrifuge tubes, reproducible detection levels could not be obtained. Under these and other experimental conditions (see Materials and Methods for more details) RT-PCR can detect as low as 50 ag or about 2200 molecules of RNase A (Figure 3.17).

From previous nanopore experiments with RNase A, 10-20 thousand events with a 60% or higher blockade current could be recorded in a period of 3-5 hrs. If those events are assumed as translocation events then 10-20 thousand molecules of RNase A would be present in the *trans* chamber. Therefore, RT-PCR can be employed as a detection assay technique for testing for RNase A presence in the *trans* chamber in a nanopore experiment.

3.3.3 The effect of silver leeching and the use of salt bridges

In the initial process of determining if RNase A translocates through the α-hemolysin pore, controls were run where both chambers, *cis* and *trans*, were filled with nuclease free electrolyte solution (1 M KCl 10 mM KPi, pH 7.4) but there was no RNase A, lipid or α-hemolysin solution added to either chamber. Yet, after testing for RNase A activity there appeared to be some activity present in both chambers. Initially this was thought to be RNase A contamination

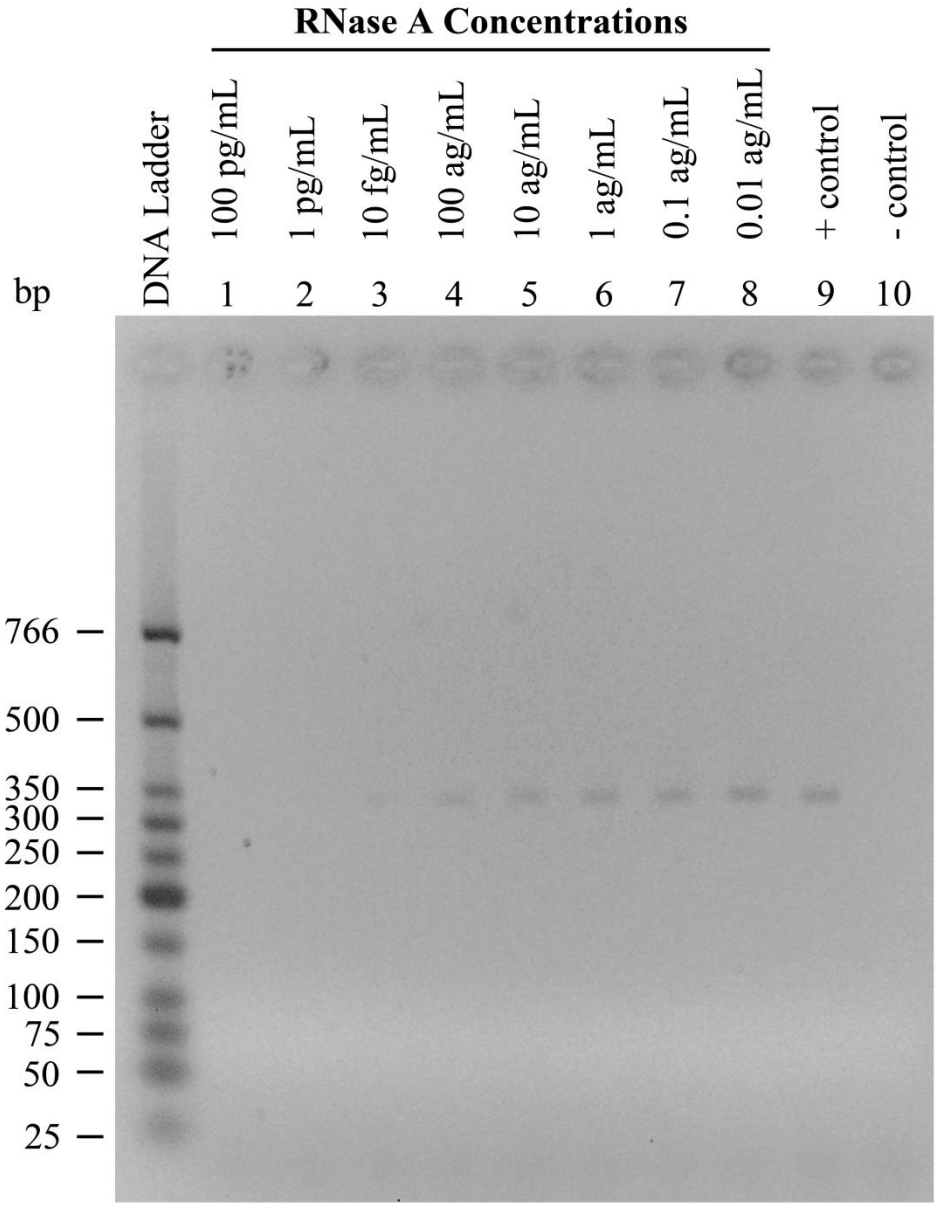

Figure 3.17. The detection limit of RT-PCR based detection assay for RNase A. Lanes 1 to 8 indicate the concentrations of RNase A. Lanes 9 is the positive control for RT-PCR which contains no RNase A. The negative control for RT-PCR, lane 10, contains no RNase A or mRNA. The concentration of mRNA is the same in lanes 1 through 9.

but after a large number of control experiments it was found that this was due to the use of Ag/AgCl electrodes. In nanopore analysis Ag/AgCl electrodes are used to apply a constant transmembrane voltage potential. This can be ruled out as RNase A contamination because the electrodes are stored overnight in bleach solution and they were pre-treated with an RNase A deactivating solution (RNase Zap, Applied Biosystems, Mississauga, Ontario) before running an experiment. So why is the use of Ag/AgCl electrodes resulting in false positive detection of RNase A? The simplest explanation is that there is silver leaching from the electrodes. The silver (I) leaching from the electrodes would bind to phosphate groups of the RNA backbone or to electron donor atoms on nucleobases (Arakawa *et al.*, 2001; Marino *et al.*, 2012). This binding forms ternary complexes between Ag (I) and nucleotides, cytosine and guanine (Arakawa *et al.*, 2001; Marino *et al.*, 2012). As a result of this binding, there would be a reduction in reverse-transcription of the mRNA. This hypothesis was tested directly by running control experiments where the *cis* and *trans* solutions were incubated with and without Ag/AgCl electrodes in the absence of RNase A, lipid, and α-hemolysin. After 1 hr incubation period, the solutions were transferred to microcentrifuge tubes and the mRNA was added to each solution and then left for 24 hr incubation at 37 ^{o}C. The mRNA from each solution was then used as a source of template RNA for RT-PCR. As shown in Figure 3.18a (lanes 1 and 2), in the absence of electrodes there was successful reverse transcription of the mRNA (same intensity as the control lane, lane 5). In the presence of Ag/AgCl electrodes there is very little reverse-transcription of mRNA (Figure 3.18a, lanes 3 and 4). Upon this discovery agarose salt bridges were then used to avoid direct contact of the Ag/AgCl electrodes with the solutions of either *cis* or *trans* chambers. With the use of agarose salt bridges there is no effect on the reverse transcription of RT-PCR (Figure 3.18b, lanes 1 and 2). Figure 3.18b (lanes 3 and 4) shows another important control where addition of RNase A to the *cis* side results in no translocation to the *trans* side in the presence of a membrane even after few hours of incubation. Both of these findings are very important: the first finding shows the importance of salt bridges in nanopore analysis of nucleic acids and the latter finding confirms what is already expected; that is in the absence of a pore there will be no protein translocation. This led us to examine the effect of salt bridges in nanopore analysis of proteins.

To determine if salt bridges have any effect in nanopore analysis of proteins it was decided to study MBP since this protein has been previously studied in detail (Section 3.2.4). Here,

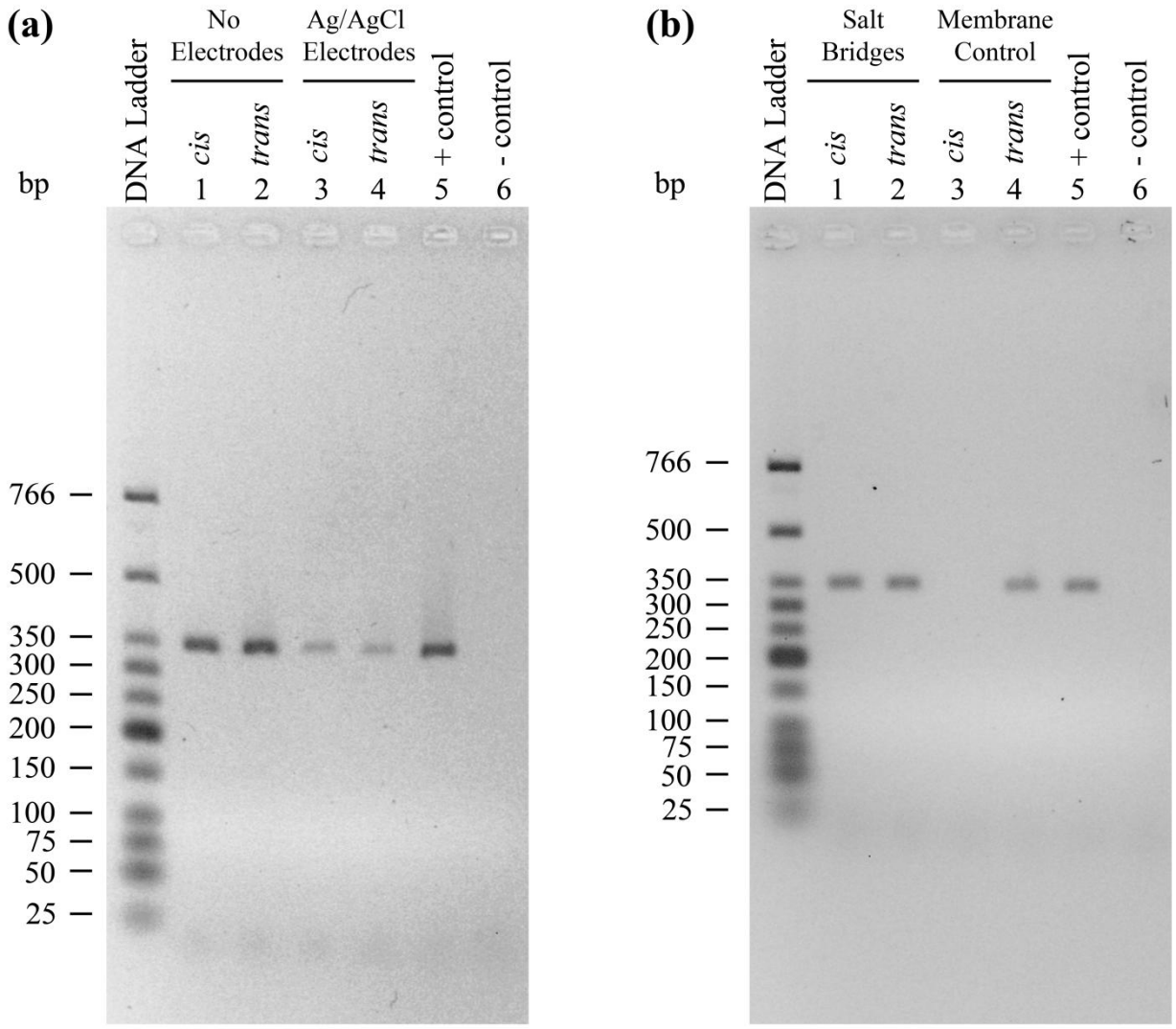

Figure 3.18. Effect of Ag/AgCl electrodes on RNase A detection assay. (a) Lanes 3 and 4 show reverse transcription of mRNA when there are Ag/AgCl electrodes immersed in the solution, whereas lanes 1 and 2 show reverse transcription of mRNA when there are no electrodes immersed in solution. (b) Lanes 1 and 2 show reverse transcription of mRNA when there are agarose salt bridges immersed in the solution instead of Ag/AgCl electrodes. Lanes 3 and 4 show the *cis* and *trans* solutions, respectively, after adding RNase A to the *cis* chamber with the lipid bilayer membrane separating the two chambers.

MBP was studied using salt bridges in HEPES buffer in the presence and absence of EDTA. One of the main observations made with salt bridges was that the frequency of events with salt bridges was much lower than without them (see current traces in Figure 3.19). The results obtained with the use of salt bridges are shown in Figure 3.19b and 3.20b. Parts (a) of Figure 3.19 and 3.20 show the result previously reported without the use of salt bridges. As shown in Figure 3.20 and Table 3.13, there is very little difference when using salt bridges. This clearly indicates that there is some interaction between the silver leaching from Ag/AgCl electrodes and the protein. However, the amount of silver leaching from the electrodes might be extremely small compared to the amount of protein added (µg/mL) in the *cis* chamber and hence the very small change in the current blockade histogram profiles for MBP. In the case of mRNA, the amount of mRNA (pg/mL) might be comparable to the amount of silver leaching from the electrodes. These results demonstrate the importance of analysing proteins with nanopores in a silver free environment.

3.3.4 Addition of natively folded ribonuclease A to the *cis* chamber and subsequent testing for ribonuclease A activity in the *trans* chamber

The detection assay established in section 3.3.2 was used to determine if RNase A translocates through the α-hemolysin pore. In the first part of the process, a typical nanopore experiment utilizing agarose salt bridges was carried out. After successful insertions of the desired number of pores, the natively folded protein was added to the *cis* chamber at a final concentration of about 20 µM. Once the protein was added, the experiment was run for an average period of about 3-6 hrs (some experiments were run longer) and the number of events with current blocks of 60% or higher was recorded. Interestingly, similar to MBP, a decrease in the frequency of events was observed when using salt bridges. Upon recording a high number of events with blockade currents of 60% or higher, the experiment was stopped and solution from both chambers were collected. The solution collected from each chamber was a fraction of the total volume in the chamber. This was done to avoid breaking of the membrane and in turn false translocation of the protein through the 150 µm aperture. If the large blockade events are putative translocation events then there should be enough RNase A molecules in the *trans* chamber to test for activity using the detection assay developed earlier.

In the second part of the process, the RT-PCR detection assay was used to test for RNase A

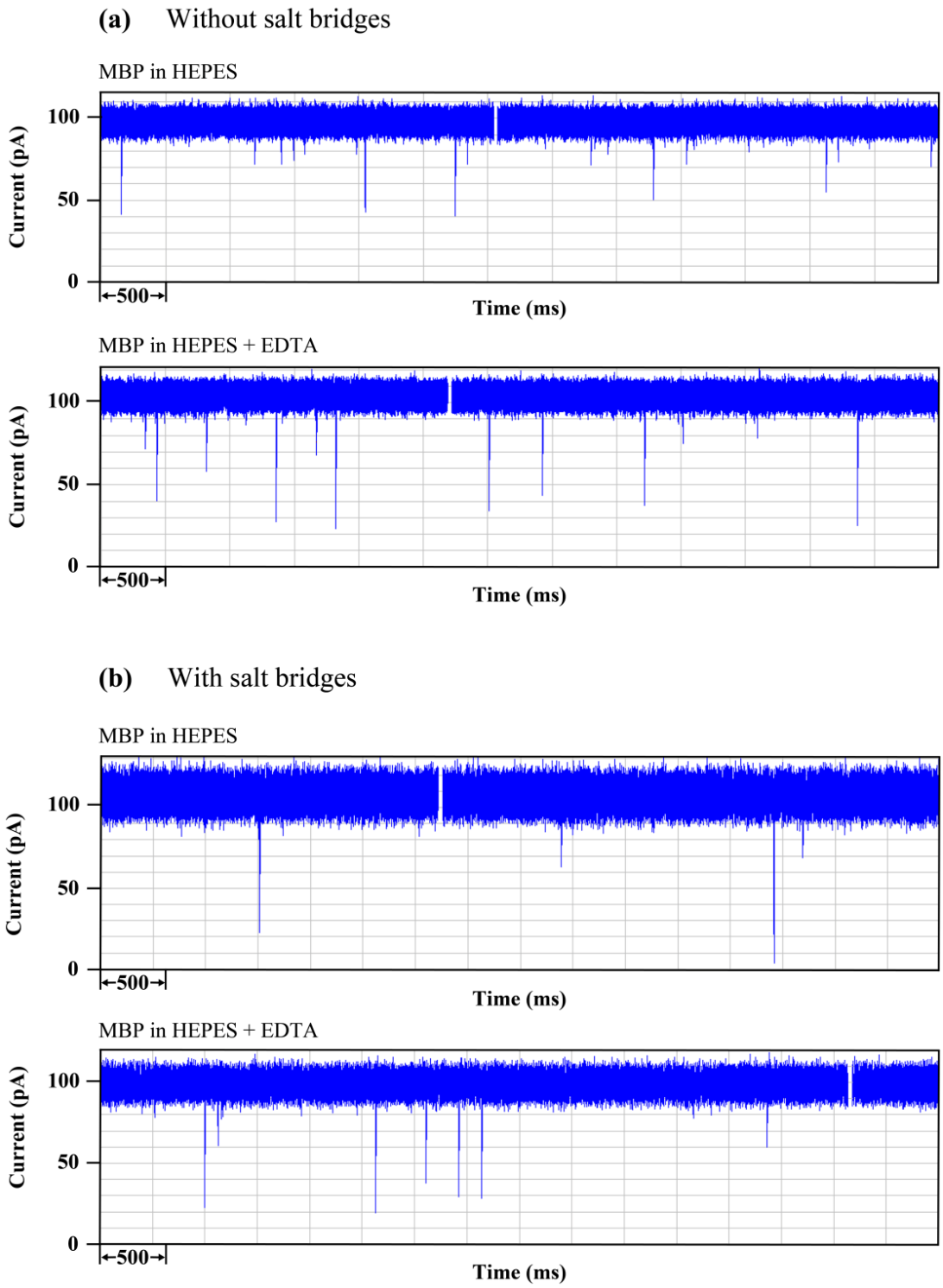

Figure 3.19. Segments of current traces for the interaction of MBP with the α-hemolysin pore in HEPES buffer with or without 1 mM EDTA conducted (a) without the use of salt bridges or (b) with the use of salt bridges. Note the change in frequency of events observed with the use of salt bridges.

(a) Without salt bridges

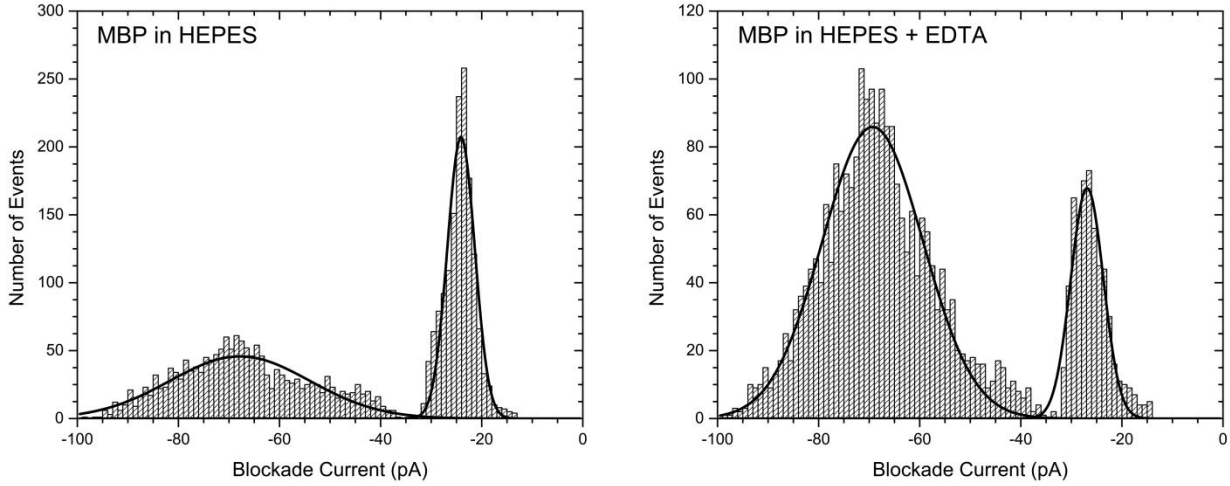

(b) With salt bridges

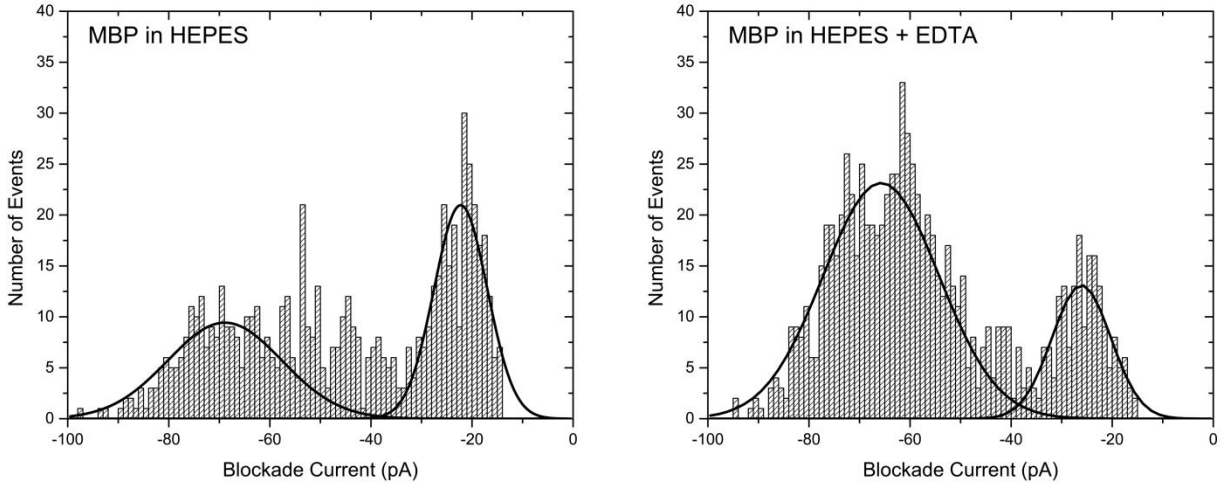

Figure 3.20. Effect of salt bridges on the interaction of MBP with the α-hemolsyin in HEPES buffer in the presence and absence of EDTA. (a) Blockade current histogram profiles obtained for MBP in HEPES with and without EDTA when using Ag/AgCl. (b) Blockade current histogram profiles obtained for MBP in HEPES with and without EDTA with the use of agarose salt bridges are. The peak blockade current values and the duration times are presented in Table 3.13.

Table 3.13. The effect of salt bridges on event parameters for MBP in HEPES buffer in the absence and the presence of EDTA.

Parameter[a]	Without salt bridges		With salt bridges	
	MBP	MBP + EDTA	MBP	MBP + EDTA
I_1 (pA)[b]	-24.1	-26.9	-22.2	-26.1
I_2 (pA)	-67.9	-69.3	-68.9	-65.7
T_1 (ms)[c]	0.20	0.14	0.03	0.04
T_2 (ms)	0.20	0.14	0.15	0.15
A_1 (%)[d]	47.1	20.3	49.0	22.6
A_2 (%)	52.9	79.7	51.0	77.4

[a] I_1, I_2, T_1, and T_2 represent the amplitudes and the durations of the current blockades of the respective event populations presented in Figure 3.20. A_1 and A_2 are percent of total events forming each respective population. The peaks are numbered from right to left.
[b] The error is estimated to be ±1 pA.
[c] The error is estimated to be ± 10%.
[d] The error is estimated to be ± 1%.

activity in solutions collected from the nanopore experiments. As shown in Figure 3.21 (lane 4) there was no enzyme activity detected in the *trans* chamber. If there was any activity then the band in lane 4 would not be there or would be of lesser intensity than that of the positive control (lane 6). However, as expected there was RNase A activity in the *cis* chamber where the protein was added. Lanes 1 and 2 indicate controls where solutions were collected from both chambers prior to adding RNase A to the *cis* chamber. This was to ensure that the buffer and apparatus used are RNase A free. These experiments have been repeated numerous times (i.e more than 10 times). Therefore, the results shown in Figure 3.21 indicate that the large blockade events observed with RNase A are intercalation rather than translocation. This is very important results because it is the first report that uses direct evidence to determine if a protein (i.e larger than the smallest diameter of the pore) translocates through the α-hemolysin pore.

To determine if the size is the limiting factor for RNase A translocation through α-hemolysin pore, positive control experiments were run where the protein was added to the *cis* side but there was no membrane or pore present. Therefore, if size was the limiting factor then the protein could easily translocate through the 150 μm aperture joining the two chambers. Indeed, as shown in Figure 3.22 (lane 4) the protein readily translocated through the 150 μm aperture even in the absence of applied voltage; thus, indicating that protein translocation can be diffusion controlled. The same experiment was repeated when applying 100 mV (*cis* side grounded) and the protein translocated again (Figure 3.22, lane 6). These control experiments confirm that the size of the pore is the limiting factor for large protein translocation. Furthermore, if the pore is large enough then protein translocation can be diffusion controlled.

3.3.5 Addition of completely unfolded ribonuclease A to the *cis* chamber and subsequent testing for ribonuclease A activity in the *trans* chamber

It has been reported that RNase A can be fully unfolded in 4 M GdnHCl (a denaturing agent) and in 100-fold molar excess of TCEP (a reducing agent) (Bastings *et al.*, 2008; Jacob *et al.*, 2007). To examine if the unfolded RNase A would translocate the α-hemolysin, the completely unfolded protein was added to the *cis* chamber and a nanopore experiment was carried out. However, in the process of conducting a nanopore experiment with the completely unfolded protein several issues were encountered which prevented successful completion of the experiment. First, because of the presence of denaturing and reducing agents, the membrane

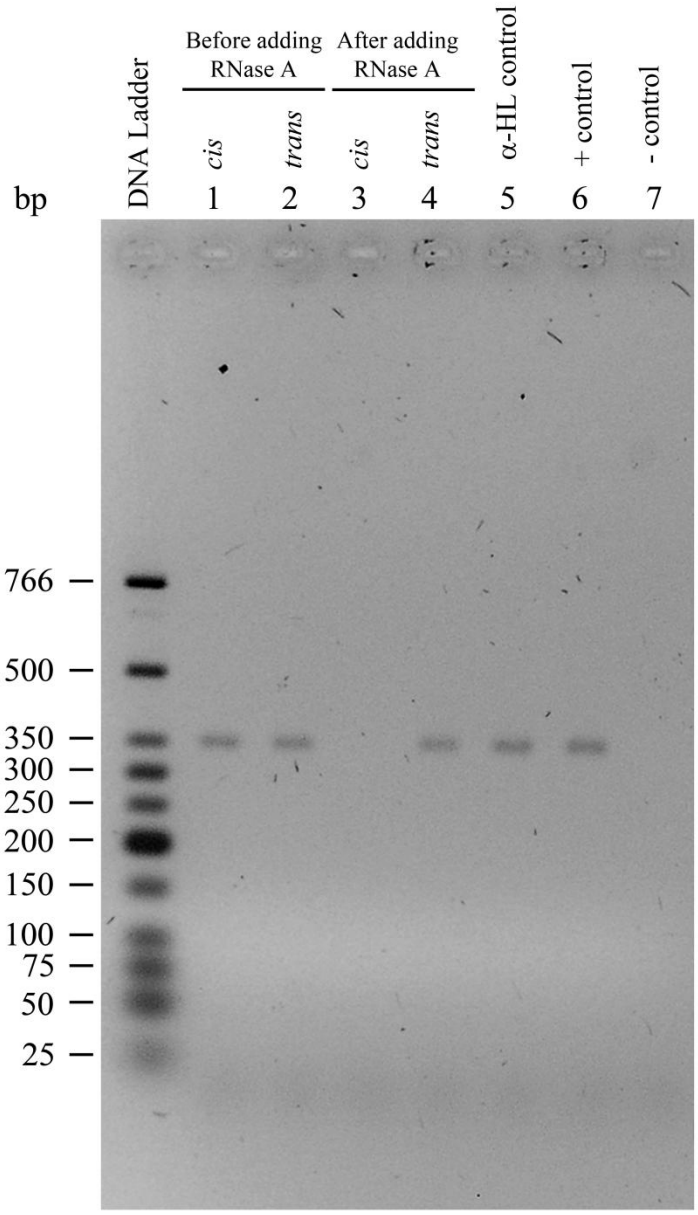

Figure 3.21. RT-PCR based detection of RNase A in the *trans*-chamber. Lanes 1 and 2 represent the solutions collected from *cis* and *trans* chambers, respectively, before adding RNase A. Lanes 3 and 4 represent the solutions collected from *cis* and *trans* chambers, respectively, after adding RNase A to the *cis* chamber and conducting a nanopore experiment. The solutions used for lanes 3 and 4 were collected after the nanopore experiment and while the lipid bilayer separating the two chambers was still intact. Lane 5 represents a control for α-hemolysin solution used in the nanopore experiment where the α-hemolysin solution was tested for RNase A activity. Lanes 6 and 7 are positive and negative controls, respectively, for RT-PCR.

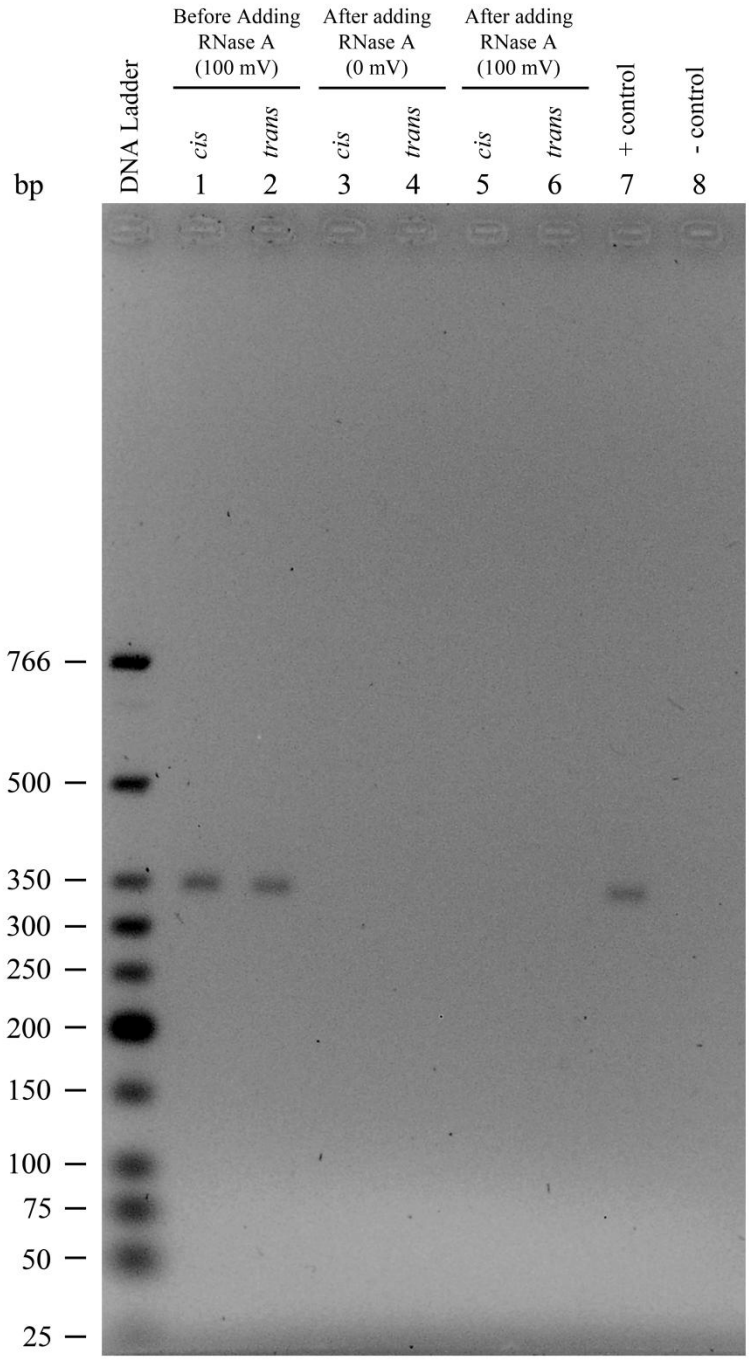

Figure 3.22. Translocation of RNase A through the 150 µm aperture. Lanes 1 and 2 are the solutions collected from the *cis* and *trans* chambers, respectively, before adding RNase A and while applying a potential of 100 mV. Lanes 3 and 4 are the solutions collected from *cis* and *trans* chambers, respectively, after adding RNase A to the *cis* chamber and under no applied voltage. Lanes 5 and 6 are similar to 3 and 4, respectively, but there was 100 mV applied. There was no lipid bilayer painted over the 150 µm aperture. Lanes 6 and 7 are positive and negative controls, respectively, for RT-PCR.

was unstable and as a result it would break after a short period of time. While this might be acceptable in a typical nanopore experiment, this is not the case here because once the membrane breaks a new experiment must be restarted in order to prevent false positive translocations through the 150 µM aperture present in the cup. Second, after only few minutes of adding the unfolded RNase A to the *cis* chamber, the α-hemolysin pores would permanently block. This in turn made it impossible to record sufficient number of large blockade events (i.e putative translocations). Finally, the third issue encountered was the frequency of events observed with unfolded protein. The unfolded protein induced far fewer events than the folded protein. In an attempt to increase the frequency of events, the experiment was repeated in the presence of 1 M GdnHCl. Interestingly, the presence of GdnHCl in both chambers improves the frequency dramatically but the presence of GdnHCl in *cis* chamber alone does not. However, having GdnHCl in the *trans* chamber will produce a false negative result on the RNase A detection assay. This is because even if the unfolded protein translocated the pore it will not be able to fold back into an active confirmation in the presence of denaturing agent. Hence, as a result of the limitations outlined here, a detection assay could not be carried out to determine if the unfolded RNase A translocates through the α-hemolysin pore.

3.4 Translocation of proteins through solid-state pores

3.4.1 Introduction

Solid-state pores have proven to be a powerful alternative to biological pores in nanopore sensing. Many research groups have utilized solid-state pores in nanopore analysis of proteins (Cressiot *et al.*, 2012; Firnkes *et al.*, 2010; Fologea *et al.*, 2007; Freedman *et al.*, 2011; Oukhaled *et al.*, 2011; Stefureac *et al.*, 2010b; Talaga and Li, 2009). As outlined in the introduction of this thesis, solid-state pores overcome some of the shortcomings encountered in nanopore sensing with biological pores such as, fixed diameter of the pore, limited lifespan of the experiment, and limited experimental conditions (eg. pH, denaturant concentrations, applied voltages, etc). Some of these shortcomings were also encountered and discussed in the earlier results of this thesis. For example, the limited lifespan of the experiment due to fragility of the lipid bilayer prevented us from determining if unfolded proteins translocate the α-hemolysin pore. In addition, there is already direct proof of protein translocation through a solid-state

pore. Fologea *et al*. demonstrated that running a nanopore experiment for 50 hrs will allow enough BSA molecules to translocate a solid-state pore where their presence in the opposite chamber can be detected by a chemiluminescent BSA enzyme linked immunosorbent assay (Fologea *et al.*, 2007). Therefore, we reasoned that solid-state nanopores can be used as positive controls for RNase A translocation through a nanopore. While similar positive control experiment was carried out with the 150 μM pore in the cup (Figure 3.22), it's important to conduct the same experiment with pores of nanometer scale.

Solid-state nanopores of 10 and 20 nm diameters were chosen. As stated earlier, the largest dimension of the folded RNase A is 3.8 nm (Joseph-McCarthy *et al.*, 1996). Therefore, the folded protein should readily translocate through these solid-state pores. Furthermore, high concentration of GdnHCl will not impact the lifespan of the experiment. Moreover, the low frequency of events should not hinder the RNase A detection assay since it should be possible to run a nanopore experiment for an extended period of time (eg. 50 hrs). Thus, translocation of sufficient number of RNase A molecules to the *trans* chamber should be possible. Hence, direct evidence of folded and unfolded RNase A through solid-state pores can be obtained by using the detection assay described in section 3.3 and in turn providing positive controls for the experiments carried out with the α-hemolysin pore.

3.4.2 Translocation of ribonuclease A through solid-state pores

To perform the RNase A translocation experiments through solid-state pores, twenty Si_3N_4 nanopores were purchased from Nanopore Solutions (Cascais, Portugal) with diameters of 10 and 20 nm. The current-voltage curve (I/V curve) was obtained for each pore prior to addition of RNase A protein in order to calculate the conductance of the pore (i.e the slope of the I/V curve) and to ensure there were no leaks. As expected, the I/V curves obtained for each pore indicated a linear relationship between the current and the voltage applied. Figure 3.23 shows typical I/V curves obtained for a 10 nm and a 20 nm pore. However, conductance values calculated from the I/V curves were much larger than expected. For example, from the I/V curves of the 10 and 20 nm pores shown in Figure 3.23, conductance values of 85.5 and 170.4 nS were calculated, respectively. In contrast, using equation (1), listed in the materials and methods section, to calculate the theoretical conductance values for 10 and 20 nm pores, conductance values of 41.0 and 121.6 nS are obtained, respectively. Therefore, the observed

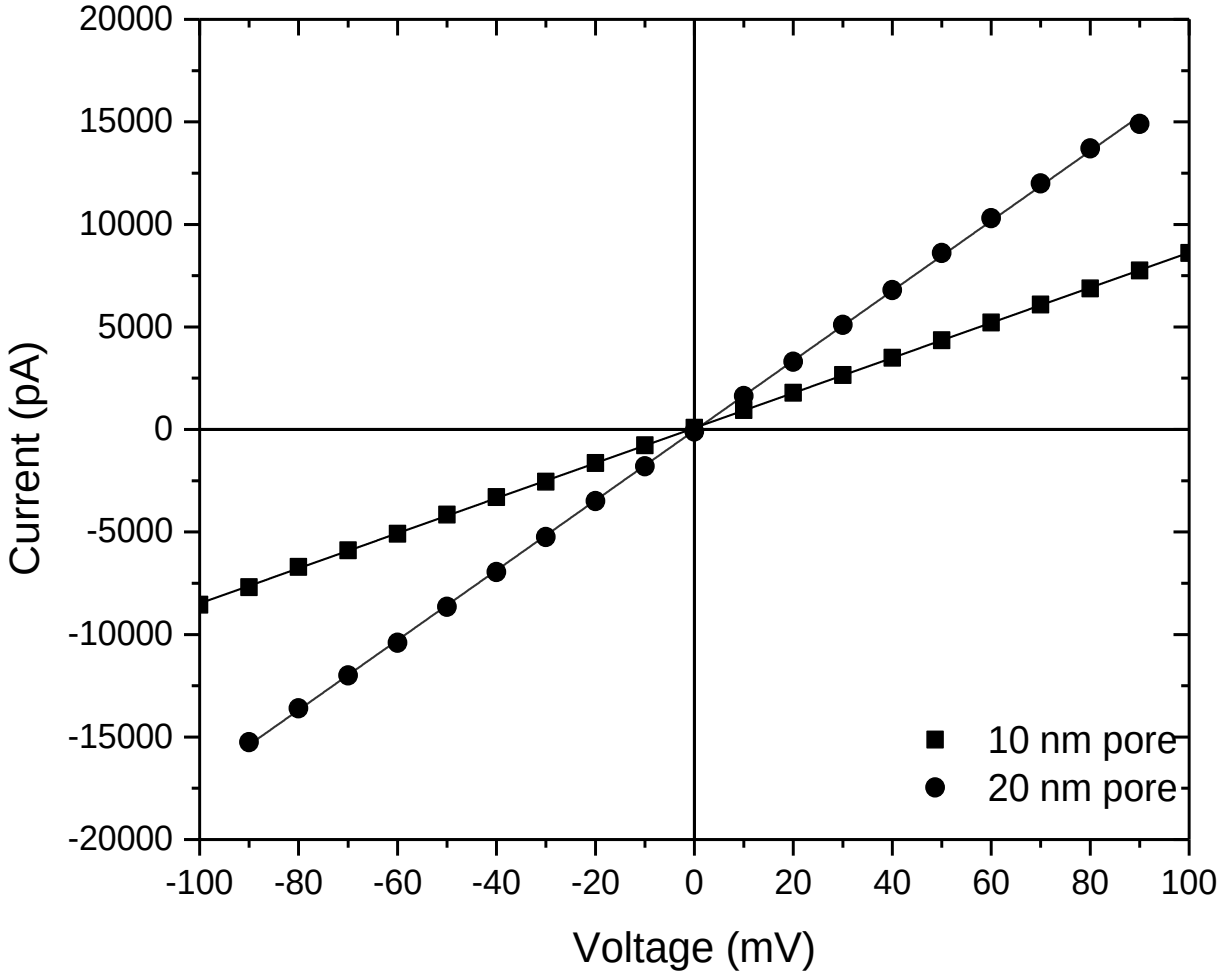

Figure 3.23. Current-voltage curves for a typical 10 nm (squares) and a 20 nm (circles) pore recorded in 1 M KCl, 10 mM Tris-HCl, pH 7.4.

conductance is much larger than the theoretical conductance. As shown in Figure 3.24, high current noise levels were also observed for all pores, ranging between 200 - 250 pA. These current noise levels are much higher than what is reported in the literature for similar pores. Although the observed conductance values and current noise levels were very high, RNase A translocation experiments were attempted (Figure 3.24).

Upon adding RNase A to the *cis* chamber (*cis* chamber grounded) there were no events observed with any of the pores (Figure 3.24b). To ensure that this is not as a result of the translocation being hindered by the electrophoretic field, the same experiments were repeated with the *trans* chamber being grounded (Figure 3.24c). However, there were still no events observed. Even if the protein translocates through the pore, events might not be distinguishable from the current noise since the observed current noise is very high. For this reason, translocation of MBP, which is three times as large as RNase A was examined in all the solid-state pores. Similar to RNase A, there were no events observed for all pores except one (Figure 3.24d). When the same experiment with the same pore was repeated, there were no events observed during the second try. It should be noted that all pores were remounted at least once and the same results were obtained.

These results confirm that solid-state pores are still behind biological pores in terms of reproducibility and reliability. While the quantity and quality of research done with solid-state pores is very high, it's important to note that only a fraction of solid-state pores tested tend to work. For example, in our lab group so far there has been about a 20% success rate with all tested solid-state pores (Stefureac, 2012). This is one of the main reasons why many nanopore research groups continue to work with biological pores rather than solid-state pores and why the quest for new biological pores continues. Therefore, RNase A translocation experiments through solid-state pores could not be carried out at this point.

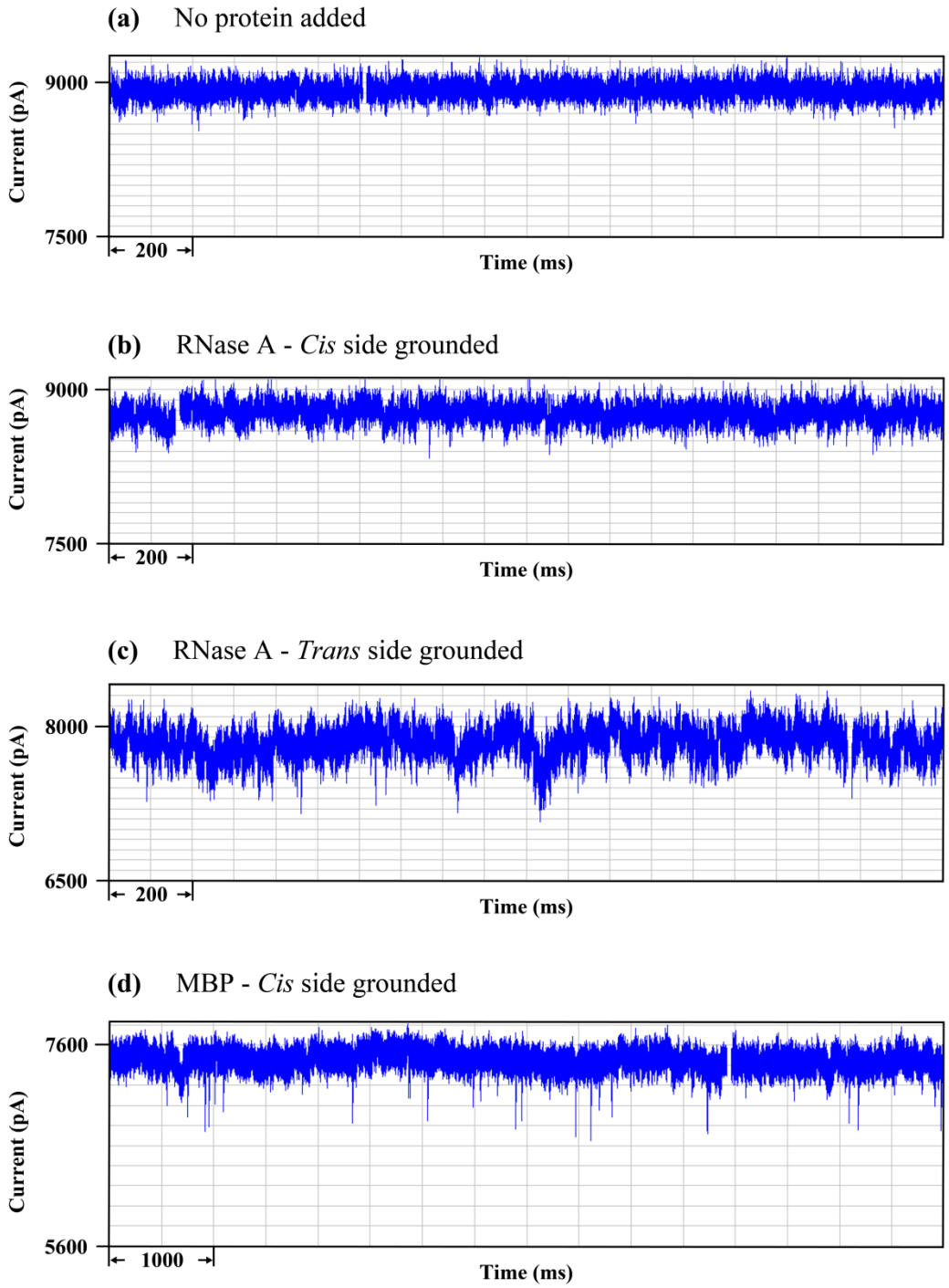

Figure 3.24. Segments of current traces obtained for a 10 nm solid-state pore (a) before adding any protein, (b) after adding RNase A to the *cis* chamber with the *cis* side being grounded (i.e negatively biased), and (c) after adding RNase A to the *cis* chamber but reversing polarity (i.e *trans* chamber being negatively biased). (d) Current traces obtained for translocation of MBP through a different 10 nm solid-state pore, *cis* side grounded.

4.0 DISCUSSION

4.1 The sensitivity of nanopore sensing

As outlined in the introduction and results sections of this thesis, nanopore sensing is a very sensitive technique and can detect minor alterations to the structure of peptides and small proteins. The results obtained from the analysis of the R, D, and RI isomers of glucagon and Fmoc-$D_2A_{10}K_2$ peptide are another confirmation of the sensitivity of nanopore sensing. The analysis of the four isomers of Fmoc-$D_2A_{10}K_2$ show that nanopore sensing coupled with wild-type α-hemolysin can readily differentiate between the directional isomers (i.e L vs R and D vs RI) but not between chiral isomers (i.e L vs D and R vs RI). The chiral isomers are non-superimposable images of each other, where the chirality of each amino acid is inverted in one of the isomers. However, in the directional isomers the chirality of each amino acid is unchanged but the sequence is reversed (Fischer, 2003).

It is clear, that interaction of the chiral Fmoc-$D_2A_{10}K_2$ peptides with the α-hemolysin pore induce similar populations of events in the current blockade histograms (Figure 3.2). For example, in the normal-sequenced peptides (L and D peptides), there is only one population of events observed. The L-Fmoc-$D_2A_{10}K_2$ peptide has been subjected to nanopore analysis before and this population of events was shown to belong to translocation of the peptide through the pore (Stefureac *et al.*, 2006). Based on this and other studies with other peptides, it can be hypothesized that the blockade events induced by the D-Fmoc-$D_2A_{10}K_2$ are as result of the translocation of the peptide through the pore (Christensen *et al.*, 2011; Meng *et al.*, 2010; Movileanu *et al.*, 2005; Stefureac *et al.*, 2010a; Sutherland *et al.*, 2004; Zhao *et al.*, 2009b). The presence of only one population of events with the L and D peptides shows that these two isomers readily translocate through the pore. In contrast, the peptides with the reversed sequence show two populations of events. The population of events with the large current blockades are attributed to translocation of the peptides through the pore, whereas the population with small current blockades are bumping events. The proportion of bumping events is less than 10% of the total events. The translocation times obtained for the reverse-sequenced peptides are at least twice as fast as those obtained for the normal-sequenced peptides (Table 3.1). Under the experimental conditions used (the electrode in the *trans* chamber is positively biased) the translocation of negatively charged peptides is facilitated by

the electrophoretic force. Therefore, in the normal peptides the translocation of N-terminal first is favoured, where in the reverse-sequenced peptides the opposite is true. In the reverse-sequenced peptides there are three negative charges at the C-terminus compared to two in N-terminus of the normal-sequenced peptides. Hence, the electrophoretic force acting on the C-terminus of the reverse-sequenced peptides is higher than that acting on the N-terminal of the normal-sequenced peptides, thus explaining faster translocation times for R- and RI-Fmoc-$D_2A_{10}K_2$ peptides.

It's important to note that while the highest degree of differentiation is between the directional isomers, one can argue that there is some level of differentiation between the chiral isomers of the Fmoc-$D_2A_{10}K_2$ as well (Table 3.1). However, the difference between the chiral isomers is very subtle and very close to the standard error. Therefore, for this reason it cannot be concluded that nanopore sensing coupled with wild-type α-hemolysin can differentiate between chiral isomers of the Fmoc-$D_2A_{10}K_2$ family. The differentiation between the chiral isomers might be improved if the peptides are added to the *trans* chamber, thereby the molecules will enter stem side first. For example, Kang *et al*. showed that the degree of differentiation between R- and S-enantiomers of drug molecules depended on whether these drug molecules enter the pore from *cis* or *trans* side (Kang *et al.*, 2006). In addition, the differentiation might also be improved by attaching another molecule inside the pore. For example, Boersma and Bayley demonstrated that a modified α-hemolysin can differentiate between single D- and L-amino acids (Boersma and Bayley, 2012). The α-hemolysin was modified with a covalently attached phenanthroline ring inside the β-barrel of the pore, which coordinates a Cu(II) ion While these approaches might be necessary to differentiate between chiral isomers of simple peptides such as the Fmoc-$D_2A_{10}K_2$ family, this might not be necessary for more complex peptides.

Nanopore analysis of the four glucagon isomers produced more complex blockade histograms. Unlike the Fmoc-$D_2A_{10}K_2$ family, the blockade histograms of glucagon isomers show three peaks instead of typical two observed with most peptides (Figure 3.3). The far left peak is attributed to the translocation of the peptides through the pore, whereas the middle and far right peak are bumping events. The middle peak is unlikely to be translocation events because the blockade amplitudes are too small for a peptide of this size (Christensen *et al.*, 2011; Meng *et al.*, 2010; Movileanu *et al.*, 2005; Stefureac *et al.*, 2006; Sutherland *et al.*, 2004;

Zhao *et al.*, 2009b). In addition, it's unlikely that these events are produced by dimer formation because in the presence of 1 M GdnHCl (Figure 3.3e), the peak remains present. Therefore, the events forming the middle peak are likely bumping events. The presence of two bumping populations are as a result of the glucagon peptide bumping into the pore in two different orientations. The sequences of the glucagon peptides (Table 2.3) show that all charged amino acids are found in the middle of the peptide. Therefore, translocation of the C-terminal first might be favoured for all four isomers. If all the parameters of the interaction between the peptides and the α-hemolysin are taken into consideration (Table 3.2), it is clear that nanopore sensing coupled with wild-type α-hemolysin is capable of differentiating between all four isomers. This is an indication that the pore is interrogating both structure and sequence of the peptide. It's important to state that while there are differences between all four isomers, the differentiation between directional isomers is significantly better than that between chiral isomers.

In conclusion, these results demonstrate the true sensitivity of nanopore sensing technique. For example, while some antibodies cannot differentiate between an RI-peptide and an L-peptide (for reasons specified in Section 3.1.1), nanopore sensing can (Benkirane *et al.*, 1995; Briand *et al.*, 1995; Muller *et al.*, 1995). Furthermore, the CD analysis of Fmoc-$D_2A_{10}K_2$ and glucagon isomers (Figure 3.4) shows that CD was only able to discriminate between chiral isomers. While, the discrimination of isomers is readily achieved with nanopore sensing coupled with wild-type α-hemolysin, the degree of discrimination can be further improved in the future by using a modified α-hemolysin pore. Moreover, investigating other interaction parameters between the pore and the isomers (eg. association and dissociation constants, frequency of events, etc) or changing the experimental set-up (eg. adding isomers to the *trans* chamber) might also further improve the separation of isomers.

4.2 Nanopore analysis of proteins

4.2.1 Interaction of proteins with the α-hemolysin pore

Nanopore analysis of proteins with different chemical and physical properties shows that all examined proteins give rise to a significant number of events with both large and small % current blockades even in the absence of denaturants. The interaction of RNase A protein with

the α-hemolysin pore induces a significant number of large blockade events even though the protein has positive net charge and under the experimental conditions the translocation direction is opposite to the electrophoretic force. For example, the *trans* chamber is positively biased yet the positively charged protein goes towards that electrode. The possibility that the events observed with RNase A are due to contaminants was ruled out since even after RNase A was subjected to a second purification by gel exclusion and ion exchange chromatography, there was no significant change in the event frequency and profile (Figure 3.6). With small peptides and polynucleotides the large blockade events would be attributed to translocation of the molecule through the pore. However, native RNase A is larger than the smallest diameter of the pore and it has four disulfide bonds. Therefore in order for the protein to translocate it would have to unfold. Considering the presence of the disulfide bonds this is highly unlikely to happen in the absence of reducing and/or denaturing agent.

Even after reducing the disulfide bonds, the interaction of the reduced RNase A with the α-hemolysin still gave rise to a similar percentage of large blockade events with the same blockade amplitudes. This indicates that the reduction of the disulfide bonds alone has no overall effect on the interaction of the protein with the pore. In contrast, when examining the protein in the presence of 1 M GdnHCl there is a significant change on the interaction of the protein with the pore. The frequency of the events together with the proportion of the large blockade events are significantly increased. At this concentration of denaturant the protein is expected to be only partially unfolded (Bastings *et al.*, 2008; Neira and Rico, 1997). Thus, the entry of a chain of a protein into the pore will be favoured. This in turn will explain the increase in percentage of events with large blockade events, independent of whether the events are intercalation or translocation. A similar effect of GdnHCl has been reported with MBP (Oukhaled *et al.*, 2007). However, in the case of MBP the authors reported no events in the absence of denaturant.

The completely unfolded protein was also subjected to nanopore analysis. One would expect that the unfolded protein would produce a larger percentage of large blockade events. From the inspection of Figure 3.6e, this was not the case. In fact, the proportion of the large blockade events was smaller compared to the folded or partially unfolded protein. The simplest explanation for this result is that the large blockade events observed with the completely unfolded protein are indeed due to translocation of the protein through the pore, whereas with

the partially unfolded or the native protein the large blockade events are due to intercalation of the protein. This is because the translocation of the fully unfolded protein would not be hindered by the size of the pore, whereas for partially unfolded protein the size of the pore will be a limiting factor. The subject of translocation and intercalation will be discussed in greater detail in the coming sections. Another explanation for this might be that the unfolded protein refolds once added to the *cis* chamber.

The analysis of a series of model proteins with different physical and chemical properties (lysozyme, calmodulin, human thioredoxin, *E. coli* thioredoxin, BPTI, ubiquitin) also produced unexpected, but interesting results. As stated earlier, the goal of these analyses was to gain more insight into protein interaction with the α-hemolysin pore. In other words, to determine how a physical or chemical property of a protein (eg. presence of disulfide bonds) affects the interaction of the protein with the pore. For example, there are conflicting reports as to whether large folded proteins induce blockade events with the α-hemolysin pore (Oukhaled *et al.*, 2007). In addition, some studies have reported no blockade events when the protein goes against the electrophoretic force, while others have shown that protein translocation can still occur even against electrophoresis if the translocation is facilitated by electroosmosis and/or diffusion (Firnkes *et al.*, 2010; Fologea *et al.*, 2007). Indeed, the results obtained with these proteins do show that presence of blockade events cannot be simply explained by electrophoresis. For example, based on electrophoresis one could assume that RNase A (124 amino acids and +4 net charge) would induce a smaller proportion of translocation/intercalation events than *E. coli* thioredoxin (108 amino acids and -5 net charge). However, the results obtained indicate the opposite (Figure 3.6 and Figure 3.10d).

The conclusion that can be reached from the examination of these proteins is that there are no obvious correlations between the results obtained and properties of the proteins. For example, human and *E. coli* thioredoxin proteins are very similar in structure, yet the results (Figure 3.8b and Figure 3.10d) are very different (Katti *et al.*, 1990; Weichsel *et al.*, 1996). On the other hand, ubiquitin and BPTI have different properties (Table 3.5) yet their current blockade histograms (Figure 3.8c, d) are very similar. This suggests that the interaction of proteins with the pore is based on a combination of protein properties.

4.2.2 Importance of adding EDTA

Metal ions are essential for the activity of many proteins (Dudev and Lim, 2008; Rees, 2002). In some cases metal ions serve as cofactors and in others cases metal ions are essential for the correct folding of the protein. Zn-finger, Zif268 folds only in the presence of the Zn^{2+} but in the absence of Zn^{2+} the protein is unfolded and only binds weakly to its DNA target (Berg and Godwin, 1997). There are also proteins where metal ions can have a deleterious effect on their activity. In particular, proteins containing free thiol groups can be inactivated by metal ions such as Cd^{2+} or Hg^{2+}, which bind tightly to thiols (Clarkson, 1993; Hamer, 1986). For Alzheimer's Aβ peptides even trace amounts of metal ions found in buffers and culture media were enough to cause the initiation of the seeding process and Aβ oligomerization (Huang *et al.*, 2004). Proteins may become contaminated with metal ions during the process of purification, or after purification, from trace levels of metal ions found on plastic and glass labware. Furthermore, water, laboratory buffers, and culture media are also a major source of metal ion contamination. Our results with MBP and *E. coli* thioredoxin (section 3.4) demonstrate that trace metals can also have unexpected effects on nanopore analysis.

First, most small proteins show an intercalation/translocation peak when the nanopore analysis is performed in a phosphate buffer. Exceptions may include very large proteins such as IgG which only give bumping events (Madampage *et al.*, 2010). Second, the addition of EDTA appears to promote intercalation whereas the deliberate addition of low concentrations of divalent metal ions suppresses these events. The phosphate buffer may partially mimic the effects of EDTA since many divalent metal ions bind tightly to phosphate (Sambrook and Russell, 2001). The original nanopore experiments on MBP, were performed in HEPES buffer without EDTA which might explain why no events were reported in the absence of denaturant (Oukhaled *et al.*, 2007). There have been three previous reports on the effect of metal ions on proteins by nanopore analysis. Zn^{2+}, but not Co^{2+} or Mg^{2+}, caused the folding of a Zn-finger but these experiments were performed in KPi by pre-incubation of the metal ion with the protein (Stefureac and Lee, 2008). Similarly Cu^{2+} does not interfere with the translocation of a β-hairpin peptide but does reduce the translocation of Cu-binding peptides derived from the prion protein (Stefureac *et al.*, 2010a). Finally, Cu^{2+} and Zn^{2+} but not Mg^{2+} cause the compaction of myelin basic protein, preventing it from translocating (Baran *et al.*, 2010). Thus these examples were all specific effects, whereas the present observations with MBP are almost certainly non-specific since there is no evidence that MBP has a metal binding site.

Surprisingly, maltose which is the natural ligand of MBP with a Kd of 1200 nM, also suppresses the events with a high current blockade (Telmer and Shilton, 2003). On the other hand, lactose does not bind to MBP and has little effect (Doring *et al.*, 1999). Incidentally, the effect of maltose strongly supports the view that the observed intercalation/translocation events are not caused by peptide impurities since there is no evidence that maltose binds to peptides.

Finally, why do divalent metal ions (and maltose in the case of MBP) decrease the frequency of intercalation events? The simplest explanation is that any ligand which binds preferentially to the folded state compared to the unfolded state will, by the law of mass action, stabilize the folded state (Fig. 4.1). Metal ions will tend to bind more tightly to the folded conformation since the local negative charge density is higher and thus the frequency of partially unfolded loops or ends which might be available for intercalation will be reduced. Similarly, NMR studies have shown that upon binding maltose the domains of the protein are much more rigid which again would prevent partial unfolding (Doring *et al.*, 1999).

In conclusion, our results with MBP and *E. coli* thioredoxin demonstrate that transient or partial unfolding of proteins can be detected by nanopore analysis confirming the usefulness of this technique for conformational studies or for protein/ligand interactions. As well, the presence of low concentrations of divalent metal ions can have a profound effect on the event profile and thus, the choice of buffer is critical in these experiments.

4.2.3 Identifying events: intercalation or translocation

4.2.3.1 Indirect approach: the effect of voltage

Over the past decade nanopore analysis utilizing α-hemolysin has been applied to numerous peptides and proteins. There have been several reports of peptide and protein translocation through the α-hemolysin pore. However, as stated earlier there is no direct evidence, as yet, that proteins can translocate the α-hemolysin pore. The current measurements provide indirect proof at best. For example, the blockade events observed with proteins could be as results of protein translocation or non-specific protein binding/unbinding to the pore. Therefore, the voltage effect on the interaction of the proteins with the pore was taken as an indirect approach to determine if the examined proteins are translocating or intercalating.

For RNase A, a protein with a +4 net charge, the blockade current was proportional to the

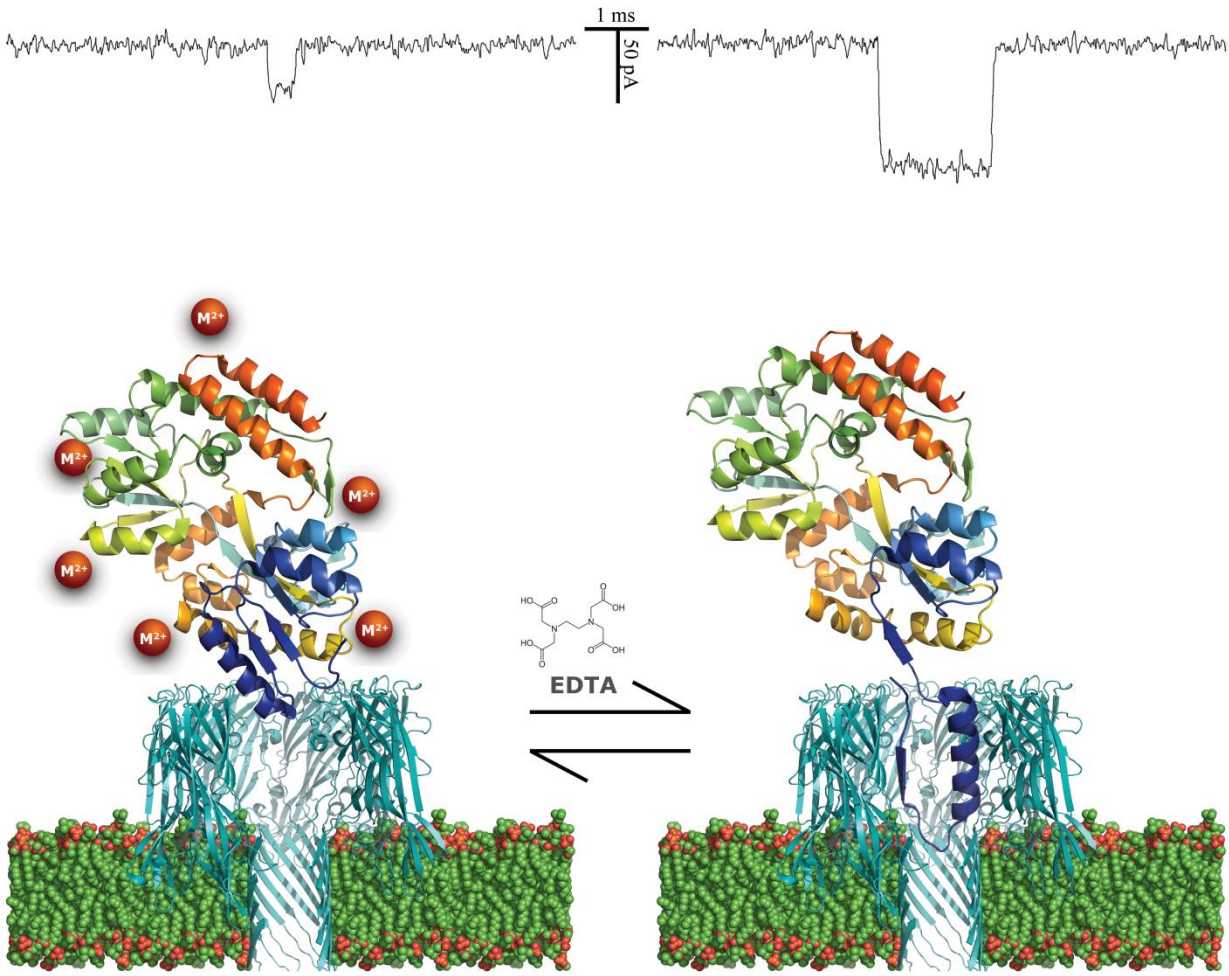

Figure 4.1. Schematic representation of the possible effect of EDTA on the interaction of MBP (PDB ID: 1JW4) with the α-hemolysin pore (PDB ID: 7AHL). In the presence of low concentrations of divalent metal ions, MBP gives rise to mostly bumping events with a small current blockade. Upon removal of the metal ions with EDTA, a loop of the protein can partially enter the pore giving rise to events with a much larger current blockade.

voltage but there was no significant change in the translocation times. This was unexpected because an increase or decrease in duration times was expected as a function of applied voltage. Considering the positive net charge and the experimental set up, if RNase A were to translocate through the pore then an increase in voltage would result in an increase in the duration times. Therefore, it is unclear if the events are translocation or intercalation. Similar result was also obtained with the negatively charged MBP. Unlike RNase A, MBP has a negative net charge (-8). In contrast, for *E. coli* thioredoxin and calmodulin the duration times decreased with decreasing voltage and the largest effect was for calmodulin which has the highest net charge density. This result is intuitively reasonable since higher net charge density would results in higher electrophoretic force acting on the protein. Since both *E. coli* thioredoxin and calmodulin are negatively charged the decrease in duration times with decreasing voltage indicates that these proteins do not translocate but rather intercalate.

The effect of voltage on the interaction of MBP with the α-hemolysin pore was also studied in the presence of 1.5 GdnHCl. At this GdnHCl concentration, MBP is completely unfolded and should translocate the α-hemolysin pore (Betton and Hofnung, 1996; Oukhaled *et al.*, 2007). Therefore, an increase in applied voltage is expected to decrease the event times. Indeed, the duration times for the large blockade events increased with decreasing voltage, suggesting translocation of the protein through the pore in the presence of 1.5 GdnHCl. The effect of voltage on the interaction of MBP with the aerolysin pore in the presence of 1.5 GdnHCl has also been investigated by Juan Pelta's group and similar results were observed (Pastoriza-Gallego *et al.*, 2011).

The voltage effect on the interaction of the proteins with α-hemolysin did not answer all our questions. For example, are the large blockade events observed with MBP and RNase A translocation or intercalation or possibly some other type of event? Why are there events observed for RNase A protein even though the protein is going against the electric field? Firnkes *et al*. has shown that translocation of proteins through solid-state pores can still occur even when going against the electric field (Firnkes *et al.*, 2010). They demonstrated that the translocation of proteins through solid-state pores is a conjoint and competitive action of diffusion, electrophoresis, and electroosmosis. Electroosmosis can enhance or counteract electrophoresis depending on the zeta potentials of the protein and the pore. In addition, it was shown that translocation can still occur even when electroosmosis and electrophoresis cancel

each other. In such a case the translocation is diffusion controlled, driven by the concentration gradient between the two chambers. However, it should be noted that in their study the size of the pore was not a limiting factor on translocation of the protein. Therefore, the proteins could readily translocate folded. Japrung *et al*. also observed events for a protein which was thought to be going against the electrophoretic flow (Japrung *et al.*, 2013). However, upon measuring the zeta potential of the protein it was found that the zeta potential of the protein was negative although the protein has a positive net charge, thus indicating charge reversal. The charge reversal was occurring at high salt concentrations of about 200 mM KCl. As shown in section Figure 3.16 charge reversal can occur when there is build up of counter ions around the protein.

Interestingly the zeta potential obtained for RNase A was negative when measured in the same buffer as the nanopore electrolyte but with lower salt concentration. Zeta potential measurements could not be carried out at high salt concentrations because of the high voltages. A negative zeta potential was also obtained in the same buffer but without salt. Considering that the pH of the solution was lower than the pI of the protein, a positive zeta potential was expected in both cases (Firnkes *et al.*, 2010). The negative zeta potential indicates that RNase A undergoes a charge reversal under the nanopore experimental conditions. Therefore, because of the charge reversal the electric field will actually facilitate the translocation of the protein rather than hinder it. In addition, since the α-hemolysin pore is slightly anion selective its zeta potential is expected to be very small and negative. Since both the pore and protein have negative zeta potentials, the small electroosmotic flow will counteract the electrophoresis. However, the zeta potential of the pore is expected to be much smaller than that of the protein and thus the translocation direction would be electrophoretic. This explains the large blockade events observed with RNase A. In addition, the magnitude of the zeta potential explains the lack of duration time dependence on voltage. The zeta potential of RNase A was also measured in buffers of different pHs. At pH 4 which is much lower than the pI 9.5, a positive zeta potential was obtained as expected. Also at a pH higher than the pI a negative zeta potential was obtained. Additionally, zeta potential measurements were also conducted for MBP and Calmodulin. The results obtained for these two proteins are as expected and indicate no charge reversal.

In conclusion, for ss-DNA the effect of voltage on blockade time and current is consistent with a simple electrophoretic model of translocation. For proteins, there are clearly other

parameters involved such as unfolding and orientation. Thus, a definitive answer to the question of protein translocation through the α-hemolysin pore cannot be obtained through the indirect approach. Furthermore, since nanopore experiments are usually performed with solutions of high salinity, our results highlight the importance of considering the zeta potential when performing nanopore analysis of proteins.

4.2.3.2 Direct approach: testing for enzyme activity in the *trans* chamber

Nanopore sensing with α-hemolysin pore has been applied to proteins for a variety of studies, such as protein folding/unfolding, protein-ligand interactions, and enzymatic kinetics. One of the main difficulties of nanopore analysis of proteins with α-hemolysin pore is the ability to discriminate between translocation and other events (eg. intercalation events or other protein-pore interaction events). As seen in this thesis most proteins are larger than the α-hemolysin pore but they still induce large blockade events. With ss-DNA and small peptides these are interpreted as translocation events. In contrast, with proteins it is more complex because they are larger than the smallest diameter of the pore, thus the events cannot be translocation if the protein is folded. However, some computer simulation studies have shown that if an unstructured segment of a protein goes into the pore then the electric field acting on the protein will be sufficient in facilitating protein unfolding and subsequent translocation (Makarov, 2009). In a different study, Bayley and coworkers attached an oligonucleotide (high net charge density) to the C-terminus of a mutant *E. coli* thioredoxin which was used to facilitate the threading of the C-terminal end of the protein into the pore (Figure 1.11) (Rodriguez-Larrea and Bayley, 2013). In addition, it was used to provide sufficient driving force under an electric field for protein unfolding and translocation. Therefore, the events observed with some of the proteins examined here (eg. proteins without disulfide bonds or reduced proteins) could be translocation events but direct evidence is required to be certain.

Direct evidence is difficult to obtain with proteins since the α-hemolysin pore on average remains viable for a very short period of time before the lipid membrane breaks and thus very few putative translocations can be achieved. Considering the low number of putative translocations a very sensitive detection assay is required for protein detection. This is why the RNase A detection assay is ideal for this experiment. Our detection assay relies on RT-PCR, which is highly specific.

The detection assay was designed to test for RNase A activity in the *trans* chamber. As stated previously, RNase A was chosen as a model enzyme for this analysis because it is very robust (eg. can withstand temperatures up to 100 ^{o}C) and after unfolding with denaturants and/or disulphide reducing agents, it readily refolds to an active conformation (Bastings *et al.*, 2008; Miyamoto *et al.*, 2009; Neira and Rico, 1997; Reinstadler *et al.*, 1996; Wedemeyer *et al.*, 2000). Based on the experimental conditions, the designed assay is successful in detecting as low as 2200 molecules of the enzyme. In other words, 2200 molecules of RNase A will be sufficient in cleaving enough globin mRNA molecules to produce a detectable change in the intensity of the bands in agarose gel. However, because only about 25% of the total volume in the *trans* chamber is used to carry out the detection assay then a total of about 10 000 molecules of the protein must go through the pore in order for the detection assay to work. Furthermore, it was reasoned that events with blockade currents of 60% or higher could be translocation on the basis that if a protein molecules translocated it will do so unfolded. From a theoretical point of view, translocation of an unfolded protein will then resemble that of a long peptide. Typical peptide translocations are 50-100% blocks. Therefore, a minimum of 10 000 events with 60% or higher block were recorded in total before conducting an RNase A detection assay.

Many control experiments were carried out in the process of RNase A detection experiments. The controls conducted were to ensure that there was no RNase A contamination in any of the steps along the process. In addition, some of the controls were carried out to ensure no false translocations occur during the nanopore experiments. For example, addition of RNase A to the *cis* chamber results in no translocation to the *trans* side when a membrane is painted over the 150 µm aperture (Figure 3.18b). This was an important result because it confirmed that in the absence of pores, the protein could not translocate through the membrane. In addition, it shows that there is no contamination by aerosols in the process since this control was run for 2 - 3 hours (i.e same length as a typical nanopore experiment). The same experiment was carried out but without the membrane painted over the 150 µm aperture as a positive control for RNase A translocation through a pore. The largest dimension of the protein is 3.8 nm, thus the translocation of the protein will not be limited by the pore size. This experiment was conducted with and without applied voltage. In both cases, there was RNase A activity detected in the *trans* chamber (Figure 3.22). From these results two conclusions can be

reached. First, the result shows that the detection assay is competent in observing RNase A translocation through a pore. The RNase A detected in the *trans* chamber is as a result of translocation through the 150 μm pore and not buffer or apparatus contamination because as shown in lanes 1 and 2 in Figure 3.22, there was no RNase A detected in the *trans* chamber prior to adding the protein to the *cis* chamber. In addition, the RNase A detected in the *trans* chamber cannot be contamination by aerosols because as it was shown earlier this doesn't occur in this experimental time frame. Second, the result obtained with no applied voltage indicates that the translocation of the RNase A can be diffusion controlled when the size of the pore is not a limiting factor. Thus, the concentration gradient is sufficient in facilitating the translocation of the protein through the micrometer pore. Together, the control experiments confirmed the feasibility of our approach in determining if RNase A translocates through the α-hemolysin pore.

The experiment with RNase A added to the *cis* chamber (*cis* side grounded) and α-hemolysin pores inserted into the lipid bilayer shows no translocations to the *trans* chamber. This experiment was repeated more than five times to confirm the results. In one occasion, the nanopore experiment was run for 13 hrs without the membrane breaking, yet there was no enzyme activity detected in the *trans* chamber. Thus this indicates that the protein is not translocating the pore. In other words, the large blockade events observed with the protein are not translocation events. The number of events recorded in each of the experiments was much greater than the minimum required for the detection assay to work. One might argue that since the protein has to unfold in order to translocate then once in the *trans* chamber it might not refold back to an active confirmation. However, RNase A has been shown to become active even after denaturing it by autoclave sterilization (heating it up to 121 °C for 20 min) (Miyamoto *et al.*, 2009). In addition, even if there is some lost activity due to disulfide interchange, the detection assay should still detect some activity since the number of putative translocations is much greater than the minimum required. Therefore, it's highly unlikely that there is non-active RNase A in the *trans* chamber. In the earlier section it was discussed that electrophoresis and diffusion are acting in favour of RNase A translocation through the pore. Based on this result it can be concluded that the two forces acting on the protein are not sufficient in facilitating its unfolding and subsequent translocation. For this reason, the protein was deliberately unfolded prior to adding it to the *cis* chamber.

The experiments attempted with the unfolded RNase A could not be successfully completed. This was because the nanopore experiment could not be run for long periods of time to record sufficient number of putative translocations and therefore the detection assay could not be performed. The factors preventing this were the stability of the pore and lipid bilayer in the presence of denaturing and reducing agents, low frequency of events, and the permanent pore blockades caused by the unfolded protein. It's important to restate that while the α-hemolysin pore and lipid bilayer are stable in the presence of GdnHCl and TCEP to carry out a typical nanopore experiment, that's not the case here. In these experiments in order for the detection assay to work the lipid bilayer formed in the beginning of the nanopore experiment must remain intact till the end of the experiment (i.e for several hours) or otherwise false translocations will occur. In terms of the frequency of events, this was partially contributed by the presence of GdnHCl in one chamber and not both. It's not clear why the presence of GdnHCl in both chambers causes an increase in the frequency of events. One explanation might be that the diffusion rate of unfolded proteins increases with increasing GdnHCl (Waldauer *et al.*, 2010). So, in the absence of GdnHCl the diffusion rate will be slower. Moreover, with folded RNase A there was charge reversal occurring whereas with the unfolded protein this is likely not the case. Hence, the electric field would be hindering the translocation of the protein with net positive charge (i.e opposite directions) under the current experimental set up which in turn can translate to lower frequency of events. Furthermore, the local negative charge density is lower and thus the frequency of events will be reduced

Overall, the direct approach shows that natively folded RNase A added to the *cis* chamber doesn't unfold to translocate, thus indicating that the electrophoretic force acting on the protein is not large enough to facilitate unfolding of the protein. Moreover, the limiting factor to the protein translocation through the α-hemolysin pore is indeed the diameter of the pore. Therefore, the large blockade events induced by RNase A are simply interactions between the pore and the protein (eg. intercalation events) but not translocations. However, it still remains unknown if the unfolded RNase A translocates through the α-hemolysin pore. A different direct approach must be taken in order to obtain a definitive answer.

4.3 Solid-state pores

The nanopore experiments with the solid-state pores were not successful. Most of the shortcomings discussed in the literature were also encountered here (Stefureac, 2012; Tabard-Cossa *et al.*, 2007). For example, poor pore-to-pore reproducibility, large open pore current noise (about 200-250 pA), and larger than expected conductance were the most common issues in all of the 20 pores tested. Analysis of RNase A was carried out with all the solid-state pores under different experimental conditions but there were no events observed with any of the pores. In addition to RNase A, MBP was analyzed as well and similar observations were made with 19 out of the 20 pores. In one of the pores there were events observed with MBP.

Under the experimental conditions used the zeta potential of both proteins are negative (section 3.2.5.3). In addition, the zeta potential of the pores is expected to be negative (Firnkes *et al.*, 2010). Therefore, the electroosmotic flow will counteract electrophoresis. If the zeta potential of the pore is much greater than that of the protein, then electroosmosis will dominate and the translocation direction will be electroosmotic. In contrast, if the zeta potential of the protein is greater than that of the pore, electrophoresis would dominate. However, it's unlikely that the absence of events with RNase A and MBP is related to electroosmosis or electrophoresis. This is because the protein was added to the *cis* chamber and positive and negative potentials were applied. Hence, independent of the magnitude of the zeta potential of the pore the translocation of the proteins would be favoured by the larger force at least under one of the set-ups, whether it's electroosmosis or electrophoresis.

For RNase A, the events might not be distinguishable from the noise level. So even if there are translocation events they will be within the current noise levels. Based on the physical characteristics of a pore of 10 nm diameter, a theoretical volume of 1178.1 nm^3 is obtained. However, based on the measured conductance for the 10 nm pore shown in Figure 3.24, the actual diameter and volume are calculated to be 15.8 nm and 2935.4 nm^3, respectively. Stefureac *et al*. has shown that when the proteins which have dimensions much smaller than the pore will translocate in a folded confirmation (Stefureac *et al.*, 2010b). If RNase A is assumed to have a sphere-like shape, then its volume would be 44.6 nm^3 with the 0.7 nm water shell added (Ebbinghaus *et al.*, 2007). Therefore, as the protein passes through the pore, the volume excluded will be 1.52% of the total pore volume. The 10 nm pore shown in Figure 3.24b had an open pore current of about 8600 pA. Thus, 1.52% of the open pore current is only 130 pA block, which is lower than the current noise and thus would not be distinguishable. In the same

pore, MBP would be expected to induce a blockade of 315 pA, which is slightly larger than the current noise. However, there were no events observed with MBP for this pore. On the other hand, if similar calculations are done for MBP and the pore shown in Figure 3.24c (calculated volume and diameter of 2477.3 nm^3 and 14.5 nm, respectively) then a blockade of about 323 pA would be expected.

While the large current noise can be used to explain the absence of events with RNase A protein, it still doesn't explain the results obtained with MBP which is a much larger protein and based on the calculations, the events should be distinguishable from the current noise. In addition, the events observed with the pore in Figure 3.24c cannot be explained by the calculations since the blockades shown in the figure are larger that the calculated current block. This indicates that in addition to the current noise levels, other factors might be responsible for the absence of events.

The conclusion that can be drawn from these studies is that solid-state pore production still needs improvement before they reach the reproducibility and reliability of biological pores. Since our lab is not equipped for the production of solid-state pores, we must rely on commercial solid-state pores. Considering the cost and the success rate with the solid-state pores, this is a limit to the number of pores that we can test.

4.4 Future directions

The experiments conducted in this thesis have demonstrated nanopore sensing as a powerful single molecule technique for studying proteins and peptides. The analysis of the peptide isomers validated the true sensitivity of nanopore sensing as a single molecule technique. With the analysis of different proteins under different experimental conditions we were able to exhibit nanopore analysis as a powerful technique for studying protein folding/unfolding, protein conformational changes, and protein ligand interactions. Together, these experiments have laid a foundation for future analysis of biomolecules.

The sensitivity of the technique was put to the test with the analysis of the glucagon and Fmoc-$D_2A_{10}K_2$ peptide isomers. For the Fmoc-$D_2A_{10}K_2$ peptide isomers, the α-hemolysin pore was able to differentiate between directional isomer but not between chiral isomers. In contrast, for the more complex glucagon peptide isomers, the pore was successful in differentiating between all four isomers, thus indicating that pore is recognizing structure and

sequence. The analysis of other peptide isomers with different properties and degrees of complexity would be of interest in order to obtain a better understanding of how the pore is interrogating different peptides. Furthermore, it would be of interest to examine if adding isomers on the stem side of the pore shows a better degree of discrimination. Moreover, the pore can be engineered to introduce chiral groups within the lumen (eg. β-cyclodextrin) to improve the pore's discrimination ability. Potentially, nanopore sensing can be developed into a method for screening and detecting isomer purity in a heterogeneous mixture. This would be of considerable importance in pharmacological applications where peptides are being explored as immunomodulatory agents, hormone agonists/antagonists, and vaccines (Brinckerhoff *et al.*, 1999; Green *et al.*, 2004; Powell *et al.*, 1993; Werle and Bernkop-Schnurch, 2006). One of the disadvantages of using peptides (eg. L peptides) for therapeutic applications is their sensitivity to biological degradation. However, RI peptides demonstrate comparable activity to the L peptides and can resist proteolytic degradation (Briand *et al.*, 1995; Goodman and Chorev, 1979; Kindrachuk *et al.*, 2011; Taylor *et al.*, 2000; Werle and Bernkop-Schnurch, 2006). Therefore, the ability to examine isomer purity at low cost and high speed would make nanopore sensing an attractive technique in pharmacological applications.

The experiments conducted with proteins of different chemical and physical properties revealed important information about nanopore analysis of proteins. Unexpectedly, all proteins induced large blockade events and there are no obvious correlations between the results obtained and the properties of the proteins. Furthermore, all proteins produced distinct current blockade histograms indicating the power of nanopore sensing to distinguish between proteins. It's been shown that very large proteins such as IgG give only bumping events (Madampage *et al.*, 2010). Therefore, it would be important to analyze more proteins ranging in size from a few kDa to more than a hundred kDa (IgG size) to determine at what point do large blockade events (eg. intercalation events) start disappearing and why.

In addition, the results obtained with MBP and *E. coli* thioredoxin demonstrate that transient or partial unfolding of proteins can be detected by nanopore analysis confirming the usefulness of this technique for conformational studies or for protein/ligand interactions. As well, the presence of low concentrations of divalent metal ions can have a profound effect on the event profile and thus, the choice of buffer or use of EDTA is critical in these experiments.

Furthermore, it was found there is silver leaching from the Ag/AgCl electrodes and that can in turn bind to nucleic acids and proteins being analyzed and induce an effect on the event profile. Therefore, the use of salt-bridges and/or EDTA must be considered in future analysis of biomolecules. Together, these findings represent a fundamental step towards the use of nanopore sensing for protein conformational studies, for protein/ligand interactions, and detection of metal poisoning of proteins, a characteristic of a single molecule technique.

In an attempt to determine the identity of the large blockade events induced by all examined proteins two approaches were taken: an indirect approach and a direct approach. The indirect approach relied on voltage effect on the interaction of the protein with the pore whereas in the direct approach the opposite chamber to where the enzyme was added was tested for enzyme activity at the end of a nanopore experiment. The indirect approach failed to provide answers for some of the examined proteins (i.e no voltage effect on the duration times). In contrast, the direct approach showed that RNase A doesn't translocate through the α-hemolysin pore. This is the first report of direct evidence that proves that proteins larger than α-hemolysin pore do not translocate. For future work it would be of interest to apply our direct approach to translocation of RNase A through a larger biological pore where translocation of the protein would not be hindered by the diameter of the pore. For example, our lab is currently working on producing and isolating the ExeD pore which is larger and more stable than the α-hemolysin pore. The ExeD pore is a homododecamer pore produced by *Aeromonas hydrophila* and one of its functions is to excrete fully folded proteins. The smallest internal diameter of the pore is 6.8 nm and forms a highly stable structure that is capable of withstanding boiling in SDS. Therefore, this would be an ideal pore to use as a positive control for RNase A translocation experiments. Furthermore, since this pore is believed to be more stable under a range of experimental conditions and remain viable for longer periods of time, it will be possible to apply the direct approach to translocation of completely unfolded RNase A which was not possible with α-hemolysin pore. In addition, ExeD pore is highly stable at high temperatures and thus can be used to study thermal unfolding of proteins (Ast *et al.*, 2002; Guilvout *et al.*, 2008; Nouwen *et al.*, 1999; Strozen *et al.*, 2011). Considering the reproducibility and reliability of biological pores, the use of ExeD pore would be an attractive alternative to solid-state pores.

Finally, the findings in this thesis have provided an overall better understanding of the nanopore sensing technique and can be applied to analysis of peptides and proteins in the

future. For example, special consideration must be given to the choice of buffer, use of salt bridges, and measurement of zeta potential when examining proteins by nanopore sensing.

5.0 REFERENCES

Akeson, M., Branton, D., Kasianowicz, J.J., Brandin, E., and Deamer, D.W. (1999). Microsecond time-scale discrimination among polycytidylic acid, polyadenylic acid, and polyuridylic acid as homopolymers or as segments within single RNA molecules. Biophys. J. *77*, 3227-3233.

Aksimentiev, A., and Schulten, K. (2005). Imaging alpha-hemolysin with molecular dynamics: ionic conductance, osmotic permeability, and the electrostatic potential map. Biophys. J. *88*, 3745-3761.

Albrecht, T., Edel, J.B., and Winterhalter, M. (2010). New developments in nanopore research-from fundamentals to applications. J. Phys.: Condens. Matter *22*, 450301.

Ang, Y.S., and Yung, L.Y. (2012). Rapid and label-free single-nucleotide discrimination via an integrative nanoparticle-nanopore approach. ACS Nano *6*, 8815-8823.

Arakawa, H., Neault, J.F., and Tajmir-Riahi, H.A. (2001). Silver(I) complexes with DNA and RNA studied by Fourier transform infrared spectroscopy and capillary electrophoresis. Biophys. J. *81*, 1580-1587.

Arjmandi, N., Van Roy, W., Lagae, L., and Borghs, G. (2012). Measuring the electric charge and zeta potential of nanometer-sized objects using pyramidal-shaped nanopores. Anal. Chem. *84*, 8490-8496.

Asandei, A., Apetrei, A., Park, Y., Hahm, K.S., and Luchian, T. (2011). Investigation of single-molecule kinetics mediated by weak hydrogen bonds within a biological nanopore. Langmuir *27*, 19-24.

Ascenzi, P., Bocedi, A., Bolognesi, M., Spallarossa, A., Coletta, M., De Cristofaro, R., and Menegatti, E. (2003). The bovine basic pancreatic trypsin inhibitor (Kunitz inhibitor: A milestone protein. Curr. Protein Pept. Sci. *4*, 231-251.

Ashkin, A. (2000). History of optical trapping and manipulation of small-neutral particle, atoms, and molecules. IEEE J. Sel. Topics Quantum Electron. *6*, 841-856.

Ast, V.M., Schoenhofen, I.C., Langen, G.R., Stratilo, C.W., Chamberlain, M.D., and Howard, S.P. (2002). Expression of the ExeAB complex of Aeromonas hydrophila is required for the localization and assembly of the ExeD secretion port multimer. Mol. Microbiol. *44*, 217-231.

Astier, Y., Braha, O., and Bayley, H. (2006). Toward single molecule DNA sequencing: direct identification of Ribonucleoside and Deoxyribonucleoside 5‘-Monophosphates by using an

engineered protein nanopore equipped with a molecular adapter. J. Am. Chem. Soc. *128*, 1705-1710.

Bahrami, A., Dogan, F., Japrung, D., and Albrecht, T. (2012). Solid-state nanopores for biosensing with submolecular resolution. Biochem. Soc. Trans. *40*, 624-628.

Baran, C., Smith, G.S., Bamm, V.V., Harauz, G., and Lee, J.S. (2010). Divalent cations induce a compaction of intrinsically disordered myelin basic protein. Biochem. Biophys. Res. Commun. *391*, 224-229.

Barford, A.M., Gilliland, G.L., and Morgan, D.W. (1986). Growing calmodulin crystals for X-ray diffraction studies at room temperature in 2 days. Anal. Biochem. *158*, 361-364.

Bastings, M.M., van Baal, I., Meijer, E.W., and Merkx, M. (2008). One-step refolding and purification of disulfide-containing proteins with a C-terminal MESNA thioester. BMC Biotechnol *8*, 76.

Bayley, H., and Cremer, P.S. (2001). Stochastic sensors inspired by biology. Nature *413*, 226-230.

Bayley, H., and Martin, C.R. (2000). Resistive-pulse sensing from microbes to molecules. Chem. Rev. *100*, 2575-2594.

Beamish, E., Kwok, H., Tabard-Cossa, V., and Godin, M. (2012). Precise control of the size and noise of solid-state nanopores using high electric fields. Nanotechnology *23*, 405301.

Benkirane, N., Guichard, G., Van Regenmortel, M.H.V., Briand, J.-P., and Muller, S. (1995). Cross-reactivity of antibodies to retro-inverso peptidomimetics with the parent protein Histone H3 and chromatin core particle: specificity and kinetic rate-constant measurments. J. Biol. Chem. *270*, 11921-11926.

Benner, S., Chen, R.J.A., Wilson, N.A., Abu-Shumays, R., Hurt, N., Lieberman, K.R., Deamer, D.W., Dunbar, W.B., and Akeson, M. (2007). Sequence-specific detection of individual DNA polymerase complexes in real time using a nanopore. Nat. Nanotechnol. *2*, 718-724.

Berg, J.M., and Godwin, H.A. (1997). Lessons from zinc-binding peptides. Annu. Rev. Biophys. Biomol. Struct. *26*, 357-371.

Betton, J.M., and Hofnung, M. (1996). Folding of a mutant maltose-binding protein of Escherichia coli which forms inclusion bodies. J. Biol. Chem. *271*, 8046-8052.

Bhattacharya, S., Derrington, I.M., Pavlenok, M., Niederweis, M., Gundlach, J.H., and Aksimentiev, A. (2012). Molecular dynamics study of MspA Arginine mutants predicts slow

DNA translocations and ion current blockades indicative of DNA sequence. ACS Nano *6*, 6960-6968.

Billingsley, D.J., Bonass, W.A., Crampton, N., Kirkham, J., and Thomson, N.H. (2012). Single-molecule studies of DNA transcription using atomic force microscopy. Phys. Biol. *9*, 021001.

Binnig, G., Quate, C.F., and Gerber, C. (1986). Atomic force microscope. Phys. Rev. Lett. *56*, 930-933.

Bockelmann, U. (2004). Single-molecule manipulation of nucleic acids. Curr. Opin. Struct. Biol. *14*, 368-373.

Boersma, A.J., and Bayley, H. (2012). Continuous stochastic detection of amino acid enantiomers with a protein nanopore. Angew. Chem. Int. Ed. *51*, 9606-9609.

Bornschlogl, T., and Rief, M. (2011). Single-molecule protein unfolding and refolding using atomic force microscopy. Methods Mol. Biol. *783*, 233-250.

Braha, O., Gu, L.-Q., Zhou, L., Lu, X., Cheley, S., and Bayley, H. (2000). Simultaneous stochastic sensing of divalent metal ions. Nat. Biotechnol. *18*, 1005-1007.

Braha, O., Walker, B., Cheley, S., Kasianowicz, J.J., Song, L.Z., Gouaux, J.E., and Bayley, H. (1997). Designed protein pores as components for biosensors. Chem. Biol. *4*, 497-505.

Branton, D., Deamer, D.W., Marziali, A., Bayley, H., Benner, S.A., Butler, T., Di Ventra, M., Garaj, S., Hibbs, A., Huang, X.H., *et al.* (2008). The potential and challenges of nanopore sequencing. Nat. Biotechnol. *26*, 1146-1153.

Braz, V.A., and Howard, K.J. (2009). Separation of protein oligomers by blue native gel electrophoresis. Anal. Biochem. *388*, 170-172.

Briand, J.-P., Guichard, G., Dumortier, H., and Muller, S. (1995). Retro-inverso peptidomimetics as new immunological probes. J. Biol. Chem. *270*, 20686-20691.

Brinckerhoff, L.H., Kalashnikov, V.V., Thompson, L.W., Yamshchikov, G.V., Pierce, R.A., Galavotti, H.S., Engelhard, V.H., and Slingluff, C.L., Jr. (1999). Terminal modifications inhibit proteolytic degradation of an immunogenic MART-1(27-35) peptide: implications for peptide vaccines. Int. J. Cancer *83*, 326-334.

Butler, T.Z., Pavlenok, M., Derrington, I.M., Niederweis, M., and Gundlach, J.H. (2008). Single-molecule DNA detection with an engineered MspA protein nanopore. Proc Natl Acad Sci U S A *105*, 20647-20652.

Cai, Q., Ledden, B., Krueger, E., Golovchenko, J.A., and Li, J. (2006). Nanopore sculpting with noble gas ions. J. Appl. Phys. *100*, 024914-024916.

Cao, A., Welker, E., and Scheraga, H.A. (2001). Effect of mutation of proline 93 on redox unfolding/folding of bovine pancreatic ribonuclease A. Biochemistry. *40*, 8536-8541.

Cao, L.X., and Wang, Y.G. (2009). Fabrication and investigation of single track-etched nanopore and its applications. Radiat. Meas. *44*, 1093-1099.

Casuso, I., Rico, F., and Scheuring, S. (2011). High-speed atomic force microscopy: Structure and dynamics of single proteins. Curr. Opin. Chem. Biol. *15*, 704-709.

Cecconi, C., Shank, E.A., Bustamante, C., and Marqusee, S. (2005). Direct observation of the three-state folding of a single protein molecule. Science *309*, 2057-2060.

Cherf, G.M., Lieberman, K.R., Rashid, H., Lam, C.E., Karplus, K., and Akeson, M. (2012). Automated forward and reverse ratcheting of DNA in a nanopore at 5-A precision. Nat. Biotechnol. *30*, 344-348.

Chin, D., and Means, A.R. (2000). Calmodulin: a prototypical calcium sensor. Trends Cell Biol. *10*, 322-328.

Christensen, C., Baran, C., Krasniqi, B., Stefureac, R.I., Nokhrin, S., and Lee, J.S. (2011). Effect of charge, topology and orientation of the electric field on the interaction of peptides with the alpha-hemolysin pore. J. Pept. Sci. *17*, 726-734.

Clarke, J., Wu, H.-C., Jayasinghe, L., Patel, A., Reid, S., and Bayley, H. (2009). Continuous base identification for single-molecule nanopore DNA sequencing. Nat. Nanotechnol. *4*, 265-270.

Clarkson, T.W. (1993). Molecular and ionic mimicry of toxic metals. Annu. Rev. Pharmacol. Toxicol. *33*, 545-571.

Cornish, P.V., and Ha, T. (2007). A survey of single-molecule techniques in chemical biology. ACS Chem. Biol. *2*, 53-61.

Coulter, W.H. (1953). Means for counting particles suspended in a fluid. U.S. Patent 2,656,508

Cozmuta, I., O'Keeffe, J.T., Bose, D., and Stolc, V. (2005). Hybrid MD-Nernst Planck model of α-hemolysin conductance properties. Mol. Simulat. *31*, 79-93.

Cressiot, B., Oukhaled, A., Patriarche, G., Pastoriza-Gallego, M., Betton, J.M., Auvray, L., Muthukumar, M., Bacri, L., and Pelta, J. (2012). Protein transport through a narrow solid-state nanopore at high voltage: experiments and theory. ACS Nano *6*, 6236-6243.

Davis, R.E., and Green, R.E. (1967). Automatic platelet counting with the Coulter particle counter. J. Clin. Pathol. *20*, 777-779.

Deamer, D. (2010). Nanopore analysis of nucleic acids bound to exonucleases and polymerases. Annu. Rev. Biophys. *39*, 79-90.

DeBlois, R.W., and Bean, C.P. (1970). Counting and sizing of submicron particles by the resistive pulse technique. Rev. Sci. Instrum. *41*, 909-916.

Dekker, C. (2007). Solid-state nanopores. Nat. Nanotechnol. *2*, 209-215.

Delgado, A.V., González-Caballero, F., Hunter, R.J., Koopal, L.K., and Lyklema, J. (2005). Measurement and interpretation of electrokinetic phenomena. Pure Appl. Chem. *77*, 1753-1805.

Ding, S., Gao, C., and Gu, L.Q. (2009). Capturing single molecules of immunoglobulin and ricin with an aptamer-encoded glass nanopore. Anal. Chem. *81*, 6649-6655.

Doring, K., Surrey, T., Nollert, P., and Jahnig, F. (1999). Effects of ligand binding on the internal dynamics of maltose-binding protein. Eur. J. Biochem. *266*, 477-483.

Duan, X., and Quiocho, F.A. (2001). Structural evidence for a dominant role of nonpolar interactions in the binding of a transport/chemosensory receptor to its highly polar ligands. Biochemistry. *41*, 706-712.

Dudev, T., and Lim, C. (2008). Metal binding affinity and selectivity in metalloproteins: insights from computational studies. Annu. Rev. Biophys. *37*, 97-116.

Ebbinghaus, S., Kim, S.J., Heyden, M., Yu, X., Heugen, U., Gruebele, M., Leitner, D.M., and Havenith, M. (2007). An extended dynamical hydration shell around proteins. Proc. Natl. Acad. Sci. *104*, 20749-20752.

Eisenstein, M. (2012). Oxford Nanopore announcement sets sequencing sector abuzz. Nat. Biotechnol. *30*, 295-296.

Eun, H.-M. (1996). DNA polymerases. In Enzymology Primer for Recombinant DNA Technology (San Diego: Academic Press), pp. 345-489.

Faller, M., Niederweis, M., and Schulz, G.E. (2004). The structure of a mycobacterial outer-membrane channel. Science *303*, 1189-1192.

Fennouri, A., Przybylski, C., Pastoriza-Gallego, M., Bacri, L., Auvray, L., and Daniel, R. (2012). Single molecule detection of Glycosaminoglycan Hyaluronic Acid Oligosaccharides and Depolymeri-zation enzyme activity using a protein nanopore. ACS Nano *6*, 9672-9678.

Firnkes, M., Pedone, D., Knezevic, J., Doblinger, M., and Rant, U. (2010). Electrically facilitated translocations of proteins through silicon nitride nanopores: conjoint and competitive action of diffusion, electrophoresis, and electroosmosis. Nano Lett. *10*, 2162-2167.

Fischer, P.M. (2003). The design, synthesis and application of stereochemical and directional peptide isomers: a critical review. Curr. Protein. Pept. Sci. *4*, 339-356.

Flashner, M.S., and Vournakis, J.N. (1977). Specific hydrolysis of Rabbit globin messenger-RNA by S1-nuclease. Nucleic Acids Res. *4*, 2307-2319.

Fologea, D., Ledden, B., McNabb, D.S., and Li, J. (2007). Electrical characterization of protein molecules by a solid-state nanopore. Appl. Phys. Lett. *91*, 053901-053903.

Fologea, D., Uplinger, J., Thomas, B., McNabb, D.S., and Li, J. (2005). Slowing DNA translocation in a solid-state nanopore. Nano Lett. *5*, 1734-1737.

Freedman, K.J., Jürgens, M., Prabhu, A., Ahn, C.W., Jemth, P., Edel, J.B., and Kim, M.J. (2011). Chemical, thermal, and electric field induced unfolding of single protein molecules studied using nanopores. Anal. Chem. *83*, 5137-5144.

Garaj, S., Hubbard, W., Reina, A., Kong, J., Branton, D., and Golovchenko, J.A. (2010). Graphene as a subnanometre trans-electrode membrane. Nature *467*, 190-193.

Goodman, M., and Chorev, M. (1979). On the concept of linear modified retro-peptide structures. Acc. Chem. Res. *12*, 1-7.

Goodrich, C.P., Kirmizialtin, S., Huyghues-Despointes, B.M., Zhu, A., Scholtz, J.M., Makarov, D.E., and Movileanu, L. (2007). Single-molecule electrophoresis of β-hairpin peptides by electrical recordings and Langevin Dynamics Simulations. J. Phys. Chem. B *111*, 3332-3335.

Gottschalk, M., Venu, K., and Halle, B. (2003). Protein self-association in solution: the bovine pancreatic trypsin inhibitor decamer. Biophys. J. *84*, 3941-3958.

Graham, M.D. (2003). The Coulter principle: foundation of an industry. J. Assoc. for Lab. Autom. *8*, 72-81.

Green, B.D., Mooney, M.H., Gault, V.A., Irwin, N., Bailey, C.J., Harriott, P., Greer, B., O'Harte, F.P., and Flatt, P.R. (2004). N-terminal His(7)-modification of glucagon-like peptide-

1(7-36) amide generates dipeptidyl peptidase IV-stable analogues with potent antihyperglycaemic activity. J. Endocrinol. *180*, 379-388.

Gu, L.-Q., Braha, O., Conlan, S., Cheley, S., and Bayley, H. (1999). Stochastic sensing of organic analytes by a pore-forming protein containing a molecular adapter. Nature *398*, 686-690.

Gu, L.-Q., Cheley, S., and Bayley, H. (2001). Prolonged residence time of a noncovalent molecular adapter, β-cyclodextrin, within the lumen of mutant α-hemolysin pores. J. Gen. Physiol. *118*, 481-494.

Guilvout, I., Chami, M., Berrier, C., Ghazi, A., Engel, A., Pugsley, A.P., and Bayan, N. (2008). In Vitro Multimerization and Membrane Insertion of Bacterial Outer Membrane Secretin PulD. J. Mol. Biol. *382*, 13-23.

Ha, T. (2001a). Single-molecule fluorescence resonance energy transfer. Methods *25*, 78-86.

Ha, T. (2001b). Single-molecule FRET. Single Molecules *2*, 283-284.

Ha, T., Enderle, T., Ogletree, D.F., Chemla, D.S., Selvin, P.R., and Weiss, S. (1996). Probing the interaction between two single molecules: fluorescence resonance energy transfer between a single donor and a single acceptor. Proc. Natl. Acad. Sci. *93*, 6264-6268.

Haddad, F., and Baldwin, K.M. (2010). Reverse transcription of the ribonucleic acid: the first step in RT-PCR assay. Methods Mol. Biol. *630*, 261-270.

Hall, A.R., Scott, A., Rotem, D., Mehta, K.K., Bayley, H., and Dekker, C. (2010). Hybrid pore formation by directed insertion of alpha-haemolysin into solid-state nanopores. Nat. Nanotechnol. *5*, 874-877.

Hamer, D.H. (1986). Metallothionein. Annu. Rev. Biochem. *55*, 913-951.

Han, A., Schurmann, G., Mondin, G., Bitterli, R.A., Hegelbach, N.G., de Rooij, N.F., and Staufer, U. (2006). Sensing protein molecules using nanofabricated pores. Appl. Phys. Lett. *88*, 093901-093903.

Haque, F., Geng, J., Montemagno, C., and Guo, P. (2013a). Incorporation of a viral DNA-packaging motor channel in lipid bilayers for real-time, single-molecule sensing of chemicals and double-stranded DNA. Nat. Protoc. *8*, 373-392.

Haque, F., Li, J., Wu, H.-C., Liang, X.-J., and Guo, P. (2013b). Solid-state and biological nanopore for real-time sensing of single chemical and sequencing of DNA. Nano Today *8*, 56-74.

Henriquez, R.R., Ito, T., Sun, L., and Crooks, R.M. (2004). The resurgence of Coulter counting for analyzing nanoscale objects. Analyst *129*, 478-482.

Hille, B. (2001). Ion channels of excitable membranes, 3rd edn (Sounderland, MA: Sinauer Associates Inc).

Holmgren, A. (1985). Thioredoxin. Annu. Rev. Biochem. *54*, 237-271.

Howorka, S., Cheley, S., and Bayley, H. (2001a). Sequence-specific detection of individual DNA strands using engineered nanopores. Nat. Biotechnol. *19*, 636-639.

Howorka, S., Movileanu, L., Braha, O., and Bayley, H. (2001b). Kinetics of duplex formation for individual DNA strands within a single protein nanopore. Proc. Natl. Acad. Sci. *98*, 12996-13001.

Howorka, S., and Siwy, Z.S. (2012). Nanopores as protein sensors. Nat. Biotechnol. *30*, 506-507.

Huang, X., Atwood, C.S., Moir, R.D., Hartshorn, M.A., Tanzi, R.E., and Bush, A.I. (2004). Trace metal contamination initiates the apparent auto-aggregation, amyloidosis, and oligomerization of Alzheimer's Aß peptides. J. Biol. Inorg. Chem. *9*, 954-960.

Hunter, R.J. (1988). Zeta potential in colloid science: principles and applications (London, UK: Academic Press).

Hurley, J. (1970). Sizing particles with a Coulter counter. Biophys. J. *10*, 74-79.

Iqbal, S.M., Akin, D., and Bashir, R. (2007). Solid-state nanopore channels with DNA selectivity. Nat. Nanotechnol. *2*, 243-248.

Jacob, J., Dothager, R.S., Thiyagarajan, P., and Sosnick, T.R. (2007). Fully reduced ribonuclease A does not expand at high denaturant concentration or temperature. J. Mol. Biol. *367*, 609-615.

Japrung, D., Dogan, J., Freedman, K.J., Nadzeyka, A., Bauerdick, S., Albrecht, T., Kim, M.J., Jemth, P., and Edel, J.B. (2013). Single-molecule studies of intrinsically disordered proteins using solid-state nanopores. Anal. Chem. *85*, 2449-2456.

Jetha, N.N., Feehan, C., Wiggin, M., Tabard-Cossa, V., and Marziali, A. (2011). Long dwell-time passage of DNA through nanometer-scale pores: kinetics and sequence dependence of motion. Biophys. J. *100*, 2974-2980.

Jetha, N.N., Semenchenko, V., Wishart, D.S., Cashman, N.R., and Marziali, A. (2013). Nanopore analysis of wild-type and mutant Prion protein (PrP(C)): single molecule discrimination and PrP(C) kinetics. PLoS One *8*, e54982.

Joseph-McCarthy, D., Fedorov, A.A., and Almo, S.C. (1996). Comparison of experimental and computational functional group mapping of an RNase A structure: implications for computer-aided drug design. Protein Eng. *9*, 773-780.

Kang, X.-f., Cheley, S., Guan, X., and Bayley, H. (2006). Stochastic detection of enantiomers. J. Am. Chem. Soc. *128*, 10684-10685.

Kang, X.-f., Gu, L.-Q., Cheley, S., and Bayley, H. (2005). Single protein pores containing molecular adapters at high temperatures. Angew. Chem. Int. Ed. *44*, 1495-1499.

Kasas, S., Thomson, N.H., Smith, B.L., Hansma, P.K., Miklossy, J., and Hansma, H.G. (1997). Biological applications of the AFM: from single molecules to organs. Int. J. Imag. Syst. Tech. *8*, 151-161.

Kasianowicz, J.J., Brandin, E., Branton, D., and Deamer, D.W. (1996). Characterization of individual polynucleotide molecules using a membrane channel. Proc. Natl. Acad. Sci. *93*, 13770-13773.

Katti, S.K., LeMaster, D.M., and Eklund, H. (1990). Crystal structure of thioredoxin from Escherichia coli at 1.68 Å resolution. J. Mol. Biol. *212*, 167-184.

Kelly, S.M., Jess, T.J., and Price, N.C. (2005). How to study proteins by circular dichroism. Biochimica et Biophysica Acta (BBA) - Proteins and Proteomics *1751*, 119-139.

Kelly, S.M., and Price, N.C. (2000). The use of circular dichroism in the investigation of protein structure and function. Curr. Protein Pept. Sci. *1*, 349-384.

Kerscher, O., Felberbaum, R., and Hochstrasser, M. (2006). Modification of proteins by ubiquitin and ubiquitin-like proteins. Annu. Rev. Cell Dev. Biol. *22*, 159-180.

Kindrachuk, J., Scruten, E., Attah-Poku, S., Bell, K., Potter, A., Babiuk, L.A., Griebel, P.J., and Napper, S. (2011). Stability, toxicity, and biological activity of host defense peptide BMAP28 and its inversed and retro-inversed isomers. Biopolymers *96*, 14-24.

Kowalczyk, S.W., Wells, D.B., Aksimentiev, A., and Dekker, C. (2012). Slowing down DNA translocation through a nanopore in lithium chloride. Nano Lett. *12*, 1038-1044.

Krasniqi, B., and Lee, J.S. (2012). The importance of adding EDTA for the nanopore analysis of proteins. Metallomics *4*, 539-544.

Kukwikila, M., and Howorka, S. (2010). Electrically sensing protease activity with nanopores. J. Phys.: Condens. Matter *22*, 454103.

Kumar, S., Tao, C., Chien, M., Hellner, B., Balijepalli, A., Robertson, J.W., Li, Z., Russo, J.J., Reiner, J.E., Kasianowicz, J.J., and Ju, J. (2012). PEG-labeled nucleotides and nanopore detection for single molecule DNA sequencing by synthesis. Sci. Rep. *2*, 684.

Kurokawa, H., and Nonomura, Y. (1988). Purification of a novel 30,000 Da calcium-binding protein from bovine cerebellum. J. Biochem. (Tokyo). *103*, 8-10.

Lesieur, C., Frutiger, S., Hughes, G., Kellner, R., Pattus, F., and van der Goot, F.G. (1999). Increased stability upon heptamerization of the pore-forming toxin Aerolysin. J. Biol. Chem. *274*, 36722-36728.

Li, J., Stein, D., McMullan, C., Branton, D., Aziz, M.J., and Golovchenko, J.A. (2001). Ion-beam sculpting at nanometre length scales. Nature *412*, 166-169.

Lieberman, K.R., Cherf, G.M., Doody, M.J., Olasagasti, F., Kolodji, Y., and Akeson, M. (2010). Processive replication of single DNA molecules in a nanopore catalyzed by phi29 DNA polymerase. J. Am. Chem. Soc. *132*, 17961-17972.

Luan, B., Stolovitzky, G., and Martyna, G. (2012). Slowing and controlling the translocation of DNA in a solid-state nanopore. Nanoscale *4*, 1068-1077.

Luo, Y., Egwolf, B., Walters, D.E., and Roux, B.t. (2009). Ion selectivity of α-hemolysin with a β-cyclodextrin adapter. I. Single ion potential of mean force and diffusion coefficient. J. Phys. Chem. B *114*, 952-958.

Ma, L., and Cockroft, S.L. (2010). Biological nanopores for single-molecule biophysics. Chembiochem *11*, 25-34.

Madampage, C., Tavassoly, O., Christensen, C., Kumari, M., and Lee, J.S. (2012). Nanopore analysis: An emerging technique for studying the folding and misfolding of proteins. Prion *6*, 116-123.

Madampage, C.A., Andrievskaia, O., and Lee, J.S. (2010). Nanopore detection of antibody prion interactions. Anal. Biochem. *396*, 36-41.

Maitra, R.D., Kim, J., and Dunbar, W.B. (2012). Recent advances in nanopore sequencing. Electrophoresis *33*, 3418-3428.

Majd, S., Yusko, E.C., Billeh, Y.N., Macrae, M.X., Yang, J., and Mayer, M. (2010). Applications of biological pores in nanomedicine, sensing, and nanoelectronics. Curr. Opin. Biotechnol. *21*, 439-476.

Makarov, D.E. (2009). Computer simulations and theory of protein translocation. Acc. Chem. Res. *42*, 281-289.

Manrao, E.A., Derrington, I.M., Laszlo, A.H., Langford, K.W., Hopper, M.K., Gillgren, N., Pavlenok, M., Niederweis, M., and Gundlach, J.H. (2012). Reading DNA at single-nucleotide resolution with a mutant MspA nanopore and phi29 DNA polymerase. Nat. Biotechnol. *30*, 349-353.

Marino, T., Russo, N., Toscano, M., and Pavelka, M. (2012). Theoretical investigation on DNA/RNA base pairs mediated by copper, silver, and gold cations. Dalton Trans *41*, 1816-1823.

Mathe, J., Visram, H., Viasnoff, V., Rabin, Y., and Meller, A. (2004). Nanopore unzipping of individual DNA hairpin molecules. Biophys. J. *87*, 3205-3212.

Mattern, C.F.T., Brackett, F.S., and Olson, B.J. (1957). Determination of number and size of particles by electrical gating: blood cells. J. Appl. Physiol. *10*, 56-70.

Meller, A., Nivon, L., Brandin, E., Golovchenko, J., and Branton, D. (2000). Rapid nanopore discrimination between single polynucleotide molecules. Proc. Natl. Acad. Sci. *97*, 1079-1084.

Meller, A., Nivon, L., and Branton, D. (2001). Voltage-driven DNA translocations through a nanopore. Phys. Rev. Lett. *86*, 3435-3438.

Menestrina, G. (1986). Ionic channels formed by Staphylococcus aureus alpha-toxin: Voltage-dependent inhibition by divalent and trivalent cations. J. Membr. Biol. *90*, 177-190.

Meng, H., Detillieux, D., Baran, C., Krasniqi, B., Christensen, C., Madampage, C., Stefureac, R.I., and Lee, J.S. (2010). Nanopore analysis of tethered peptides. J. Pept. Sci. *16*, 701-708.

Merchant, C.A., and Drndic, M. (2012). Graphene nanopore devices for DNA sensing. Methods Mol. Biol. *870*, 211-226.

Merchant, C.A., Healy, K., Wanunu, M., Ray, V., Peterman, N., Bartel, J., Fischbein, M.D., Venta, K., Luo, Z., Johnson, A.T.C., and Drndić, M. (2010). DNA translocation through graphene nanopores. Nano Lett. *10*, 2915-2921.

Merlini, G., and Bellotti, V. (2005). Lysozyme: A paradigmatic molecule for the investigation of protein structure, function and misfolding. Clin. Chim. Acta *357*, 168-172.

Merstorf, C., Cressiot, B., Pastoriza-Gallego, M., Oukhaled, A., Betton, J.M., Auvray, L., and Pelta, J. (2012). Wild type, mutant protein unfolding and phase transition detected by single-nanopore recording. ACS Chem. Biol. *7*, 652-658.

Michalet, X., Weiss, S., and Jäger, M. (2006). Single-molecule fluorescence studies of protein polding and conformational dynamics. Chem. Rev. *106*, 1785-1813.

Miles, B.N., Ivanov, A.P., Wilson, K.A., Dogan, F., Japrung, D., and Edel, J.B. (2013). Single molecule sensing with solid-state nanopores: novel materials, methods, and applications. Chem. Soc. Rev. *42*, 15-28.

Miyamoto, T., Okano, S., and Kasai, N. (2009). Irreversible thermoinactivation of ribonuclease-A by soft-hydrothermal processing. Biotechnol. Prog. *25*, 1678-1685.

Mohammad, Prakash, S., Matouschek, A., and Movileanu, L. (2008). Controlling a single protein in a nanopore through electrostatic traps. J. Am. Chem. Soc. *130*, 4081-4088.

Mohammad, M.M., Howard, K.R., and Movileanu, L. (2011). Redesign of a plugged β-barrel membrane protein. J. Biol. Chem. *286*, 8000-8013.

Molleman, A. (2003). Patch clamping: An introductory guide to patch clamp electrophysiology. (Chichester, UK: John Wiley & Sons, Ltd).

Movileanu, L., Howorka, S., Braha, O., and Bayley, H. (2000). Detecting protein analytes that modulate transmembrane movement of a polymer chain within a single protein pore. Nat. Biotechnol. *18*, 1091-1095.

Movileanu, L., Schmittschmitt, J.P., Scholtz, J.M., and Bayley, H. (2005). Interactions of peptides with a protein pore. Biophys. J. *89*, 1030-1045.

Mulero, R., Prabhu, A.S., Freedman, K.J., and Kim, M.J. (2010). Nanopore-based devices for bioanalytical applications. Jala *15*, 243-252.

Muller, S., Guichard, G., Benkirane, N., Brown, F., Van Regenmortel, M.H., and Briand, J.P. (1995). Enhanced immunogenicity and cross-reactivity of retro-inverso peptidomimetics of the major antigenic site of foot-and-mouth disease virus. Pept. Res. *8*, 138-144.

Mussi, V., Fanzio, P., Repetto, L., Firpo, G., Scaruffi, P., Stigliani, S., Menotta, M., Magnani, M., Tonini, G.P., and Valbusa, U. (2010a). Electrical characterization of DNA-functionalized solid state nanopores for bio-sensing. J. Phys.: Condens. Matter *22*, 454104.

Mussi, V., Fanzio, P., Repetto, L., Firpo, G., Scaruffi, P., Stigliani, S., Tonini, G.P., and Valbusa, U. (2010b). DNA-functionalized solid state nanopore for biosensing. Nanotechnology *21*, 145102.

Mussi, V., Fanzio, P., Repetto, L., Firpo, G., Stigliani, S., Tonini, G.P., and Valbusa, U. (2011). "DNA-Dressed Nanopore" for complementary sequence detection. Biosens. Bioelectron. *29*, 125-131.

Neher, E., and Sakmann, B. (1976). Single-channel currents recorded from membrane of denervated frog muscle fibres. Nature *260*, 799-802.

Neher, E., Sakmann, B., and Steinbach, J. (1978). The extracellular patch clamp: A method for resolving currents through individual open channels in biological membranes. Pflügers Archiv *375*, 219-228.

Neira, J.L., and Rico, M. (1997). Folding studies on ribonuclease A, a model protein. Fold. Des. *2*, R1-R11.

Neuman, K.C., and Block, S.M. (2004). Optical trapping. Rev. Sci. Instrum. *75*, 2787-2809.

Niedzwiecki, D.J., Grazul, J., and Movileanu, L. (2010). Single-molecule observation of protein adsorption onto an inorganic surface. J. Am. Chem. Soc. *132*, 10816-10822.

Nivala, J., Marks, D.B., and Akeson, M. (2013). Unfoldase-mediated protein translocation through an alpha-hemolysin nanopore. Nat. Biotechnol. *31*, 247-250.

Nouwen, N., Ranson, N., Saibil, H., Wolpensinger, B., Engel, A., Ghazi, A., and Pugsley, A.P. (1999). Secretin PulD: Association with pilot PulS, structure, and ion-conducting channel formation. Proc. Natl. Acad. Sci. *96*, 8173-8177.

Oukhaled, A., Bacri, L., Pastoriza-Gallego, M., Betton, J.M., and Pelta, J. (2012). Sensing proteins through nanopores: fundamental to applications. ACS Chem. Biol. *7*, 1935-1949.

Oukhaled, A., Cressiot, B., Bacri, L., Pastoriza-Gallego, M., Betton, J.M., Bourhis, E., Jede, R., Gierak, J., Auvray, L., and Pelta, J. (2011). Dynamics of completely unfolded and native proteins through solid-state nanopores as a aunction of electric driving force. ACS Nano *5*, 3628-3638.

Oukhaled, G., Mathe, J., Biance, A.L., Bacri, L., Betton, J.M., Lairez, D., Pelta, J., and Auvray, L. (2007). Unfolding of proteins and long transient conformations detected by single nanopore recording. Phys. Rev. Lett. *98*, 158101.

Pastoriza-Gallego, M., Gibrat, G., Thiebot, B., Betton, J.-M., and Pelta, J. (2009). Polyelectrolyte and unfolded protein pore entrance depends on the pore geometry. Biochim. Biophys. Acta *1788*, 1377-1386.

Pastoriza-Gallego, M., Oukhaled, G., Mathe, J., Thiebot, B., Betton, J.-M., Auvray, L., and Pelta, J. (2007). Urea denaturation of alpha-hemolysin pore inserted in planar lipid bilayer detected by single nanopore recording: loss of structural asymmetry. FEBS Lett. *581*, 3371-3376.

Pastoriza-Gallego, M., Rabah, L., Gibrat, G., Thiebot, B., van der Goot, F.G., Auvray, L., Betton, J.M., and Pelta, J. (2011). Dynamics of unfolded protein transport through an aerolysin pore. J. Am. Chem. Soc. *133*, 2923-2931.

Payet, L., Martinho, M., Pastoriza-Gallego, M., Betton, J.-M., Auvray, L., Pelta, J., and Mathé, J. (2012). Thermal unfolding of proteins probed at the single molecule level using nanopores. Anal. Chem. *84*, 4071-4076.

Pedone, D., Firnkes, M., and Rant, U. (2009). Data analysis of translocation events in nanopore experiments. Anal. Chem. *81*, 9689-9694.

Penner, R. (1995). A practical guide to patch clamping. In Single-Channel Recording, B. Sakmann, and E. Neher, eds. (New York: Springer US), pp. 3-30.

Pennisi, E. (2012). Search for pore-fection. Science *336*, 534-537.

Petkova, V., Benattar, J.-J., and Nedyalkov, M. (2002). How to control the molecular architecture of a monolayer of proteins supported by a lipid bilayer. Biophys. J. *82*, 541-548.

Pickart, C.M. (2001). Mechanisms underlying ubiquitination. Annu. Rev. Biochem. *70*, 503-533.

Plesa, C., Kowalczyk, S.W., Zinsmeester, R., Grosberg, A.Y., Rabin, Y., and Dekker, C. (2013). Fast translocation of proteins through solid state nanopores. Nano Lett. *13*, 658-663.

Postma, H.W.C. (2010). Rapid sequencing of individual DNA molecules in graphene nanogaps. Nano Lett. *10*, 420-425.

Powell, M.F., Stewart, T., Otvos, L., Jr., Urge, L., Gaeta, F.C., Sette, A., Arrhenius, T., Thomson, D., Soda, K., and Colon, S.M. (1993). Peptide stability in drug development. II. Effect of single amino acid substitution and glycosylation on peptide reactivity in human serum. Pharm. Res. *10*, 1268-1273.

Raines, R.T. (1998). Ribonuclease A. Chem. Rev. *98*, 1045-1066.

Rees, D.C. (2002). Great metalloclusters in enzymology. Annu. Rev. Biochem. *71*, 221-246.

Reinstadler, D., Fabian, H., Backmann, J., and Naumann, D. (1996). Refolding of thermally and urea-denatured ribonuclease A monitored by time-resolved FTIR spectroscopy. Biochemistry. *35*, 15822-15830.

Rhee, M., and Burns, M.A. (2006). Nanopore sequencing technology: research trends and applications. Trends Biotechnol. *24*, 580-586.

Rincon-Restrepo, M., Mikhailova, E., Bayley, H., and Maglia, G. (2011). Controlled translocation of individual DNA molecules through protein nanopores with engineered molecular brakes. Nano Lett. *11*, 746-750.

Ritort, F. (2006). Single-molecule experiments in biological physics: methods and applications. J. Phys.: Condens. Matter *18*, R531.

Rodriguez-Larrea, D., and Bayley, H. (2013). Multistep protein unfolding during nanopore translocation. Nat. Nanotechnol. *8*, 288–295.

Rosenstein, J.K., Wanunu, M., Merchant, C.A., Drndic, M., and Shepard, K.L. (2012). Integrated nanopore sensing platform with sub-microsecond temporal resolution. Nat. Methods *9*, 487-492.

Rotem, D., Jayasinghe, L., Salichou, M., and Bayley, H. (2012). Protein detection by nanopores equipped with aptamers. J. Am. Chem. Soc. *134*, 2781-2787.

Roy, R., Hohng, S., and Ha, T. (2008). A practical guide to single-molecule FRET. Nat. Methods *5*, 507-516.

Safarian, S., and Moosavi-Movahedi, A. (2000). Binding patterns and kinetics of RNase A interaction with RNA. J. Protein Chem. *19*, 335-344.

Sambrook, J., and Russell, D.W. (2001). Molecular cloning: a laboratory manual, 3 edn (New York: Cold Spring Harbor Laboratory Press).

Samorì, B., Zuccheri, G., and Baschieri, P. (2005). Protein unfolding and refolding under force: methodologies for nanomechanics. Chemphyschem *6*, 29-34.

Santos, N.C., and Castanho, M.A.R.B. (2004). An overview of the biophysical applications of atomic force microscopy. Biophys. Chem. *107*, 133-149.

Sasaki, K., Dockerill, S., Adamiak, D.A., Tickle, I.J., and Blundell, T. (1975). X-ray analysis of glucagon and its relationship to receptor binding. Nature *257*, 751-757.

Schneider, G.F., and Dekker, C. (2012). DNA sequencing with nanopores. Nat. Biotechnol. *30*, 326-328.

Schneider, G.g.F., Kowalczyk, S.W., Calado, V.E., Pandraud, G.g., Zandbergen, H.W., Vandersypen, L.M.K., and Dekker, C. (2010). DNA translocation through graphene nanopores. Nano Lett. *10*, 3163-3167.

Schuhmann, R., and Muller, R.H. (1998). Optimization of sample preparation for coulter counter measurements. Pharm. Ind. *60*, 157-163.

Sela, M., and Anfinsen, C.B. (1957). Some spectrophotometric and polarimetric experiments with ribonuclease. Biochim. Biophys. Acta *24*, 229-235.

Selvin, P.R., and Ha, T. (2008). Single-molecule techniques: a laboratory manual (New York: Cold Spring Harbor Laboratory Press).

Sethuraman, A., and Belfort, G. (2005). Protein structural perturbation and aggregation on homogeneous surfaces. Biophys. J. *88*, 1322-1333.

Sexton, L.T., Horne, L.P., Sherrill, S.A., Bishop, G.W., Baker, L.A., and Martin, C.R. (2007). Resistive-pulse studies of proteins and protein/antibody complexes using a conical nanotube sensor. J. Am. Chem. Soc. *129*, 13144-13152.

Sexton, L.T., Mukaibo, H., Katira, P., Hess, H., Sherrill, S.A., Horne, L.P., and Martin, C.R. (2010). An adsorption-based model for pulse duration in resistive-pulse protein sensing. J. Am. Chem. Soc. *132*, 6755-6763.

Siwy, Z., Gu, Y., Spohr, H.A., Baur, D., Wolf-Reber, A., Spohr, R., Apel, P., and Korchev, Y.E. (2002). Rectification and voltage gating of ion currents in a nanofabricated pore. Europhys. Lett. *60*, 349.

Siwy, Z., Trofin, L., Kohli, P., Baker, L.A., Trautmann, C., and Martin, C.R. (2005). Protein biosensors based on biofunctionalized conical gold nanotubes. J. Am. Chem. Soc. *127*, 5000-5001.

Smeets, R.M.M., Keyser, U.F., Wu, M.Y., Dekker, N.H., and Dekker, C. (2006). Nanobubbles in solid-state nanopores. Phys. Rev. Lett. *97*, 088101.

Smeets, R.M.M., Kowalczyk, S.W., Hall, A.R., Dekker, N.H., and Dekker, C. (2009). Translocation of RecA-coated double-stranded DNA through solid-state nanopores. Nano Lett. *9*, 3089-3095.

Song, L., Hobaugh, M.R., Shustak, C., Cheley, S., Bayley, H., and Gouaux, J.E. (1996). Structure of staphylococcal alpha-hemolysin, a heptameric transmembrane pore. Science *274*, 1859-1866.

Soskine, M., Biesemans, A., Moeyaert, B., Cheley, S., Bayley, H., and Maglia, G. (2012). An engineered ClyA nanopore detects folded target proteins by selective external association and pore entry. Nano Lett. *12*, 4895-4900.

Spurlino, J.C., Lu, G.Y., and Quiocho, F.A. (1991). The 2.3-A resolution structure of the maltose- or maltodextrin-binding protein, a primary receptor of bacterial active transport and chemotaxis. J. Biol. Chem. *266*, 5202-5219.

Stefankova, P., Kollarova, M., and Barak, I. (2005). Thioredoxin - structural and functional complexity. Gen. Physiol. Biophys. *24*, 3-11.

Stefureac, R. (2012). Nanopore analysis of peptides and proteins. Ph.D. Thesis. University of Saskatchewan, Saskatoon.

Stefureac, R., Long, Y.-T., Kraatz, H.-B., Howard, P., and Lee, J.S. (2006). Transport of alpha-helical peptides through alpha-hemolysin and aerolysin pores. Biochemistry. *45*, 9172-9179.

Stefureac, R., Waldner, L., Howard, P., and Lee, J.S. (2008). Nanopore analysis of a small 86-residue protein. Small *4*, 59-63.

Stefureac, R.I., Kachayev, A., and Lee, J.S. (2012). Modulation of the translocation of peptides through nanopores by the application of an AC electric field. Chem. Commun. *48*, 1928-1930.

Stefureac, R.I., and Lee, J.S. (2008). Nanopore analysis of the folding of zinc fingers. Small *4*, 1646-1650.

Stefureac, R.I., Madampage, C.A., Andrievskaia, O., and Lee, J.S. (2010a). Nanopore analysis of the interaction of metal ions with prion proteins and peptides. Biochem. Cell Biol. *88*, 347-358.

Stefureac, R.I., Trivedi, D., Marziali, A., and Lee, J.S. (2010b). Evidence that small proteins translocate through silicon nitride pores in a folded conformation. J. Phys.: Condens. Matter *22*, 454133.

Stoloff, D.H., and Wanunu, M. (2012). Recent trends in nanopores for biotechnology. Curr. Opin. Biotechnol.

Storm, A.J., Chen, J.H., Ling, X.S., Zandbergen, H.W., and Dekker, C. (2003). Fabrication of solid-state nanopores with single-nanometre precision. Nature Mater. *2*, 537-540.

Storm, A.J., Chen, J.H., Ling, X.S., Zandbergen, H.W., and Dekker, C. (2005). Electron-beam-induced deformations of SiO2 nanostructures. J. Appl. Phys. *98*, 014307 - 014315.

Strozen, T.G., Stanley, H., Gu, Y., Boyd, J., Bagdasarian, M., Sandkvist, M., and Howard, S.P. (2011). Involvement of the GspAB complex in assembly of the type II secretion system secretin of Aeromonas and Vibrio species. J. Bacteriol. *193*, 2322-2331.

Sugita, T., Hiramatsu, K., Ikeda, S., and Matsumura, M. (2013). Fabrication of pores in a silicon carbide wafer by electrochemical etching with a glassy-carbon needle electrode. ACS Appl. Mater. Interfaces *5*, 2580-2584.

Sutherland, T.C., Long, Y.T., Stefureac, R.I., Bediako-Amoa, I., Kraatz, H.B., and Lee, J.S. (2004). Structure of peptides investigated by nanopore analysis. Nano Lett. *4*, 1273-1277.

Tabard-Cossa, V., Trivedi, D., Wiggin, M., Jetha, N., N., and Marziali, A. (2007). Noise analysis and reduction in solid-state nanopores. Nanotechnology *18*, 305505.

Takahashi, T., Irie, M., and Ukita, T. (1969). A comparative study on enzymatic activity of bovine pancreatic ribonuclease A, ribonuclease S and ribonuclease S'. J. Biochem. (Tokyo). *65*, 55-62.

Talaga, D.S., and Li, J. (2009). Single-molecule protein unfolding in solid state nanopores. J. Am. Chem. Soc. *131*, 9287-9297.

Tavassoly, O., and Lee, J.S. (2012). Methamphetamine binds to alpha-synuclein and causes a conformational change which can be detected by nanopore analysis. FEBS Lett. *586*, 3222-3228.

Taylor, E.M., Otero, D.A., Banks, W.A., and O'Brien, J.S. (2000). Retro-inverso prosaptide peptides retain nioactivity, are stable in vivo, and are blood-brain barrier permeable. J. Pharmacol. Exp. Ther. *295*, 190-194.

Telmer, P.G., and Shilton, B.H. (2003). Insights into the conformational equilibria of maltose-binding protein by analysis of high affinity mutants. J. Biol. Chem. *278*, 34555-34567.

Tinoco, I., and Gonzalez, R.L. (2011). Biological mechanisms, one molecule at a time. Genes Dev. *25*, 1205-1231.

Tsitrin, Y., Morton, C.J., el-Bez, C., Paumard, P., Velluz, M.C., Adrian, M., Dubochet, J., Parker, M.W., Lanzavecchia, S., and van der Goot, F.G. (2002). Conversion of a transmembrane to a water-soluble protein complex by a single point mutation. Nat. Struct. Biol. *9*, 729-733.

Unger, R.H., and Orci, L. (1976). Physiology and pathophysiology of glucagon. Physiol. Rev. *56*, 778-826.

Venkatesan, B.M., Dorvel, B., Yemenicioglu, S., Watkins, N., Petrov, I., and Bashir, R. (2009). Highly sensitive, mechanically stable nanopore sensors for DNA analysis. Adv. Mater. *21*, 2771-2776.

Venkatesan, B.M., Shah, A.B., Zuo, J.-M., and Bashir, R. (2010). DNA sensing using nanocrystalline surface-enhanced Al2O3 nanopore sensors. Adv. Funct. Mater. *20*, 1266-1275.

Vercoutere, W., Winters-Hilt, S., Olsen, H., Deamer, D., Haussler, D., and Akeson, M. (2001). Rapid discrimination among individual DNA hairpin molecules at single-nucleotide resolution using an ion channel. Nat. Biotechnol. *19*, 248-252.

Vercoutere, W.A., Winters-Hilt, S., DeGuzman, V.S., Deamer, D., Ridino, S.E., Rodgers, J.T., Olsen, H.E., Marziali, A., and Akeson, M. (2003). Discrimination among individual Watson–Crick base pairs at the termini of single DNA hairpin molecules. Nucleic Acids Res. *31*, 1311-1318.

Vijay-Kumar, S., Bugg, C.E., and Cook, W.J. (1987). Structure of ubiquitin refined at 1.8Åresolution. J. Mol. Biol. *194*, 531-544.

Waldauer, S.A., Bakajin, O., and Lapidus, L.J. (2010). Extremely slow intramolecular diffusion in unfolded protein L. Proc. Natl. Acad. Sci. *107*, 13713-13717.

Walsh, M. (1983). Calmodulin and its roles in skeletal muscle function. Canadian Anaesthetists' Society Journal *30*, 390-398.

Wang, H.Y., Li, Y., Qin, L.X., Heyman, A., Shoseyov, O., Willner, I., Long, Y.T., and Tian, H. (2013). Single-molecule DNA detection using a novel SP1 protein nanopore. Chem. Commun. *49*, 1741-1743.

Wang, H.Y., Ying, Y.L., Li, Y., Kraatz, H.B., and Long, Y.T. (2011a). Nanopore analysis of beta-amyloid peptide aggregation transition induced by small molecules. Anal. Chem. *83*, 1746-1752.

Wang, Y., Zheng, D., Tan, Q., Wang, M.X., and Gu, L.Q. (2011b). Nanopore-based detection of circulating microRNAs in lung cancer patients. Nat. Nanotechnol.

Wanunu, M. (2012). Nanopores: A journey towards DNA sequencing. Phys. Life Rev. *9*, 125-158.

Wanunu, M., Dadosh, T., Ray, V., Jin, J., McReynolds, L., and Drndic, M. (2010). Rapid electronic detection of probe-specific microRNAs using thin nanopore sensors. Nat. Nanotechnol. *5*, 807-814.

Wedemeyer, W.J., Welker, E., Narayan, M., and Scheraga, H.A. (2000). Disulfide bonds and protein folding. Biochemistry. *39*, 4207-4216.

Wei, R., Gatterdam, V., Wieneke, R., Tampe, R., and Rant, U. (2012). Stochastic sensing of proteins with receptor-modified solid-state nanopores. Nat. Nanotechnol. *7*, 257-263.

Weichsel, A., Gasdaska, J.R., Powis, G., and Montfort, W.R. (1996). Crystal structures of reduced, oxidized, and mutated human thioredoxins: evidence for a regulatory homodimer. Structure (London, England : 1993) *4*, 735-751.

Wells, D.B., Belkin, M., Comer, J., and Aksimentiev, A. (2012). Assessing graphene nanopores for sequencing DNA. Nano Lett. *12*, 4117-4123.

Wendell, D., Jing, P., Geng, J., Subramaniam, V., Lee, T.J., Montemagno, C., and Guo, P. (2009). Translocation of double-stranded DNA through membrane-adapted phi29 motor protein nanopores. Nat. Nanotechnol. *4*, 765-772.

Werle, M., and Bernkop-Schnurch, A. (2006). Strategies to improve plasma half life time of peptide and protein drugs. Amino Acids *30*, 351-367.

Wolfe, A.J., Mohammad, M.M., Cheley, S., Bayley, H., and Movileanu, L. (2007). Catalyzing the translocation of polypeptides through attractive interactions. J. Am. Chem. Soc. *129*, 14034-14041.

Wu, H.-C., Astier, Y., Maglia, G., Mikhailova, E., and Bayley, H. (2007). Protein nanopores with covalently attached molecular adapters. J. Am. Chem. Soc. *129*, 16142-16148.

Wu, M.Y., Krapf, D., Zandbergen, M., Zandbergen, H., and Batson, P.E. (2005). Formation of nanopores in a SiN/SiO2 membrane with an electron beam. Appl. Phys. Lett. *87*, 113106-113109.

Xie, H., Braha, O., Gu, L.-Q., Cheley, S., and Bayley, H. (2005). Single-molecule observation of the catalytic subunit of cAMP-dependent protein kinase binding to an inhibitor Peptide. Chem. Biol. *12*, 109-120.

Yang, S., and Neimark, A.V. (2012). Adsorption-driven translocation of polymer chain into nanopores. J. Chem. Phys. *136*, 214901.

Yeh, L.H., Zhang, M., Joo, S.W., and Qian, S. (2012). Slowing down DNA translocation through a nanopore by lowering fluid temperature. Electrophoresis *33*, 3458-3465.

Ying, Y.-L., Wang, H.-Y., Sutherland, T.C., and Long, Y.-T. (2011). Monitoring of an ATP-binding aptamer and its conformational changes using an α-hemolysin nanopore. Small *7*, 87-94.

Yusko, E.C., Johnson, J.M., Majd, S., Prangkio, P., Rollings, R.C., Li, J.L., Yang, J., and Mayer, M. (2011). Controlling protein translocation through nanopores with bio-inspired fluid walls. Nat. Nanotechnol. *6*, 253-260.

Yusko, E.C., Prangkio, P., Sept, D., Rollings, R.C., Li, J., and Mayer, M. (2012). Single-particle characterization of Abeta oligomers in solution. ACS Nano *6*, 5909-5919.

Zhang, H., and Liu, K.-K. (2008). Optical tweezers for single cells. J. R. Soc. Interface *5*, 671-690.

Zhao, Q., de Zoysa, R.S., Wang, D., Jayawardhana, D.A., and Guan, X. (2009a). Real-time monitoring of peptide cleavage using a nanopore probe. J. Am. Chem. Soc. *131*, 6324-6325.

Zhao, Q., Jayawardhana, D.A., and Guan, X. (2008a). Stochastic study of the effect of ionic strength on noncovalent interactions in protein pores. Biophys. J. *94*, 1267-1275.

Zhao, Q., Jayawardhana, D.A., Wang, D., and Guan, X. (2009b). Study of peptide transport through engineered protein channels. J. Phys. Chem. B *113*, 3572-3578.

Zhao, Q.T., Wang, D., Jayawardhana, D.A., and Guan, X.Y. (2008b). Stochastic sensing of biomolecules in a nanopore sensor array. Nanotechnology *19*, 505504.